AD-A081 915 VIRGINIA POLYTECHNIC INST AND STATE UNIV BLACKSBURG --ETC F/G 11/4
THERMAL-MECHANICAL AND THERMAL BEHAVIOR OF HIGH-TEMPERATURE STR--ETC(U)
DEC 79 D P HASSELMAN, P F BECHER, L D BENTSEN N00014-78-C-0431

UNCLASSIFIED NL

1 OF 3

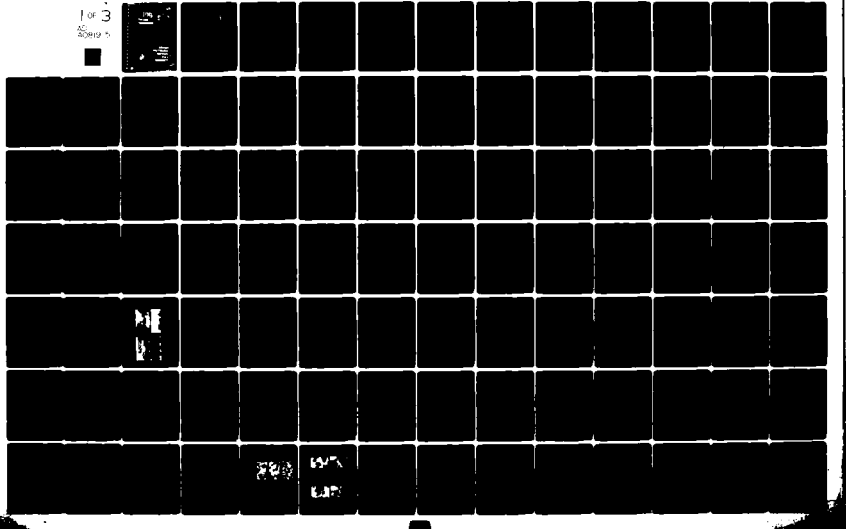

THERMAL-MECHANICAL AND THERMAL BEHAVIOR OF HIGH-TEMPERATURE STRUCTURAL MATERIALS

Interim Report to
Office of Naval Research
Agreement No. N00014-78-C-0431
January 1, 1979 - December 31, 1979

by

D. P. H. Hasselman

in cooperation with

P. F. Becher, L. D. Bentsen, M. P. Kamat, K. Mazdiyasni, R. J. Pallicka, B. R. Powell, J. A. Rubin, K. Satyamurthy, J. P. Singh W. M. Su, J. R. Thomas, G. E. Youngblood and G. Ziegler

Department of Materials Engineering
Department of Mechanical Engineering
Department of Engineering Science and Mechanics
Virginia Polytechnic Institute and State University
Blacksburg, Virginia 24061

THERMO-MECHANICAL AND THERMAL BEHAVIOR OF HIGH-TEMPERATURE STRUCTURAL MATERIALS

PREFACE

Technical ceramics because of their chemical inertness, high melting point, good wear resistance, excellent mechanical stability at high temperature and other unique properties, represent a class of materials eminently suited for many critical engineering applications. Unfortunately, because of their brittleness and unfavorable combination of pertinent material properties, technical ceramics generally are highly susceptible to catastrophic failure in non-uniform thermal environments, which give rise to thermal stresses of high magnitude.

Thermal stress failure analysis of structural materials represents a multi-disciplinary problem which involves the principles of heat transfer, mechanics and materials engineering. Over the last few decades much general understanding of the nature of thermal stress failure of brittle materials has been generated. However, due to the multi-disciplinary nature of the problem, the ability to predict thermal stress failure quantitatively for design or other purposes has lagged behind the progress made in other engineering fields. The objective of the present program is to improve the qualitative and quantitative understanding of the nature of thermal stress failure of brittle structural materials. In order to achieve this objective, the participating investigators and scope of the program are organized such that full advantage is taken of the combined inputs from a number of engineering disciplines. This report, in the form of individual chapters, presents studies completed for publication during the period 1/1/79 to 12/31/79. For one study, because of its length and to keep the printing cost to a minimum, only the abstract is given. Upon publication, reprints can be sent to the readers interested in further detail. Together with the eleven papers reported previously, the papers contained in the present report bring the total number of completed studies to twenty-three for the contract period to date (4/1/78 - 12/31/79).

The readers of this report are invited to provide their comments.

UNCLASSIFIED
SECURITY CLASSIFICATION OF THIS PAGE (When Data Entered)

REPORT DOCUMENTATION PAGE

READ INSTRUCTIONS BEFORE COMPLETING FORM

1. REPORT NUMBER
2. GOVT ACCESSION NO.
3. RECIPIENT'S CATALOG NUMBER

4. TITLE (and Subtitle)
Thermo-Mechanical and Thermal Behavior of High-Temperature Structural Materials

5. TYPE OF REPORT & PERIOD COVERED
Interim report
1/1/79 - 12/31/79

6. PERFORMING ORG. REPORT NUMBER

7. AUTHOR(s)
D. P. H. Hasselman

8. CONTRACT OR GRANT NUMBER(s)

9. PERFORMING ORGANIZATION NAME AND ADDRESS
Virginia Polytechnic Institute and State University, Blacksburg, Virginia 24061

10. PROGRAM ELEMENT, PROJECT, TASK AREA & WORK UNIT NUMBERS

11. CONTROLLING OFFICE NAME AND ADDRESS
Office of Naval Research
Arlington, VA. 22217

12. REPORT DATE
December 31, 1979

13. NUMBER OF PAGES

14. MONITORING AGENCY NAME & ADDRESS(if different from Controlling Office)

15. SECURITY CLASS. (of this report)
Unclassified

15a. DECLASSIFICATION/DOWNGRADING SCHEDULE

16. DISTRIBUTION STATEMENT (of this Report)
See distribution list. Do not release to NTIS

17. DISTRIBUTION STATEMENT (of the abstract entered in Block 20, if different from Report)

18. SUPPLEMENTARY NOTES

19. KEY WORDS (Continue on reverse side if necessary and identify by block number)
Absorption coefficient; composites (Al_2O_3-BN, BeO-SiC, glass-Ni, ZrC-graphite); crack propagation, fracture, micro-cracking, porosity, silicon nitride, thermal conductivity, thermal diffusivity, thermal radiation, thermal stress, thermal shock, transient heating

20. ABSTRACT (Continue on reverse side if necessary and identify by block number)
This report contains studies completed over the period 1/1/79 to 12/31/79 as part of a research program on the thermo-mechanical and thermal behavior of high-temperature structural materials, reported in the form of individual chapters as follows:

DD FORM 1 JAN 73 1473 EDITION OF 1 NOV 65 IS OBSOLETE
S/N 0102-LF-014-6601

Unclassified
SECURITY CLASSIFICATION OF THIS PAGE (When Data Entered)

I. J.P. Singh, J.R. Thomas, Jr., and D.P.H. Hasselman, "Analysis of Effect of Heat Transfer Variables on Thermal Stress Resistance of Brittle Ceramics Measured by Quenching Experiments,"

II. K. Satyamurthy, M.P. Kamat and D.P.H. Hasselman, "Effect of Spatially Varying Thermal Conductivity on Magnitude of Thermal Stress in Brittle Ceramics Subjected to Convective Heating,"

III. G. Ziegler and D.P.H. Hasselman, "Effect of Data Scatter on Apparent Thermal Stress Failure Mode of Brittle Ceramics,"

IV. K. Satyamurthy, J.P. Singh, M.P. Kamat and D.P.H. Hasselman, "Effect of Spatially Varying Porosity on Magnitude of Thermal Stress During Steady-State Heat Flow,"

V. Bob R. Powell, Jr., C.E. Youngblood, D.P.H. Hasselman and Larry D. Bentsen, "Effect of Thermal Expansion Mismatch on the Thermal Diffusivity of Glass-Ni Composites,"

VI. D.P.H. Hasselman, P.F. Becher and K.S. Mazdiyasni, "Analysis of the Resistance of High-E, Low-E Brittle Composites to Failure by Thermal Shock,"

VII. K. Satyamurthy, J.P. Singh, M.P. Kamat and D.P.H. Hasselman, "Thermal Stress Analysis of Brittle Ceramics with Density Gradients Under Conditions of Transient Convective Heat Transfer,"

VIII. J.R. Thomas, Jr., J.P. Singh and D.P.H. Hasselman, "Analysis of Thermal Stress Resistance of Partially Absorbing Ceramic Plate Subjected to Assymmetric Radiation, I: Convective Cooling at Rear Surface,"

IX. J.P. Singh, D.P.H. Hasselman, W.M. Su, J.A. Rubin and R. Palicka, "Observations on the Nature of Micro-Cracking in Brittle Composites,"

X. K. Satyamurthy, J.P. Singh, D.P.H. Hasselman and M.P. Kamat, "Transient Thermal Stresses in Cylinders with Square Cross-Section Under Conditions of Convective Heat Transfer,"

XI. D.P.H. Hasselman, "Effect of Micro-Cracking on Thermal Conductivity: Analysis and Experiment,"

XII. J.R. Thomas, J.P. Singh and D.P.H. Hasselman, "Role of Thermal Expansion in the Thermal Stress Resistance of Semi-Absorbing Brittle Materials Subjected to Severe Thermal Radiation."

CHAPTER I

ANALYSIS OF EFFECT OF HEAT TRANSFER VARIABLES ON THERMAL STRESS RESISTANCE OF BRITTLE CERAMICS MEASURED BY QUENCHING EXPERIMENTS

by

J. P. Singh, J. R. Thomas and D. P. H. Hasselman

Departments of
Materials and Mechanical Engineering
Virginia Polytechnic Institute and State University
Blacksburg, Virginia 24061

ABSTRACT

Heat transfer theory was used to analyze the variables which control the thermal stress fracture of brittle ceramic specimen subjected to rapid cooling by quenching into fluid media. Expressions were derived for the maximum quenching temperature difference to which circular solid cylindrical specimens can be subjected in terms of the pertinent properties of the material and fluid media. Appropriate thermal stress resistance parameters were derived. The specimen density was introduced as an additional property which controls thermal stress resistance. Recommendations were made for procedures to be followed in conducting quenching experiments.

List of Symbols

A	A constant
A_p	Projected area (dL)
α	Coefficient of thermal expansion
α_1	Thermal diffusivity
B	A Constant
β	Biot's number $(\frac{dh}{2K_s})$
C, C_1, C_2, C_3, C_r	Constants whose value depend on the value of N_{Gr}, N_{pr} and N_{Re}
C_{pf}	Specific heat of fluid
d	Diameter of the rod
E	Young's modulus of elasticity
F	Shear force $(\frac{f_D \rho_f V_t^2 A_p}{2g})$
f_D	Friction factor
γ	Volume coefficient of expansion
h	Surface heat transfer coefficient
H	Height above the fluid surface from which the specimen is dropped into the quenching bath.
H_m	Optimum height
K_f	Thermal conductivity of the fluid
K_s	Thermal conductivity of the specimen
L	Length of the rod specimen
m, n	Constants whose values depend on the value of N_{Gr}, N_{Pr} and N_{Re}.
N_{Gr}	Grashof number $(g\gamma(T_w - T_\infty)d^3/\nu_f^2)$
N_{Pr}	Prandtl number (ν_f/α_1)

List of Symbols (cont'd)

ν	Poisson's ratio
ν_f	Fluid viscosity
ρ_f	Density of the fluid
R_f	Thermal stress resistance parameter in forced convection mode of heat transfer
R_n	Thermal stress resistance parameter in natural convection mode of heat transfer.
ρ_s	Density of the solid specimen
S_t	Tensile strength of the specimen
σ^*_{max}	Non-dimensional stress $(\frac{(1-\nu)\sigma_\theta}{\alpha E \Delta T})$
σ_θ	Tangential stress
T	Temperature
T_w	Specimen wall temperature
T_∞	Fluid temperature before the hot specimen is dropped into it.
ΔT	Temperature difference between the specimen wall and the fluid medium
$(\Delta T)_{max}$	Maximum temperature difference between the specimen wall and the fluid medium.
V_a	Free fall velocity of the specimen ($\sqrt{2gH}$)
V_t	Terminal velocity

I. Introduction

Technical ceramics due to their unique physical properties, are excellent candidate materials for engineering applications involving extreme thermal and chemical environments. Unfortunately, due to their brittle nature, ceramic materials are highly susceptible to catastrophic failure due to high thermal stresses encountered during transient or steady state heat transfer. For this reason, proper selection of materials for high temperature application is critical to maintain structural integrity. Such selection can be based on theoretical analysis[1,2] as well as on experimental testing[3-7]. A popular test for the thermal stress resistance of brittle ceramics consists of quenching specimens from higher temperatures in a fluid bath at lower temperature. Such fluids may include water, oil, eutectic mixtures of salt and fluidized beds. These tests are useful for assessing relative difference in thermal stress resistance of different materials. Unfortunately, however, at this time due to the complex nature of heat transfer, quenching experiments do not appear to be very suitable for a quantitative assessment of thermal stress resistance. It is the purpose of this paper to discuss the variables which affect heat transfer in quenching tests, and to derive appropriate expression for the heat transfer coefficient in order to provide an improved quantitative basis for the interpretation of the results for thermal stress resistance determined by quenching experiments.

II. Analysis

A. General.

In general, quenching experiments can be performed in two different ways, each corresponding to a different mode of heat transfer. In one

type of experiment[3-5], the specimen is preheated to thermal equilibrium at a specified temperature and then quickly transferred to the fluid bath where it is held stationary. In this situation the heat is transferred from the specimen surface by natural convection due to the fluid motion resulting from the density change caused by the heating process[8]. In the second type of experiments, the preheated specimen is dropped[6] into and falls through the stationary fluid. In this case, there is a relative motion between the fluid and the specimen and the heat transfer takes place by forced convection as a result of the imposed fluid flow by a stream around the heated object[9]. General equations for heat transfer will be obtained for both modes namely 'natural' and 'forced' convection. For convenience of mathematical analysis, the simple specimen geometry of a circular horizontal cylinder will be considered. However, the analysis can easily be extended to different geometries. Also the analysis will be limited to the conditions where nucleate boiling and film formation do not take place.

B. Natural Convection (stationary specimen).

The average heat transfer coefficient h from an immersed horizontal cylinder in a stationary fluid is given by[8]:

$$h = C(N_{Gr} \cdot N_{Pr})^n \frac{K_f}{d} \qquad (1)$$

where n and C are constants which depend on the value of $(N_{Gr} \cdot N_{Pr})$, d is the diameter of the cylinder and subscript 'f' refers to the fluid property values at the film temperature, generally taken as the mean of the specimen surface and the fluid temperature.

Using the definition of N_{Gr} and N_{Pr}, the value of h can be obtained from equation 1 in terms of material and environment properties. Thus,

$$h = C(g\gamma\rho_f C_{pf}/\nu_f)^n (\Delta T)^n d^{3n-1} K_f^{1-n} \qquad (2)$$

C. Forced Convection (falling specimen).

In addition to many other parameters, the heat transfer by forced convection also depends upon the velocity with which the specimen falls through the fluid in a quenching experiment. It is important, therefore, to evaluate the specimen velocity before the general expression for h can be obtained. In a quenching experiment, while the specimen is falling through the fluid bath, the downward force due to the specimen weight is opposed by the upward buoyancy and shear force*. When the upward forces balance the weight of the specimen, the specimen attains an equilibrium constant velocity frequently termed as terminal velocity[10]. For mathematical simplicity it can be assumed that the specimen attains the terminal velocity as soon as it hits the fluid surface.

For a horizontal cylinder with its axis perpendicular to flow, at terminal velocity V_t,

$$\frac{\pi}{4} d^2 L\rho_s = \frac{\pi}{4} d^2 L\rho_f + F \qquad (3)$$

where F is given by[11] $f_D \rho_f V_r^2 A_p/2g$, friction coefficient f_D is a function of Reynold's number and A_p is the projected area. Using the appropriate values for f_D from Table I, the values of V_t are obtained as:

$N_{Re} < 0.5$

$$V_t = \frac{1}{16} d^2 g\left(\frac{\rho_s}{\rho_f} - 1\right) \nu_f^{-1} \left(2.002 - \ln \frac{V_t d}{\nu_f}\right) \qquad (3a)$$

* Shear force is a function of the specimen velocity.

$0.5 < N_{Re} < 10$

$$V_t = 0.267\, g^{0.714} d^{1.143} \left(\frac{\rho_s}{\rho_f} - 1\right)^{0.714} \nu_f^{-0.429} \qquad (3b)$$

$10 < N_{Re} < 40$

$$V_t = 0.5 g^{0.588} d^{0.765} \left(\frac{\rho_s}{\rho_f} - 1\right)^{0.588} \nu_f^{-0.176} \qquad (3c)$$

$40 < N_{Re} < 400$

$$V_t = 0.4513\, g^{0.6035} d^{0.8105} \left(\frac{\rho_s}{\rho_f} - 1\right)^{0.6035} \nu_f^{-0.2070} \qquad (3d)$$

$4 \times 10^2 < N_{Re} < 4 \times 10^5$

$$V_t = 1.45\, g^{0.5} d^{0.5} \left(\frac{\rho_s}{\rho_f} - 1\right)^{0.5} \qquad (3e)$$

These values of the terminal velocity were used in the expression for N_{Re} and the equations for heat transfer coefficient were obtained for the range of Reynold's number commonly encountered in the thermal quenching experiments.

The average heat transfer coefficient h in forced convection for a circular cylinder in a fluid with its axis perpendicular to the flow is given by[14].

$$h = C_r (N_{Re})^m (N_{Pr})^{\frac{1}{3}} \frac{K_f}{d} \qquad (4)$$

where m and C_r are constants whose values depend on N_{Pr} and N_{Re}. As far as the heat transfer is concerned, this case is identical to one in which a horizontal cylinder falls through the stationary fluid, since in both cases the heat is transferred due to the relative motion between the cylinder and the fluid.

Substituting for N_{Re} and N_{Pr} in terms of velocity and fluid properties and using equation (3e)* for velocity, h can be expressed as:

* Equation (3e) has been used for the velocity to obtain an expression for h because this represents the range of Reynold's number typical for laboratory thermal quench experiments. However, other equations should be used whenever appropriate.

$$400 < N_{Re} < 4000,\ N_{Pr} > 0.6$$

$$h = C_r \left[2.1g\left(\frac{\rho_s}{\rho_f} - 1\right)\right]^{\frac{m}{2}} \nu_f^{\frac{1}{3}} - m\ \rho_f^{\frac{1}{3}} C_{pf}^{\frac{1}{3}} K_f^{\frac{2}{3}} d^{\frac{3}{2}m-1} \qquad (5)$$

where $m = 0.466$ and $C_r = 0.683$

It should be pointed out that the equations 2 and 5 represent the average value of h over the surface of the specimen. There are, in fact, local variations[13] in h over the specimen surface. To incorporate this effect in the quantitative evaluation of thermal stress resistance is the topic of future research.

D. Calculation of $(\Delta T)_{max}$.

The maximum temperature differenct $(\Delta T)_{max}$, to which the specimen can be subjected without failure in a thermal quench experiment, can be obtained by equating the maximum thermal stress to the tensile strength S_t of the specimen. The exact solutions[15] of the thermal stresses developed in a circular cylinder in case of transient cooling are too complex to yield any simple analytical solution of $(\Delta T)_{max}$ for a given heat transfer coefficient value. However, when the maximum tangential stress σ_θ[15] was plotted as a function of Biot's number (figure not shown here), it resulted in a straight line represented by:

$$\frac{1}{\sigma^*_{max}} = 1.451\ (1 + \frac{3.41}{\beta}) \qquad (6)$$

where $\sigma^*_{max} = (1-\nu)\sigma_\theta/(\alpha E \Delta T)$

For thermal fracture during transient cooling, the tangential stress σ_θ is the relevant stress to consider since the other stresses are either equal to or smaller than σ_θ. Thus, equating σ_θ to the tensile strength S_t of the specimen, the maximum temperature difference $(\Delta T)_{max}$,

to which the specimen can be subjected without fracture, can be given by:

$$(\Delta T)_{max} = \frac{1.451\ S_t(1-\nu)}{\alpha E}\ (1 + 6.82\ \frac{K_s}{hd}) \qquad (7)$$

D1. Natural Convection (Stationary Specimen).

Substituting the value of h from equation (2) in equation (7) yields:

$$(\Delta T)_{max} = \frac{1.451\ S_t(1-\nu)}{\alpha E}\ [1 + 6.82\ \frac{K_s}{C}(\frac{\nu_f}{g\gamma\rho_f C_{pf}})^n \frac{1}{d^{3n} K_f^{1-n} (\Delta T)^n}] \qquad (8)$$

It is important to note that ΔT in the right hand side of the equation (8) is the temperature difference between the specimen wall and the fluid at any time whereas $(\Delta T)_{max}$ is the maximum or initial temperature difference. However, for small β, the relative surface temperature of the specimen remains close[1] to the initial temperature during the time period when the maximum stress is reached in the specimen. Thus, in this case, ΔT can be assumed to be approximately equal to $(\Delta T)_{max}$ for thermal fracture predictions. Also, for a small value of β, the second term in the parenthesis of equation (8) is much greater than 1 and therefore, $(\Delta T)_{max}$ can be approximated to be:

$$(\Delta T)_{max} \simeq C_1 [\frac{S_t(1-\nu)}{\alpha E} \frac{K_s}{d^{3n}} (\frac{\nu_f}{g\rho_f C_{pf}\gamma})^n \frac{1}{K_f^{1-n}}]^{\frac{1}{n+1}} \qquad (9)$$

where C_1 is a constant which depends upon the value of $(N_{Gr} \cdot N_{Pr})$. For a given quenching medium and specimen size, if β is small,

$$(\Delta T)_{max} \simeq C_2 [\frac{S_t(1-\nu)}{\alpha E} \frac{K_s}{}]^{\frac{1}{n+1}} \qquad (10)$$

D2. Forced Convection (falling specimen)

From equations (5) and (7), $(\Delta T)_{max}$ is given by:

$$(\Delta T)_{max} = \frac{1.451 S_t(1-\nu)}{\alpha E}\left[1 + \frac{6.82 K_s}{C_r}\{2.1g(\frac{\rho_s}{\rho_f} - 1)\}^{-\frac{m}{2}} \nu_f^{m-\frac{1}{3}} C_{pf}^{-\frac{1}{3}} K_f^{-\frac{2}{3}} \rho_f^{-\frac{1}{3}} d^{-\frac{3}{2}m}\right] \quad (11)$$

Similar to equation (10), for a given quenching medium and specimen size, if β is small, equation 11 yields:

$$(\Delta T)_{max} = C_3 \frac{S_t(1-\nu)}{\alpha E} K_s (\frac{\rho_s}{\rho_f} - 1)^{-\frac{m}{2}} \quad (12)$$

III. Discussion and Conclusions

The analyses presented above have a number of implications for the quantitative significance of the experimental results of quenching experiments and for the procedures to be followed in conducting such experiments. To date, the interpretation of the quenching experiments is based on the assumption that the heat transfer coefficient, h, is constant for a given quenching medium irrespective of the specimen size and the quenching conditions. With the assumption of a constant h for a given material, the magnitude of thermal stress is uniquely defined by the value of the Biot's number, β. However, equations (1), (2), (4) and (5) indicate that the heat transfer coefficient, h, is a function of specimen size, specimen velocity and the instantaneous temperature difference between the specimen surface and the fluid medium in addition to the pertinent fluid properties. These factors render the interpretation of quenching experiments considerably more complex,

especially when comparing the thermal quench data for specimens of different materials having large differences in $(\Delta T)_{max}$ values as well as for specimens of a given material which differ significantly in size. Throughout the following discussion, it will be assumed that Biot's number is sufficiently small ($\beta < 1$) for the natural convection case of heat transfer so that over the period of maximum stress, the change in the relative specimen surface temperature is small. Therefore, to a good approximation $\Delta T \simeq (\Delta T)_{max}$.

A. Effect of Specimen Size on $(\Delta T)_{max}$

For a heat transfer coefficient independent of specimen size, thermal stress analysis[1] predicts that $(\Delta T)_{max}$ in a quenching experiment is inversely proportional to the speciman size, which can be expressed, in general, as:

$$(\Delta T)_{max} = A + Bd^{-1} \tag{13}$$

where A and B are constants.

The results of the present analysis suggest, however, that this approach requires modification. In the present analysis, the heat transfer coefficient, h, is found to depend on the specimen size as shown in equation (5). Thus, $(\Delta T)_{max}$, based on the size-dependent heat transfer is given by equation (11) and can be written in the general form:

$$(\Delta T)_{max} = A + Bd^{-\frac{3}{2}m} \tag{14}$$

For forced convection heat transfer conditions typically encountered in laboratory quenching experiments, $m \sim 0.466$, which yields:

$$(\Delta T)_{max} = A + Bd^{-0.699} \tag{15}$$

Comparison of equations (13) and (15) shows that in forced convection heat transfer, where h is given by equation (5), $(\Delta T)_{max}$ is less dependent on specimen size than for a size-independent heat transfer coefficient. This conclusion is important for the interpretation of experimental data for $(\Delta T)_{max}$ as a function of specimen size. Equation (13) indicates that a plot of $(\Delta T)_{max}$ versus d^{-1} should yield an intercept equal to A at $d^{-1} = 0$, from which a value of $S_t(1-\nu)/\alpha E^*$ can be obtained. However, if h is a function of specimen size, the value of A obtained from equation (13) is an overestimate. The present analysis indicates that for a size-dependent h, the appropriate value of A is obtained by plotting $(\Delta T)_{max}$ against $d^{-0.699}$.

It is critical to note that in forced convection heat transfer (falling specimen), the value of the exponent of the diameter (equation 5) depends on the value of m. For this reason, especially for large specimen sizes and/or low specimen velocities in highly viscous fluid, the nature of heat transfer must be analyzed quantitatively in order to establish the proper size dependence for a correct interpretation of the experimental data.

For natural convection heat transfer, the size-dependence of $(\Delta T)_{max}$ is more complex for the reason that the heat transfer coefficient h itself depends on ΔT. However, for $\beta < 1$, the second term in equation (8) is large as compared to unity and the change in the relative specimen surface temperature is small before the maximum stress is reached. Thus, $\Delta T \simeq (\Delta T)_{max}$ so that the size dependence of $(\Delta T)_{max}$

* The terms $S_t(1-\nu)/\alpha E$ and $S_t(1-\nu)K_s/\alpha E$ will be frequently used throughout discussion because these terms represent well known thermal stress resistance parameters R and R'[16] respectively.

can be expressed as:

$$(\Delta T)_{max} \propto d^{-3n/n+1} \tag{16}$$

For $n = \frac{1}{4}$ (for laboratory quenching conditions), equation 16 yields:

$$(\Delta T)_{max} \propto d^{-0.6} \tag{17}$$

which indicates that for natural convection heat transfer, a plot of $(\Delta T)_{max}$ versus $d^{-0.6}$ should yield a straight line. Equation (17) indicates that similar to the forced convection case, for natural convection heat transfer with a size-dependent heat transfer coefficient, $(\Delta T)_{max}$ is less dependent on specimen size than for a size-independent heat transfer coefficient expressed by equation (13).

For natural convection heat transfer, caution should be exercised in extrapolation of a plot of $(\Delta T)_{max}$ versus $d^{-0.6}$ to high values of d. Such an extrapolation includes values of the Biot's number $\beta >> 1$ which violates the assumption $\Delta T \simeq (\Delta T)_{max}$. Unless accompanied by extensive numerical analysis for the variation of h with ΔT during the quench test, such an extrapolation is not expected to result in a meaningful value of the intercept. For this reason, a reliable determination of the quantity $S_t(1-\nu)/\alpha E$ should be based on quenching tests using falling specimens rather than stationary specimens.

B. Dependence of h on ΔT

For heat transfer by natural convection (stationary specimen), the heat transfer coefficient h is a function of the instantaneous temperature difference between the specimen surface and the quenching fluid (see equation 2). This implies that different materials with varying values of $(\Delta T)_{max}$ are subjected to different heat transfer

conditions. Due to this reason, for dissimilar materials, no direct proportionality is expected between $(\Delta T)_{max}$ and the quantities $S_t(1-\nu)/\alpha E$ or $S_t(1-\nu)K_s/\alpha E$. To examine the role of these quantities in establishing $(\Delta T)_{max}$, equation (9) (for $\beta<1$ and $n=\frac{1}{4}$) can be written as:

$$(\Delta T)_{max} \propto \{S_t(1-\nu)K_s/\alpha E\}^{4/5} \tag{18}$$

Equation 18 indicates that the relative difference in thermal stress resistance of different materials as measured by $(\Delta T)_{max}$ in a quenching experiment is less than the relative difference in the respective quantities of $S_t(1-\nu)K_s/\alpha E$. In order to obtain linearity for the purpose of inter- or extrapolation, it is recommended that a plot be obtained of $(\Delta T)_{max}^{5/4}$ versus $S_t(1-\nu)K_s/\alpha E$. Conversely, linearity can be also achieved by plotting $(\Delta T)_{max}$ against the thermal stress resistance parameter, R_n given by:

$$R_n = \{S_t(1-\nu)K_s/\alpha E\}^{4/5} \tag{19}$$

appropriate for the natural convection heat transfer with a ΔT-dependent heat transfer coefficient and low β.

C. Effect of Specimen Density on $(\Delta T)_{max}$

As indicated by equations (3e), (5) and (11), for a quenching experiment involving forced convection (falling specimen) the specimen velocity and therefore the heat transfer coefficient and $(\Delta T)_{max}$ are function of the ratio of specimen to fluid density. For this reason, different materials with identical values for the quantity $S_t(1-\nu)K_s/\alpha E$ can still exhibit different values of $(\Delta T)_{max}$ due to possible difference in densities. This effect should be taken into account in the interpretation of experimental data for $(\Delta T)_{max}$. The direct transfer of the

relative thermal stress resistance for different materials as measured by $(\Delta T)_{max}$ in a falling specimen method to the experimental conditions where the specimen densities do not affect the magnitude of thermal stress resistance could lead to considerable error. To avoid such error, it is proposed that the values of $(\Delta T)_{max}$ be correlated with the thermal stress resistance parameter R_f given by:

$$R_f = \{\frac{S_t(1-\nu)K_s}{\alpha E}\}\{\frac{\rho_s}{\rho_f} - 1\}^{-\frac{m}{2}} \tag{20}$$

The value of $\frac{S_t(1-\nu)K_s}{\alpha E}$ can be easily extracted from equation (20) for known values of $\frac{\rho_s}{\rho_f}$ and m. It should be noted that the quantity R_f depends on the value of the exponent m. Thus, the nature of the heat transfer in a thermal quench experiment must be assessed quantitatively in terms of the pertinent fluid properties, specimen size and terminal velocity before a valid correlation between the theory and experiments can be obtained.

The effect of specimen density on $(\Delta T)_{max}$ also can play a significant role in the effect of porosity on thermal stress resistance for a given material. This effect can be measured by changes in $(\Delta T)_{max}$ in the falling specimen method. An increase in porosity, (i.e., a decrease in density) for a porous specimen whose density approaches the fluid density will result in an increase in $(\Delta T)_{max}$ due to large increase in $\{\frac{\rho_s}{\rho_f} - 1\}^{-\frac{m}{2}}$. In contrast, for specimens with densities much higher than the fluid density, the increase in porosity is expected to decrease $(\Delta T)_{max}$ due to greater decrease in the value of $S_t(1-\nu)K_s/\alpha E$. In general, the effect of porisity on thermal stress resistance will depend on the method of measurement. For valid comparison of the results obtained by different testing methods including the falling

specimen method, the effect of specimen density must be taken into account.

D. Recommendations for Quantitative Quenching Experiments

The general analytical results of the present study also lead to a number of recommendations for procedures to be followed in quenching experiments.

As indicated by equations (2) and (5) for both natural convection (stationary specimen) and forced convection (falling specimen), the heat transfer coefficient is a function of properties of the fluid medium. Many of these fluid properties, especially the viscosity, are strongly temperature-dependent. For this reason it is critical to define the temperature of the quenching bath in reporting values for $(\Delta T)_{max}$. Because of the relatively rapid variation of fluid properties with temperature, reporting bath temperature as "room temperature" which can vary by as much as five to ten degrees, must not be considered adequate. In order to facilitate comparisons of data obtained by different investigators or laboratories, it is recommended that bath temperature be controlled and maintained at an internationally agreed-upon value. A temperature recommended here, which should be easily accomodated in most studies, is 35°C ± 0.5°C. This temperature is slightly above the room temperature in the vast majority of cases and can be maintained with minimum requirement for heating and control devices.

Another recommendation for the quantitative evaluation of $(\Delta T)_{max}$ data obtained by the falling specimen method concerns the velocity with which the specimen falls through the fluid. The present analysis is based on the assumption that the specimen falls through the fluid with its terminal velocity. Therefore, to avoid any undue complexity in

the data analysis it is desirable that the specimen should move with its terminal velocity over the time-period between entering the fluid till the time of failure. Any deviation from the terminal velocity, especially at the time of specimen entry into the fluid, will introduce transient effects in heat transfer. Such transient effects can be eliminated if the specimens were to hit the fluid surface with its terminal velocity. This can be accomplished by dropping the specimen from a pre-determined optimum height such that the velocity of the free fall (in air) corresponds to the terminal velocity when it hits the fluid surface. This height can be determined as follows:

For a free fall through height H in air, the specimen velocity V_a (neglecting air friction) just before it touches the fluid surface is given by,

$$V_a = \sqrt{2gH} \tag{21}$$

The terminal velocity V_t of a circular rod specimen falling horizontally through the fluid can be expressed as,

$$V_t = \left[\frac{\pi}{2f_D} g \left(\frac{\rho_s}{\rho_f} - 1\right) d\right]^{\frac{1}{2}} \tag{22}$$

where f_D is a function of the Reynold's number as shown in Table I. For the optimum height, $V_a = V_t$, and therefore, from equations (21) and (22), the optimum height H_m can be given by:

$$H_m = \frac{\pi}{4f_D} \left(\frac{\rho_s}{\rho_f} - 1\right)d \tag{23}$$

For fluid properties and specimen velocities commonly encountered in laboratory experiments, $4x10^2 < N_{Re} < 4x10^5$ which corresponds to a value of $f_D = 0.75$ such that

$$H_m \sim 1.05 \left(\frac{\rho_s}{\rho_f} - 1\right)d \tag{24}$$

The values of H_m for typical ceramics and specimen sizes encountered in practice correspond to heights of a few centimeters. In general for a given fluid and specimen of arbitrary size and density, the Reynold's number needs to be established before the optimim height can be calculated.

Finally, it is recommended that a careful consideration should be given to the depth of the quenching bath used for the falling specimen. In general, the thermal stresses do not reach their maximum value at the instant the specimen hits the fluid surface. For fluids with relatively low heat transfer coefficient values in combination with high thermal conductivity and small size of the specimen (i.e., low Biot's number), the time to maximum stress could be on the order of a few seconds. Under these conditions, the specimen will take less time to hit the bottom of the bath than the time required to reach the maximum stress. Consequently, the heat transfer coefficient would not be constant over the time period required to reach maximum stress which could introduce considerable error in quantitative analysis of $(\Delta T)_{max}$. In addition, a meaningful comparison cannot be made of $(\Delta T)_{max}$ data obtained from different laboratories where the bath depts could be quite different. Thus, the heat transfer properties of the fluid medium and the thermo-mechanical response of the specimen must be well understood for any quantitative interpretation of thermal quench data.

Acknowledgments

The present study was performed as a part of a research program supported by the Office of Naval Research under Contract No. N00014-78-C-0431 and by the Department of Mechanical Engineering at Virginia Polytechnic Institute and State University.

TABLE I

Drag coefficient for laminar flow past immersed body[12]

Surface	Reynold's number	Drag Coefficient
Circular cylinder with axis perpendicular to flow.	$N_{Re}<0.5$	$f_D = \frac{8\pi}{Re(2.002-\ln Re)}$
	$0.5<N_{Re}<10$	$f_D = \frac{10}{Re^{0.6}}$ *
	$10<N_{Re}<40$	$f_D = \frac{5}{Re^{0.3}}$ *
	$40<N_{Re}<400$	$f_D = \frac{5.87}{Re^{0.343}}$ *†
	$400<N_{Re}<4\times10^5$	$f_D = 0.75$*

* These equations are obtained by curve fitting the expermental data.
† Reference 13.

Reference:

1. W. D. Kingery, "Factors Affecting Thermal Stress Resistance of Ceramic Materials," J. Am. Ceram. Soc., 38 [1] 3-15 (1955).

2. B. A. Boley and J. H. Weiner, Theory of Thermal Stresses, John Wiley & Sons, Inc., New York, 1960.

3. J. A. Ainsworth and R. H. Herron, "Thermal Shock Damage Resistance of Refractories," J. Am. Ceram. Soc., 53 [7] 533-38 (1974).

4. S. S. Manson and R. W. Smith, "Quantitative Evaluation of Thermal-Shock Resistance," Trans. of the ASME, 533-44 (1956).

5. C. E. Curtis, "Development of Zirconia Resistant to Thermal Shock," J. Am. Ceram. Soc., 30 [6] 180-96 (1947).

6. D. P. H. Hasselman, "Strength Behavior of Polycrystalline Alumina Subjected to Thermal Shock," J. Am. Ceram. Soc., 53 [9] 490-94 (1970).

7. A. Aris, "Thermal Shock Resistance of Zirconia with 15 Mole % Titanium," J. Am. Ceram. Soc., 49 [6] 334-38 (1966).

8. J. P. Holman, Heat Transfer; p. 187, McGraw-Hill Book Company, New York, 1963.

9. B. Gebhart, Heat Transfer; p. 225. McGraw-Hill Book Company, New York, 1961.

10. B. S. Massey, Mechanics of Fluids; p. 155, Van Nostrand Reinhold Company, London, 1970.

11. J. G. Knudsen and D. L. Katz, Fluid Dynamics and Heat Transfer; pp. 248-49, McGraw-Hill Book Company, New York, 1958.

12. ibid.; pp. 300-301

13. J. P. Holman, Heat Transfer; p. 214, McGraw-Hill Book Co., New York, 1976.

14. R. H. Perry and C. H. Chilton, Chemical Engineers' Handbook; pp. 10-13, McGraw-Hill Book Company, New York, 1973.

15. J. C. Jaeger, "On Thermal Stresses in Circular Cylinders," Philosophical Magazine, 36, 418-28 (1945).

16. D. P. H. Hasselman, "Thermal Stress Resistance Parameters for Brittle Refractory Ceramics: A Compendium," J. Amer. Ceram. Soc., 49 [12] 1033-37 (1970).

CHAPTER II

EFFECT OF SPATIALLY VARYING THERMAL CONDUCTIVITY ON MAGNITUDE OF THERMAL STRESS IN BRITTLE CERAMICS SUBJECTED TO CONVECTIVE HEATING

by

K. Satyamurthy, M. P. Kamat and D. P. H. Hasselman

Departments of Materials Engineering and
Engineering Science and Mechanics
Virginia Polytechnic Institute and State University
Blacksburg, Virginia 24061

ABSTRACT

The effect of a spatial variation of the thermal conductivity on the magnitude of the maximum tensile thermal stress in a solid circular cylinder subjected to sudden convective heating was calculated by finite element methods. The general results show that by lowering the thermal conductivity in the surface region of the cylinder, the magnitude of the maximum tensile thermal stress at the center of the cylinder is reduced significantly. Also, the time to maximum stress is increased substantially as well. It is also shown, that a change in the thermal diffusivity affects the time of maximum tensile thermal stress but not its magnitude.

I. Introduction

Brittle ceramic materials for high-temperature applications are highly susceptible to catastrophic failure due to thermal stresses which result from constrained thermal expansions[1]. A detailed analysis of the magnitude and distribution of the thermal stresses and selection of materials with good thermal stress resistance is an essential feature of the design and construction of structures or components operating at non-ambient environments. The selection of material with optimum thermal stress resistance can be based on "thermal stress resistance" parameters or "figures-of-merit", derived[2-6] for a number of heat transfer conditions, performance criteria and failure modes as reviewed recently[7].

Unfortunately, even the best material, selected on this basis, may be unable to withstand thermal stresses encountered in severe thermal environment. A partial solution of this problem is to develop new or improved materials. Another approach is to reduce the magnitude of thermal stress to which any given material may be subjected. In respect to this latter approach, it should be noted that the magnitude of maximum thermal stress in a structure or component is a function of the maximum difference of temperature in the structure and the manner in which the temperature is distributed. In principle then, the magnitude of thermal stress can be reduced by modifications of the temperature distribution. One technique by which this can be accomplished is to introduce a spatially varying thermal conductivity in the structure. In a recent study, Hasselman and Youngblood[8] demonstrated that a spatially varying thermal conductivity in a hollow cylinder can cause a significant reduction in the magnitude of the tensile

thermal stress under conditions of steady-state heat flow. It is the purpose of the present study to investigate whether a spatially varying thermal conductivity will also reduce the magnitude of the maximum tensile thermal stress under transient conditions.

II. Analysis

An infinitely long solid circular cylinder is selected as a geometry appropriate for the present study. The cylinder is subjected to sudden heating by convective Newtonian heat transfer, from an initial temperature, T_o to the final temperature of the surrounding, T_∞.

The spatial variation of the thermal conductivity is arbitrarily chosen to be of the form:

$$K(r) = K_o[1 - C(r/a)^n] \tag{1}$$

where n and C ($0 < C < 1$) are constants, r is the radial coordinate, a is the radius of the cylinder and K_o is the thermal conductivity corresponding to the value for the uniformly distributed thermal conductivity. Eq. 1 indicates that at $r = 0$, $K = K_o$ for any value of C and n. For $0 < r < a$, $K < K_o$, which implies that the spatial variation of the thermal conductivity is such that the thermal conductivity is decreased with respect to its value at the center. The lowest value of thermal conductivity $K = K_o(1 - C)$ occurs at $r = a$. In order to establish the effect of the spatial variation of the thermal conductivity on the magnitude of thermal stress alone, all other pertinent material properties are assumed to be spatially and temperature invariant.

It should be noted that for a spatially uniform thermal conductivity closed form solutions for the transient temperatures and thermal stresses

in solid circular cylinder are available in the literature[9,10]. However, calculations for the transient temperature, and thermal stresses in a solid circular cylinder with a spatially varying thermal conductivity distribution requires numerical methods such as finite element analysis selected for the present study.

The differential equation governing the present heat transfer problem is:

$$\frac{\partial}{\partial r}\left\{rK(r)\,\frac{\partial T}{\partial r}\right\} = \rho c\,\frac{\partial T}{\partial t} \tag{2}$$

where ρ and c are the density and specific heat of the cylinder and T is the instantaneous temperature. For the present problem the boundary conditions are:

$$\frac{\partial T}{\partial r} = 0 \quad \text{at } r = 0 \tag{3a}$$

and

$$\left\{rK(r)\,\frac{\partial T}{\partial r}\right\} + rh(T - T_\infty) = 0 \text{ at } r = a \tag{3b}$$

Since the heat flow in the cylinder occurs in the radial direction only, the transient temperatures can be obtained with a consistent one-dimensional (radial) element formulation with two nodes per element and continuity of only the nodal temperature across the inter-element boundaries. Using a finite element code compiled for this program, the temperatures are obtained with a radial element configuration composed of 33 elements.

Because of the radial and tangential symmetry it is sufficient to analyze a sector of the circular cross-section for the calculation of the thermal stresses from the temperature distribution. This sector is being modelled as an assemblage of 23 quadrilateral elements and imposing the condition

that the displacement field is radial only. Conditions of plane strain and linear elastic behavior are assumed throughout. For purposes of a slight computational advantage, the quadrilateral elements can be generated from an assemblage of four triangular elements followed by a static condensation to eliminate the common internal node. The reader is referred to the text of Zienkiewicz[11] for further details on the finite element method. The validity of this finite element program was established by verifying the analytical results of Jaeger[10], which resulted in excellent agreement.

For convenience and for purposes of comparison, the numerical results are reported in terms of the non-dimensional thermal stress, $\sigma^* = \sigma(1-\nu)/\alpha E\Delta T$, the non-dimensional time, $\tau^* = \kappa t/a^2$ where κ is the thermal diffusivity, $K_o/\rho c$ and t is the time, the non-dimensional radial coordinate, r/a and the Biot number, $\beta_o = ah/K_o$.

As a final remark, it should be noted that only sufficient numerical results are obtained to indicate the general trends, rather than making calculations of the thermal stresses for specific thermal shock experiments.

III. Numerical Results and Discussion

Since brittle ceramic materials are far more susceptible to failure in tension than in compression, in this study the tensile thermal stresses are of primary interest. For a solid circular cylinder subjected to convective heating, the tensile thermal stresses have their maximum at the center of the cylinder (r = 0). Figure 1 shows the time dependence of the maximum value of the tensile thermal stress for values of C = 0.9 and 0.99 and n = 5 and 10, for the Biot number $\beta_o = 5$. For the purpose of comparison the maximum tensile stress for a spatially invariant thermal conductivity is included in Figure 1 as well. Comparison of the curves

shows that the effect of the spatially varying thermal conductivity is to decrease the magnitude of the tensile thermal stress at any value of τ^* by a significant fraction. Noteworthy also is that the spatial variation in thermal conductivity leads to a significant increase in the values of τ^* at which the tensile thermal stresses reach their maximum values.

Figures 2a and 2b show the temperatures and the thermal stresses as a function of the radial distance at the instant at which the tensile thermal stresses reach their maximum values for the values of C, n and β_o shown in Fig. 1. As indicated by Fig. 2a, the effect of the spatial variation of thermal conductivity is to cause a significant change in the temperature distribution in support of the hypothesis on which this study is based. Figure 2b indicates that the decrease in the value of maximum tensile stress at r/a = 0 is accompanied by an increase in the value of compressive stress in the surface at r/a = 1.

For $\beta_o = 5$, Fig. 3 gives the values of the maximum tensile thermal stress for a range of values of C and n. Generally, the higher the value of C (i.e., the lower the relative thermal conductivity at the surface), the lower is the value of tensile thermal stress. However, for a given value of C, the maximum value of thermal stress is a function of n, with a general inverse dependence between C and n.

For $\beta_o = 5$, Fig. 4 shows the values of time, τ^* as a function of C and n, at which the tensile thermal stresses reach their maximum values. For high values of C and lower values of n, the values of τ^* are significantly higher than the value of $\tau^* \approx 0.11$ for constant thermal conductivity.

Figure 5 shows the maximum tensile thermal stress, σ^* for C = 0.9 and n = 3 as a function of the Biot number, β_o. For comparison, the

value of σ^* for constant thermal conductivity is included in Fig. 5 as well. These results indicate that the relative reduction in the maximum value of the tensile thermal stress is greater for the higher values of the Biot number. The excessive computer time required precluded a complete optimization of the values of σ^* as a function of β_o for all possible variations of C and n. As a result, the values of σ^* as a function of β_o shown in Fig. 5 could even be lower than indicated.

Additional calculations were made for the magnitude of thermal stresses for the same values of C, n and β_o as indicated in Fig. 1, but for convective cooling rather than heating. The results showed that the magnitude of the stresses are identical to the heating case but of opposite sign. This result implies that in case of cooling, for the spatial variation of thermal stresses in fact, will be increased. It appears then that for a decrease in the tensile thermal stresses on cooling, a thermal conductivity distribution must be chosen which differs from the one given by eq. 1.

A further calculation concerned the time at which the tensile stress reaches its maximum value. For a constant thermal conductivity distribution, the magnitude of the thermal diffusivity controls the time at which the stresses reach their maximum value, but not their magnitude. To cneck whether this still holds for a spatially varying thermal conductivity, the maximum tensile stresses were calculated for C = 0.999, n = 20 and two values of ρc = 0.997 and 1.994. Here the value of thermal diffusivity was varied by a factor of 2 keeping K constant. The above values of C and n were chosen deliberately to obtain an extreme variation in thermal conductivity. The numerical results show in Fig. 6 indeed indicate that the magnitude of thermal stress is not affected by changes in the thermal diffusivity. As for the constant thermal conductivity case, the inverse dependence of time of maximum stress and thermal diffusivity is maintained.

The general results of this study may have practical significance. For constant thermal conductivity, increase in thermal stress resistance (for all other properties being constant) requires an increase in thermal conductivity. For nominally pure, fully-dense materials, such increase in thermal conductivity may be hard to obtain. Increasing thermal stress resistance by lowering the thermal conductivity in the outer surface as suggested by the present result should be much easier to obtain. Such spatially varying thermal conductivity may be accomplished by spatially varying pore content, non-uniformly distributed impurities or solid-solution content, composites with graded compositions, a spatially non-uniform degree of crystallization in glass ceramics and perhaps by a host of other special techniques which will depend on the specific material under consideration.

The data shown in Fig. 5 should be of particular siginficance to high-temperature technology. The large decreases in tensile thermal stresses are obtained at the high values of the Biot number, β_o. High values of β_o generally imply high heat flux, large structure size, or low thermal conductivity. Under these conditions, brittle ceramic materials are particularly susceptible to thermal fracture, because of the generally high magnitude of thermal stress. For this reason, the results of this study are most appropriate for those environments for which the thermal fracture problem is more severe. In particular, thermal fatigue life, because of its extreme stress dependence, should exhibit orders of magnitude improvement.

It will be recalled that for the purpose of reporting convenience, the values of maximum tensile thermal stresses were compared at a given value of the Biot number (β_o) corresponding to the value of thermal conductivity, K_o. However, for a spatial variation of the thermal conductivity described by eq. 1, the relative thermal conductivity at the surface is decreased by a

factor equal to (1 - C), with a corresponding increase in the Biot number by the factor 1/1-C. If the comparison of the stresses would take this change in Biot number into account as well, the reduction in thermal stress level due to the spatially varying thermal conductivity is even greater. For this reason, comparison of the stresses on the basis of K_o, in fact, yields a conservative estimate of the stress reductions which can be obtained.

As noted earlier, the spatial variation in the thermal conductivity described in eq. 1 in convective cooling leads to an increase in the magnitude of tensile thermal stresses in the surface as compared to the stress level for constant thermal conductivity. Under these conditions, then, the spatial variation in thermal conductivity can lead to a decrease in thermal stress resistance. This problem, however, can be overcome by superposing on the thermal stresses an internal stress distribution which is highly compressive in the surface and has a relatively low tensile stress in the interior of the cylinder. This type of internal stress distribution, frequently encountered in glassy materials strengthened by ion-exchange, should be particularly effective for materials which fail in tension from surface flaws. In this manner, then, by combining a spatially varying thermal conductivity (with low surface values) with surface-compression strengthening, improvements in thermal stress resistance for both convective heating and cooling can be obtained.

In summary, it can be concluded that spatial variations in thermal conductivity can lead to significant decreases in the magnitude of the tensile thermal stresses generated during transient convective heating.

Acknowledgment

The present study was carried out as part of a larger research program on the thermo-mechanical and thermal properties of high-temperature structural materials, supported by the Office of Naval Research under contract N00014-78-C-0431. The authors are indebted to Dr. J. P. Singh for many helpful discussions and review of the manuscript.

References

1. W. D. Kingery, "Factors Affecting the Thermal Stress Resistance of Brittle Ceramics," J. Amer. Ceram. Soc., 38 (1) 3-15 (1955).

2. W. B. Crandall and J. Ging, "Thermal Shock Analysis of Spherical Shapes," J. Amer. Ceram. Soc., 38 (1) 44-56 (1955).

3. W. R. Buessum, "Resistance of Ceramic Bodies to Temperature Fluctuations," Sprechasaal, 93 (6) 137-41 (1960).

4. D. P. H. Hasselman, "Thermal Shock by Radiation Heating," J. Amer. Ceram. Soc., 46 (9) 229-34 (1963).

5. D. P. H. Hasselman, "Unified Theory of Thermal Shock Fracture Initiation and Crack Propagation in Brittle Ceramics," J. Amer. Ceram. Soc., 52 (11) 600-07 (1969).

6. D. P. H. Hasselman, "Role of Physical Properties in the Resistance of Brittle Ceramics to Failure in Thermal Buckling," J. Amer. Ceram. Soc., (in press).

7. D. P. H. Hasselman, "Figures-of-Merit for the Thermal Stress Resistance of High-Temperature Brittle Materials: A Review," Ceramurgia International (in press).

8. D. P. H. Hasselman and C. E. Youngblood, "Enhanced Thermal Stress Resistance of Structural Ceramics with Thermal Conductivity Gradient," J. Amer. Ceram. Soc., 61 (1) 49-52 (1978).

References (Cont'd)

9. H. S. Carslaw and J. C. Jaeger, Conduction of Heat in Solids, 2nd Ed., Oxford at the Clarendon Press (1959).

10. J. C. Jaeger, "On Thermal Stresses in Circular Cylinders," Phil. Mag. 36, 418-28 (1945).

11. O. C. Zienkiewicz, "The Finite Element Method," Third Edition, McGraw Hill Book Company, (1977).

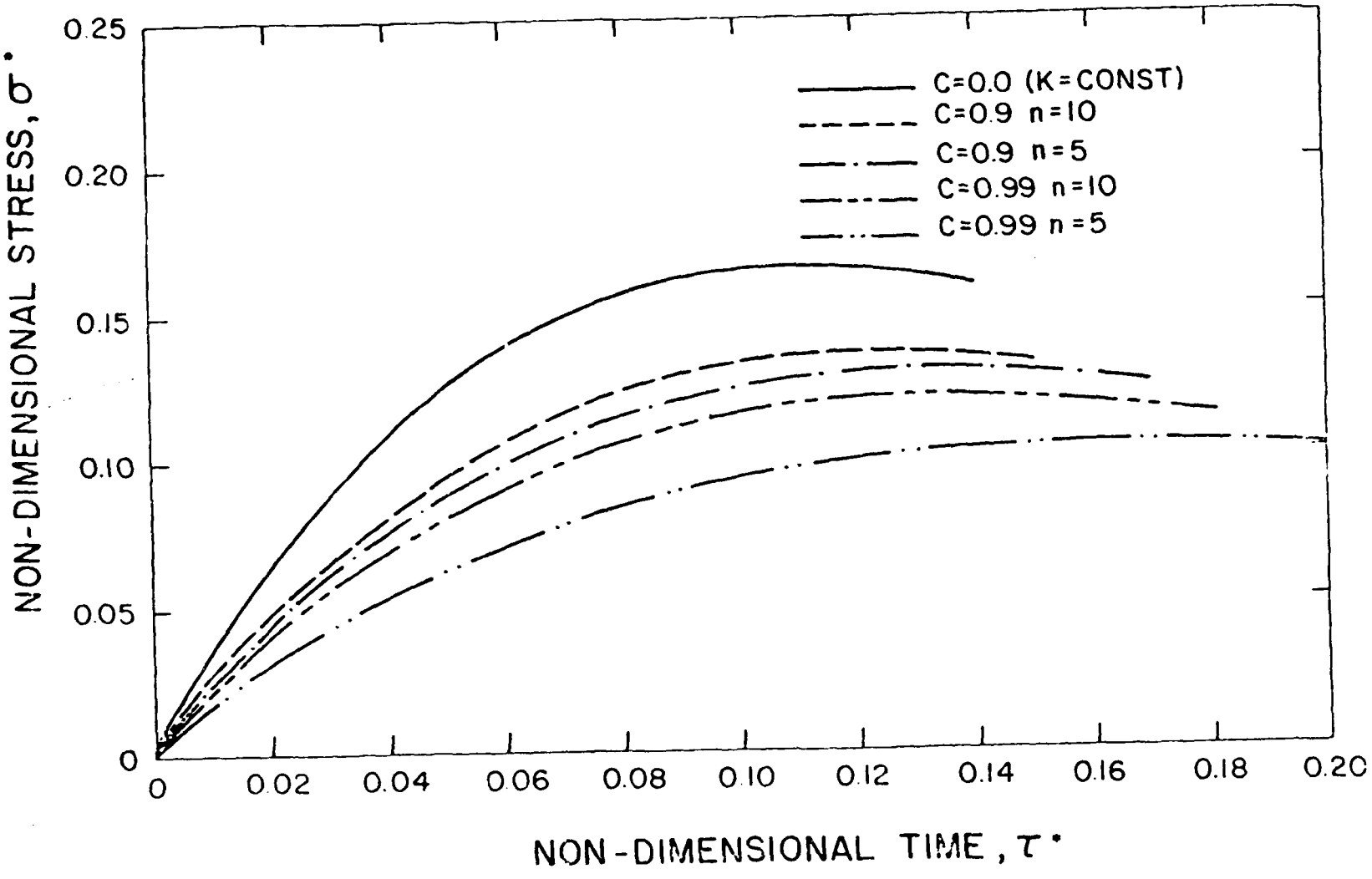

Fig. 1. Time dependence of maximum tensile thermal stress at center of solid circular cylinder subjected to sudden convective heating for a number of different spatial distributions of the thermal conductivity (see eq. 1).

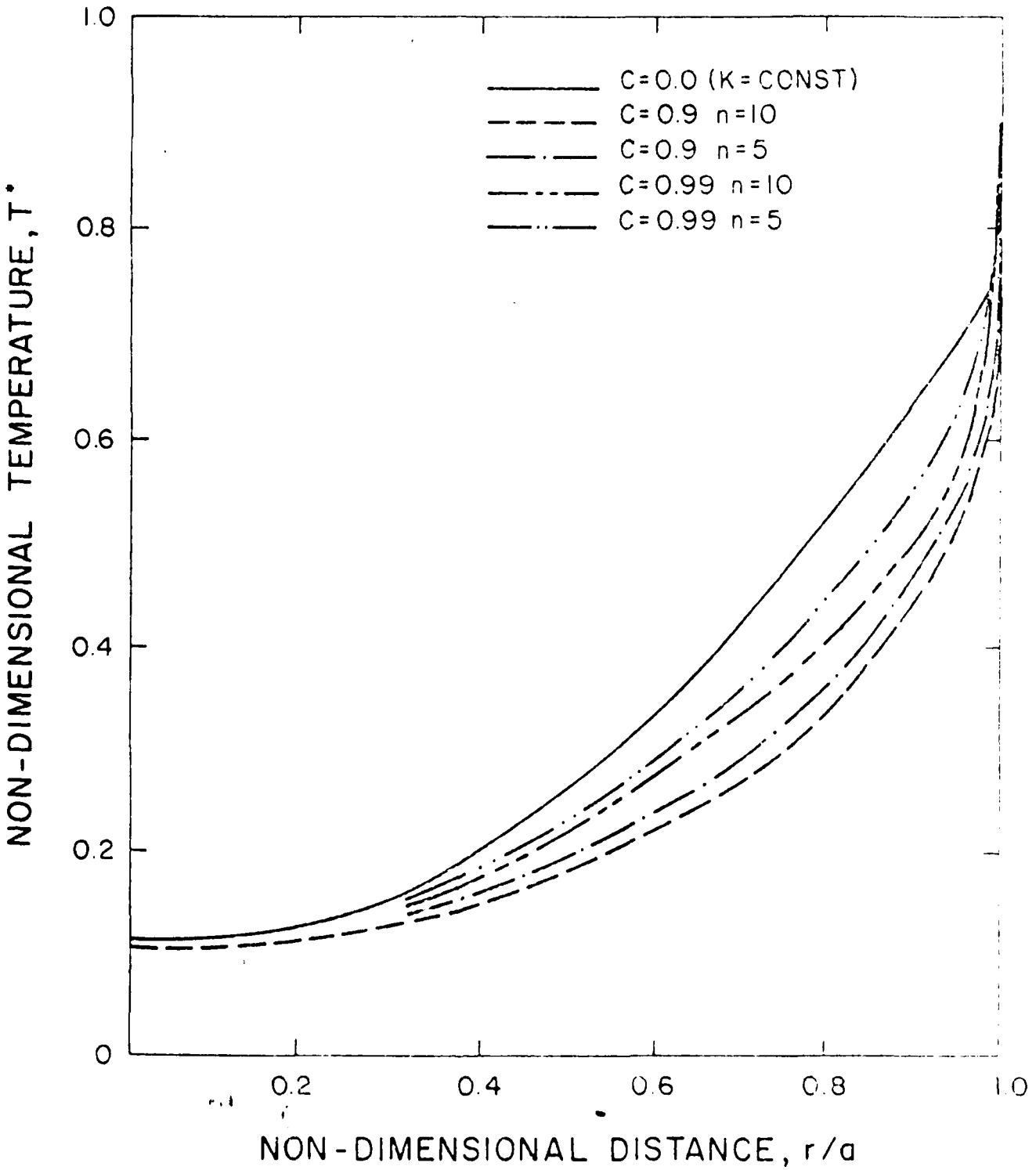

Fig. 2a. Transient temperature distributions in solid circular cylinders subjected to sudden convective heating at time of maximum tensile stress for the spatial distributions of the thermal conductivity given in fig. 2.

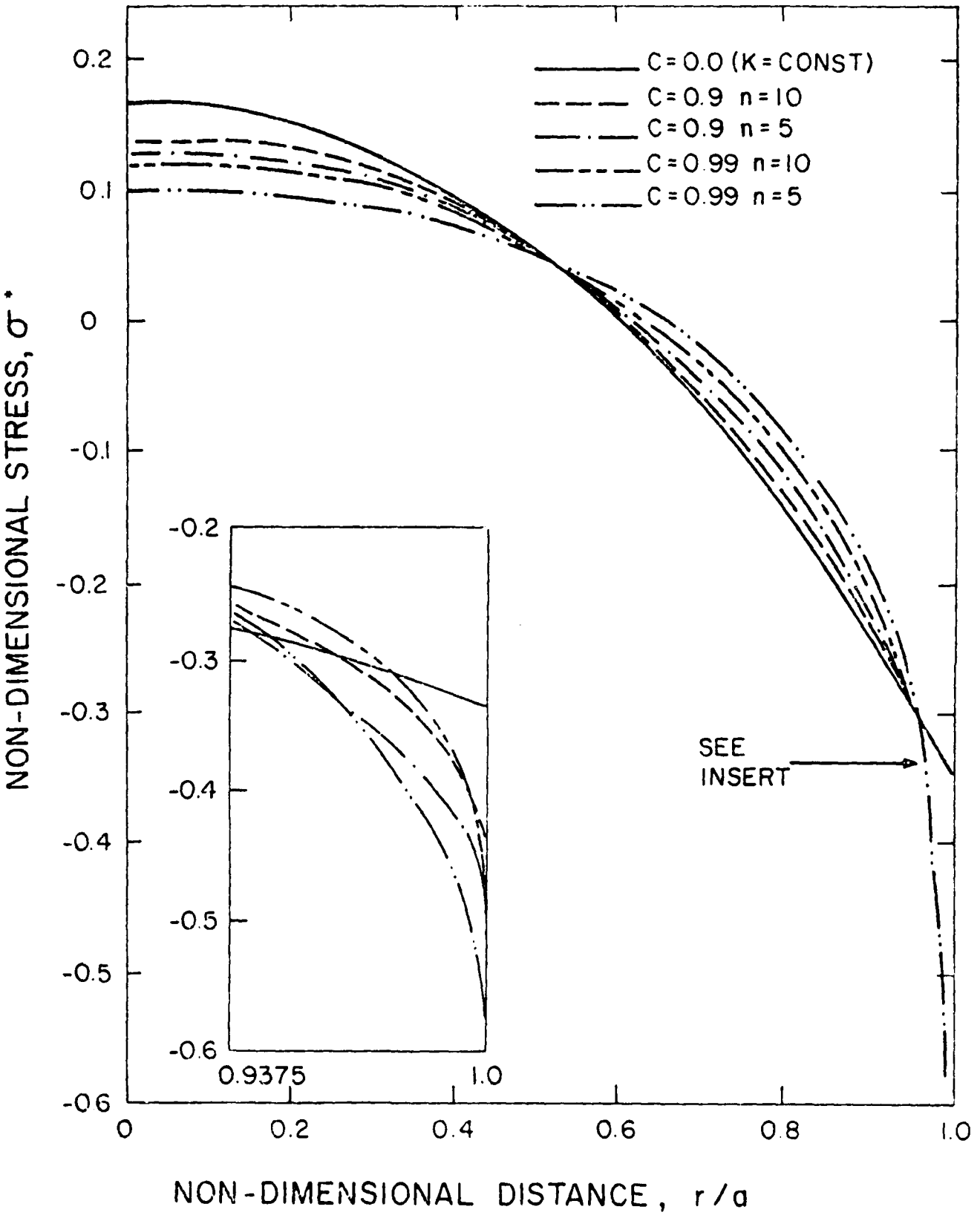

Fig. 2b. Transient thermal stress distributions in solid circular cylinder subjected to sudden convective heating at time of maximum tensile stress, for the spatial variations of the thermal conductivity given in Fig. 2.

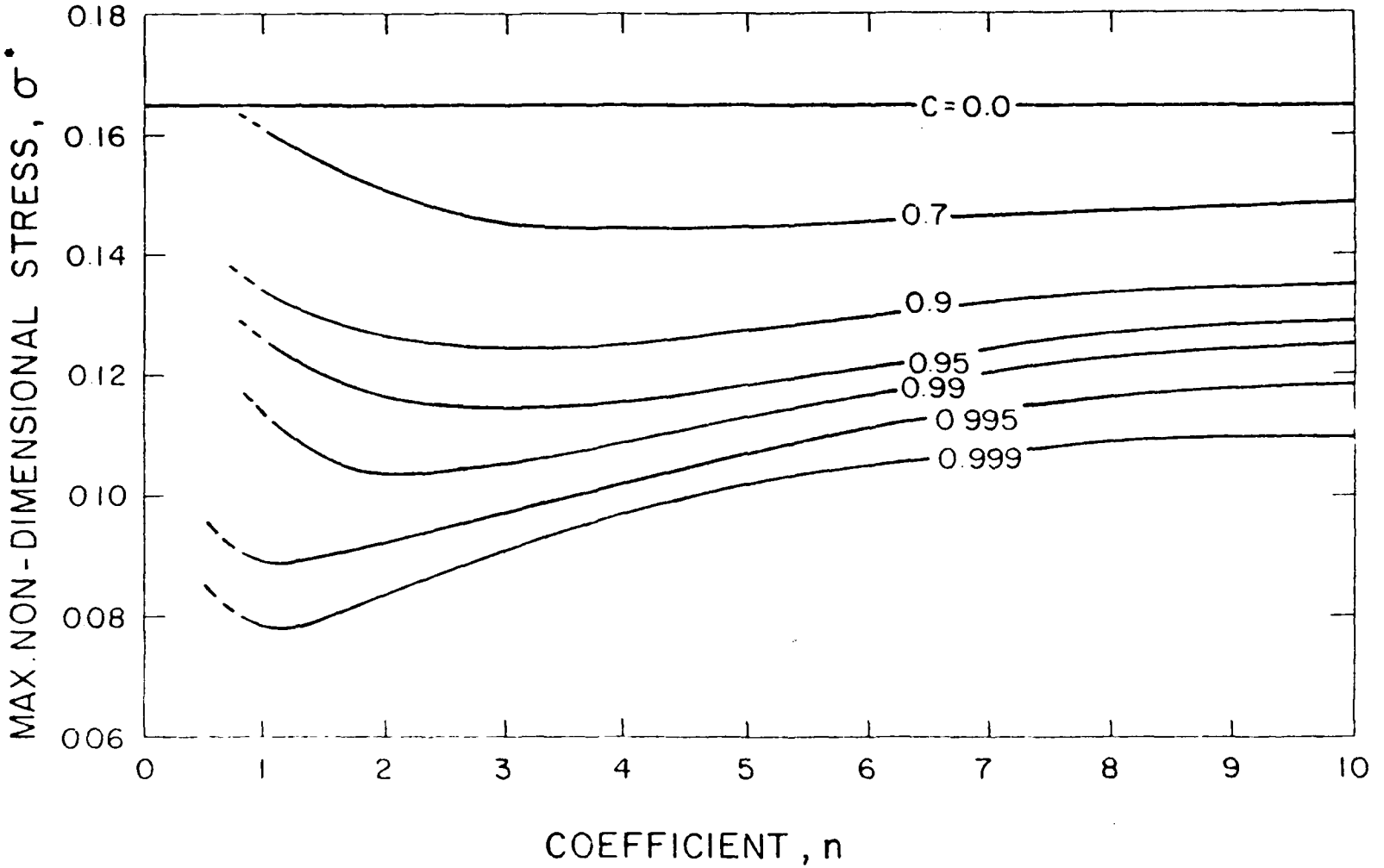

Fig. 3. Maximum tensile thermal stress in solid circular cylinder subjected to sudden convective heating for a number of spatial distributions of the thermal conductivity given by eq. 1.

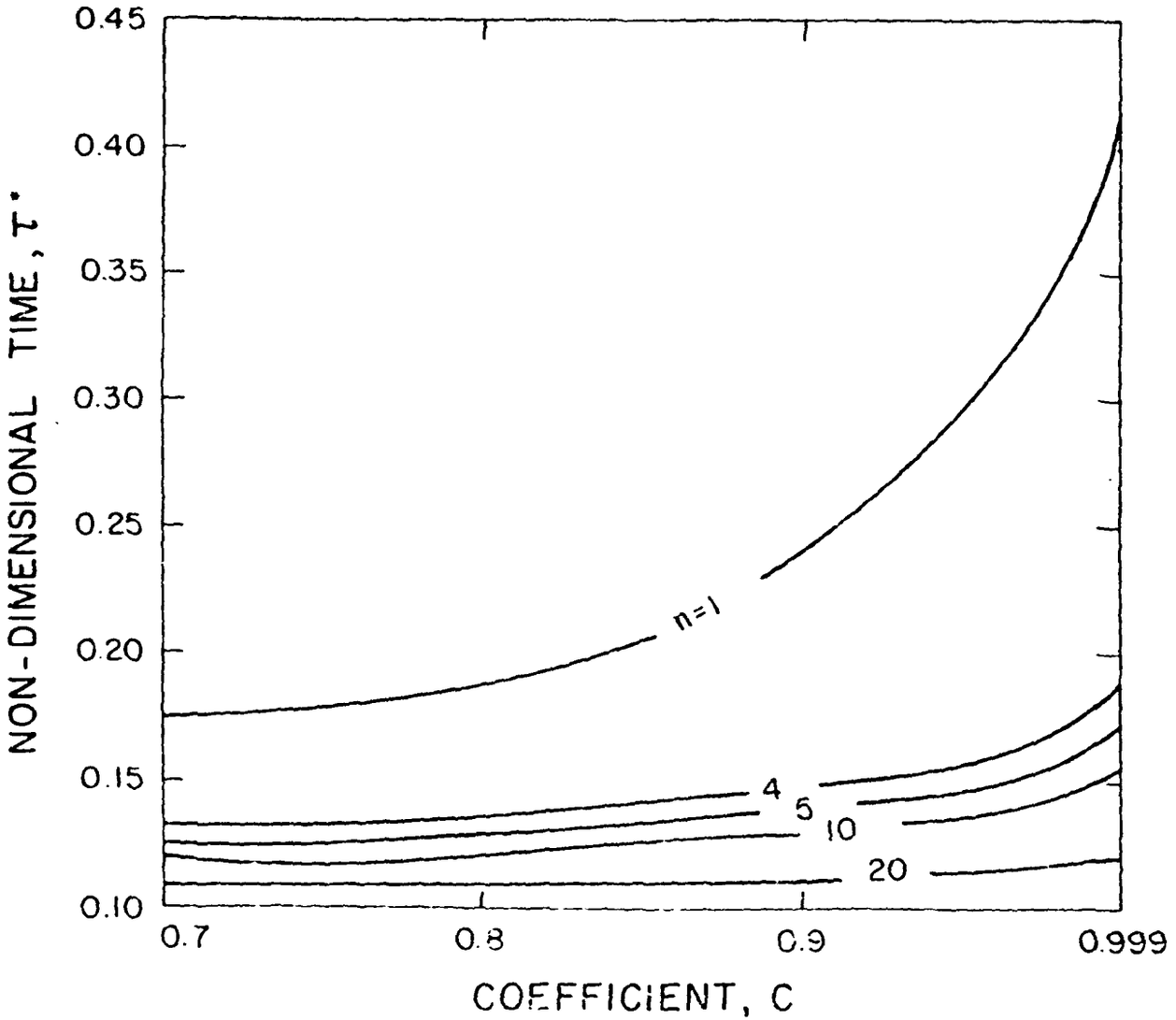

Fig. 4. Time of maximum tensile thermal stress for spatial distribution of the thermal conductivity given in Fig. 4.

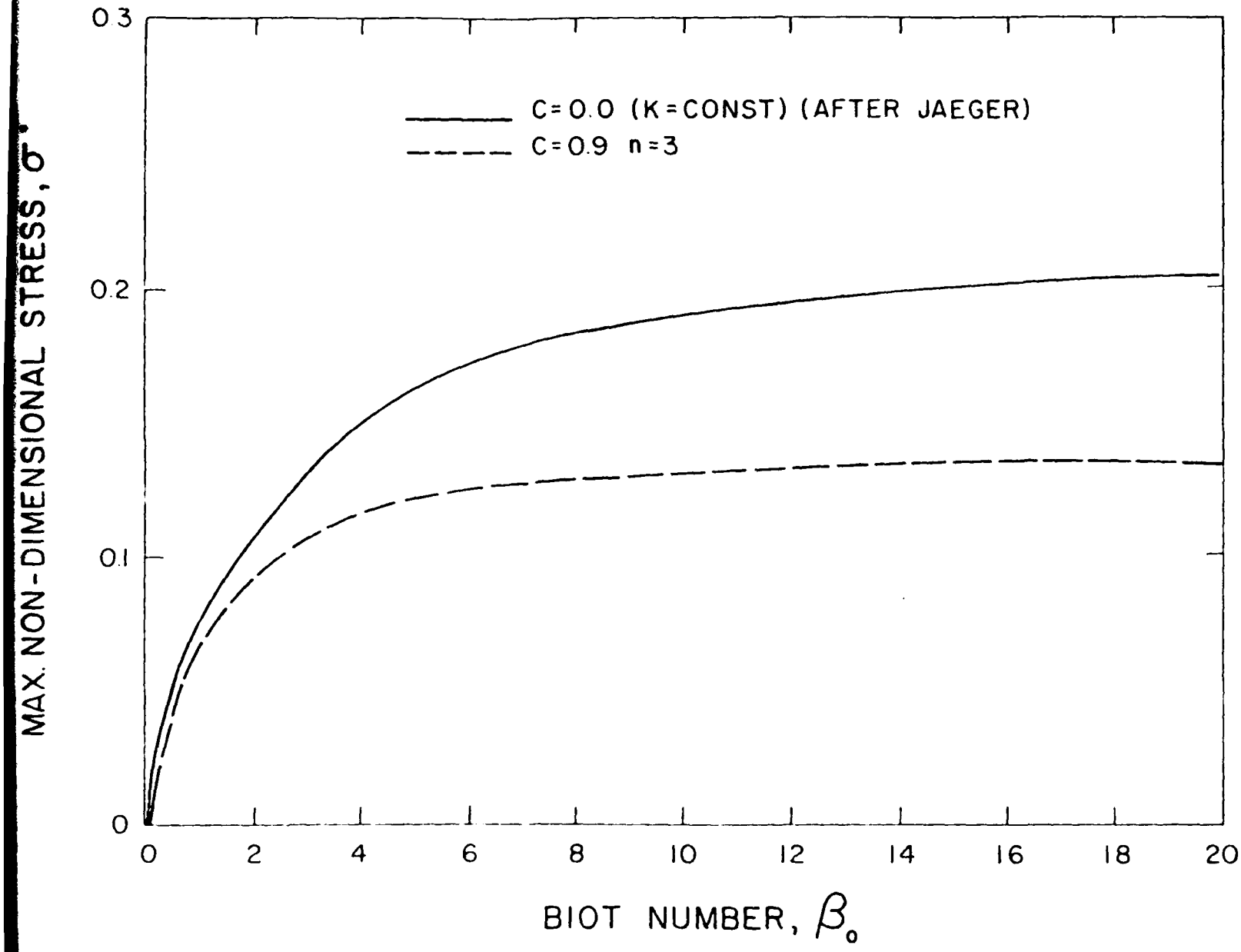

Fig. 5. Dependence on Biot number of the maximum tensile thermal stress in a solid circular cylinder with constant and spatially varying thermal conductivity (n = 3, C = 0.9) subjected to **sudden** convective heating.

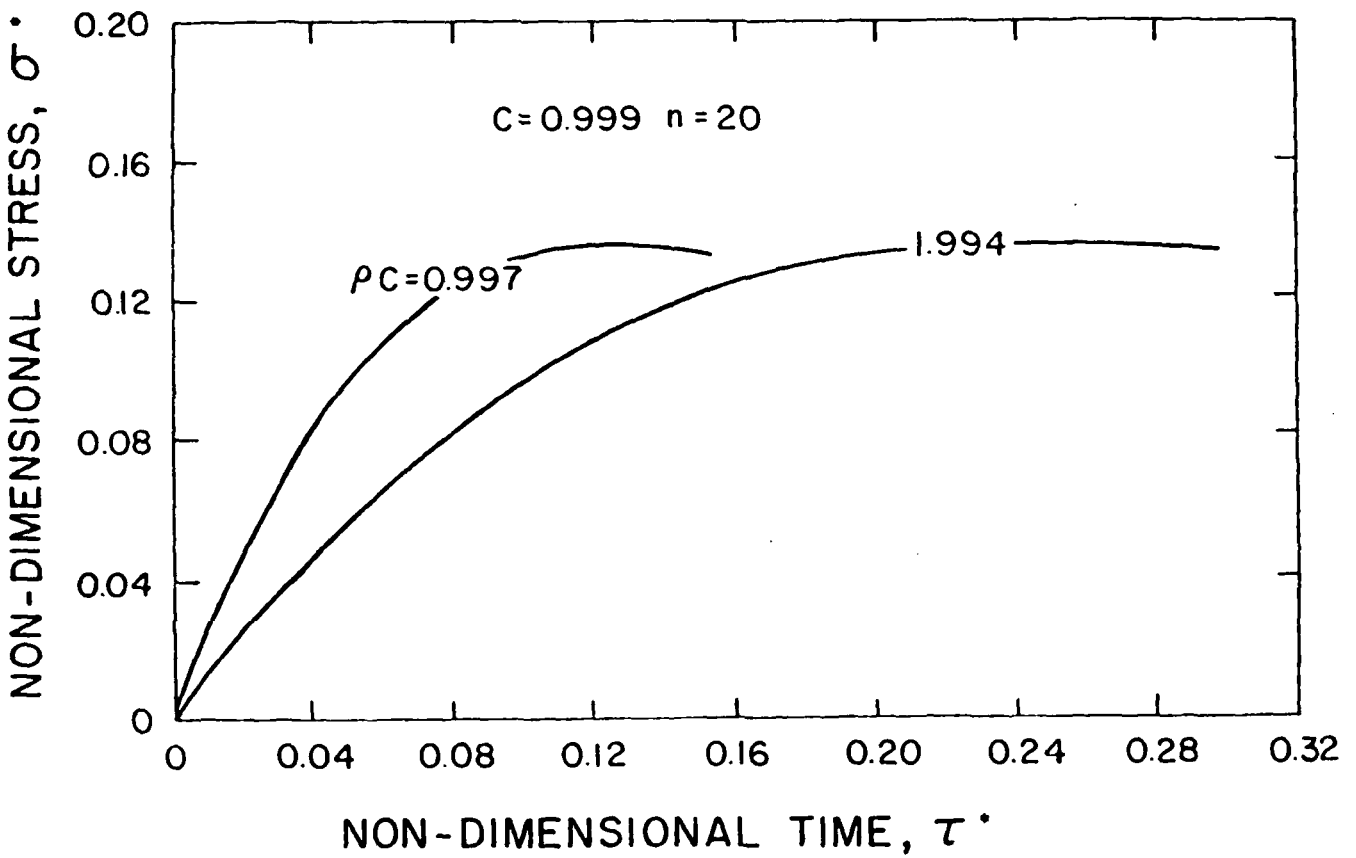

Figure 6. Transient maximum tensile thermal stress in solid circular cylinder, with spatially varying thermal conductivity (C = 0.999, n = 20) for two values of the specific heat per unit volume.

CHAPTER III

EFFECT OF DATA SCATTER ON APPARENT THERMAL STRESS FAILURE MODE OF BRITTLE CERAMICS

by

G. Ziegler*

and

D. P. H. Hasselman§

*Institut für Werkstoff-Forschung
DFVLR, 5000 Köln 90, W. Germany

§Department of Materials Engineering
Virginia Polytechnic Institute and
State University
Blacksburg, Va. 24061, USA.

Fracture of brittle materials subjected to thermal stress can occur by unstable or stable crack propagation[1-6]. In terms of the strength retained as a function of temperature difference of thermal shock such as in quenching tests, unstable crack propagation is manifested by a precipitous decline in strength at a critical temperature difference, ΔT_c. Stable crack propagation, in contrast, is characterized by a monotonic decrease in strength with increasing temperature difference. Generally, if sufficient data for the retained strength are obtained over the total range of temperature difference, for most literature data the stable or unstable nature of crack propagation can be established unequivocally.

Nevertheless, the usual scatter in material properties relevant to thermal stress fracture can introduce a complexity in the characterization of the failure mode. In this respect, due to variation in crack depth and geometry and/or local variations in fracture toughness, strength represents the most significant variable. For a given set of specimens subjected to a quenching test, those with a higher value of tensile strength will require a higher temperature difference to induce failure than those with the lower values of tensile strength. As a direct result, at values of ΔT near ΔT_c for a set of specimens only a fraction within the set may undergo fracture, with the remainder surviving intact. For specimens which undergo relatively large strength losses on fracture and for which the coefficients of variations of the surviving and failed specimens are relatively small, the distribution of the strength values for all specimens shows a pronounced bi-modal distribution[7]. Clearly, in this case it is inappropriate to judge the strength loss behavior on the basis of the averages of all

specimens tested at a given value of ΔT. Instead, the strength loss behavior properly should be judged on the averages of each mode of the bi-modal distribution.

However, the situation can arise that in unstable fracture, the distributions of the two modes of the bi-modal distribution show significant overlap, so that the clear-cut bi-modal nature becomes less apparent. This is expected to be the case for materials with moderate strength which undergo only a small relative strength loss. In this case, the determination of the thermal stress failure mode becomes ambiguous, and so could lead to an erroneous interpretation. The purpose of the present note is to illustrate these observations by data for the thermal shock behavior of a reaction sintered silicon nitride.

Quenching experiments were carried out with commercial reaction-sintered silicon-nitride with a density of 2.31 g/cm^3 and an average size of a small pores of 0.05 μm, but with single pores up to 30 μm. Rectangular rods 6 cm long and with cross-section of 6 mm by 6 mm were used. The rods in the as-nitrided form were quenched from a range of higher temperatures into a silicone oil[§] bath at R.T., followed by a strength test in 4-pt bending with a total span of 40 mm and 20 mm between the central loading points at a cross-head speed of 0.05 mm/min in laboratory air at R.T.

The individual data points for all specimens are shown in Fig. 1. Table I lists the average and standard deviations for each set of specimens tested at a given value of ΔT. Note the relatively large scatter

§ Dow Corning, Type 705, 125 Ct.

in strength data in the as-nitrided ($\Delta T = 0$) specimens. Scanning electron microscopy revealed that the relatively large scatter most likely is due to large structural inhomogenities in the near-surface layer of about 200 μm in thickness, shown in Fig. 2. Major decreases in strength occur over the temperature range 725 to 975°C. In this range, the strength data scatter exceeds that at R.T. For ΔT · 975°C, the mean values show no statistical significant difference with R.T. data. For $\Delta T_c \geq 975°C$, there is a significant difference between the mean values of these temperatures and R.T. at the 99.5% significance level. Note that for $725°C < \Delta T < 975°C$ there is no visually obvious evidence for the existence of a bi-modal strength distribution. As a result, the relative strength behavior must be judged by the averages of all specimens tested at given ΔT values. It appears then, in the absence of additional information, that failure in these specimens must have occurred by crack propagation in the stable mode.

The validity of the above conclusion can be examined on the basis of an approximate analysis. As derived for a two-dimensional model with N cracks of half-length ℓ per unit area, uniaxially constrained in the direction perpendicular to the cracks and constrained from shrinkage on cooling, the critical temperature difference ΔT_c required for crack instability and propagation is[2]:

$$\Delta T_c = (2G/\alpha^2 E\ell)^{\frac{1}{2}} (1+2\pi N\ell^2) \tag{1}$$

where G is the fracture surface energy required to create unit area of fracture surface, α is the coefficient of thermal expansion and E is Young's modulus of the crack-free plate. In stable fracture[2] the term $2\pi N\ell^2$ dominates such that eq. 1 can be written:

$$\Delta T_c \simeq 2\pi N(2G/\alpha^2 E)^{\frac{1}{2}}\ell^{3/2} \tag{2}$$

By noting that strength is proportional to the reciprocal square root of crack length, from eq. 2 the ratio of strength values σ_1, and σ_2 of specimens subjected to temperature differences ΔT_1 and ΔT_2 can be derived to be:

$$(\sigma_2/\sigma_1) = (\Delta T_1/\Delta T_2)^{1/3} \tag{3}$$

Note that eq. 3 predicts the relative strength behavior in stable crack propagation and therefore does not depend on the specific geometry of the test specimen, with the exception that the derivation of eq. 1 assumes the absence of the effects of crack interaction and a specific dependence of the effective Young's modulus of the plate and crack length. For this reason, eq. 3 at least to a first approximation can be applied to the present specimens.

For the present data with crack propagation occurring over the range of 725°C < ΔT < 975°C, $(\Delta T_1/\Delta T_2)^{1/3} \simeq 0.91$. The corresponding observed strength ratio $\sigma_2/\sigma_1 \simeq 0.16$, which is much smaller than the predicted value. This large discrepancy between predicted and observed strength behavior indicates that the strength loss is much too great over the temperature difference between 725 to 975°C for crack propagation to have occurred in a stable manner. For this reason, in spite of the absence of direct experimental evidence, it must be concluded that at least the majority of specimens must have failed by unstable crack propagation.

The correctness of the latter conclusion was verified experimentally by carrying out a similar series of quenching experiments as shown in Fig. 1, using an additional set of specimens of the same original batch which were surface-ground to remove the structural inhomogenities in the surface. The grinding consisted of removing a surface layer

of approximately 500 μm with a diamond wheel with particle size of 64 μm at a surface speed of 18 m/min in a direction parallel to the length of the specimen. The mean surface roughness of the ground specimens was 3.5 μm.

Figure 3 shows the strength behavior as a function of quenching temperature difference for these ground specimens. Comparisons of Figs. 1 and 3 and Table 1 show that the grinding treatment increased the average strength somewhat, primarily by elimination of the low strength data of the non-ground specimens. Since in unstable fracture the retained strength after fracture is an inverse function of the strength before fracture, removal of the low strength specimens prior to the quench also removed the high strength specimens from the strength distributions after failure. As a result, the strength distributions over the range of 725°C $\leq \Delta T <$ 925°C now clearly indicate a pronounced bi-modal distribution as expected from unstable fracture when only a fraction of the specimens tested at a given value of ΔT undergo failure.

The data presented herein suggest that for materials which exhibit significant data scatter, the thermal shock behavior should be analyzed very carefully in order to clearly elucidate the mode of crack propagation. As indicated by the present data, excessive coefficients of variation within the range of ΔT at which failure occurs may be indicative of an unstable failure mode obscured by data scatter. For purpose of engineering design it is critical that the proper failure mode be established. The situation could arise that a material is selected for its apparent stable mode of failure, when in fact crack propagation will occur in the less desirable unstable mode of crack propagation.

References

1. D. P. H. Hasselman, "Unified Theory of Thermal Shock Fracture Initiation and Crack Propagation of Brittle Ceramics," J. Am. Ceram. Soc., 52 (11), 600-04 (1969).

2. D. P. H. Hasselman, "Thermal Stress Crack Stability and Propagation in Severe Thermal Environments," pp. 89-103 in Materials Science Research, Vol. V, Ceramics in Severe Environments, Ed. by W. W. Kriegel and H. Palmour III, Plenum, N.Y. (1971).

3. D. P. H. Hasselman, "Strength Behavior of Polycrystalline Alumina Subjected to Thermal Shock," J. Am. Ceram. Soc., 53, (9) 490-95 (1970).

4. D. R. Larson, J. A. Coppola, D. P. H. Hasselman and R. C. Bradt, "Fracture Toughness and Spalling Behavior of High-Alumina Refractories," J. Am. Ceram. Soc., 57, (10) 417-31 (1974).

5. T. K. Gupta, "Strength Degradation and Crack Propagation in Thermally Shocked Al_2O_3," J. Am. Ceram. Soc., 55, (5), 249-53 (1972).

6. Y. W. Mai and A. G. Atkins, "Fracture Strength Behavior of Tool Carbides Subjected to Thermal Shock," J. Am. Ceram. Soc., 54, (6), 593 (1975).

7. D. A. Krohn and D. P. H. Hasselman, "Thermal Stress Fracture of a Surface-Compression Strengthened Aluminum Oxide," Problemy Prochnosti, 5, 14-18 (1975).

Acknowledgments

The present study was supported in part by the Deutsche Forschungsgemeinschaft (D-5300 Bonn-Bad Godesberg, Kennedy Allee 40) and in part by the Office of Naval Research under contract No. N00014-C-78-0431.

Table 1: Mean Strength and Standard Deviation for As-nitrided and Ground Reaction-sintered Silicon-Nitride in the As-nitrided Specimens and after Oil Quenching

Quenching Temperature Difference (^{o}C)	Mean strength MN/m^2		Standard deviation (MN/m^2)		Coefficient of variation (%)	
	as-nitrided	ground	as-nitrided	ground	as-nitrided	ground
as-nitrided ($\Delta T=0$)	112.2	125.3	20.2	15.1	18.0	12.1
675	125.6	126.2	18.4	9.1	14.6	7.2
725	123.7	120.9 + 41.1	24.9	14.8	20.1	12.2
775	75.7	135.6 + 35.4	51.6	10.5	68.2	7.7
875	66.1	151.5 + 44.5	47.0	10.4	71.1	23.3
925	74.5	115.9 + 37.0	62.8	18.8	84.4	50.9
975	20.1	32.8	20.2	11.3	100.5	34.6
1075	21.9	27.1	20.7	3.2	103.0	11.9

+) bimodal distribution

Fig. 1: Strength behavior as a function of quenching temperature difference for the as-nitrided specimens of reaction-sintered silicon nitride.

Fig. 2. Scanning electron micrographs of the as-nitrided specimens: structural inhomogenities in the near-surface layer which cause the relatively large scatter in strength.

Fig. 3. Strength behavior as a function of quenching temperature difference for the ground specimens of reaction-sintered silicon nitride.

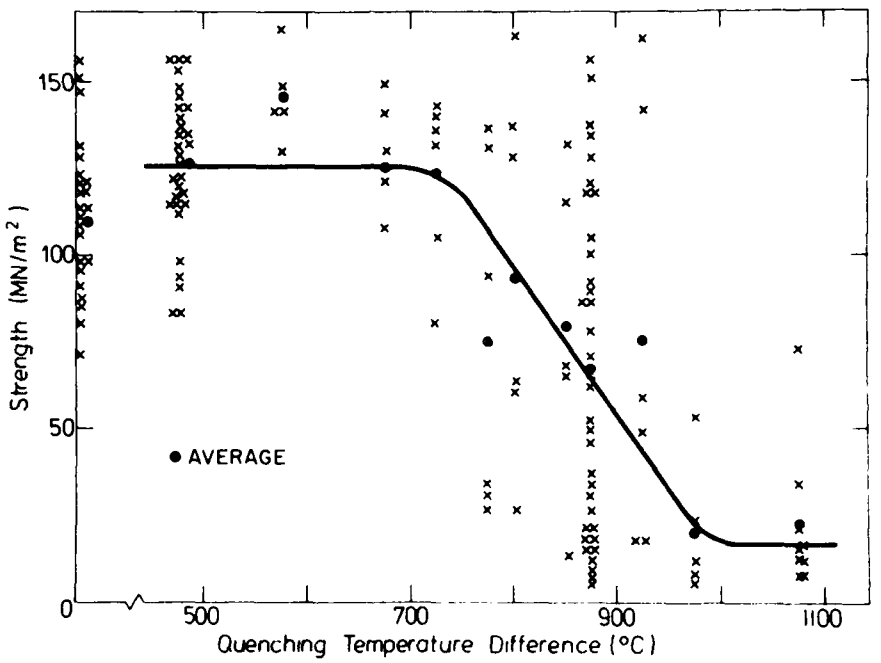

Fig. 1. Strength behavior as a function of quenching temperature difference for the as-nitrided specimens of reaction-sintered silicon nitride.

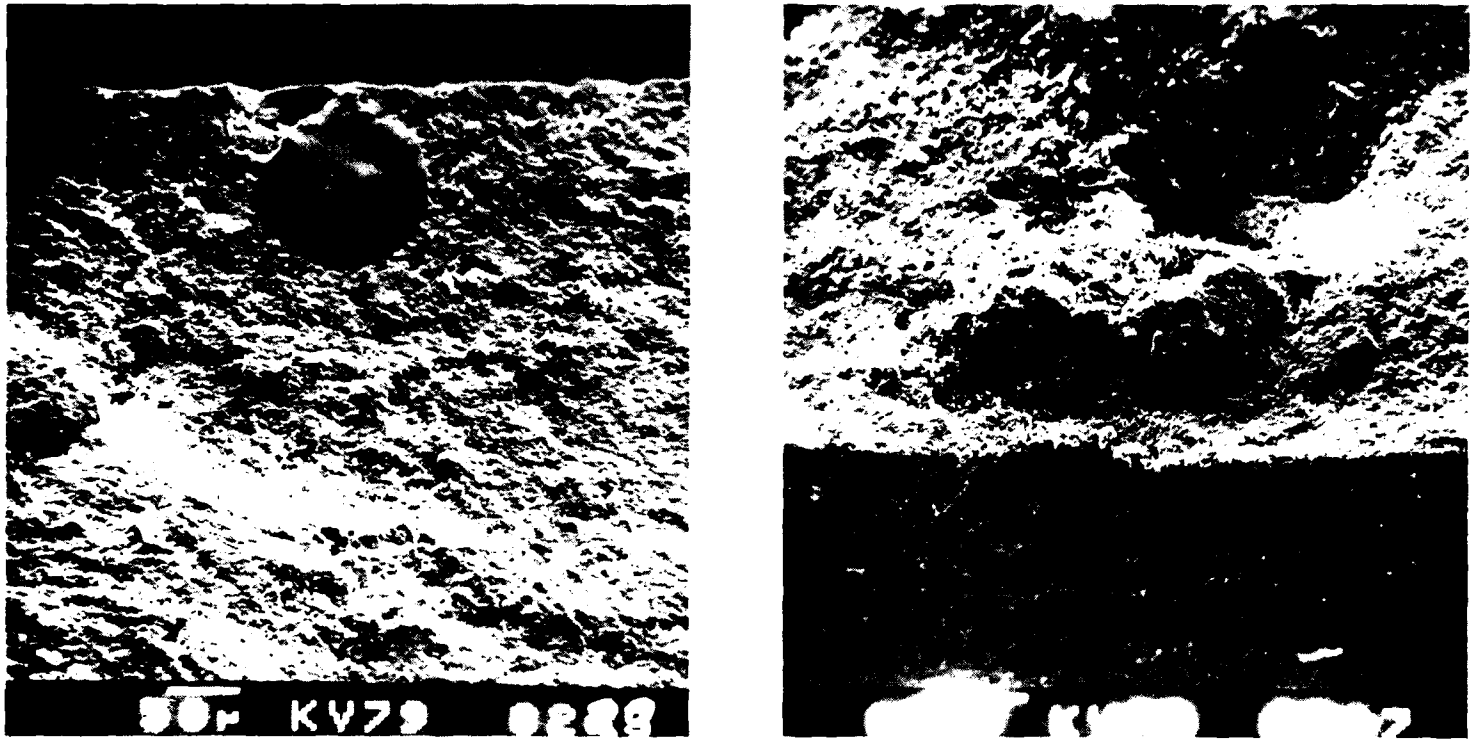

Fig. 2. Scanning electron micrographs of the as-nitrided specimens: structural inhomogenities in the near-surface layer which cause the relatively large scatter in strength.

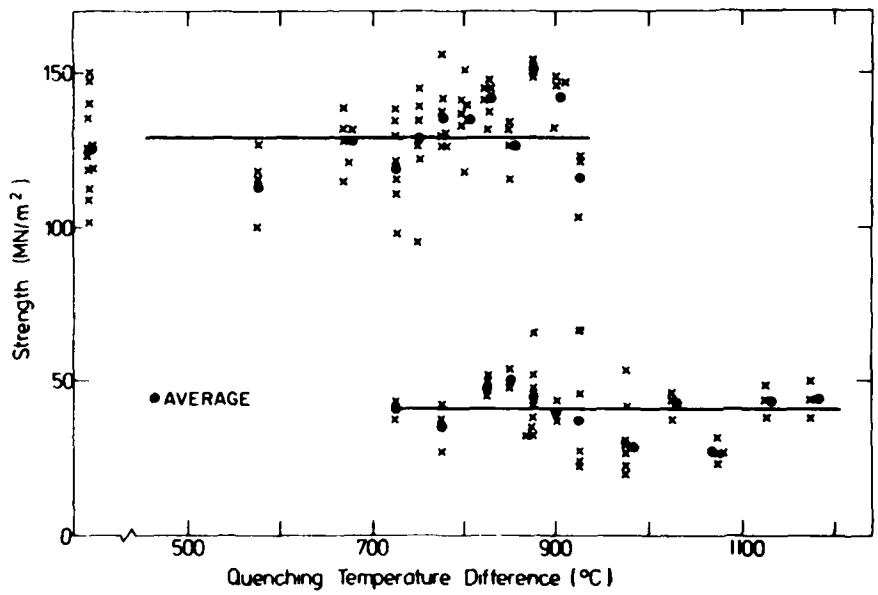

Fig. 3. Strength behavior as a function of quenching temperature difference for the surface-ground specimens of reaction-sintered silicon nitride.

CHAPTER IV

EFFECT OF SPATIALLY VARYING POROSITY ON MAGNITUDE OF THERMAL STRESS DURING STEADY-STATE HEAT FLOW

by

K. Satyamurthy, J.P. Singh, M.P. Kamat and D.P.H. Hasselman

Departments of Materials Engineering
and Engineering Science and Mechanics
Virginia Polytechnic Institute and State University
Blacksburg, Virginia 24061

As a partial solution to the critical problem of the low thermal stress resistance of many materials for high-temperature applications, the results of two recent studies[1,2] showed that the magnitude of tensile thermal stresses can be reduced appreciably by the introduction of a spatially varying conductivity.

An effective way of instroducing a spatially varying thermal conductivity is to introduce a spatially varying pore content. This should have the added advantage of lowering Young's modulus as well. Furthermore, if the pore phase is distributed such that full density is maintained in the region of maximum tensile stress within the structure or component, the adverse effect of porosity on tensile strength is avoided. The purpose of this study is to establish the quantitative improvement in thermal stress resistance under steady-state heat flow due to a spatially varying pore phase.

The geometry selected for this study consisted of an infinitely long hollow cylinder with inner radius a and outer radius b. The cylinder is subjected to radially outward or inward heat flow, which results in a temperature difference ΔT across the tube wall.

For radially outward heat flow the porosity distribution was arbitrarily taken as:

$$P = P_o\{(b-r)/(b-a)\}^n \qquad (1)$$

where P_o is the porosity at r = a and n is the porosity distribution coefficient.

For radially inward heat flow the porosity was assumed to be distributed according to:

$$P = P_o\{(r-a)/(b-a)\}^n \qquad (2)$$

The effect of the pore phase on the thermal conductivity, K and Young's modulus, E was taken as[3]:

$$K,\ E = K_o,\ E_o e^{-bP} \qquad (3)$$

where the subscript refers to the non-porous material and b is a numerical constant taken as b = 3 and 4 for K and E, resp. Clearly, for a specific material the values of b must be established experimentally. Poisson's ratio and the coefficient of thermal expansion were assumed to be unaffected by the pore phase.

The thermal stresses were evaluated by the finite element method, using a computer program developed by Satyamurthy et al[2]. The validity of this numerical program was established by verifying the analytical results of Hasselman and Youngblood[1], which gave excellent agreement.

Figures 1a and 1b, for radially outward and inward heat flow, resp., show the values of the non-dimensional maximum tensile stress, $\sigma^* = \sigma(1-\nu)/\alpha E_o \Delta T$ as a function of the coefficient n, for three values of b/a and $P_o = 0.3$, which is a reasonable value achievable in practice. To a first approximation the thermal stresses are independent of n. As the result of the spatial variation in strength for value of $n < 1$ and a value of b = 6 (in eq. 3) to express the effect of porosity on relative tensile strength, failure can occur within the cylinder away from the region of maximum tensile thermal stress. For radially outward heat flow with b/a = 10 and for radially inward heat flow with b/a = 1.1 the reduction in the maximum tensile thermal stress is about 33 and 22%, resp. Since the failure stress at the site of maximum stress is not affected by the pore phase, these reductions in thermal stress, result in corresponding increases in thermal stress resistance. Similarly, somewhat smaller increases in thermal stress resistance are obtained for the other values of b/a.

Figures 2a and 2b give the magnitude of the maximum tensile stress as a function of pore content, P_o for radially outward and inward heat flow, resp., corresponding to the value of n for which the stresses are minimum as indicated by Fig. 1. These results indicate that to a first approximation the reduction in thermal stress is a linear function of porosity.

It should be noted that the improvement in thermal stress resistance due to the presence of a pore phase, is not expected from thermo-elastic theory based on spatially invariant physical properties. In fact, a uniformly distributed pore phase is expected to decrease thermal stress resistance[4,5]. For steady-state heat flow, thermal stress resistance as measured in terms of a maximum temperature difference which can be imposed on a structure for a given coefficient of thermal expansion and Poisson's ratio is governed by the ratio of tensile strength and Young's modulus of elasticity. For a uniform porosity, P = 0.3 and b = 4 and 6 (eq. 2) for Young's modulus and tensile strength[6], resp., thermal stress resistance would be reduced by nearly a factor of two.

These results indicate that for structures or components which do not permit design modification or material substitution, the incidence of thermal stress failure may be reduced by the incorporation of a spatially varying pore phase.

ACKNOWLEDGMENTS

The present study was conducted as part of a larger program on the thermo-mechanical and thermal behavior of high-temperature structural material funded by the Office of Naval Research under contract No. 00014-78-C-0431.

REFERENCES

1. D. P. H. Hasselman and G. E. Youngblood, "Enhanced Thermal Stress Resistance of Structural Ceramics with Thermal Conductivity Gradient," J. Amer. Ceram. Soc., 61, 49-52 (1978).
2. K. Satyamurthy, M.P. Kamat and D.P.H. Hasselman, "Effect of Spatially Varying Thermal Conductivity on Magnitude of Thermal Stress in Convection Heating," J. Amer. Ceram. Soc., (in review).
3. R. M. Spriggs, "Expression for Effect of Porosity on Elastic Modulus of Polycrystalline Refractory Materials, Particularly Aluminum Oxide," J. Amer. Ceram. Soc., 44 (12) 628-29 (1961).
4. R. L. Coble and W. D. Kingery, "Effect of Porosity on Thermal Stress Fracture," J. Amer. Ceram. Soc., 38 (1) 33-37 (1955).
5. S. Kato and H. Okuda, "Relations Among Porosity, Thermal Shock Resistivity, and Some Physical Constants of Porcelain," Nagoya Kogyo Gijutsu Shikensko Hokoku, 8 [5] 37-43 (1959); Ceram. Abstracts, 1959, Nov. p. 287a.
6. F. P. Knudsen, "Dependence of Mechanical Strength of Brittle Polycrystalline Specimens on Porosity and Grain Size," J. Amer. Ceram. Soc., 42 (8) 376-87 (1959).

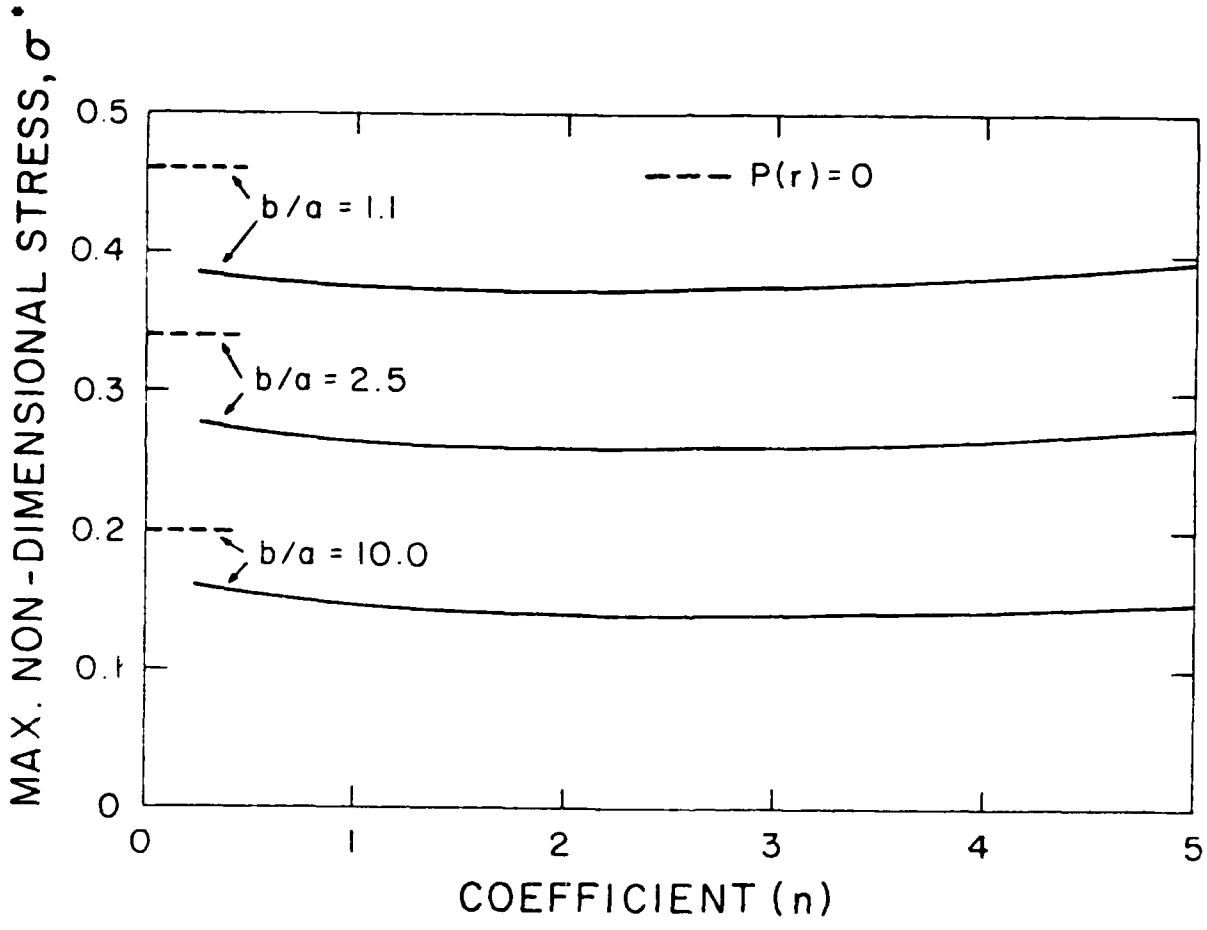

Fig. 1a. Maximum tensile thermal stress in hollow cylinder under conditions of steady-state radially outward heat-flow with spatially varying pore content according to eq. 1 with $P_o(r=a) = 0.3$.

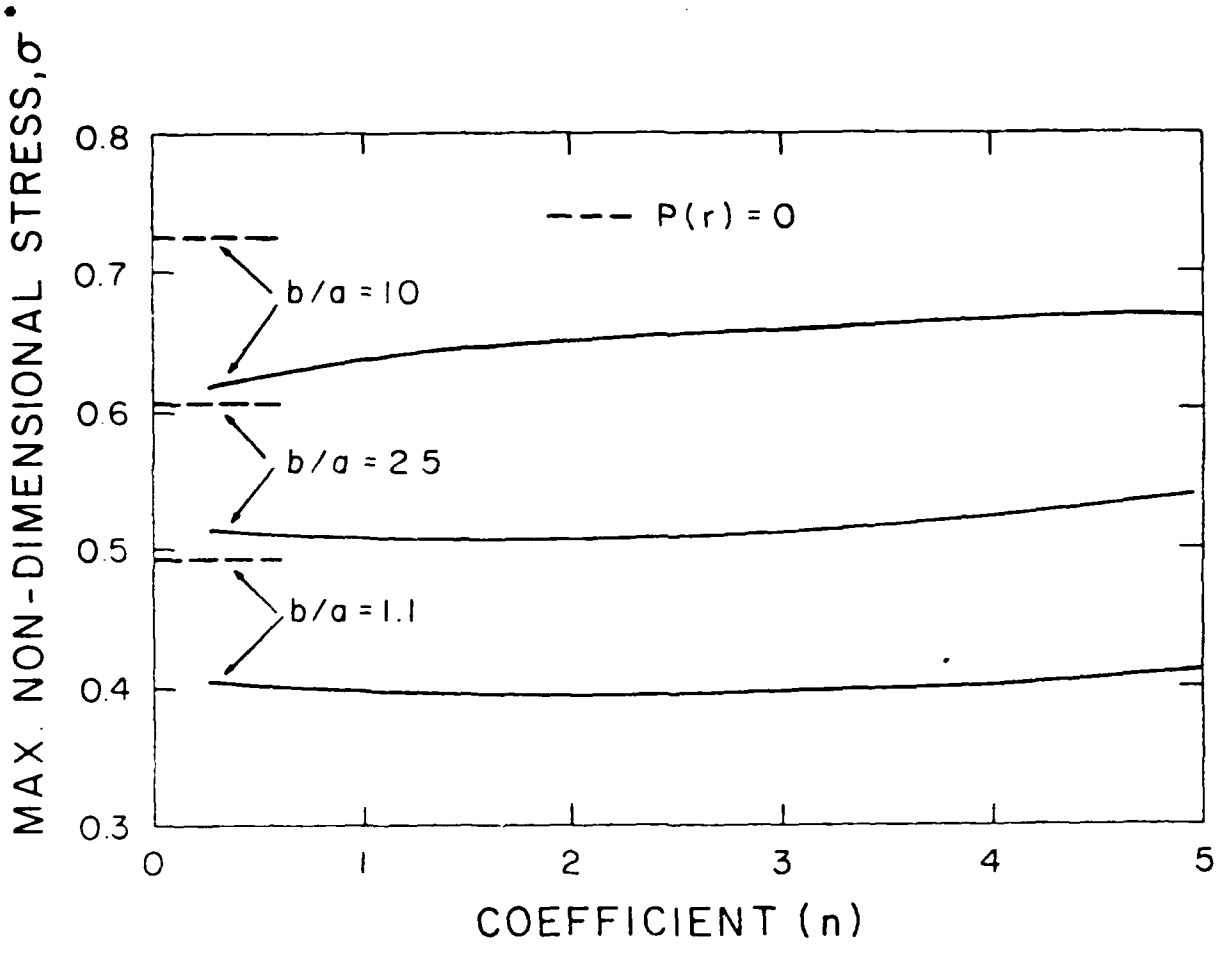

Fig. 1b. Maximum tensile thermal stress in hollow cylinder under conditions of steady-state radially inward heat flow with spatially varying pore content according to eq. 1 with $P_o(r=b) = 0.3$.

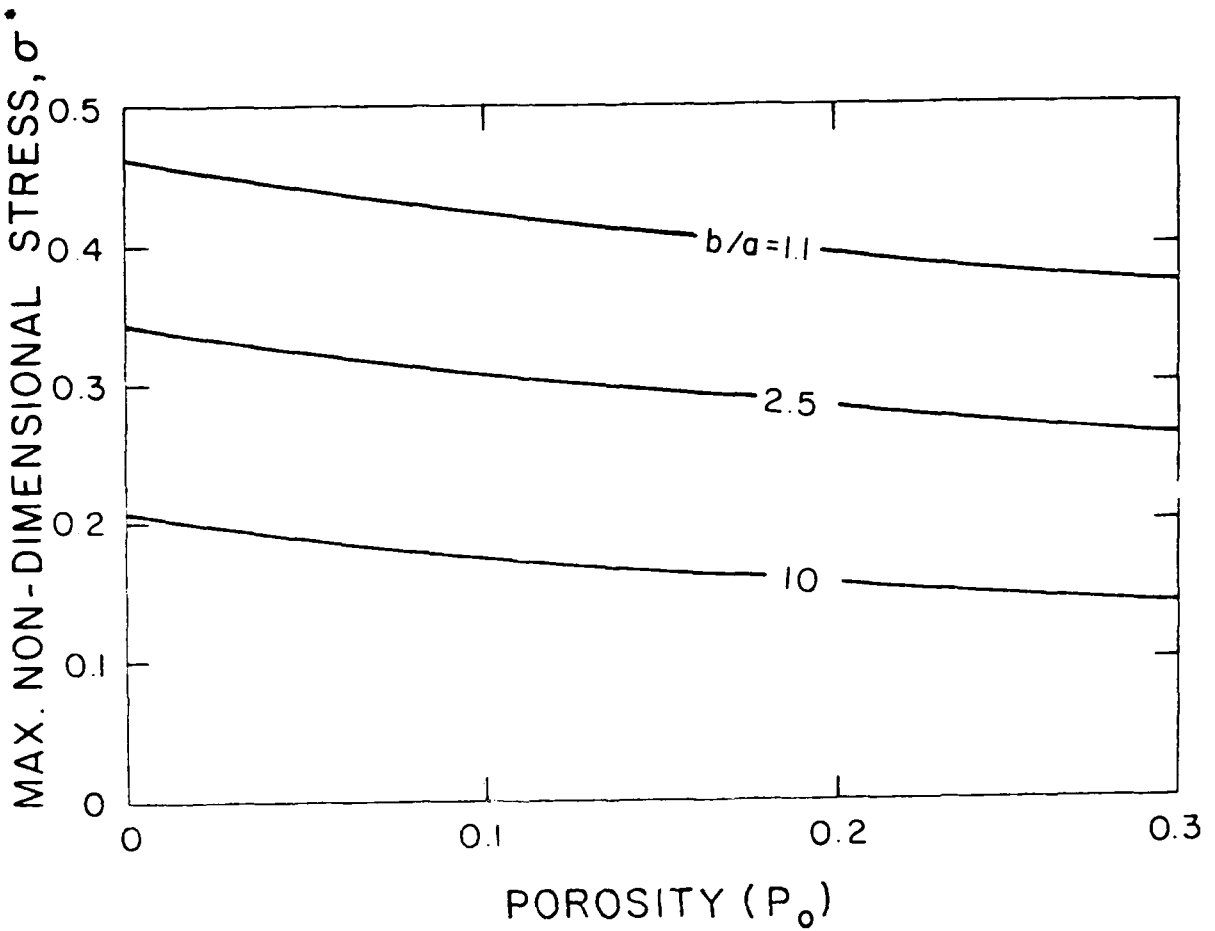

Fig. 2a. Maximum tensile thermal stress in hollow cylinder under conditions of steady-state radially outward heat flow with spatially varying pore content as a function of maximum porosity, $P_o(r=a)$.

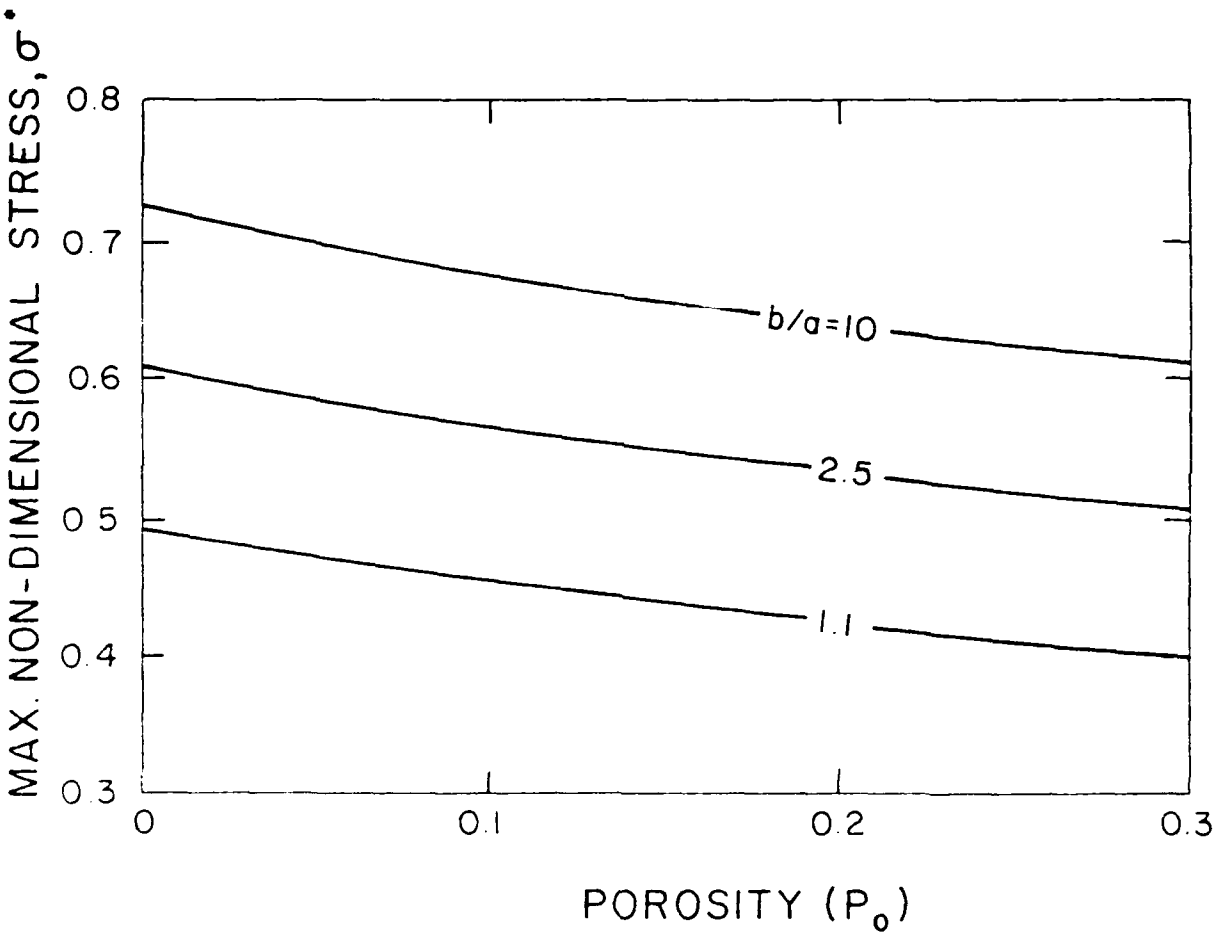

Fig. 2b. Maximum tensile thermal stress in hollow cylinder under conditions of steady-state radially inward heat flow with spatially varying pore content as a function of maximum porosity, $P_o(r=b)$.

CHAPTER V

EFFECT OF THERMAL EXPANSION MISMATCH ON THE THERMAL DIFFUSIVITY OF GLASS-NI COMPOSITES

by

Bob R. Powell, Jr.,[§+] G. E. Youngblood,[*] D. P. H. Hasselman,[+]
and
Larry D. Bentsen[*]

[§]Department of Materials Science and Engineering
University of California
Berkeley, California 94720

[*]Montana Energy and MHD Research and Development
Institute, Butte, Montana 59701

[+]Department of Materials Engineering, Virginia
Polytechnic Institute and State University
Blacksburg, Virginia 24061

[+]Now with General Motors Research Laboratories, Warren, Michigan 48090

ABSTRACT

The effect of interfacial de-cohesion, due to the thermal expansion mismatch, on the thermal diffusivity of a hot-pressed glass matrix with a dispersed phase of nickel was investigated by the laser-flash technique over the temperature range of 25 to 600°C. The interfacial gap formed on cooling acts as a barrier to heat flow and lowers the thermal diffusivity to values below those predicted from composite theory and also creates a temperature dependence of the thermal diffusivity which is strongly positive. Preoxidation of the Ni spheres promotes interfacial bonding to yield values of thermal diffusivity higher than those for non-oxidized spheres and a thermal diffusivity which is relatively temperature independent. The results of the present study also confirm the criteria for the effective thermal diffusivity of composites established by Lee and Taylor.

EFFECT OF THERMAL EXPANSION MISMATCH ON THE THERMAL DIFFUSIVITY OF GLASS-NI COMPOSITES

Bob R. Powell, Jr., G. E. Youngblood, D. P. H. Hasselman
and Larry D. Bentsen

I. INTRODUCTION

Numerous composite materials have been developed to meet the special requirements for many engineering applications. Such composites frequently exhibit favorable properties not found in the individual components. The science of "composite theory" for the calculation of the properties of composites from the properties of the components represents a very active field.

For the calculation of the thermal conductivity of composites for a wide variety of phase compositions and distributions, many expressions are available from the literature.[1,2,3,4] These theories, however, generally assume that perfect bonding exists between the components. For this reason, the interfacial boundaries offer no resistance to the transport of heat through the composite. In practice, however, many composites will exhibit less than perfect bonding between the components as the direct result of poor wettability or the absence of good mechanical adhesion. This problem is expected to be especially severe for composites with a large mismatch in the coefficients of thermal expansion of the components. Changes in temperature of such composites can lead to the formation of high values of "internal" stress, which can lead to "micro-cracking" of the components or to interfacial separation, depending on the direction of the mismatch. Such micro-

cracking also can occur in polycrystalline materials which exhibit a high degree of thermal expansion anisotropy of the individual grains. In these latter materials micro-cracking has been shown to result in major decreases in the thermal diffusivity,[5,6] in accordance with analytical results for the effect of cracks on thermal conductivity.[7] Similar effects would be expected for composites with a large mismatch in thermal expansion. However, as far as these writers are aware no such experimental data exist in the literature.

The purpose of the present study was to investigate the effect of the mismatch in thermal expansion on the thermal diffusivity of a bonded and non-bonded composite consisting of a low thermal expansion matrix containing a high thermal expansion dispersed phase. On cooling of such a composite, de-cohesion between the phases results in the formation of a interfacial gap, which in analogy to micro-cracks is expected to have a large effect on the transport of heat through the composite.

II. EXPERIMENTAL

A. Materials, Preparation and Characterization

D-glass of the same composition (16% Na_2O, 14% B_2O_3 and 70% SiO_2) are used in previous investigations[8,9,10] was chosen as a suitable matrix phase. The dispersed phase consisted of near spherical particles of Ni with a diameter, $45 < D < 53$ μm. Composites contained nickel in the "raw" (non-oxidized) form or nickel particles with an oxide coating produced by oxidation in air to a weight gain of 1 percent. As found in an earlier study,[10] the presence of an oxide coating promoted the adherence

of the glass and nickel phase. The composites were prepared by vacuum-hot-pressing mixtures of the Ni and glass in powder form in graphite dies at a pressure of 14 MPa at 700°C for 10 min. The initial heating rate was ~ 9 °C/min. After hot-pressing the specimens were permitted to cool naturally within the graphite die within the hot-pressing chamber maintained at vacuum.

The density of the composites was determined by the Archimedes principle with H_2O as the fluid medium, from the same specimens used for the measurement of the thermal diffusivity. The experimental and theoretical densities are compared in Table 1. The sample containing 45 vol.% Ni exhibits a density greater than theoretical. This may be due to a Ni concentration somewhat higher than 45% or due to uncertainties in the density of the glass. A density less than theoretical is attributable to the existence of a pore phase created during cooling from the hot-pressing temperature, as the direct result of the expansion mismatch.

Figure 1 shows optical micrographs of the glass with 15, 30 and 45 percent Ni. Direct Ni particle-to-particle contact is evident especially at 45% Ni. Although most particles are very close to being spherical, some are tear-shaped or ellipsoidal in shape. As indicated by the theoretical results of Bruggeman[11] and Niesel[12] a deviation from perfectly spherical shape should have no effect on the thermal conductivity and thermal diffusivity as long as the dispersed particles are oriented randomly.

Figures 2 and 3 show scanning electron fractographs for the glass containing raw and oxidized Ni dispersions, respectively. It is evident that during fracture the raw Ni particles were easily pulled from the

glass matrix indicative of a lack of adhesion. For the oxidized Ni the fractographs indicate that the Ni and glass show good adherence. In these composites the thermal expansion mismatch appears to be accommodated by visco-elastic deformation of the glass, which resulted in the formation of a highly porous fibrous glass phase in the immediate vicinity of the Ni-glass interface. Such a fibrous glass phase most likely occurred at temperatures immediately below the hot-pressing temperatures at which such visco-elastic deformation most likely is expected to occur.

B. Measurement of Thermal Diffusivity

The thermal diffusivity was measured over the temperature range 25°C to 600°C by the laser-flash technique.[13] A single flash (∿ 1 msec) from a glass Nd laser[+] irradiated the front face of the specimen (1/2 inch diameter by 2.0 mm thick). An intrinsic thermocouple[14] (low temperature) or an infrared detector[*] (high temperature) was used to monitor the temperature transient at the back face. The typical steady-state temperature rise of the specimen was kept below 3°C.

For low temperature measurements (25°C-400°C) the specimens were held by three alignment pins inside a wire-wound temperature controlled split-tube furnace with air atmosphere. The specimen front face was coated with carbon[**] to ensure uniform absorptivity. A 1/4 inch diameter Ag-print spot was painted onto the specimen backface to average local heating effects and to provide electrical continuity for a Chromel-Constantan (type E) intrinsic thermocouple spring-loaded to press up

[+]Korad K-1, 70 Joules maximum per flash, Santa Monica, CA.
[*]Barnes Engineering IT-7B (InSb) Stamford, CT.
[**]Miracle DGF spray, Miracle Power Products Co., Cleveland, OH.

firmly against the backface to monitor the chamber temperature as well as the transient temperature of the sample.

At higher temperatures (200°C-600°C) at which the IR detector was used for monitoring the specimen temperature, the specimens with each face coated with carbon were held in a split-tube graphite holder in a carbon resistance furnace[++] with nitrogen atmosphere.

The transient temperature response from either the thermocouple or infra-red detector was fed into an oscilloscope[†] equipped with signal storage. The thermal diffusivity (α) of the composite sample was calculated from

$$\alpha = 0.1388\ L^2/t_{1/2} \qquad (1)$$

where L is the specimen thickness and $t_{1/2}$ is the time required for the temperature of the back surface of the specimen to reach half its final value. The measured values of the thermal diffusivity were corrected for heat losses in a manner described by Heckman.[15] These corrections amounted to only a few percent at low temperature and increased to about 5 percent at 1000°C. No corrections for finite pulse width were necessary. The equipment was calibrated against Armco iron which resulted in agreement to within 3% of standard values[16] for the infra-red detector and within 11% for the thermo-couple. These discrepancies could be due to heat losses along the thermo-couple and because above the Curie point the thermal diffusivity appears to be a function of thermal history.[15] Also, intrinsic thermocouples are known to produce lower diffusivity values than infra-red detectors.[14]

[++]Astro Model 1000A, Santa Baraba, CA.
[†]Tektronix 5111 with plug-ins, Beaverton, OR.

In order to establish whether the value of thermal diffusivity obtained by the laser-flash method represents the effective thermal diffusivity, the ratios of thermal properties and micro-structural parameters of the present composites were compared with the limits of non-homogeneity established by Lee and Taylor.[17] Briefly, Lee and Taylor showed that the concept of a "homogeneous" thermal diffusivity of a composite is valid for ratios of 0.48-1137 for α_d/α_m; 0.02-1.16 for $(\rho_d C_d V_d)/(\rho_m C_m V_m)$; 3.8-2857 for L/D; 0.23-0.88 for nD/L and 0.012-0.34 for V_d, where α is the thermal diffusivity, ρ is the density, C is the specific heat, V is the volume fraction, L is the sample thickness, D is the particle diameter, $n = [V_d L^3/1.33\pi(D/2)^3]^{1/3}$ is the total number of particles in the sample thickness direction, and the subscripts d and m refer to the dispersed and the continuous phase, repsectively. Table II lists the thermal properties at room temperature of the Ni and glass respectively. Table III lists the values of the above ratios for the composites studied.

It is noted that all of the various ratios fall within the experimental bounds established by Lee and Taylor except nD/L for the 45 v/o Ni sample. Thus, with the possible expception of interfacial resistance the measured values of thermal diffusivity represent the "homogeneous" thermal diffusivity of the composites.

III. RESULTS AND DISCUSSION

The experimental data for the thermal diffusivity for D-glass and D-glass with 15, 30, and 45 volume percent dispersed nickel spheres are shown in Figures 4 and 5 for the glass with raw and oxidized nickel

spheres, respectively. The dashed curves in each figure show the thermal diffusivity calculated from the Bruggeman[11] variable dispersion (BVD) relation for the conductivity of a composite (λ_c):

$$\frac{\lambda_c - \lambda_d}{\lambda_m - \lambda_d} \left(\frac{\lambda_m}{\lambda_c}\right)^{1/3} = 1 - V_d \qquad (2)$$

the volumetric heat capacity:

$$\rho_c C_c = \rho_m C_m V_m + \rho_d C_d V_d \qquad (3)$$

and the relation: $\alpha = k/\rho C$ (4)

The implicit assumption in the derivation of eq. 2 is that the components are perfectly bonded with no thermal resistance at the interface. It may also be noted that the BVD relation gives a better prediction of the "homogeneous" thermal diffusivity in the range of volume fractions being considered here than does the Rayleigh - Maxwell Equation.[17]

As may be noted from Figure 4 the thermal diffusivity, α, of the 15 and 30 v/o raw Ni/glass composites from room temperature to $\sim$ 300°C matches the values of thermal diffusivity of 100% D-glass while α of the 45 v/o Ni composite is about twice that of the D-glass. Above 300°C, α has a high positive temperature dependence. Values of α for the 15 and 30 v/o raw-Ni composites increase with increasing temperature until they show excellent agreement with values calculated by the BVD relation at 600°C, near the fabrication temperature of 700°C. For the 45 v/o Ni composite, the thermal diffusivity increases to values above that predicted by the BVD theory for temperatures above 500°C. The Curie point transition at 358°C for nickel is readily observable in the

Ni glass composites, although the minimum in α appears displaced to slightly lower temperatures.

For the oxidized Ni/glass composites measured α values are lower than those calculated by the BVD relation for all temperatures, as shown in Figure 5. However, at room temperature α values for the composites with oxidized nickel spheres are higher than α values for composites with raw nickel spheres of corresponding concentration. The positive temperature dependence of α for these composites is much less than those with non-oxidized spheres. Again the effect of the Curie transition on thermal diffusivity is observable at temperatures slightly below 358°C for all three nickel concentrations.

At least qualitatively the above observations can be explained on the basis of the mismatch in the coefficients of thermal expansion and the nature of and differences in the interfacial bonds.

For the glass with raw Ni spheres, the lack of bonding is clearly evident from the SEM fractographs shown in Fig. 2. The lack of cohesion at the interface between the glass and Ni also can be justified from the magnitude of the internal stress which would have arisen for perfect bonding. After Selsing,[18] the magnitude of the radial stress (σ_r) perpendicular to the interface of a single spherical particle contained in an infinite matrix is:

$$\sigma_r = \frac{\Delta\beta\Delta T E_d}{(1+\nu_m)(E_d/2E_m)+(1-2\nu_d)} \qquad (5)$$

where $\Delta\beta$ is the mismatch in the coefficients of linear thermal expansion, ΔT is the temperature difference over which the composite is cooled and over which no stress relaxation can occur, E is Young's modulus, ν is

Poisson's ratio and, as before, subscripts d and m refer to the dispersed phase and matrix phase, respectively. With $\Delta\beta = 6.7\times10^{-6}\,°K^{-1}$, $\Delta T = 600°C$, $E_m = 6.0\times10^5$ MPa, $E_d = 20.6\times10^5$ MPa, $\nu_m = 0.3$, $\nu_d = 0.3$ yields:

$$\sigma_r \simeq 345 \text{ MPa}(50{,}000 \text{ psi})$$

This magnitude of stress quite likely exceeds the strength of the interfacial bond of a non-wetting metal-glass system such as the present, without any bonding agent. Separation of the glass-Ni interface most likely already occurs during the cooling phase immediately following hot-pressing. It is easily calculated from the thermal expansion mismatch that for a 50 μm spherical inclusion and a 600°C temperature range of cooling, the width of the interfacial gap is approximately 0.1 μm. Such a gap is expected to act as a significant barrier to the flow of heat. For this reason, the measured values of the thermal diffusivity are expected to fall well below those calculated from composite theory even at the lower temperatures.

Despite the presence of the gaps, the nickel metal still makes a contribution to the thermal diffusivity as indicated by the unique temperature dependence which reflects the presence of the Curie point in the nickel. Also, the thermal diffusivity of the glass-raw Ni composites does not fall below the value of the thermal diffusivity of the glass, which would have been expected if the Ni-phase made no contribution to the conduction of heat. The reason for this is that in the glass in which at the lower temperatures thermal transport occurs primarily by phonon transport, the thermal diffusivity is directly proportional to the product of the phonon velocity and mean free path in the direction of the

temperature gradient. The presence of the gaps increases the total distance required for phonon transport and accordingly decreases the thermal diffusivity. Furthermore if the Ni did not contribute to the conduction of heat, the thermal diffusivity would be expected to decrease with increasing Ni content (i.e., increasing number of interfacial gaps). The contribution of the Ni to the conduction of heat can occur by means of Ni particle-to-practice contact especially expected for the glass with 45 vol.% Ni. Even isolated particles however can contribute to the thermal transport since contact with the glass can occur at multiple points especially for the non-spherical particles.

With increases in temperature to the hot-pressing temperature the contact between the glass and Ni inclusions will improve. At higher temperatures, therefore, the Ni particles can make a greater contribution to the thermal transport than at the lower temperatures. This results in a positive temperature dependence of the thermal diffusivity, in agreement with observations. For the highest temperatures (600°C) excellent agreement exists between the experimental data and those calculated by the BVD composite theory for the glass with 15 and 30% Ni. This is indicative of the absence of an interfacial barrier to heat flow. For the composite with 45% Ni, the observed values exceed those predicted by the BVD theory, probably as the result of an enhanced thermal diffusivity due to direct particle-to-particle contact, not taken into account in the BVD theory. It should also be noted that the excellent agreement between the observed and calculated data for the composites with 15 and 30% Ni confirms the validity of the criteria for the thermal diffusivity established by Lee and Taylor,[17] when no significant interfacial effects are present.

The magnitude and temperature dependence of the thermal diffusivity of the glass with the oxidized Ni dispersion is expected to show different behavior. Since the fibrous glass phase at the interface provides physical contact between the glass matrix and the nickel, at least at the lower temperatures the latter can make a much larger contribution to the thermal diffusivity than the non-oxidized (raw) Ni dispersions. These should result in a higher diffusivity in agreement with observations. Because of the presence of the pores at the interface, the observed values are expected to fall below those predicted by composite theory, as observed.

The fibrous phase at the interface will form only at those temperatures at which visco-elastic deformation can take place. Below these temperatures on further cooling the thermal expansion mismatch will place the fibrous phase in tension without further changes in fiber and pore morphology. For this reason, the temperature dependence of the glass with oxidized Ni particles is expected to be less than for the glass with raw Ni dispersions, again in agreement with observations.

The results of the effect of thermal cycling (i.e. heating followed by cooling) on thermal diffusivity shown in Fig. 6, provide additional information on the nature of the interfacial bond and thermal barrier at the glass-Ni interface. For the glass with oxidized Ni spheres the experimental data on heating and cooling over one cycle were observed to be reproducible. This suggests that the interfacial bond is relatively permanent, at least over the temperature range of the thermal cycle.

For the glass with raw Ni dispersions, however, the experimental data on the cooling part of the cycle lie well above the data obtained on heating. This suggests that near 600°C the glass and nickel form a

bond of some sort which requires some degree of cooling before rupture occurs. This results in a discontinuity in slope of the thermal diffusivity as a function of temperature at ≈ 400°C. It is of interest to note that a similar "hysteresis" was observed by Siebeneck et al[5] for the effect of micro-cracking on the thermal diffusivity of iron titanate. The lack of reproducibility of the "hysteresis" curve for the glass-raw Ni composites in repeated thermal cycling is further evidence for the lack of permanance of the interfacial bond.

In summary, the results of the present study indicate that the nature of the interfacial bond between the individual components of a composite can have a profound effect on the thermal transport properties of such composites. Such effects should be taken into account in estimates of the thermal conductivity of composites which exhibit de-bonding at the interfaces. The general results of this study also suggest that controlling the degree of bonding at the interface between components, may constitute an effective mechanism for tailoring the heat conduction properties of composites.

Acknowledgements

This study was conducted as part of research programs sponsored by the Office of Naval Research under contracts N-00014-78-C-0726 and N-00014-78-C-0431. The specimens were prepared in the Department of Materials Science and Engineering at the University of California in Berkeley. The authors are indebted to C. Wood for assistance in sample characterization.

REFERENCES

1. A. E. Powers, "Conductivity in Aggregates," Knolls Atomic Power Report KAPL 2145, General Electric Company, March 6, 1961.

2. Z. Hashin, "Assessment of the Self Consistent Scheme Approximation: Conductivity of Particulate Composites," J. Comp. Mat., 2 [3] 284-300 (1968).

3. S. C. Cheng and R. I. Vachon, "The Prediction of the Thermal Conductivity of Two and Three Phase Solid Heterogeneous Mixtures," Int. J. Heat Mass. Transfer, 12, 249-64 (1969).

4. A. Nir and A. Acrivos, "The Effective Thermal Conductivity of Sheared Suspensions," J. Fluid Mech., 78 [1] 33-48 (1976).

5. H. J. Siebeneck, J. J. Cleveland, D. P. H. Hasselman and R. C. Bradt, "Effect of Microcracking on the Thermal Diffusivity of Fe_2TiO_5," J. Amer. Ceram. Soc., 59 [5-6] 241-44 (1976).

6. H. J. Siebeneck, J. J. Cleveland, D. P. H. Hasselman and R. C. Bradt, "Grain Size Microcracking Effects on the Thermal Diffusivity of $MgTiO_5$," J. Am. Ceram. Soc., 60 [7-8] 336-38 (1977).

7. D. P. H. Hasselman, "Effects of Cracks on Thermal Conductivity," J. Comp. Mat., 12, 403-07 (1978).

8. D. P. H. Hasselman and R. M. Fulrath, "Proposed Fracture Theory of a Dispersion Strengthened Glass Matrix," J. Amer. Ceram. Soc., 49, 68-71 (1966).

9. D. P. H. Hasselman and R. M. Fulrath, "Micromechanical Stress Concentrations in Two-Phase Brittle Matrix Ceramic Composites," J. Amer. Ceram. Soc., 50, 399-404 (1967).

REFERENCES (CONT'D)

10. D. O. Nason, "Effect of Interfacial Bonding on Strength of a Model Two-Phase System," M.S. Thesis, University of California, Berkeley (1962).

11. D. A. G. Bruggeman, "Dielectric Constant and Conductivity of Mixtures of Isotropic Materials," Annalen Physik, 24, 636-79 (1935).

12. W. Niesel, "The Dielectric Constants of Heterogeneous Mixtures of Isotropic and Anisotropic Substances," Annalen Physik, 10, 336-48 (1952).

13. W. J. Parker, R. J. Jenkins, C. P. Butler and G. L. Abbott, "Flash Method of Determining Thermal Diffusivity, Heat Capacity, and Thermal Conductivity," J. Appl. Phys., 32 [9] 1679-84 (1961).

14. K. D. Maglic and B. S. Marsicanin, "Factors Affecting the Accuracy of Transient Response of Intrinsic Thermocouples in Thermal Diffusivity Measurement," High Temperatures-High Pressures, 5, 105-110 (1973).

15. R. C. Heckman, "Finite Pulse-Time and Heat-Loss Effects in Pulse Thermal Diffusivity Measurements," J. Appl. Phys., 44 [4] 1455-60 (1973).

16. H. R. Shanks, A. H. Klein and G. S. Danielson, "Thermal Properties of Armco Iron," J. Appl. Phys., 38 [7] 2885-92 (1967).

17. T. Y. R. Lee and R. E. Taylor, "Thermal Diffusivity of Dispersed Materials," J. Heat Transfer, 100, 720-24 (1978).

18. J. Selsing, "Internal Stresses in Ceramics," J. Amer. Ceram. Soc., 44 [8] 419 (1961).

Table I.--Composition and Density of Glass-Nickel Composites

Sample	ρ bulk	ρ theory**	%theoretical
D-glass	2.476		100
+ 15 v/o Ni (raw)	3.44	3.44	100
+ 30 v/o Ni (raw)	4.29	4.41	97.3
+ 45 v/o Ni (raw)	5.45	5.37	101.5
+ 15 v/o Ni (ox.)	3.24	3.43	94.5
+ 30 v/o Ni (ox.)	4.24	4.38	96.8
+ 45 v/o Ni (ox.)	5.21	5.32	97.9

** Estimate made using 8.8 and 8.9 gm/cc for raw and oxidized Ni, respectively.

Table II.--Thermophysical Properties of Glass and Nickel at 27°C.

Property	Nickel*	D-glass
Density (Kg/m^3)	8900	2476
Specific Heat ($J/Kg \cdot k$)	450	840+*
Thermal Diffusivity (10^{-6} m^2/sec)	22.9	0.52
Thermal Conductivity ($W/m \cdot K$)	91	1.1
Linear Thermal Expansion ($x10^6$)($°K^{-1}$)	13.4	7.0+*

*Literature values
+Ref. 8.

Table III.--Ratios of Various Properties for Glass/Nickel Composites for Lee and Taylor Criteria.

V_d	15 v/o Ni	30 v/o Ni	45 v/o Ni
α_d/α_m (27°C)	44	44	44
α_d/α_m (358°C)	21	21	21
λ_d/λ_m (27°C)	83	83	83
$(\rho_d C_d V_d)/(\rho_m C_m V_m)$	0.37	1.02	1.64
L/D	41	41	41
nD/L	0.66	0.83	0.95

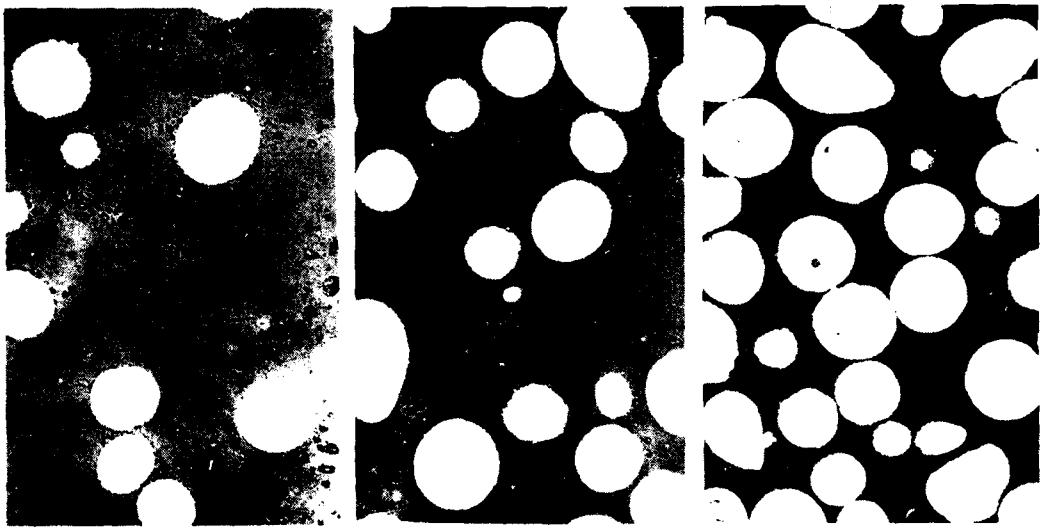

Fig. 1. Optical micrographs of D-glass containing, a: 15 vol%; b: 30 vol.% and c: 45 vol.% Ni with average diameter of approx. 50 μm.

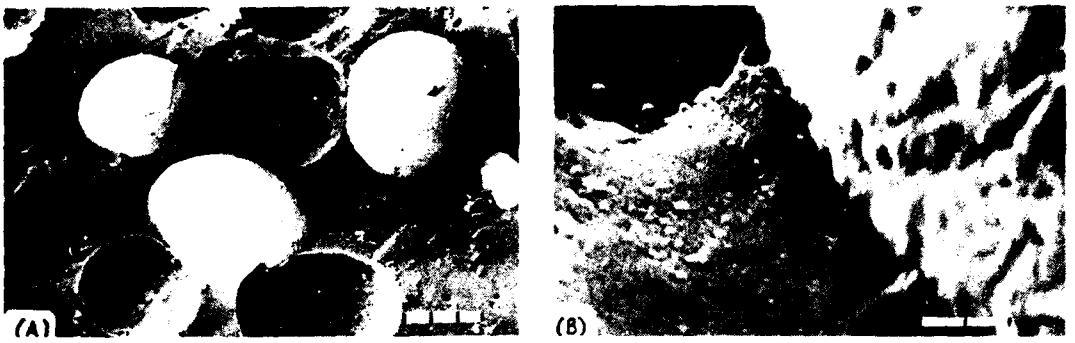

Fig. 2. Scanning electron fractographs of D-glass with 45 vol.% raw Ni. A: non-bonded Ni spheres and cavities (bar = 30 μm); B: detailed view of interfacial gap between glass and Ni (bar = 2 μm).

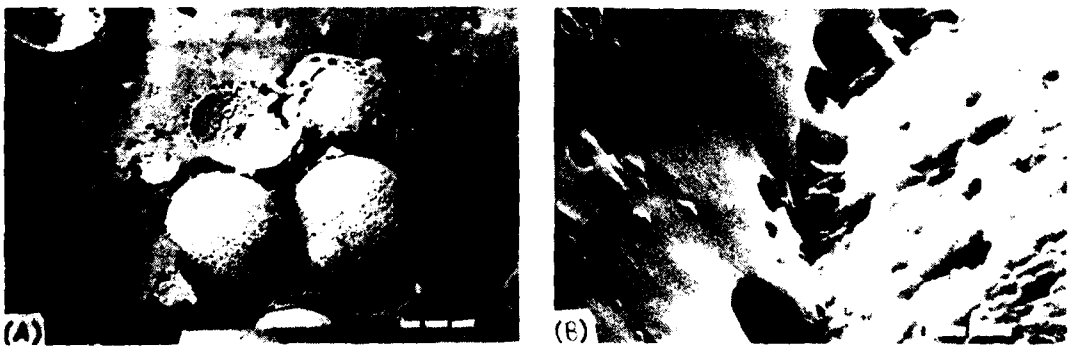

Fig. 3. Scanning electron micrographs of D-glass with oxidized Ni spheres. A: bonded Ni spheres and cavities (bar = 30 μm); B: glass-Ni interface (bar = 2 μm).

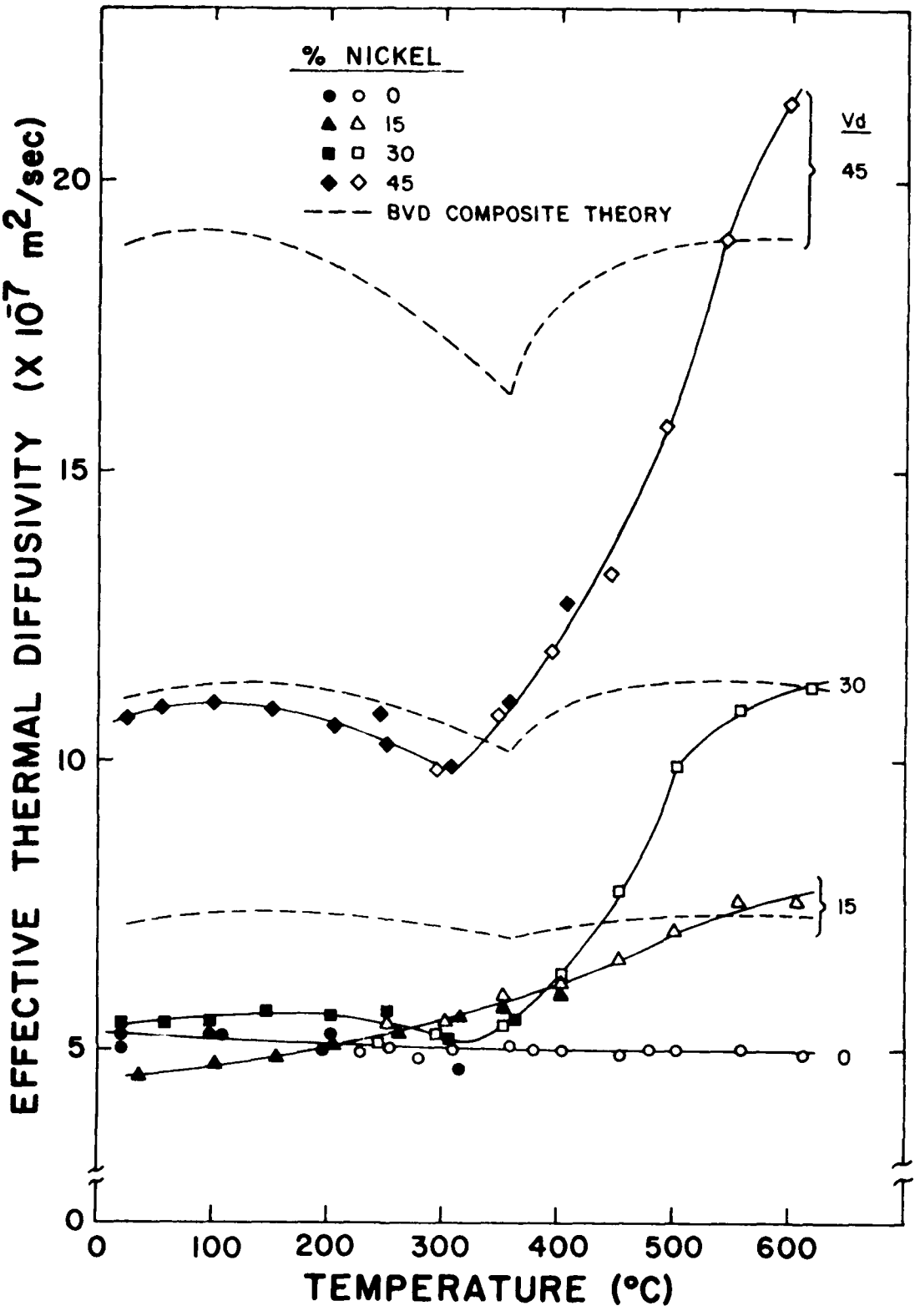

Fig. 4. Thermal diffusivity of D-glass with raw (non-oxidized) Ni inclusion (open symbols: thermocouple data; closed symbols: infra-red data).

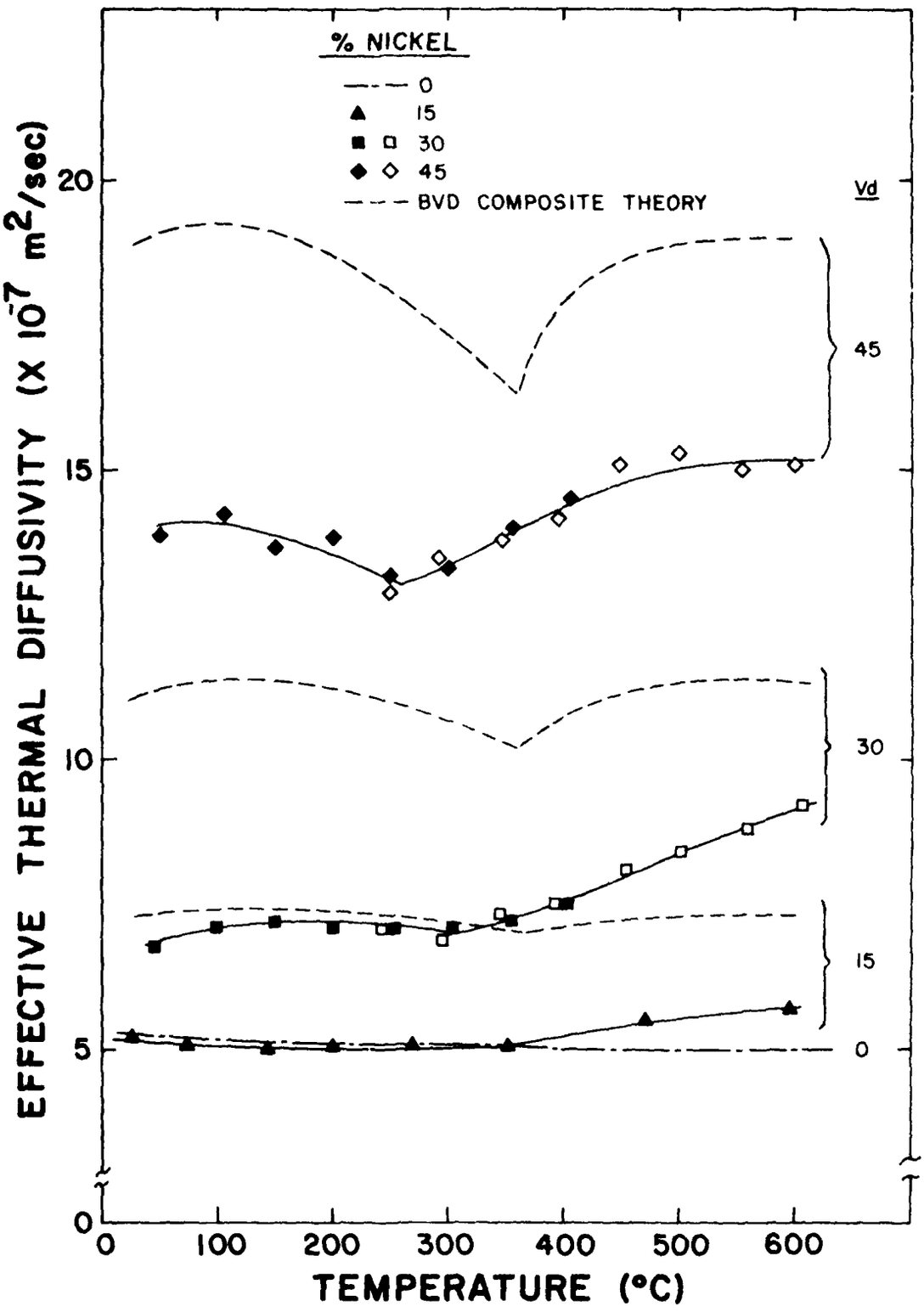

Fig. 5. Thermal diffusivity of D-glass with oxidized Ni inclusions (open symbols: thermocouple data; closed symbols: infra-red data).

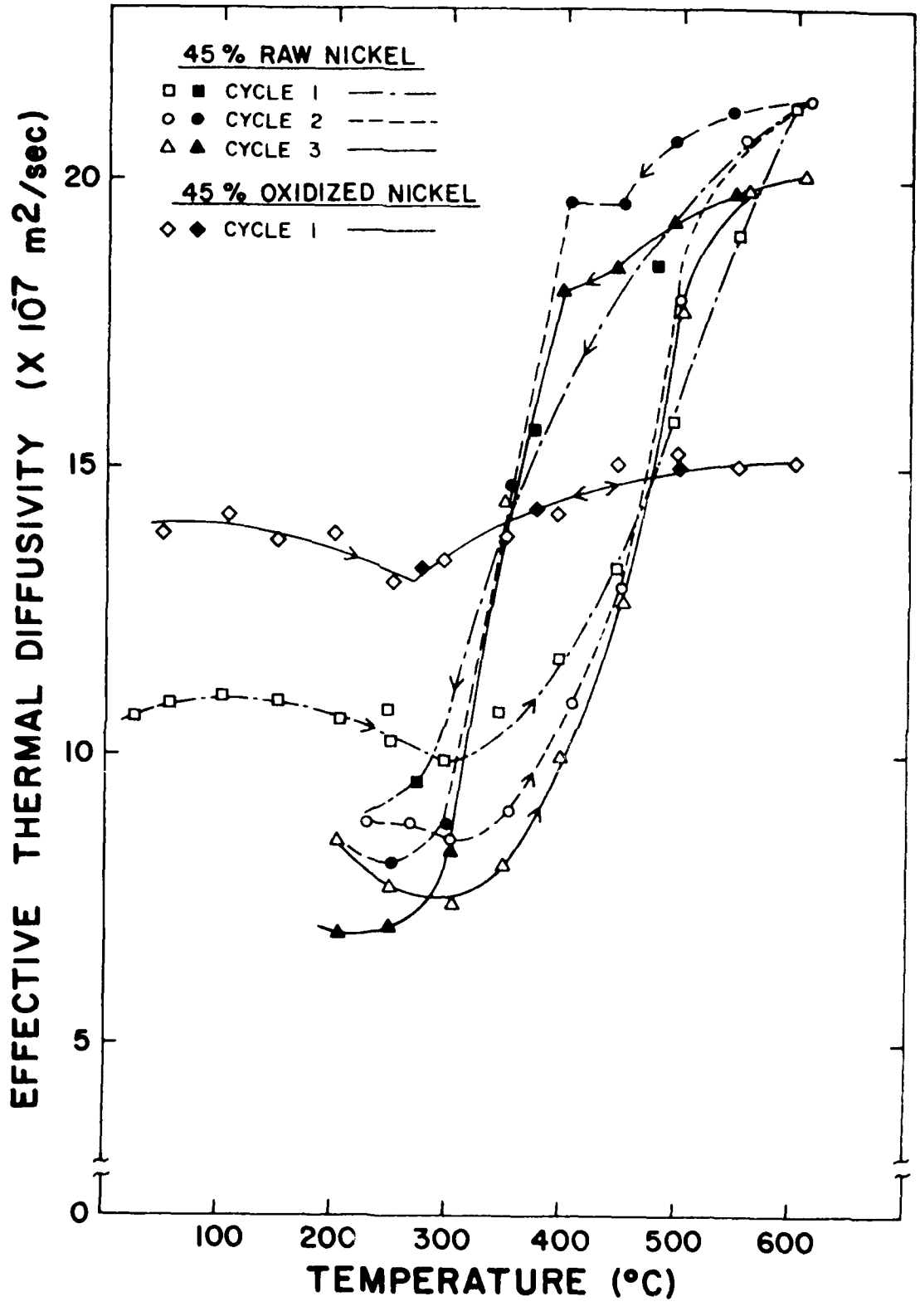

Fig. 6. Effect of heating and cooling (thermal cycling on thermal diffusivity of D-glass with 45% raw and oxidized Ni dispersions (open symbols: heating; closed symbols: cooling).

CHAPTER VI

ANALYSIS OF THE RESISTANCE OF HIGH-E, LOW-E BRITTLE COMPOSITES TO FAILURE BY THERMAL SHOCK

by

D. P. H. Hasselman*

P. F. Becher†

K. S. Mazdiyasni§

*Department of Materials Engineering
Virginia Polytechnic Institute and State University
Blacksburg, Virginia 24061 USA

†Engineering Materials Division
Naval Research Laboratory, Washington, D.C. 20375, USA

§Air Force Materials Laboratory
Wright-Patterson Air Force Base
Ohio 45433, USA

ABSTRACT

By means of the inclusion of a dispersed phase with low Young's modulus, the generally low thermal stress resistance of brittle materials for high-temperature structures can be improved significantly. An analysis of this improvement on the basis of continuum and micro-mechanical theory is presented in this paper.

The low-E phase is shown to cause a significant decrease in Young's modulus, with a negligible effect in the coefficient of thermal expansion. The relative change in thermal conductivity is a function of the thermal conductivity of the dispersed phase.

The tensile fracture stress is reduced significantly, primarily due to the mismatch in elastic properties, with smaller effects due to the mismatches in the coefficient of thermal expansion and thermal conductivity.

The relative changes in Young's modulus and tensile fracture stress are such as to result in an increase in the strain-at-fracture and a simultaneous decrease in the elastic energy at fracture, the driving force for catastrophic crack propagation. The accompanying increase in fracture energy also contributes to the improvement of thermal shock resistance. By changing the size of the low-E inclusion, trade-offs can be made between strain-at-fracture and elastic energy at fracture.

CHAPTER VII

THERMAL STRESS ANALYSIS OF BRITTLE CERAMICS WITH DENSITY GRADIENTS UNDER CONDITIONS OF TRANSIENT CONVECTIVE HEAT TRANSFER

by

K. Satyamurthy, J. P. Singh, M. P. Kamat and D. P. H. Hasselman

Departments of Materials Engineering and Engineering Science and Mechanics
Virginia Polytechnic Institute and State University
Blacksburg, Virginia 24061 USA

ABSTRACT

The effect of porosity gradient on the maximum tensile thermal stresses during transient heat flow for a circular cylinder is calculated using finite element method. It is shown that with appropriate porosity distribution, the maximum tensile thermal stress in the cylinder is substantially reduced without the loss of strength in the critical region, thus improving the thermal stress resistance of the material.

1. INTRODUCTION

Brittle ceramic materials are highly susceptible to catastrophic fracture due to thermal stresses which result from constrained thermal expansion[1]. A detailed analysis of the magnitude and distribution of such stresses is essential for the design of structures or components operating in non-ambient thermal environments. The selection of materials with optimum thermal stress resistance can be based on thermal stress resistance parameters[2,3]. Unfortunately, even the best material selected on this basis, may be unable to withstand the thermal stresses frequently encountered in practice. For such cases, new materials may have to be developed or major design changes may be called for.

For a further solution of the problem of thermal stress failure, it should be noted that the magnitude of thermal stresses in a given structure is a function of the imposed heat flux, temperature difference, etc., to which the structure is subjected as well as the distribution of temperature within the structure. Generally, little or no control exists over the external heating conditions. However, by means of appropriate design and/or materials selection, modification in the temperature distribution can be made in such a manner that the magnitude of the thermal stress is reduced. One method by which this can be achieved is to incorporate within the structure, a spatially varying thermal conductivity. The validity of this latter approach was substantiated by two recent studies by Hasselman and Youngblood[4] and Satyamurthy et al[5]. These studies showed that for both steady-state and transient convective heat transfer in a hollow and solid cylinder, resp., the magnitude of thermal stress can be lowered substantially by a spatially varying thermal conductivity distributed in such

AD-A081 915 VIRGINIA POLYTECHNIC INST AND STATE UNIV BLACKSBURG --ETC F/G 11/4
THERMAL-MECHANICAL AND THERMAL BEHAVIOR OF HIGH-TEMPERATURE STR--ETC(U)
DEC 79 D P HASSELMAN, P F BECHER, L D BENTSEN N00014-78-C-0431

UNCLASSIFIED NL

2 OF 3
AD A081915

a manner that at the hotter parts of the cylinder the thermal conductivity is lower than in the other parts of the cylinder.

An effective method of incorporating a spatially varying thermal conductivity in a material is by way of a spatially varying pore phase. However, a spatially varying pore phase also will cause spatial variations in Young's modulus and strength values. If the pore phase were distributed such that the pore content is low (or zero) in the region of maximum tensile thermal stress, to which brittle materials are most susceptible, full advantage can be taken of the spatially varying thermal conductivity and decreased Young's modulus, without the accompanying adverse effects of porosity on tensile strength. The validity of this concept was established in a thermal stress analysis of a hollow cylinder[6] subjected to steady-state heat flow. This study showed that a spatially varying pore phase with a maximum local pore content of 0.3, could improve thermal stress resistance by as much as 30%. This result is particularly noteworthy, since a uniformly distributed pore content of 0.3 can decrease thermal stress resistance by as much as a factor of two[7].

The purpose of the present study is to investigate the improvements in thermal stress resistance which can be obtained by a spatially varying pore phase under conditions of transient convective heat transfer.

2. PROCEDURES

2.1 Model and Heat Transfer Conditions

A solid circular cylinder was selected as a geometry appropriate for the present study. The cylinder, initially at uniform temperature, is subjected to uniform heating and cooling along its surface by a sudden change

in ambient temperature. Heat transfer is assumed to be Newtonian with a heat transfer coefficient h, described by the Biot number, $\beta_o = ah/K_o$, where a is the radius of the cylinder and K_o is the thermal conductivity of the non-porous material.

2.2 Porosity Distribution

2.2.1 Heating

The distribution of the pore phase for convective heating was selected arbitrarily as:

$$P = P_o(r/a)^n \tag{1}$$

where P is the fractional porosity, P_o is the maximum fractional pore content, n is a constant which may be referred to as the "porosity distribution coefficient" and r is the radial coordinate. Eq. 1 indicates that at the center of the cylinder (r=0), where the tensile thermal stresses are maximum, the pore content is zero, so that the tensile strength at r=0 is not affected.

2.2.2 Cooling

Preliminary calculations showed that a continuous function of the general form of eq. 1 would not give significant reduction in the thermal stresses. Instead, the porosity distribution was chosen as

$$P = 0 \qquad \text{for} \quad 0.9 \leq r/a \leq 1 \tag{2}$$

$$P = P_o\{1 - (r/0.9a)^n\} \quad \text{for} \quad 0 \leq r/a < 0.9 \tag{3}$$

Eqs. 2 and 3 indicate that the surface, where the tensile stresses are maximum, has a non-porous layer of thickness 0.1 r/a.

2.3 Effect of Porosity on Material Properties

The dependence of the thermal conductivity, K, Young's modulus, E and the tensile strength, σ_f ,on the porosity was chosen arbitrarily to be expressed by the well-known exponential equation[8,9]:

$$K,\ E,\ \sigma_f = K_o,\ E_o,\ \sigma_{fo} e^{-bP} \qquad (4)$$

where the zero subscript refers to the value of the non-porous material and b is a constant taken as 3, 4 and 6 for the thermal conductivity, Young's modulus and tensile strength resp. Poisson's ratio and the coefficient of thermal expansion were assumed to be unaffected by the pore phase.

2.4 Computational Method

Due to the spatial variation of the thermal conductivity and Young's modulus, the transient temperatures and thermal stresses required evaluation by numerical method. For this purpose a computer program based on finite element principles was utilized. This program was developed and used in previous studies[5,6], and gave excellent agreement with the analytical solutions of Jaeger[10] for the transient thermal stresses in a solid circular cylinder with uniform thermal conductivity. The program also was used to verify the analytical results obtained by Hasselman and Youngblood[4] for the steady-state thermal stress in a hollow cylinder with spatially varying thermal conductivity.

For convenience, the numerical results obtained in the present study were reported in terms of the non-dimensional stress, $\sigma^* = \sigma(1-\nu)/\alpha E_o \Delta T$, the non-dimensional radial coordinate r/a and the Biot number, ah/K_o, defined earlier. Since the calculations of the transient thermal stresses required

extensive computer analysis, only sufficient data points were generated to indicate the positive effect of the spatially varying pore phase on thermal stress resistance in general, rather than evaluating thermal stresses for specific applications.

3. NUMERICAL RESULTS AND DISCUSSION

3.1 Heating

Figures 1a and 1b show the spatial variation in the transient temperatures and thermal stresses for β_o = 1, 5 and 20, n = 1 and P_o = 0.3, at the instant of time the tensile thermal stresses at the center of the cylinder reach their maximum value. A value of P_o = 0.3 corresponds to a value realizable in practice. Included in figs. 1a and 1b are the temperature and thermal stress distributions for the fully dense material, P_o = 0. Comparisons of these figures show that the spatially varying pore phase causes a significant change in the temperature distribution and a corresponding decrease in the maximum tensile stress at r = 0, in agreement with the original hypothesis on which this study was based.

Figure 2 for P_o = 0.3, shows the values of the maximum tensile thermal stress at r = 0, for β_o = 1, 5 and 20 as a function of the porosity distribution function, n. For $n \geq 1$, the magnitude of the thermal stress is nearly independent of n, i.e., the manner in which the porosity is distributed. A sensitivity analysis showed that this independence of stress on n is due to the counteracting contributions of the effect of the spatial variation in the thermal conductivity and Young's modulus on the magnitude of maxinum tensile thermal stress.

Included in fig. 2 are the values of the maximum tensile thermal stress for the non-porous material, (P_o = 0). Comparison of these data

show that the spatially varying pore phase causes a significant decrease in the magnitude of the tensile thermal stress at r = 0. Since at this position (P = 0), the tensile strength of the material is not affected, the decrease in tensile thermal stress leads to a corresponding increase in thermal stress resistance. This relative increase in thermal stress resistance due to the spatially varying pore phase is shown in fig. 3 for β_o = 1, 5 and 20 and P_o = 0.3. These increases are considerable. It is, however, important to note in figure 3 that due to rapid decrease in the tensile strength close to the center of the cylinder, failure will not initiate at the center where the tensile stress is maximum but away from it where the strength to stress ratio is lower. In view of this observation a porosity distribution which includes a small core (r/a = 0.1) of fully dense material can be used to further advantage. This will not cause any significant change in stress distribution because of little change in temperature distribution and Young's modulus values. However, the strength distribution will be improved substantially in the critical region resulting in a further gain in thermal stress resistance. Additional calculations showed that the relative increase which can be obtained by a spatially varying porosity described by equation 1, is approximately a linear function of P_o, as also found in a previous study for steady-state heat flow[6].

It should be noted that the relative increase in thermal stress resistance shown in figure 3, is reported on the basis of constant Biot number, $\beta_o = ah/K_o$, where K_o is the thermal conductivity of the non-porous material. However, the porosity in the surface lowers the thermal conductivity considerably, which in effect increases the Biot number. This increase in the Biot number for spatially varying material properties

also increases the magnitude of thermal stress. In fact, if this change in Biot number had been taken into account as well, the relative increase in thermal stress resistance obtainable for the spatially varying pore phase, would be even greater. For this reason, the data reported in fig. 3 are based on the most conservative comparison.

3.2 Cooling

On convective cooling the tensile thermal stresses are maximum at the surface of the cylinder, (r=a). Preliminary calculations indicated that for a continuous porosity distribution of the form:

$$P = P_o\{1 - (r/a)^n\} \tag{5}$$

no significant improvements in thermal stress resistance could be obtained. Furthermore for $n < 1$, the tensile strength close to the surface would decrease very rapidly. Under these conditions similar to heating case, failure would not be initiated in the surface under the influence of the maximum tensile stress, but within the interior of the cylinder with a lower tensile strength to stress ratio. This latter effect, justified selecting a porosity distribution function of the type given by eqs. 2 and 3 which avoids the spatially rapid decrease in tensile strength in the immediate surface area.

Figures 4a and 4b show the spatial variation of transient temperature and thermal stresses for $n = 1$, $P_o = 3$ and for $\beta_o = 1$, 5 and 20. The data for the case of constant conductivity ($P_o = 0$) overlap with the ones for variable porosity case and hence have not been shown for the purpose of clarity. However, fig. 5 shows the plots for thermal stresses relative to the maximum stress for the zero porosity case. Included in fig. 5 is

also the strength distribution. It can be seen that the increase in thermal stress resistance is less than that obtainable for the heating case.

3.3 General

The data presented in the present paper demonstrate that a spatially varying pore phase can be used effectively to improve the thermal stress resistance of brittle ceramics. For the solid cylinder chosen for the present study, such improvements are particularly significant for thermal shock by convective heating. For other geometries, heat transfer environments and porosity distribution the improvements in thermal stress resistance which can be obtained must be investigated on an individual basis. The results presented in this paper suggest that this method can be used to advantage.

Acknowledgments

The present study was conducted as part of a larger research program on thermo-mechanical and thermal properties of structural brittle materials supported by the Office of Naval Research under contract N00014-78-C-0431.

References

1. Kingery, W. D., J. Amer. Ceram. Soc., 38 (1) 3-15 (1955).
2. Hasselman, D.P.H., Bull. Amer. Ceram. Soc., 49 (12), 1933-37 (1970).
3. Hasselman, D.P.H., Ceramurgia (in press).
4. Hasselman, D.P.H. and Youngblood, G. E., J. Amer. Ceram. Soc., 61 (1) 49-52 (1978).
5. Satyamurthy, K., Kamat, M. P., and Hasselman, D.P.H., J. Amer. Ceram. Soc., (in review).
6. Satyamurthy, K., Singh, J. P., Kamat, M. P., and Hasselman, D.P.H., J. Amer. Ceram. Soc., (in review).
7. Coble, R. L., and Kingery, W. D., J. Amer. Ceram. Soc., 38 (1) 33-37 (1955).
8. Knudsen, F. P., J. Amer. Ceram. Soc., 42 (8) 376-87 (1959).
9. Spriggs, R. M., J. Amer. Ceram. Soc., 44 (12) 628-29 (1961).
10. Jaeger, J. C., Phil. Mag. 36, 418-28 (1945).

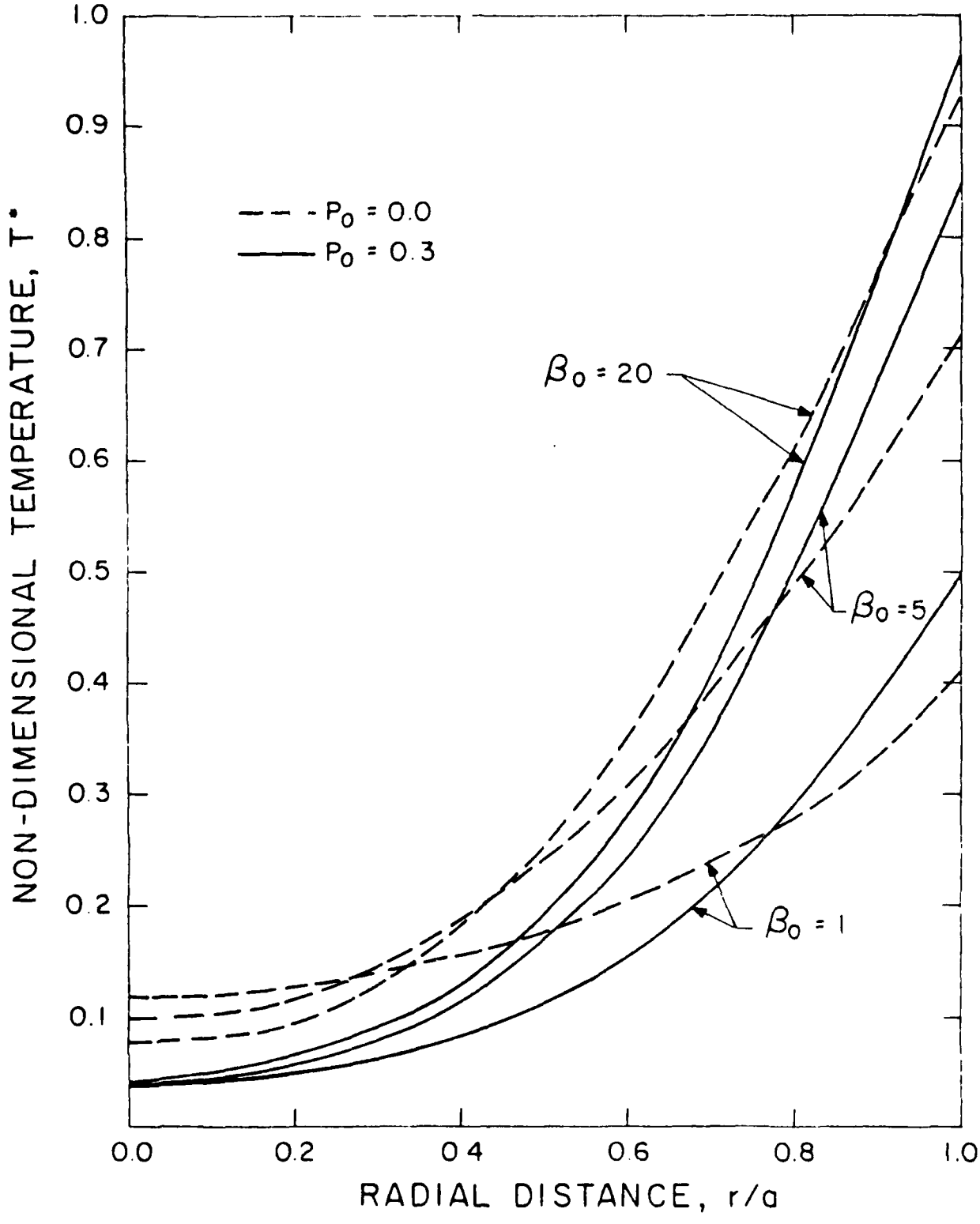

Fig. 1a. Transient temperature distribution in solid circular cylinder subjected to sudden convective heating at the time of maximum tensile stress for spatially varying porosity described by equation 1 with $n = 1$ and $P_0 = 0.3$.

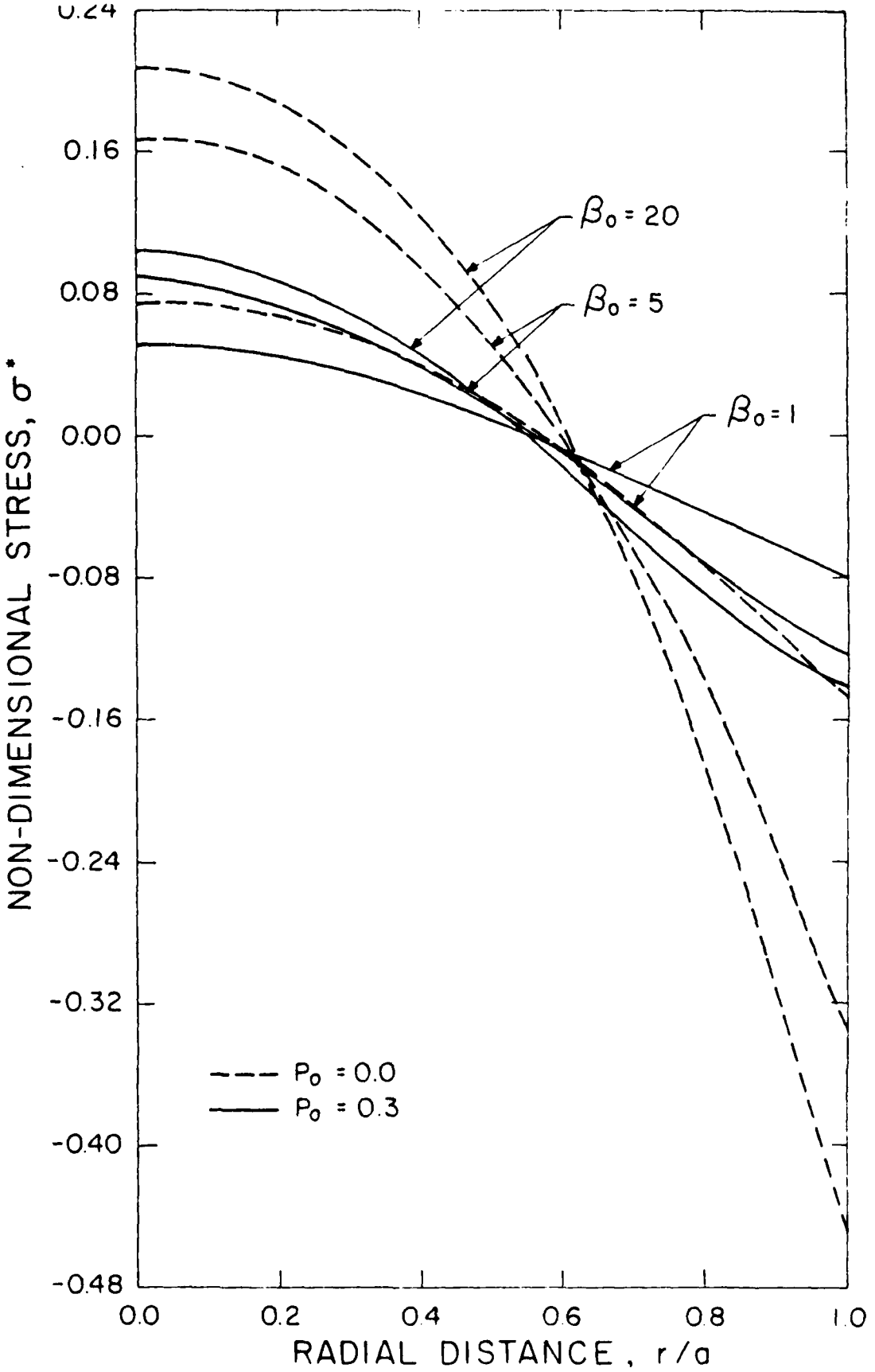

Fig. 1b. Transient thermal stress distribution in solid circular cylinder subjected to sudden convective heating at the time of maximum tensile stress for spatially varying porosity described by equation 1 with n = 1 and P_0 = 0.3.

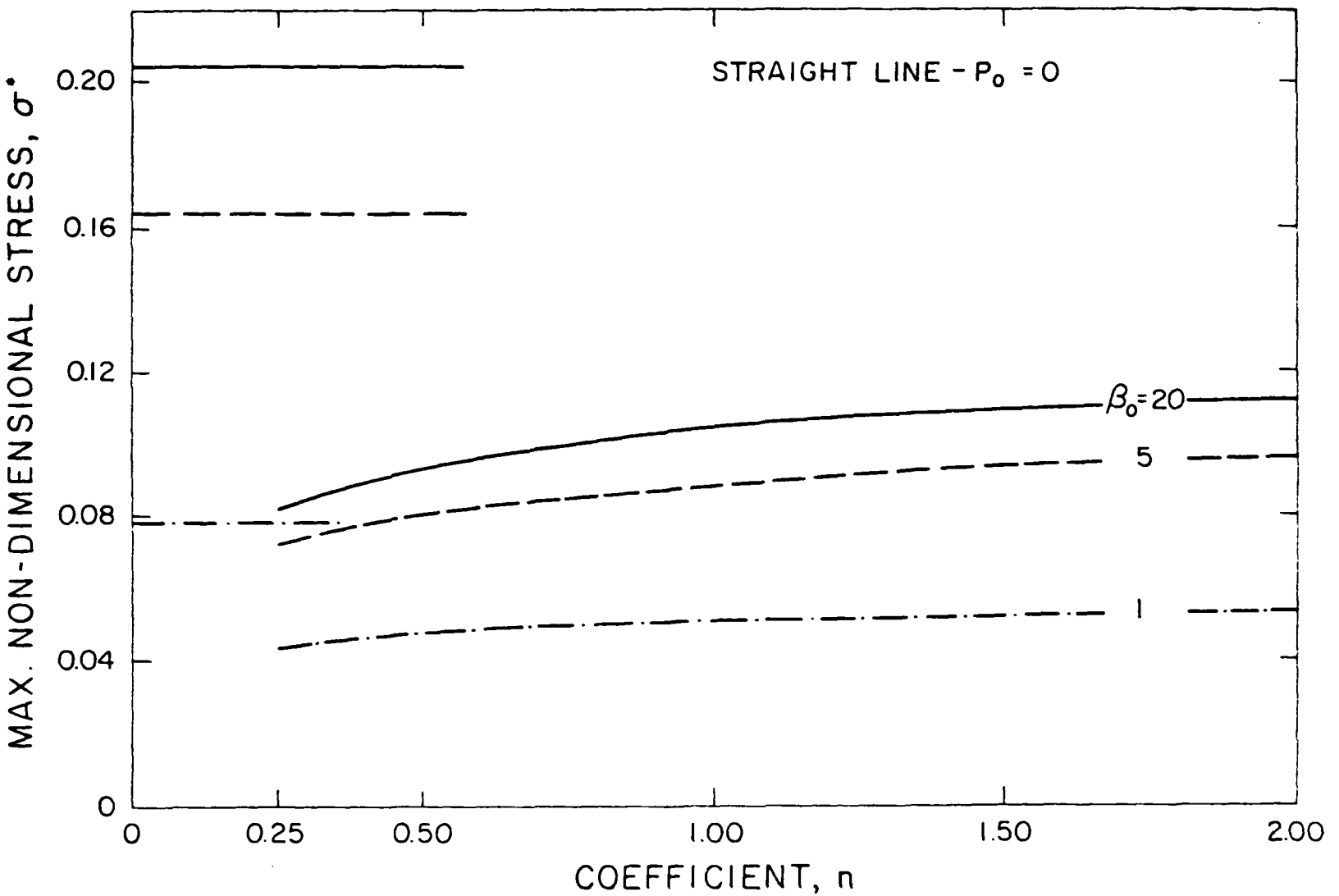

Fig. 2. Maximum tensile thermal stress in solid circular cylinder subjected to sudden convective heating for spatially varying porosity described by equation 1 with P_o = 0.3 for a range of values for n and Biot numbers.

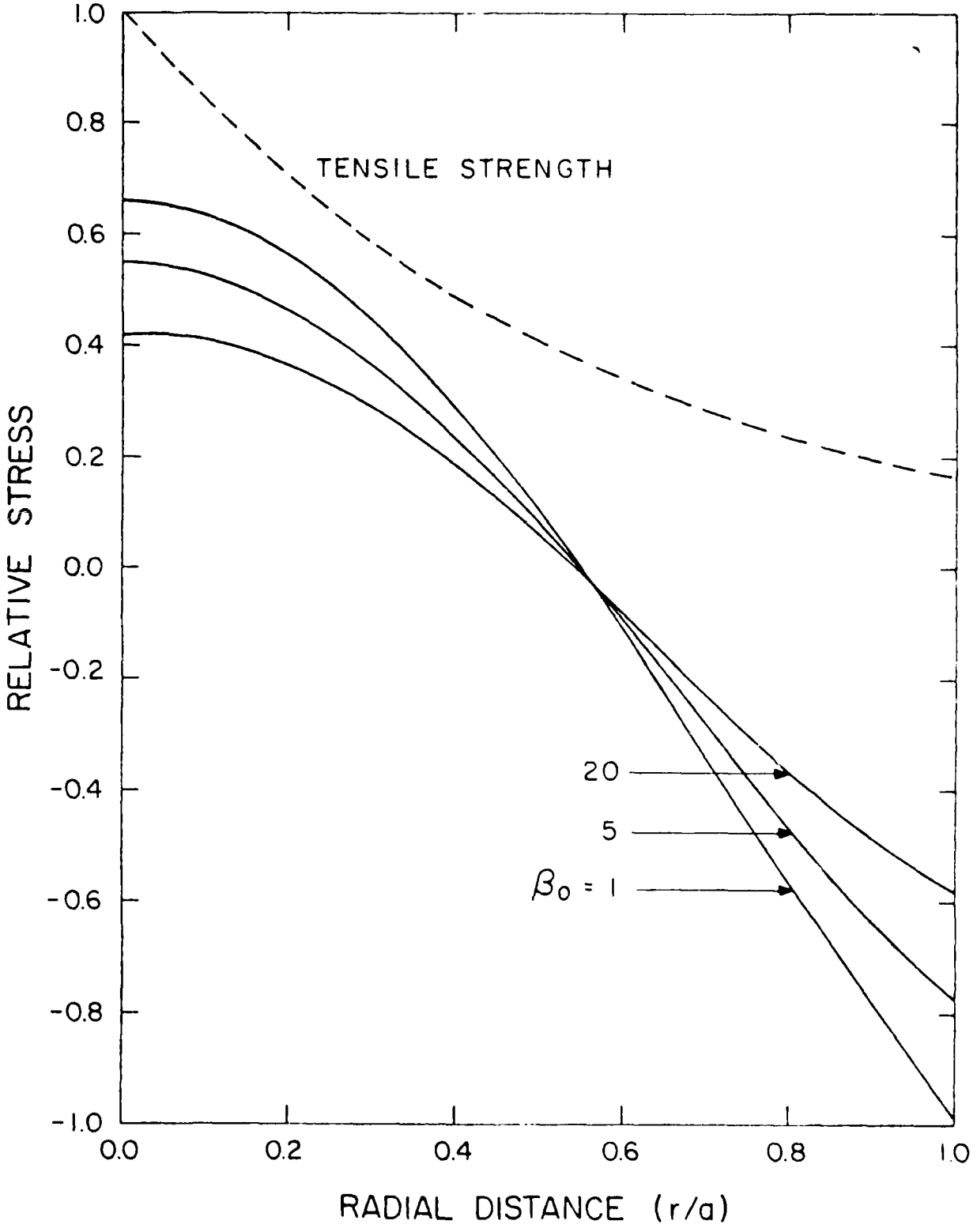

Fig. 3. Distribution of thermal stress and tensile strength for P_o=0.3 and n=1 relative to the corresponding maximum values at P_o=0 in a solid circular cylinder subjected to sudden convective heating for spatially varying porosity described by equation 1.

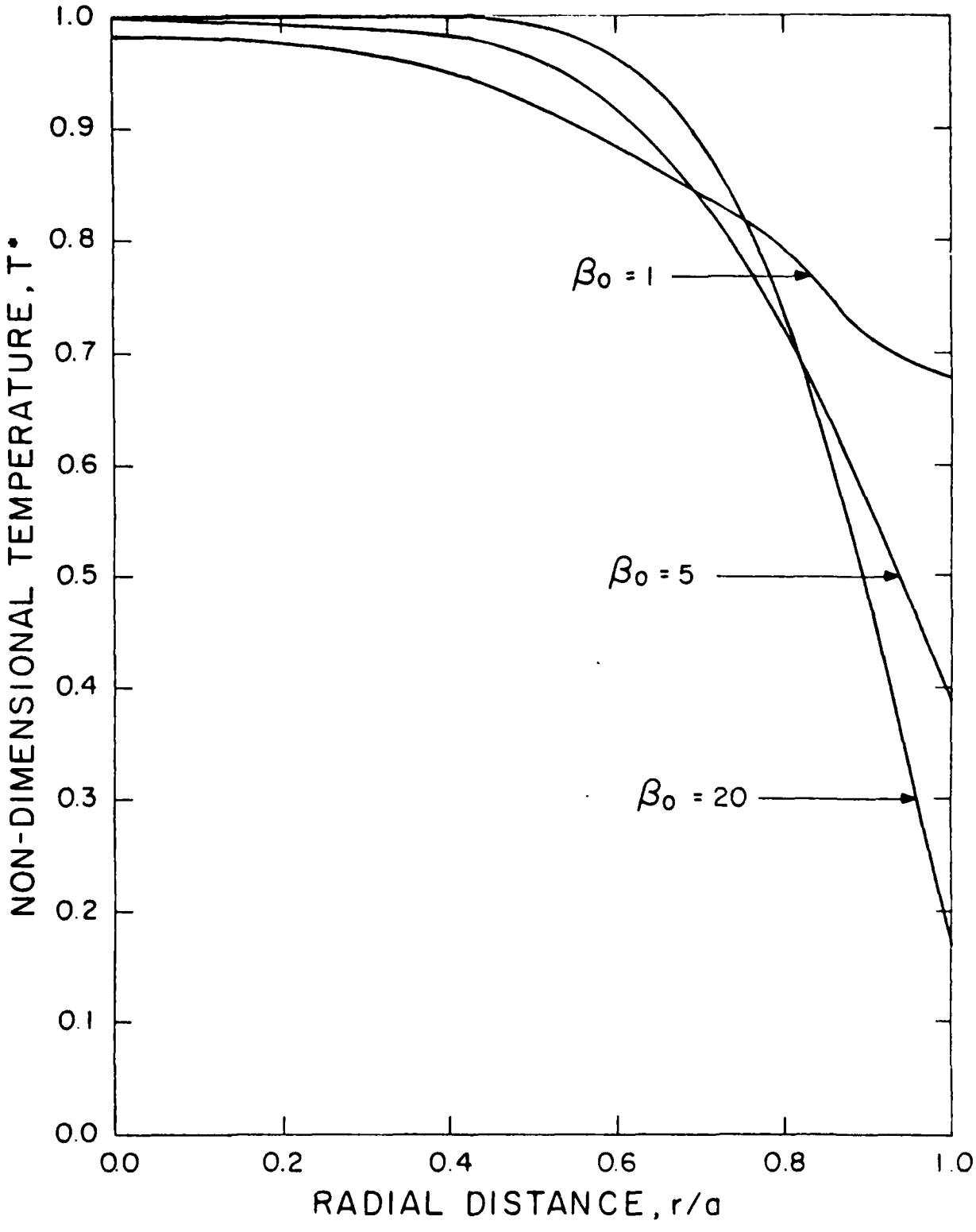

Fig. 4a. Transient temperature distribution in a solid circular cylinder subjected to sudden convective cooling at the time of maximum tensile stress for spatially varying porosity described by equations 2 and 3 with n=1 and P_o=0.3.

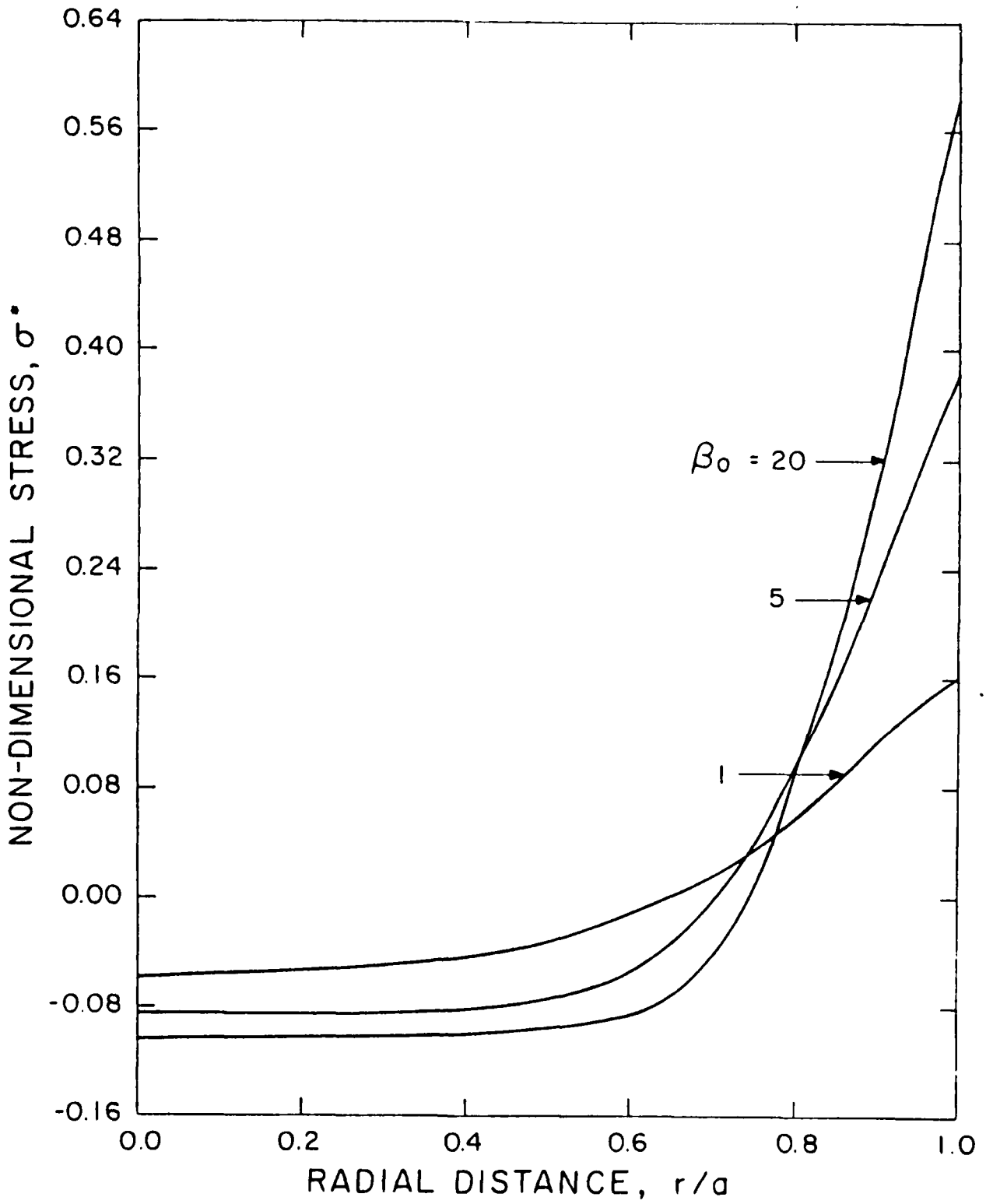

Fig. 4b. Transient thermal stress distribution in a solid circular cylinder subjected to sudden convective cooling at the time of maximum tensile stress for spatially varying porosity described by equations 2 and 3 with n=1 and P_o=0.3.

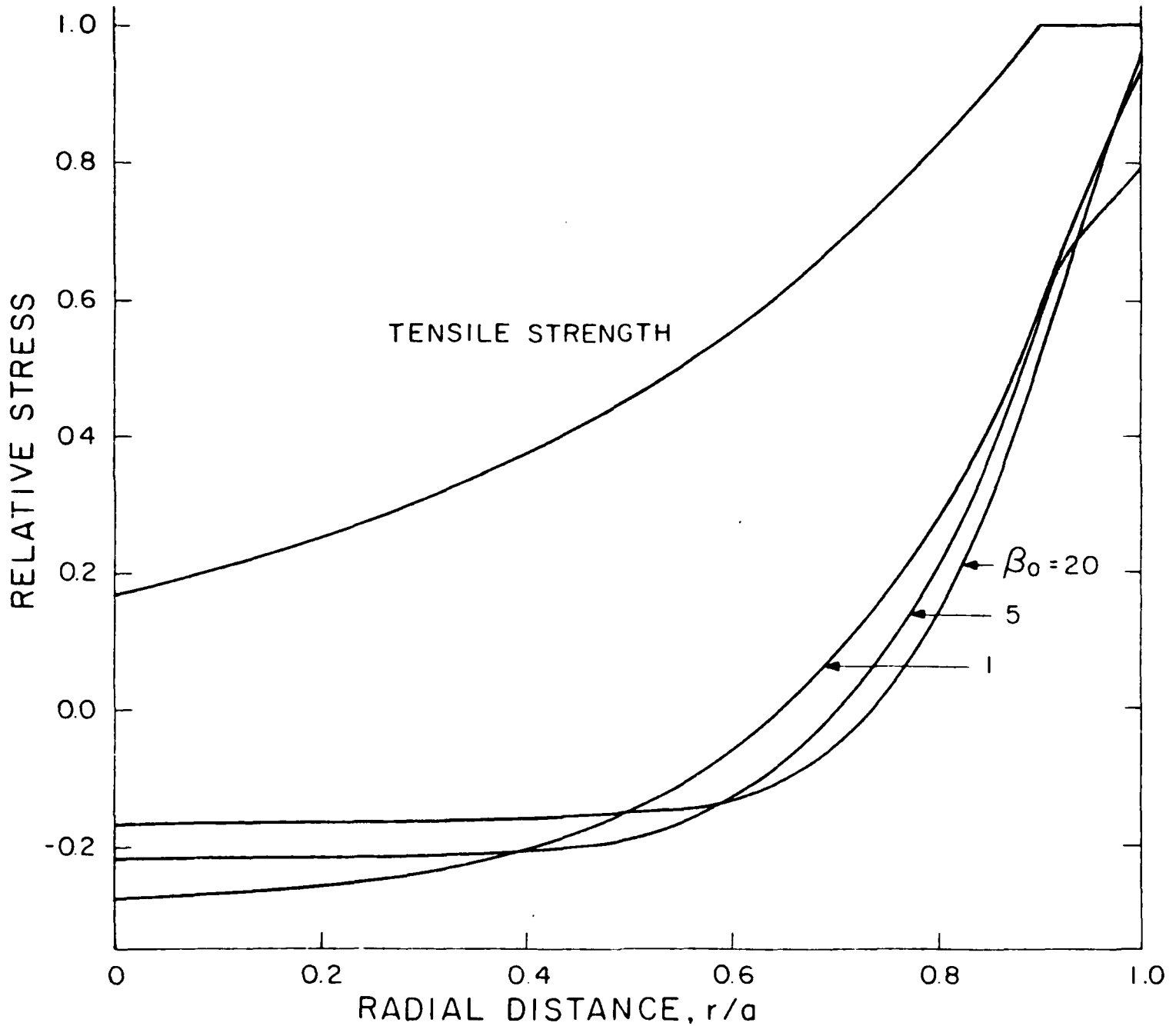

Fig. 5. Distribution of thermal stress and tensile strength for P_0=0.3 and n=1 relative to the corresponding maximum values at P_0=0 in a solid circular cylinder subjected to sudden

CHAPTER VIII

ANALYSIS OF THERMAL STRESS RESISTANCE OF PARTIALLY ABSORBING CERAMIC PLATE SUBJECTED TO ASSYMMETRIC RADIATION, I: CONVECTIVE COOLING AT REAR SURFACE

by

J. R. Thomas, Jr., J. P. Singh and D. P. H. Hasselman

Departments of Mechanical and Materials Engineering
Virginia Polytechnic Institute and State University
Blacksburg, Virginia 24061

ABSTRACT

An analysis is presented of the thermal stresses in a partially absorbing brittle ceramic flat plate assymmetrically heated by radiation on the front surface and cooled by convection on the rear surface with a heat transfer coefficient, h, being finite or zero.

For finite h, the transient thermal stresses are a function of h, whereas the steady-state thermal stresses are independent of h. The maximum value of tensile thermal stresses occurs at an optical thickness $\mu a = 2$ and equals zero for $\mu a = 0$ or ∞. For an optical thickness $\mu a < 10.7$, the steady-state thermal stresses exceed the transient stresses, with the converse being true for $\mu a > 10.7$. The maximum tensile thermal stresses occur in the front surface where the temperatures are highest.

For $h = 0$, the tensile thermal stresses increase with increasing value of optical thickness. The role of the material properties which control the thermal stress resistance under conditions of combined radiation heating and convection cooling are discussed. Appropriate thermal stress resistance parameters are proposed.

I. Introduction

Brittle ceramics are excellent candidate materials of construction for solar energy collectors involving concentrated radiation and other applications such as found in aerospace technology, subject to high-intensity radiant heat fluxes. Unfortunately, in part due to high brittleness and an unfavorable combination of other pertinent properties, ceramic materials are susceptible to catastrophic failure under the influence of the high thermal stress which inevitably accompany transient or steady state heat conduction.[1,2] For the purpose of selection of the optimum material of construction and reliable engineering design, it is imperative that the variables which control the magnitude of thermal stresses arising from radiation heating are well understood.

An earlier analysis of thermal stresses by radiation heating considered materials opaque to incident black-body radiation.[3] This analysis was extended to include materials opaque above a given wavelength of the black-body radiation and completely transparent below this value of wavelength.[4] A more recent analysis[5] concentrated on partially absorbing ceramics symmetrically heated by radiation which is absorbed as it is being transmitted through the material. This analysis showed that for ceramic plates with small optical thickness, the thermal stresses are proportional to the first or third power of the absorption coefficient, for convective cooling corresponding to heat transfer coefficients $h = 0$ and $h = \infty$, respectively.

The purpose of the present paper is to analyze the role of the pertinent material properties which control the magnitude of thermal stresses in a partially absorbing ceramic plate subjected to thermal radiation on one side and cooled by convection with values of the heat transfer coefficient h ranging from zero to infinity at the opposite side.

II. Analysis

A. Geometry and boundary conditions

The geometry selected for the analysis consisted of an unconstrained infinite flat plate of thickness 2a, located parallel to the y,z-plane and $-a < x < a$. The plate, initially at uniform temperature T_o, is subjected to a constant normally incident uniform thermal radiation at $x = -a$ beginning at time $t = 0$. At $x = a$, the plate is cooled by Newtonian convection with a heat transfer coefficient h. The optical properties of the plate were assumed to be independent of wavelength. Also, the reflectivity of the plate was assumed to be sufficiently low so that the effect of multiple reflections within the plate can be neglected. The other relevant material properties which control the magnitude of thermal stresses, such as the coefficient of thermal expansion, Young's modulus, Poisson's ratio, the thermal conductivity and thermal diffusivity were assumed to be independent of temperature.

Following the approach of the previous analyses[3,5] it will be assumed that over the time period required for the stresses to reach their maximum value, the temperature of the plate remains sufficiently low so that re-emission of the absorbed energy is negligible in comparison to the incident radiation. The validity of this assumption was demonstrated in the earlier analyses[3,5] by means of a numerical example, as will also be done in the present study.

B. Derivation of transient temperatures

For normally incident radiation of intensity q_o on the surface of the plate, the flux transmitted through the surface equals εq_o, where ε is the emissivity or $\varepsilon = 1 - r$, where r is the reflectivity.

The intensity q of the radiation within the plate at a distance x is:

$$q = \varepsilon q_o \, e^{-\mu(a + x)} \tag{1}$$

where μ is the absorption coefficient.

The rate of heat absorption (g''') at x is:

$$g''' = \mu\varepsilon q_o e^{-\mu(a + x)} \tag{2}$$

For the appropriate boundary conditions the solutions for the temperature (T) are obtained by solving the heat conduction equation[6]:

$$\partial^2 T/\partial x^2 + g'''(x)/k = (1/\kappa)\partial T/\partial x \tag{3}$$

where k is the thermal conductivity and κ is the thermal diffusivity.

Two cooling conditions of the plate at x = a were considered, namely a heat transfer coefficient $0 < h \leq \infty$ and h = 0. In this respect, it should be noted that a finite heat transfer coefficient $h \to 0$, does not correspond to the same condition obtained for $h \equiv 0$.

The solutions for the transient temperatures are as follows:

a. Finite heat transfer coefficient, h.

For this case the initial and boundary conditions are:

$$T(x,0) = T_o; \; \partial T/\partial x(-a,t) = 0 \tag{4a}$$

$$-k \, \partial T/\partial x(a,t) = h\{T(a,t) - T_o\} \tag{4b}$$

Solution of Eq. (3) for these boundary conditions yields:

$$T(x,t) = T_o + \sum_{n=0}^{\infty} B_n(t) \cos\lambda_n(x + a) \tag{5a}$$

where

$$B_n(t) = G_n\left[1 - e^{-\kappa\lambda_n^2 t}\right]/\kappa\lambda_n^2 \tag{5b}$$

$$G_n = \frac{\kappa q_o \varepsilon \mu}{N_n k}\left\{\frac{\mu + e^{-2\mu a}[\lambda_n \sin(2\lambda_n a) - \mu\cos(2\lambda_n a)]}{\mu^2 + \lambda_n^2}\right\} \tag{5c}$$

$$N_n = \frac{1}{2\lambda_n}[\sin(2\lambda_n a)\cos(2\lambda_n a) + 2\lambda_n a] \quad (5d)$$

and λ_n are the roots of the transcendental equation:

$$\lambda_n \tan(2\lambda_n a) = h/k \quad (5e)$$

A value of heat transfer coefficient $h = \infty$ represents the limiting case for the finite value of heat transfer coefficient.

For $h = \infty$, the initial and boundary conditions are:

$$T(x,0) = T(a,t) = T_o;\ \partial T/\partial x(-a,t) = 0 \quad (6)$$

Solution of Eq. (3) for these boundary conditions yields:

$$T(x,t) = T_o + \sum_{n=\text{odd}}^{\infty} \frac{16q_o\varepsilon\mu a}{n^2\pi^2 k} \frac{\mu + \left(\frac{n\pi}{4a}\right) e^{-2\mu a}}{\mu^2 + (n\pi/4a)^2} \left(1 - e^{-\kappa\lambda_n^2 t}\right) \cos\{\lambda_n(x + a)\} \quad (7a)$$

where $$\lambda_n = n\pi/4a \text{ with } n = 1, 3, 5, 7 \ldots \quad (7b)$$

b. Heat transfer coefficient $h = 0$.

The initial and boundary conditions are:

$$T(x,0) = T_o \quad (8a)$$

$$\partial T/\partial x(-a,t) = \partial T/\partial x(a,t) = 0 \quad (8b)$$

Solution of Eq. (3) for the boundary conditions of Eq. (8) yields:

$$T(x,t) = T_o + \sum_{n=0}^{\infty} C_n e^{-\kappa\lambda_n^2 t} \cos\{\lambda_n(x + a)\} - \frac{q_o\varepsilon}{k}\left[\frac{e^{-\mu(x+a)}}{\mu} - \frac{(x+a)^2}{4a}(1 - e^{-2\mu a}) + (x + a)\right] + \frac{\kappa q_o\varepsilon}{2ak}(1 - e^{-2\mu a})t \quad (9)$$

where:

$$C_n = \frac{q_o\varepsilon}{ak}\left[\frac{1 - (-1)^n e^{-2\mu a}}{\mu^2 + \lambda_n^2} - \frac{(-1)^n}{\lambda_n^2}(1 - e^{-2\mu a}) + \frac{(-1)^n - 1}{\lambda_n^2}\right], \quad n \neq 0 \quad (10a)$$

$$C_o = \frac{q_o \varepsilon}{2ak}\left[(1 - e^{-2\mu a})\left(\frac{1}{\mu^2} - \frac{2a^2}{3}\right) + 2a^2\right] \tag{10b}$$

and $$\lambda_n = n\pi/2a \text{ with } n = 0, 1, 2, 3 \ldots \tag{10c}$$

C. Derivation of the thermal stresses

From the known temperature distributions, the thermal stresses can be obtained from:[7]

$$\sigma_{y,z} = \frac{\alpha E}{1 - \nu}\left[-T + \frac{1}{2a}\int_{-a}^{a} T dx + \frac{3x}{2a^3}\int_{-a}^{a} T x dx\right] \tag{11}$$

where α is the coefficient of thermal expansion, E is Young's modulus and ν is Poisson's ratio.

For the two cooling conditions the stresses are as follows:

a. Finite heat transfer coefficient h.

For finite values of the heat transfer coefficient, from Eqs. (5) and (11), the thermal stresses can be derived to be:

$$\sigma_{y,z} = -\frac{\alpha E}{1 - \nu}\sum_{n=0}^{\infty} B_n(t)\cos\{\lambda_n(x + a)\}$$

$$+ \frac{\alpha E}{2a(1 - \nu)}\sum_{n=0}^{\infty}\frac{B_n(t)}{\lambda_n}\sin(2\lambda_n a)$$

$$+ \frac{3x\alpha E}{2a(1 - \nu)}\sum_{n=0}^{\infty} B_n(t)\left[\frac{\sin(2\lambda_n a)}{a\lambda_n} + \frac{1}{a^2\lambda_n^2}\cos(2\lambda_n a) - \frac{1}{a^2\lambda_n^2}\right] \tag{12}$$

with $B_n(t)$ and λ_n defined by Eq. (5).

For the special case of $h = \infty$ from Eqs. (7) and (11), the thermal stresses can be calculated to be:

$$\sigma_{y,z} = -\frac{\alpha E}{1-\nu}\sum_{n=\text{odd}}^{\infty}\frac{16q_o\varepsilon\mu a}{n^2\pi^2 k}\left[\frac{\mu + (n\pi/4a)e^{-2\mu a}}{\mu^2 + (n\pi/4a)^2}\left(1 - e^{-k\lambda_n^2 t}\right)\cos\{\lambda_n(x+a)\}\right]$$

$$+\frac{\alpha E}{1-\nu}\sum_{n=\text{odd}}^{\infty}\frac{8q_o\varepsilon\mu}{n^2\pi^2 k}\left[\frac{\mu + (n\pi/4a)e^{-2\mu a}}{\mu^2 + (n\pi/4a)^2}\frac{1}{\lambda_n}\left(1 - e^{-\kappa\lambda_n^2 t}\right)(-1)^{\frac{n-1}{2}}\right]$$

$$+\frac{3x\alpha E}{a^2(1-\nu)}\sum_{n=\text{odd}}^{\infty}\frac{8q_o\varepsilon\mu}{n^2\pi^2 k}\left[\frac{\mu + (n\pi/4a)e^{-2\mu a}}{\mu^2 + (n\pi/4a)^2}\left(1 - e^{-\kappa\lambda_n^2 t}\right)\left(\frac{a}{\lambda_n}(-1)^{\frac{n-1}{2}} - \frac{1}{\lambda_n^2}\right)\right] \quad (13)$$

The stresses attain their maximum value at $t = \infty$. For the maximum tensile stresses which occur at $x = -a$, Eq. (13) can be simplified for the optically thick ($\mu a \to \infty$) and the optically thin ($\mu a << 1$) plates as follows:

$$\sigma_{y,z}(-a,\infty) = 0 \qquad (\mu a \to \infty) \qquad (14a)$$

$$\sigma_{y,z}(-a,\infty) = \frac{0.2719\alpha E q_o \varepsilon \mu a^2}{(1-\nu)k} \qquad (\mu a << 1) \qquad (14b)$$

Setting $\sigma_{y,z}$ in Eq. (14) equal to the tensile strength, S_t, yields the maximum possible heat flux, q_{max}, to which the plate can be subjected without risk of failure under steady-state conditions ($t \to \infty$):

$$q_{max} \to \infty \qquad (\mu a \to \infty) \qquad (15a)$$

$$q_{max} = \frac{3.677 S_t (1-\nu)k}{\alpha E \varepsilon \mu a^2} \qquad (\mu a << 1) \qquad (15b)$$

b. Heat transfer coefficient h = 0.

For h = 0, the thermal stresses from Eqs. (9) and (11) can be derived to be:

$$\sigma_{y,z} = -\frac{\alpha E}{1-\nu}\left\{\sum_{n=1}^{\infty} C_n e^{-\kappa\lambda_n^2 t}\cos\{\lambda_n(x+a)\} - \frac{q_o\varepsilon}{k}\left[\frac{e^{-\mu(x+a)}}{\mu}\right.\right.$$

$$\left.\left. - \frac{(x+a)^2}{4a}(1-e^{-2\mu a}) + (x+a)\right]\right\}$$

$$+\frac{\alpha E}{1-\nu}\left[\frac{q_o\varepsilon}{2\mu^2 ak}(e^{-2\mu a}-1) + \frac{q_o\varepsilon a}{3k}(1-e^{-2\mu a}) - \frac{q_o\varepsilon a}{k}\right]$$

$$+\frac{3\alpha E x}{2(1-\nu)a^3}\left\{-\sum_{n=\text{odd}}^{\infty}\frac{2C_n e^{-\kappa\lambda_n^2 t}}{\lambda_n^2} + \frac{q_o\varepsilon}{\mu^3\kappa}\left[e^{-2\mu a}(\mu a+1) + (\mu a-1)\right]\right.$$

$$\left.+\frac{q_o\varepsilon a^3}{3k}(1-e^{-2\mu a}) - \frac{2q_o\varepsilon a^3}{3k}\right\} \qquad (16)$$

Eq. (16) can be simplified for an optically thick plate ($\mu a \to \infty$) and an optically thin plate ($\mu a \ll 1$). The maximum tensile stresses, which occur at $t = \infty$, are of primary interest.

For the optically thick plate the tensile thermal stresses have their maximum value at $x = 0$ and are given by:

$$\sigma_{y,z}(0,\infty) = \alpha E q_o \varepsilon a/12(1-\nu)k \qquad (\mu a \to \infty) \qquad (17a)$$

For the optically thin plate the tensile thermal stresses reach their maximum value at $x = -a$ and are given by:

$$\sigma_{y,z}(-a,\infty) = \alpha E q_o \varepsilon \mu a^2/(1-\nu)k \qquad (\mu a \ll 1) \qquad (17b)$$

In analogy to Eqs. (15a) and (15b), Eqs. (17a) and (17b), setting the maximum tensile stress, $\sigma_{y,z}$ equal to the tensile strength yields an expression for the maximum permissible radiation heat flux to which the plate can be subjected without risk of failure.

$$q_{max} = \frac{12 S_t (1-\nu)k}{\alpha E \varepsilon a} \qquad (\mu a \to \infty) \qquad (18a)$$

$$q_{max} = \frac{S_t (1-\nu)k}{\alpha E \varepsilon \mu a^2} \qquad (\mu a \ll 1) \qquad (18b)$$

III. Numerical results and discussion

The temperatures, thermal stresses and their time dependence for convenience are reported in terms of the non-dimensional temperature:

$$T^* = (T - T_o)k/\varepsilon q_o a \tag{19}$$

the non-dimensional thermal stress:

$$\sigma^* = \sigma(1 - \nu)k/\alpha E\varepsilon q_o a \tag{20}$$

and the non-dimensional time:

$$t^* = \kappa t/a^2 \tag{21}$$

For simplicity, the quantities T^*, σ^*, and t^* hereafter will be referred to as temperature, stress, and time, respectively. Because brittle ceramics generally fail in tension, the maximum tensile stresses are of primary interest.

The validity of the assumption that the stresses reach a value near or equal to their maximum value before the plate becomes hot enough that the re-emitted radiant energy must be taken into account, must be examined first. Most conveniently, this can be done for the extremes in the values of the heat transfer coefficient, i.e., $h = 0$ and $h = \infty$.

For $h = 0$, Figs. 1a and 1b show the maximum temperatures, which occur at $x = -a$, and maximum tensile thermal stresses, respectively, as a function of time, for several values of the optical thickness μa. The corresponding values for $h = \infty$ are shown in Figs. 2a and 2b. Table I lists the calculated surface temperatures for a value of incident heat flux, q_{max}, for a material with properties approximately corresponding to those of aluminum oxide. As indicated by the data in Table I, the

re-emitted heat flux is negligible compared to the incident heat flux at a time when the stresses are within 5 percent of their maximum value.

Examination of Figs. 1a and 1b show that for $h = 0$, after an initial transient, during which the stress reaches a maximum, the temperature increases linearly with time, because of the absence of cooling. In contrast, for $h = \infty$ as shown in Figs. 2a and 2b, both the temperatures and stresses after an initial transient reach steady-state values as $t^* \to \infty$.

A number of interesting features of the time dependence and the magnitude of the tensile stresses may be noted from Fig. 2b. First, the stresses increase with time to pass through a maximum followed by a decrease and then to rise again to a steady-state value as $t \to \infty$. This behavior is the direct result of a corresponding time dependence of the position within the plate at which the tensile stresses are a maximum.

Figure 2b also shows that the steady-state stresses ($t \to \infty$) increase with increasing value of optical thickness to reach a maximum at $\mu a \approx 2$, followed by a decrease as $\mu a \to \infty$. In fact, it can be shown that for $\mu a = \infty$, the steady-state thermal stresses are identically equal to zero. Furthermore, it may be noted that the steady-state stresses exceed the transient stresses or vice-versa, depending on the value of μa.

Figure 3 shows the time dependence of the stresses for $\mu a = 3$ and a range of values of the heat transfer coefficient. It can be noted that after an initial transient, the maximum tensile stress is independent of the value of h. As may be determined from the temperature solutions, the final steady-state temperatures at which the h-independent stress value occurs is inversely proportional to the heat transfer coefficient. With the exception of $h \approx 0$, these observations and conclusions can be shown to be valid for any value of μa.

Figure 4 summarizes the values of maximum tensile thermal stress as a function of optical thickness. For finite values of h or $h = \infty$, the steady-state stresses ($t \to \infty$) exceed the transient stresses for $0 < \mu a < \sim 10.7$. For $10.7 < \mu a < \infty$, the maximum transient stresses exceed the steady-state stresses. As discussed earlier, for $h = \infty$ (or finite) the stresses pass through a maximum at $\mu a \simeq 2$ and vanish for $\mu a = 0, \infty$. The data in Fig. 4 qualitatively are quite similar to the corresponding data obtained in the earlier study[5] for a symmetrically heated and cooled plate. The magnitude of maximum tensile stress found in the present study for the assymmetrically heated and cooled flat plate is less than that for the symmetrically heated and cooled plate. At least one reason for this difference is that in the assymmetrically heated and cooled plate the differential thermal strains within the plate in part can be accommodated by bending. This is not the case for symmetric heating and cooling.

Figure 5 shows the spatial distribution of the stresses at $t \to \infty$ for $h = \infty$ (or finite) for a number of values of μa. It is of interest to note that the maximum tensile stresses are formed in the front surface of the plate which is at the highest temperature. These results were unexpected and initially thought to be incorrect. However, a separate study devoted to this effect to be published elsewhere[8] showed that these results indeed were correct and could be attributed to the nature of the concavity of the temperature distribution. In principle, the present problem involves an assymmetrically non-uniform internal heat generation, which results in a temperature distribution which is concave downward. This temperature distribution contrasts with the usual concave upward temperature distributions found in many cases of thermal stresses with the heat exchanged only at the outside boundary of the structure.

A similar effect is noted for the stress distributions for h = 0 shown in Fig. 6, which indicated that at least for the small values of μa, the maximum tensile stress also is found at the position of maximum temperature at x = -a, i.e., the front surface of the plate.

The material properties which control the thermal stress resistance for the assymmetrically heated and cooled flat plate can be determined most conveniently from the equations for q_{max} for h = 0,∞ and the two limiting cases of the optically thin and thick plates. From these equations the following thermal stress resistance parameters can be obtained:

$$\{S_t(1 - \nu)k/\alpha E\mu\epsilon\} \qquad (h = 0,\infty;\ \mu a<<1) \qquad (22)$$

and

$$\{S_t(1 - \nu)k/\alpha E\epsilon\} \qquad (h = 0;\ \mu a \to \infty) \qquad (23)$$

These parameters indicate that high thermal stress resistance for heating and cooling requires high values of tensile strength and thermal conductivity in combination with low values of the coefficient of thermal expansion, Young's modulus, absorption coefficient and emissivity (high values of reflectivity). It should be noted that for h = 0 and μa<<1, thermal stress resistance is inversely proportional to the first power of the absorption coefficient. This contrasts with the findings for the symmetrically heated plate with h = 0 and μa<<1, which showed that the thermal stress resistance was an inverse function of the cube of the absorption coefficient. This suggests that in general the relative role of the material properties which effect the thermal stress resistance of brittle ceramics is a function of the specific heating and cooling conditions and will require analysis for each individual case.

It should be noted that the material requirements for high thermal stress resistance may be incompatible with the material requirements for other performance criteria. For high efficiency of flat plate solar collectors, it will be required to have high values of the absorption coefficient and emissivity to keep the amount of transmitted and reflected radiation to a minimum. Clearly, for the selection of materials for solar energy collectors trade-offs between maximum thermal stress resistance and collector efficiency will have to be made. Similar trade-offs of perhaps another nature may have to be made for aerospace structures of components subjected to intense radiation from solar or other sources.

Focussing attention on the absorption coefficient, Fig. 4 suggests that for a non-zero heat transfer coefficient and steady-state operation, intermediate values of the optical thickness, especially near $\mu a = 2$, should be avoided. The incidence of thermal stress fracture can be minimized by either setting $\mu a \to 0$ or $\mu a \to \infty$. Zero stresses are obtained for the latter case because at steady-state ($t \to \infty$) the temperature distribution within the plate becomes linear and therefore stress-free. High values of the transient stresses can be minimized by gradually increasing the heat flux towards the final steady-state value rather than subjecting the plate to the full value of heat flux at $t = 0$.

The observation that the maximum tensile stresses occur at the hottest part of the plate (i.e., the front surface) could be critical for environmental conditions which promote fatigue by stress-corrosion or other mechanisms. Stress-corrosion generally is a thermally activated process and is expected to occur at a maximum rate for the temperature and stress distributions prevalent for the heating and cooling conditions

of the present study. The magnitude of temperature at which the plate operates, however, can be minimized by having a high value of the heat transfer coefficient. As noted earlier, the steady-state stress value is independent of the heat transfer coefficient, but the steady-state temperature level is inversely proportional to the heat transfer coefficient. It appears then that, in general, the incidence of thermal stress fracture in brittle ceramic flat plates subjected to radiation heating can be kept to a minimum by a judicious selection of materials, in combination with the optimum choice of optical thickness and cooling conditions.

Acknowledgments

The present study was conducted as part of a larger research program on the thermo-mechanical and thermal behavior of high-temperature structural materials supported by the Office of Naval Research under contract N00014-78-C-0431.

Table I. Calculated Maximum Heat Flux and Temperatures in Partially Absorbing Flat Plate Assymmetrically Heated by Thermal Radiation at 95% of Value of Maximum Tensile Stress

Heat Transfer Coefficient Watts. cm^{-2} $°C^{-1}$	Optical Thickness (μa)	Time at 95% Stress (kt/a^2)	Max Heat Flux q_{max} Watts. cm^{-2}	Emitted Heat Flux Watts. cm^{-2}	Ratio Emitted to Incident Heat Flux (%)
0	5	0.5	275	1.77	0.64
∞	2	5.0	105	1.32	1.2

Property values chosen for calculation: S_t = 200 $MN.m^{-2}$; E = 4 x 10^5 $MN.m^{-2}$, ν = 0.25, k = 0.3 Watts. cm^{-1} $°C^{-1}$; ε = 0.9, α = 7 x 10^{-6} $°C^{-1}$, a = 1 cm, T_o = 273°K.

References

1. W. D. Kingery, "Factors Affecting the Thermal Stress Resistance of Brittle Ceramics," J. Amer. Ceram. Soc., 38(1) 3-15 (1955)

2. D. P. H. Hasselman, "Unified Theory of Thermal Shock Fracture Initiation and Crack Propagation in Brittle Ceramics," J. Amer. Ceram. Soc., 52(11) 600-04 (1969)

3. D. P. H. Hasselman, "Thermal Shock by Radiating Heating," J. Amer. Ceram. Soc., 46, 229-34 (1963)

4. D. P. H. Hasselman, "Theory of Thermal Stress Resistance of Semi-Transparent Ceramics Under Radiation Heating," J. Amer. Ceram. Soc., 49, 103-04 (1966)

5. D. P. H. Hasselman, J. R. Thomas, M. P. Kamat and K. Satyamurthy, "Thermal Stress Analysis of Partially Absorbing Brittle Ceramics Subjected to Symmetric Radiation Heating," J. Amer. Ceram. Soc. (in press)

6. H. S. Carslaw and J. C. Jaeger, Conduction of Heat in Solids, 2nd Ed., Oxford, at the Clarendon Press (1960) 510 pp.

7. B. A. Boley and J. H. Weiner, Theory of Thermal Stresses, John Wiley and Sons, New York, (1960) 586 pp.

8. K. Satyamurthy, D. P. H. Hasselman, and J. P. Singh, "Effect of Nature of Concavity of the Temperature Distribution on the Magnitude and Sign of Thermal Stress," (in preparation)

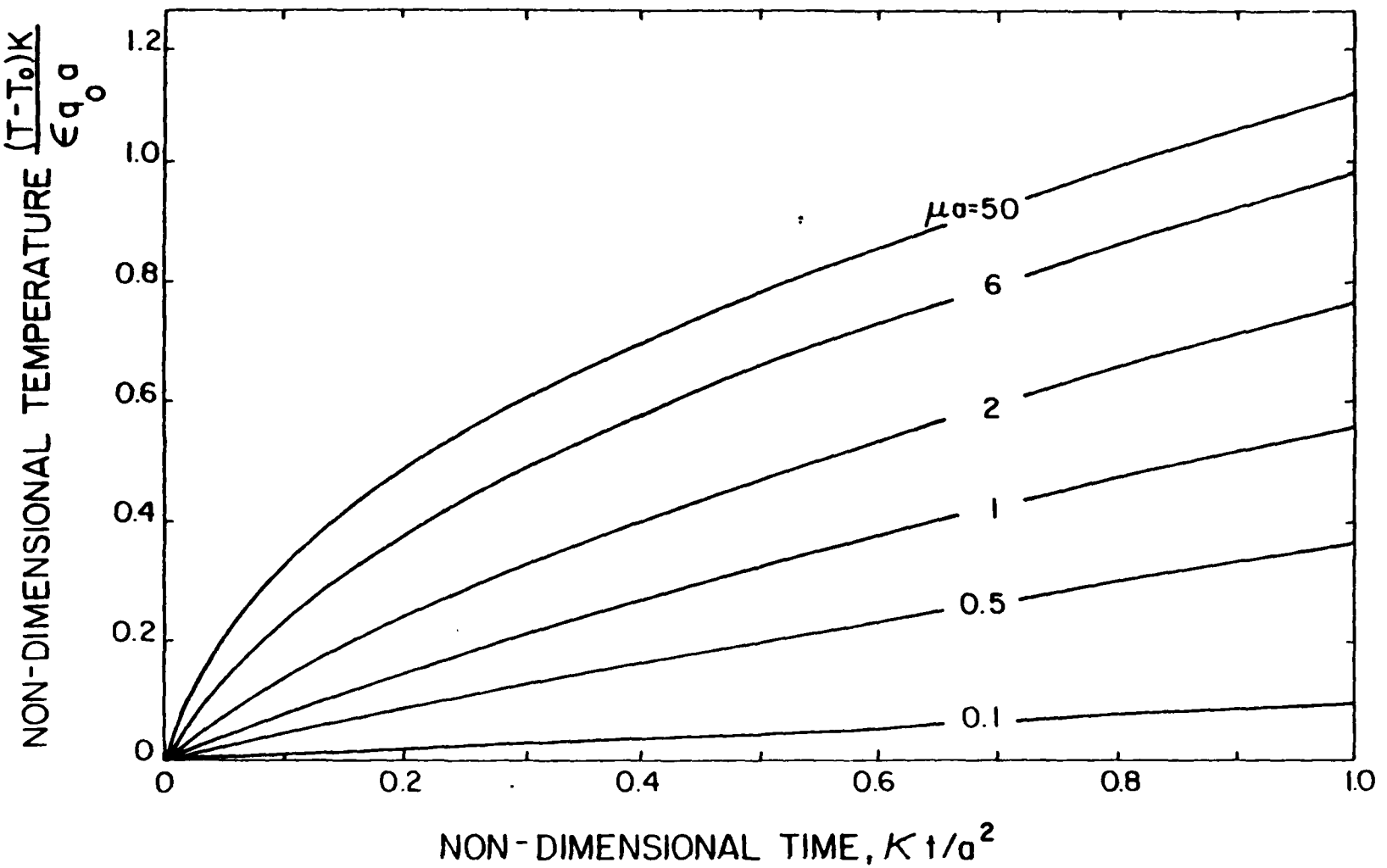

Figure 1a. Temperatures at the front face of partially absorbing flat plate assymmetrically heated in front by normally incident radiation and cooled at the rear surface by convection with heat transfer coefficient, h = 0, k = 0.3 watts. cm^{-1}. $^{\circ}c^{-1}$ and a = 1 cm.

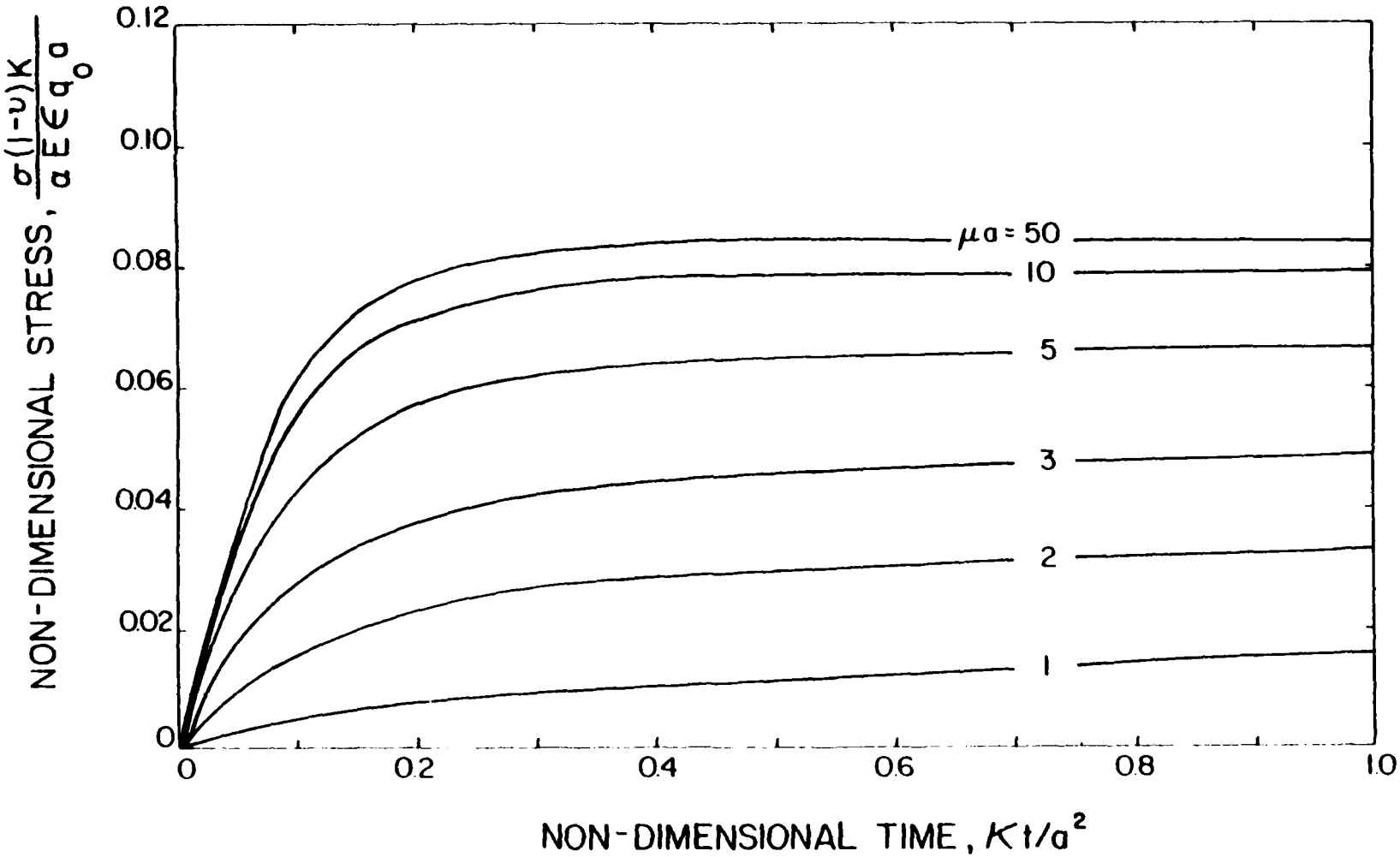

Figure 1b. Maximum tensile thermal stresses in a partially absorbing flat plate assymmetrically heated in front by normally incident radiation and cooled at the rear surface by convection with heat transfer coefficient, h = 0, K = 0.3 watts. cm^{-1}. $°c^{-1}$ and a = 1 cm.

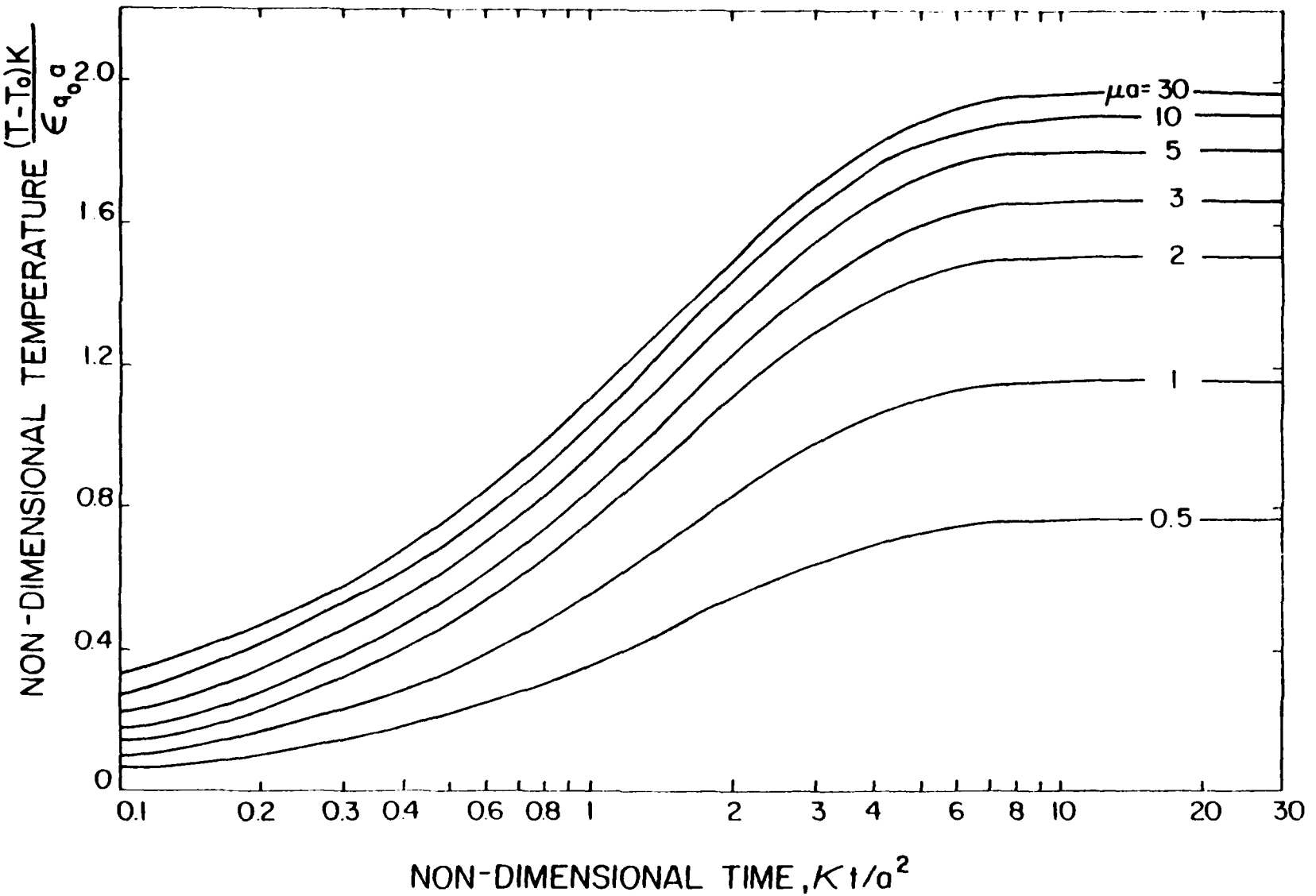

Figure 2a. Temperatures at the front face of partially absorbing flat plate assymmetrically heated in front by normally incident radiation and cooled at the rear surface by convection with heat transfer coefficient, h = ∞, K = 0.3 watts. cm^{-1}. $°c^{-1}$ and a = 1 cm.

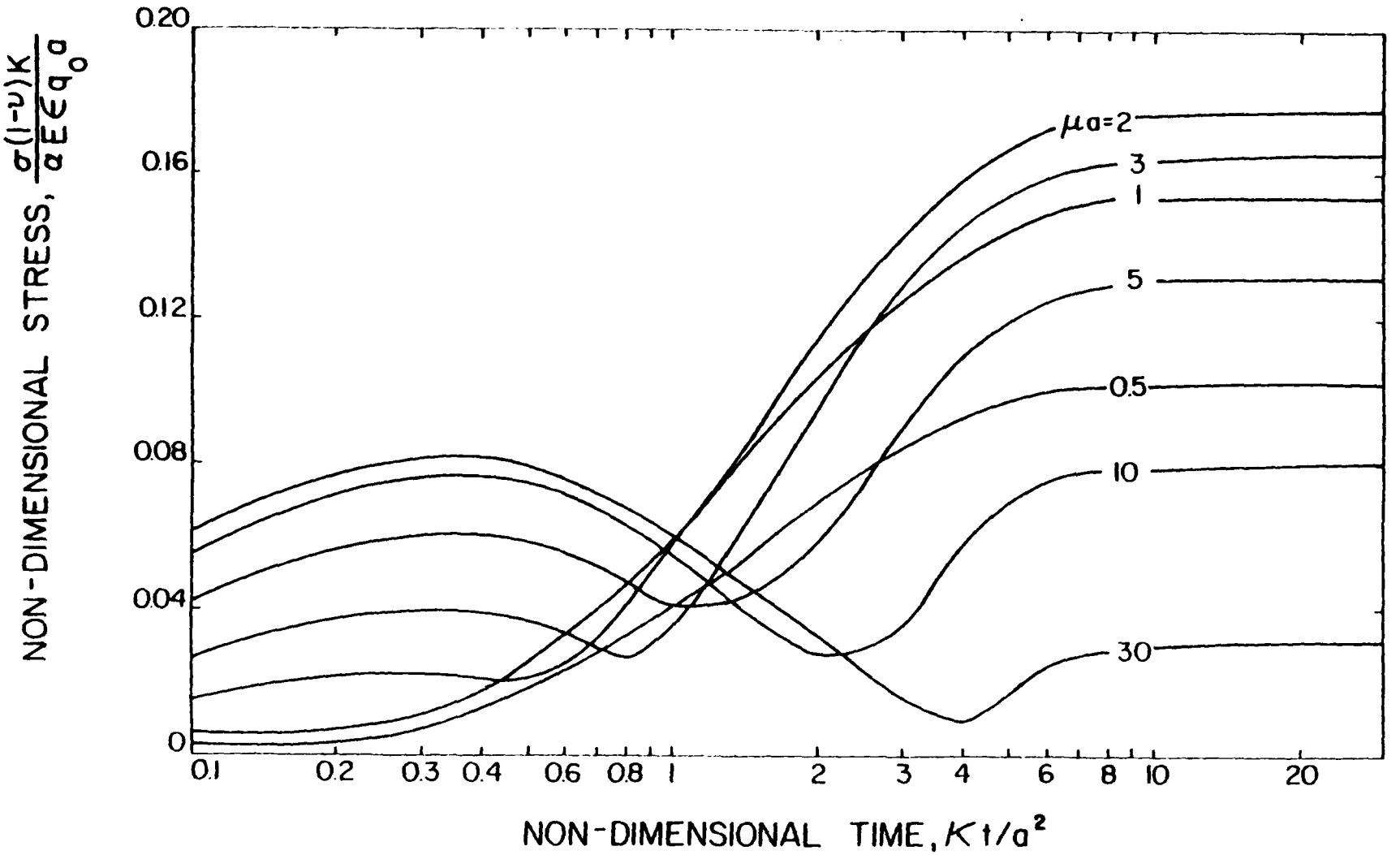

Figure 2b. Maximum tensile thermal stresses in a partially absorbing flat plate assymmetrically heated in front by normally incident radiation and cooled at the rear surface by convection with heat transfer coefficient, h = ∞, K = 0.3 watts. cm^{-1}. $°c^{-1}$ and a = 1 cm.

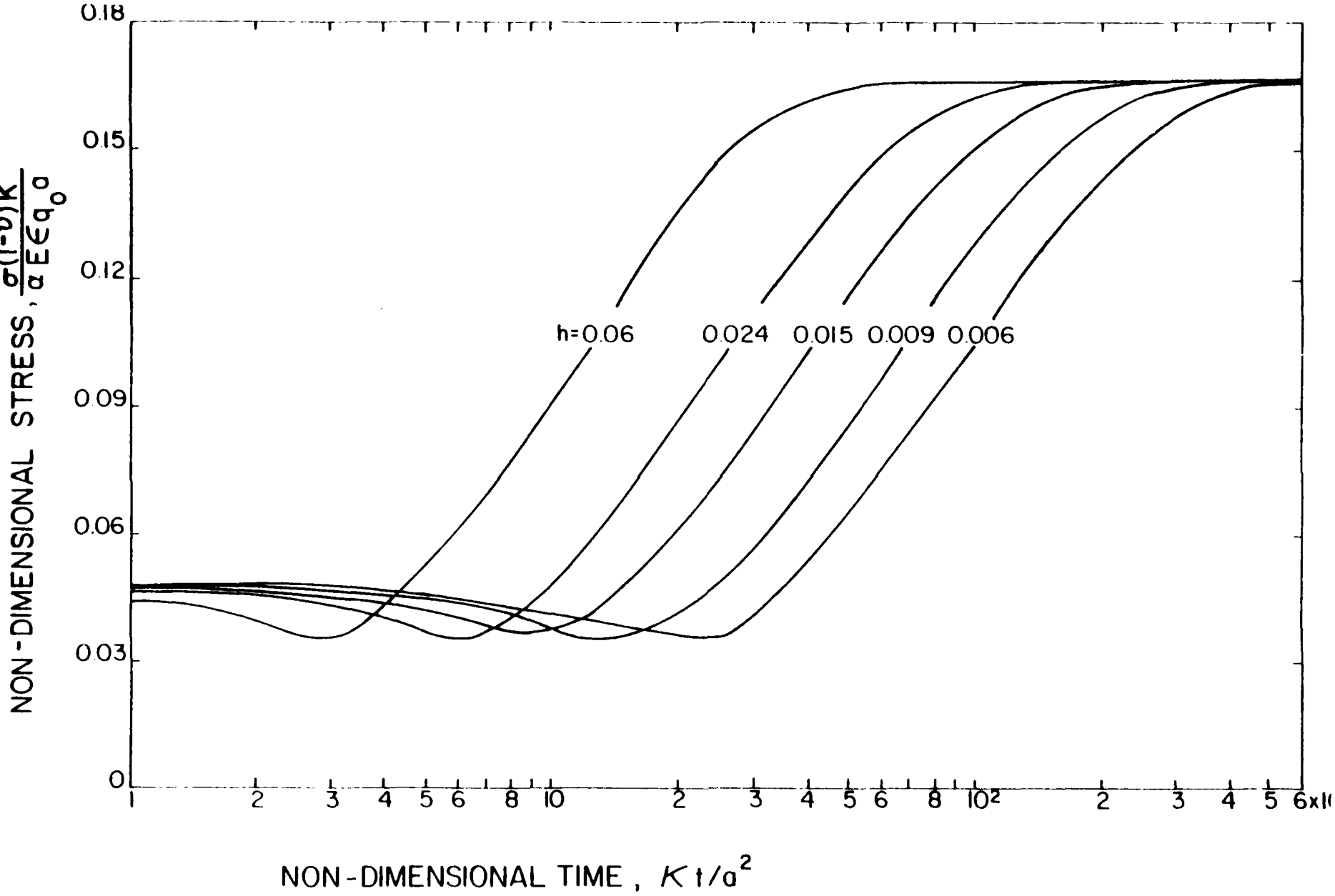

Figure 3. Time dependence of maximum tensile thermal stress in a partially absorbing flat plate with $\mu a = 3$, assymmetrically heated in front by normally incident radiation and cooled at the rear surface by convection for various values of heat transfer coefficient, h (watts. cm^{-2}. $°c^{-1}$) with K = 0.3 watts. cm^{-1}. $°c^{-1}$ and a = 1 cm.

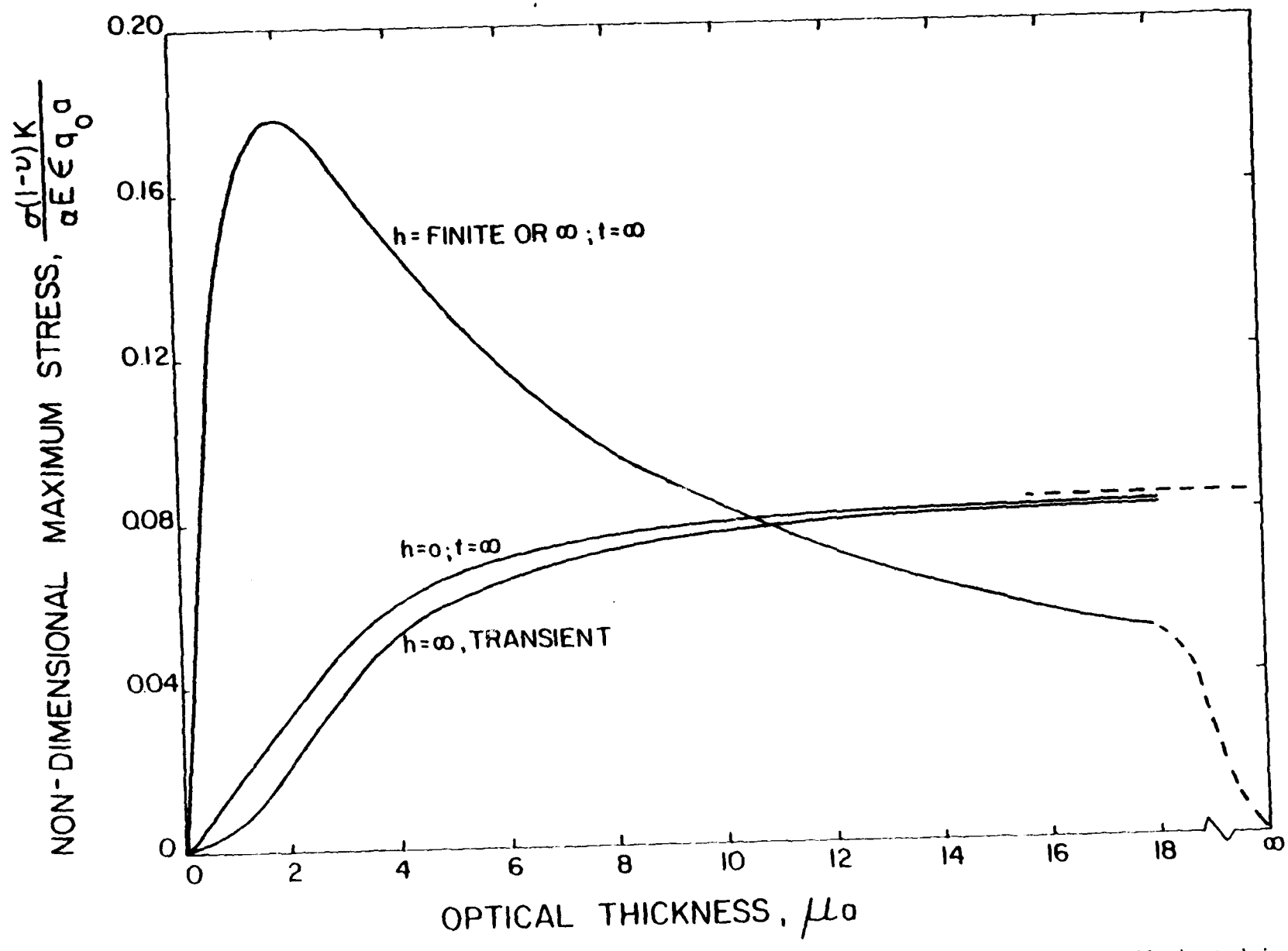

Figure 4. Maximum tensile thermal stresses in partially absorbing flat plate assymmetrically heated in front by normally incident radiation and cooled at the rear surface by convection with heat transfer coefficient, h = 0, ∞ and finite, K = 0.3 watts. cm^{-1}. $^{\circ}c^{-1}$ and a = 1 cm.

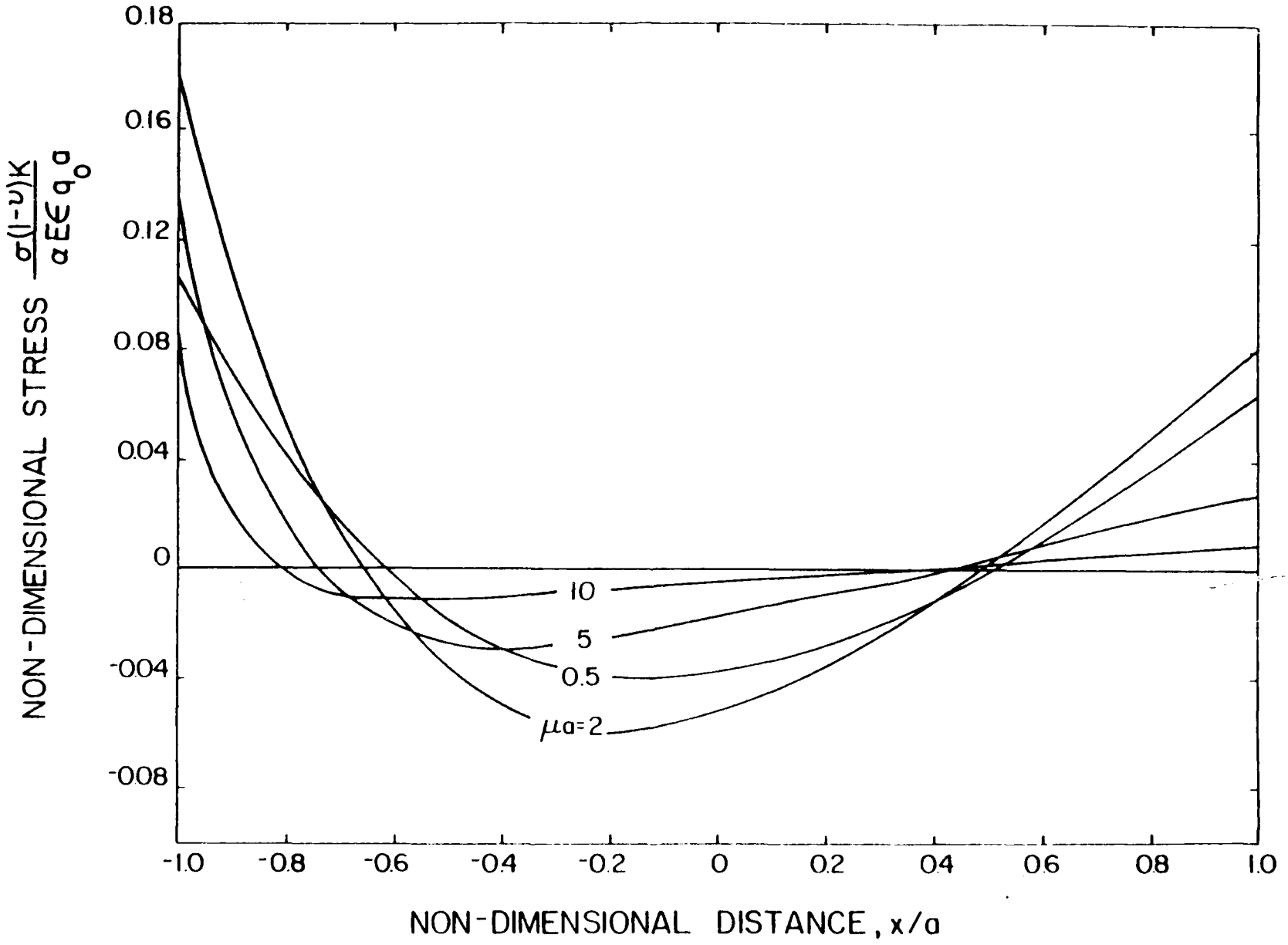

Figure 5. Spatial distribution of steady state (t = ∞) thermal stresses for various values of μa in a partially absorbing flat plate assymmetrically heated in front by normally incident radiation and cooled at the rear surface by convection with heat transfer coefficient h = ∞ (or finite), K = 0.3 watts. cm^{-1}. $°c^{-1}$ and a = 1 cm.

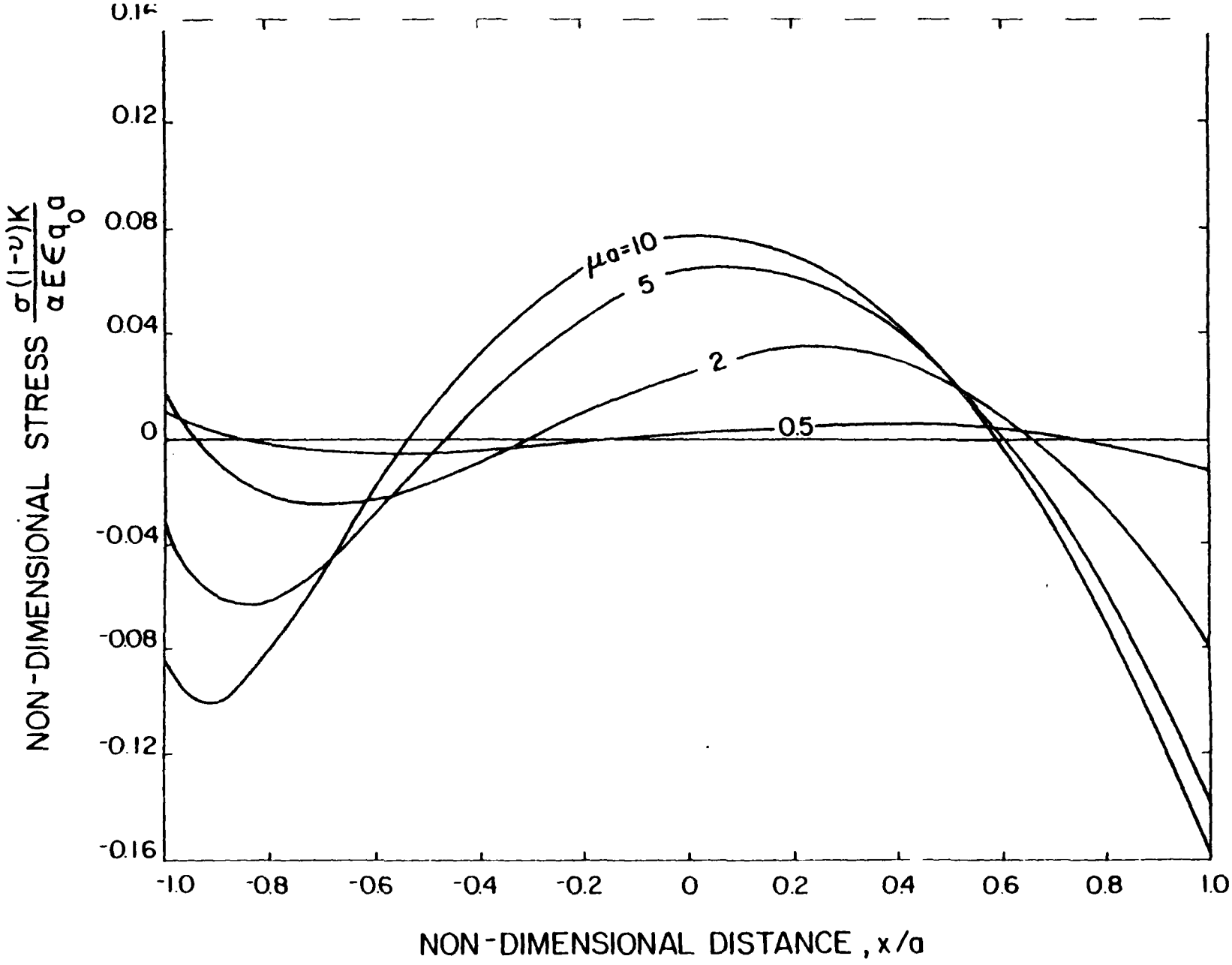

Figure 6. Spatial distribution of steady state (t = ∞) thermal stresses for various values of μa in a partially absorbing flat plate assymmetrically heated in front by normally incident radiation and cooled at the rear surface by convection with heat transfer coefficient, h = 0, K = 0.3 watts. cm^{-1}. $^{\circ}c^{-1}$ and a = 1 cm.

CHAPTER IX

OBSERVATIONS ON THE NATURE OF MICRO-CRACKING IN BRITTLE COMPOSITES

by

J. P. Singh, D. P. H. Hasselman, W. M. Su

Department of Materials Engineering
Virginia Polytechnic Institute and State University
Blacksburg, Virginia 24061

and

J. A. Rubin

Kyocera International, Inc.
San Diego, California 92123

and

R. Palicka

Ceradyne Inc.
Santa Ana, California 92705

ABSTRACT

The degree of micro-cracking in BeO-SiC composites under the influence of the internal stresses which arise due to mismatch in the coefficients of thermal expansion was studied by measuring thermal diffusivity of the composite as a function of SiC content. The experimental results on diffusivity measurement indicated that the micro-cracking was extensive at approx. 30 and 80% SiC content and minimum at ~ 50% SiC content. This was in agreement with similar observation of the effect of micro-cracking on strength, and fracture energy of other investigators.

A stress analysis indicated that these observations cannot be attributed to the difference in magnitude of internal stresses, but instead are thought to be due to statistical effects controlled by difference in stress-state in accordance with suggestions by Evans.

1. Introduction

The development of composites has led to materials with advantageous properties not found in single-phase materials. Mismatches in the coefficient of thermal expansion of the individual component within the composite can lead to the development of high levels of internal stresses on cooling the composite from its manufacturing temperature[1-7]. In composites in which one of the components is a polymer or a metal, relaxation of such internal stresses can occur by viscous or plastic flow even at relatively low temperatures. In brittle composites, internal stress relaxation can occur by diffusional creep, but only at high temperatures near the manufacturing temperature. Below these temperatures no stress relaxation can occur so that in brittle composites, for a given degree of mismatch of the coefficients of thermal expansion, the magnitude of the internal stresses will be particularly high. Such stresses, if sufficiently large, can lead to extensive "micro-cracking." Such micro-cracking can occur at the boundaries between the components or within the component with the higher coefficient of thermal expansion which generally is subjected to the high value of tensile stress. It should be noted that extensive micro-cracking can also occur in single phase non-cubic polycrystalline materials which exhibit a large degree of anisotropy in thermal expansion behavior[8,9].

Micro-cracking in brittle composites or polycrystalline materials is not necessarily disadvantageous. In fact, it can lead to major improvements in many engineering properties. As observed experimentally micro-cracking can lead to siginficant increase in fracture toughness[10], presumably due to the formation of a process-zone ahead of a propagating crack. Micro-cracking can also lead to major decrease in elastic behavior[10,11,12] and the thermal conductivity and diffusivity[13,14]. Due to a large increase in the strain-at-

fracture in combination with a stable mode of crack propagation, micro-cracked solids appear to be excellent candidate materials for applications at high temperature involving severe thermal shock[15,16]. In particular, micro-cracked materials probably are the only class of engineering materials appropriate for conditions which require high thermal shock resistance in combination with good thermal insulating ability[16]. Finally, micro-cracking can enhance the machinability of brittle materials substantially to an extent that they can be shaped by conventional metal working techniques[17].

As indicated by a large number of literature studies[1-9], methods for the calculation of the magnitude and distribution of internal stresses which arise from non-uniformities of the coefficients of thermal expansion in composites or poly-crystalline materials appear to be well developed. In general, these calculations show that the magnitude of these internal stresses is a function of the mismatch or degree of anisotropy of the thermal expansion coefficients, the range of temperature over which the composite or polycrystalline material is cooled without any stress relaxation, as well as the phase distribution of the individual components or the relative orientation of the individual grains within the poly-crystal. Of significance to the present study is that these studies show that the magnitude of the internal stresses for a given composite or non-cubic polycrystalline material is not a function of the size of the components or the grains. For this reason, if micro-cracking were controlled solely by the magnitude of internal stress, the degree of micro-cracking in terms of the number of micro-cracks formed should be independent of the scale of the microstructure.

This latter conclusion, however, is in contradiction with experimental observations. As observed by Davidge and Green[18], for a continuous matrix dispersed phase system, a minimum dispersion size was necessary for micro-

cracking to occur. Also, in polycrystalline materials with high thermal expansion anisotropy, a critical grain size is required before micro-cracking can take place. It appears then that the presence of internal stresses is a necessary but not sufficient condition for micro-cracking and that other factors need to be considered.

In providing an explanation for their observations, Davidge and Green[18] noted that the elastic energy available for crack propagation was proportional to the third power of the inclusion size. However, the total energy required to propagate a radial crack is proportional to the crack size. For this reason, below a given inclusion size insufficient elastic energy was available for the formation of a micro-crack of sufficient size to give sufficient stress relief. A similar explanation was offered by Kuszyk and Bradt[10] to explain the grain size effect on micro-cracking in polycrystalline single phase materials. It should be noted, however, that this explanation considers only the energy conditions after microcrack-formation, but does not address the condition of the onset of formation of micro-cracks.

Lange[19] based his analysis of micro-crack formation on an energy balance approach and found that below a given value of the product of the square of the stress and the particle radius, micro-crack formation cannot occur of the size of the pre-existing flaw from which the micro-crack originated.

More recently, Evans[9] pointed out that micro-crack formation most likely occurs from precursor flaws in the form of pores at grain-boundaries or triple points. The size of such pore frequently is directly related to the grain size. For this reason, the larger the grain for a given level of internal stress, the larger will be the stress intensity factor (K_I) for the precursor flaw. Micro-cracking will occur whenever $K_I \geq K_{Ic}$, the critical stress intensity factor. This latter mechanism provides a ready explanation

for the observed component or grain size effect on the incidence of micro-cracking in brittle materials. It is expected that micro-cracking originating from grain-boundary pores would be governed by statistical variables such as the size distribution and orientation of the pores as well as the magnitude and distribution of the internal stresses. Experimental data in support of this hypothesis are presented in the present paper.

2. Experimental

2.1 Materials and Experimental Method

Nearly fully-dense samples of composites of BeO and SiC made by hot-pressing were obtained from a commercial source.* Specimens of fully dense SiC made by conventional sintering were obtained as well. Figure 1 shows scanning electron micrographs of composites containing 30, 50 and 80 wt.% SiC. The grain size of BeO and SiC was below 5 μm. Due to the relatively large mismatch in their coefficients of thermal expansion, BeO-SiC composites exhibit extensive micro-cracking. As shown in Fig. 1, the isolated inter-grannular cracking is frequently observed to initiate from a triple point and propagate along one or two adjacent grain faces in agreement with Evans[7].

As shown analytically[20], micro-cracking has a pronounced effect on thermal conductivity. For this reason, the degree of micro-cracking was monitored by measurements of the thermal diffusivity by the laser-flash method[21], using equipment described elsewhere[13]. Measurements were made over the range of temperature from about 300 to 1400°C. One particular advantage of using the measurement of thermal diffusivity for monitoring the extent of micro-cracking is that the results are not affected by additional micro-crack formation due to mechanical loading as is expected to be the case during measurements of strength and fracture toughness.

*Ceradyne, Inc., Santa Ana, CA, USA; Code Ceralloy 2700 Series.

2.2 Experimental Results

Figure 2 shows the experimental data for the thermal diffusivity as a function of temperature for BeO, SiC and two of the BeO-SiC composites. The data shown in Fig. 2 were obtained by heating the specimens slowly from room temperature to 1400°C. On cooling a hysteresis effect was noted. A detailed nalysis of this latter observation is deferred to a later publication.

Figure 3 shows the thermal diffusivity as a function of SiC content for a number of temperatures as obtained by smooth curves drawn through the experimental data.

Figure 4 shows the value of the thermal conductivity (K) at 400°C calculated from the corresponding curve for the thermal diffusivity in Fig. 3 using the relation:

$$K = \alpha \rho c \qquad (1)$$

where α is the thermal diffusivity, ρ is the density and c is the specific heat. Latter two values as a function of SiC content were assumed to vary linearly between the end values for SiC and BeO.

Included in Fig. 4 is the value for the thermal conductivity as a function of SiC content for a non-microcracked composite calculated from the Rayleigh-Maxwell relation[22,23]

$$K_c = K_m \frac{1+2V(1-K_m/K_p)/(2K_m/K_p+1)}{1-V(1-K_m/K_p)/(K_m/K_p+1)} \qquad (2)$$

where K is the thermal conductivity, the subscripts c, m and p refer to the composite, matrix and dispersed phase, resp. For the numerical calculation of conductivity by eq. 2 the following data were used: SiC, ρ = 3.21 gm/cc, c = 0.255 cal $gm^{-1}{}^{\circ}K^{-1}$ and BeO, ρ = 3.008 gm/cc, c = 0.408 cal $gm^{-1}{}^{\circ}K^{-1}$.

3. Discussion and Conclusions

The discussion will primarily concentrate on the microstructural and mechanical variables which affect the formation of micro-cracks. A comparative study of the effect of micro-cracking on heat transport properties for a number of different micro-cracked composites is deferred to a subsequent publication.

The thermal conductivity for the BeO-SiC composites calculated from the Rayleigh-Maxwell theory varies monotonically between the values of the thermal conductivity of the BeO and SiC. In fact regardless of the phase-distribution of each component, the composite thermal conductivity should fall between the corresponding values of the two components[24]. For this reason the value for K for the SiC represents the lower bound on the thermal conductivity of the composite regardless of volume fraction. However, the variation of the thermal conductivity as a function of silicon carbide content inferred from the experimental data for the thermal diffusivity lies below the value for the SiC. Since these composites are fully-dense (or nearly so), this effect cannot be attributed to the presence of a pore phase. Instead, the decrease of the thermal conductivity must be attributed to the presence of the micro-cracks.

It is of particular interest to note that the decrease in thermal conductivity is most pronounced at approximately 30 and 80 % SiC. In contrast, at approximately 50% SiC the decrease in thermal conductivity is rather small, if existent at all. This observation suggests that micro-cracking is most pronounced at 30 and 80% content of SiC and appears to be absent at approximately 50% SiC. Support for this latter conclusion is provided by experimental data[25] made available to the present authors prior to future publication in detail at a later date, for the strength and fracture energy for these composites.

At approximately 20 and 75% SiC, these composites have higher values for tensile strength (measured in bending) and fracture energy as compared to the values for single phase SiC and BeO. At 40% SiC, however, the values of strength are comparable. In other words, at these compositions which exhibit a decrease in thermal conductivity, a corresponding increase in strength and fracture energy is found. The minima in the strength and fracture energy plots, however, occur at a slightly lower SiC content than the corresponding SiC content for the maxima in the diffusivity plot. This is believed to be due to the fact that during the strength and fracture energy measurements additional micro-cracks could have been formed during the loading period. These opposite effects are entirely consistent with the presence of micro-cracks which are known to enhance fracture toughness[10] and to decrease the thermal conductivity[9]. Further supporting evidence for the low degree of micro-cracking can be obtained from the experimental data for the coefficient of thermal expansion of BeO-SiC composites measured by Rossi[26]. At 50 vol.% SiC the coefficient of thermal expansion lies relatively much closer to the coefficient of thermal expansion calculated from composite theory than at 25 and 75% SiC.*

As shown analytically, the effect of randomly oriented circular cracks of equal size on thermal conductivity is given by[16]:

$$K = K_0[1 + 8\ Nb^3/9]^{-1} \qquad (3)$$

where N is the number of cracks per unit volume, and b is the crack radius. Unfortunately, the density, size and geometry of the micro-cracks cannot be

*It should be noted that Rossi draws a smooth curve through his data. Close examination of the experimental data, however, suggests that a better curve would have the same general form as the curves in Figure 3.

determined with any accuracy by metallographic methods. For this reason, the decrease in thermal conductivity cannot be estimated from prior information. Instead, from eq. 3, the value of Nb^3 can be assessed from the experimental data for thermal diffusivity. These results are shown in Fig. 5 for the case of uniformly distributed micro-cracks within the composite as a whole. Since the micro-cracks are more likely to be found within the BeO phase, Nb^3 was also evaluated by means of eq. 2 in which the thermal conductivity of the BeO phase was assumed to be given by eq. 3. As indicated in Fig. 5, the value of Nb^3 for micro-cracks in the BeO phase can go to high values, as expected, since at the higher fractions of SiC the BeO will exhibit the highest degree of micro-cracking. A value of $Nb^3 \simeq 0.5$ for uniformly distributed micro-cracking at ~ 80 SiC content suggests that for a micro-crack radius equal to the grain size (~ 5μm) approximately one half of the BeO grains contain a micro-crack. It should be noted that an estimate of the thermal conductivity of a micro-cracked composite obtained by substitution of eq. 3 in eq. 2 for the conductivity of the micro-cracked phase assumes that the effect of the micro-cracking and the presence of the dispersions on the thermal conductivity, in fact, are uncoupled. This latter assumption, however is not expected to be valid since the micro-cracking in the BeO phase is expected to occur in the immediate vicinity of the SiC matrix. An analysis of the coupling effect of dispersions and micro-cracking on thermal conductivity is recommended as a fruitful area for further theoretical and experimental work.

The question as to why at the intermediate volume fractions of the SiC phase micro-cracking appears to be largely absent, still remains to be answered. To find a solution to this problem, the internal stresses at the BeO-SiC interface were calculated for a composite sphere model in which either

the BeO or the SiC represents the outer layer. With SiC on the inside represents the SiC-BeO composite with low volume fractions of SiC. With the BeO on the inside of the composite, represents the microstructure at high volume fractions SiC at which the BeO takes the form of the dispersed phase. At infinite dilute volume fractions the answers obtained agreed with those obtained from solutions presented by Selsing[1]. Figure 6 shows the tensile radial and tangential stresses as a function of volume fraction SiC for the BeO or SiC as the outside layer of the composite sphere. It may be noted that the stresses increase linearly with increasing volume fraction SiC. Clearly, no reason exists for the absence of micro-cracking at the intermediate volume fractions of SiC.

A spherical composite model considered above, however, assumes that either the SiC or BeO phase is the dispersed phase over the total volume fraction of SiC. Near 50% SiC, however, BeO and SiC are both expected to be continuous. For this reason, a composite cylinder model for the assessment of the internal stresses appears more appropriate.

For such a composite cylinder model, solutions for the internal stresses due to the mismatch of coefficients of thermal expansion were derived by Gatewood[27]. For the SiC-BeO system the magnitude of these tensile internal stresses (in the BeO phase) are shown in Fig. 7. Again, as for the composite sphere model, these stresses increase with increasing volume fraction SiC. At first sight, from the point of view of the magnitude of stress, no reason appears to exist as to why at approx. 50 vol.% SiC the micro-cracking seems suppressed. However, it is well known that fracture of brittle materials is governed by statistical variables affected by flaw size distribution, and orientation as well as by the stress state. In respect to this effect of stress state on failure probability, it should be noted that in the composite

sphere model the tensile stress in the BeO phase at the BeO-SiC interface is uniform bi-axial in nature. Therefore at a radially oriented pore at a triple point at the BeO-SiC interface, micro-crack formation can occur regardless of the pore's other orientation. For the composite cylinder, however, which more closely represents the microstructure of the BeO-SiC composite near 50 % SiC, the maximum tensile stress in the BeO appears in the axial direction. This axial stress is of a uniaxial nature. For this reason, at a flat pore oriented radially at the BeO-SiC interface, micro-crack formation can occur only if the plane of the pore is oriented perpendicularly to the axial direction. For this reason, the probability of micro-crack formation in the composite cylinder model is less than the corresponding probability in the composite sphere model. Since the composite cylinder model approached the phase distribution of the present composites near 50% SiC, the observations reported herein are consistent with expected behavior governed by statistical variables.

In general, then, the present results and discussion suggest that theories for the formation of micro-cracks based on the magnitude of stress, elastic energy principles or stress intensity approaches also should include the statistical aspects of brittle fracture such as the size distribution of the precursor flaws, their orientation as well as the stress-state of the residual stress fields.

Acknowledgments

The present study was conducted as part of a larger programme supported by the Office of Naval Research under contract No. 0014-78-C-0431. The specimens of the SiC-BeO composites were supplied by Ceradyne Corporation,

Santa Ana, California. The gift of a specimen of SiC by Carborundum Company, Niagara Falls, NY is gratefully acknowledged. The authors are indebted to Professor M. P. Kamat for his helpful suggestions.

References

1. J. Selsing, J. Am. Ceram. Soc., 44 (1961) 419.
2. R. M. Fulrath, Chptr. 32 in Mechanical Properties of Engineering Ceramics, W. W. Kriegel and H. Palmour III, Ed., Interscience Publishers, N.Y., London (1961).
3. W. D. Kingery, J. Am. Ceram. Soc., 40 (1957) 351.
4. R. A. Schapery, J. Comp. Mat. 2(1968) 380.
5. T. T. Wang and T. K. Kwei, J. Pol. Sc., 7 (1969) 889.
6. A. A. Fahmy and A. N. Ragai, J. Appl. Phys., 41 (1970) 5108.
7. I. M. Daniel, pp. 203-221 in Thermal Expansion 6 (1978) Plenum Publishing Corporation, N.Y.
8. W. R. Bussuem, Chptr. 10 in Mechanical Properties of Engineering Ceramics, W. W. Kriegel and H. Palmour III, Ed., Interscience Publ., N.Y., London (1961)
9. A. G. Evans, Acta Met., 26 (1978) 1845.
10. J. A. Kuszyk and R. C. Bradt, J. Am. Ceram. Soc., 56 (1973) 420.
11. E. A. Bush and F. A. Hummel, J. Am. Ceram. Soc., 41 (1958) 189.
12. S. L. Dole, O. Hunter, Jr., F. W. Calderwood and D. J. Bray, J. Am. Ceram. Soc., 61 (1978) 486.
13. H. J. Siebeneck, D. P. H. Hasselman, J. J. Cleveland and R. C. Bradt, J. Am. Ceram. Soc., 59 (1976) 241.
14. H. J. Siebeneck, D. P. H. Hasselman, J. J. Cleveland and R. C. Bradt, J. Am. Ceram. Soc., 60 (1977) 336.
15. D. P. H. Hasselman, J. Am. Ceram. Soc., 52 (1969) 600.
16. D. P. H. Hasselman and J. P. Singh, Ceram. Bull (in press).
17. R. C. Rossi, Private Communication.
18. R. W. Davidge and T. G. Green, J. Mat. Sc., 3 (1968) 629.

References (Cont'd)

19. F. F. Lange, pp. 599-609 in Fracture Mechanics of Ceramics, Vol. II, Plenum Press (1974).

20. D. P. H. Hasselman, J. Comp. Mat., 12 (1978) 403.

21. W. J. Parker, R. J. Jenkins, C. P. Butler and G. L. Abbott, J. Appl. Phys., 32 (1961) 1679.

22. L. Rayleigh, Phil. Mag., 34 (1892) 481.

23. J. C. Maxwell, A Treatise on Electricity and Magnetism, I, 3rd Ed., Oxford Press (1904).

24. A. E. Powers, Knolls Atomic Power Laboratory Report - KAPL-2145, General Electric Comp. (1961).

25. J. A. Rubin, Private Communication.

26. R. C. Rossi, J. Am. Ceram. Soc., 52 (1969) 290.

27. B. E. Gatewood, Thermal Stresses, McGraw-Hill (1957).

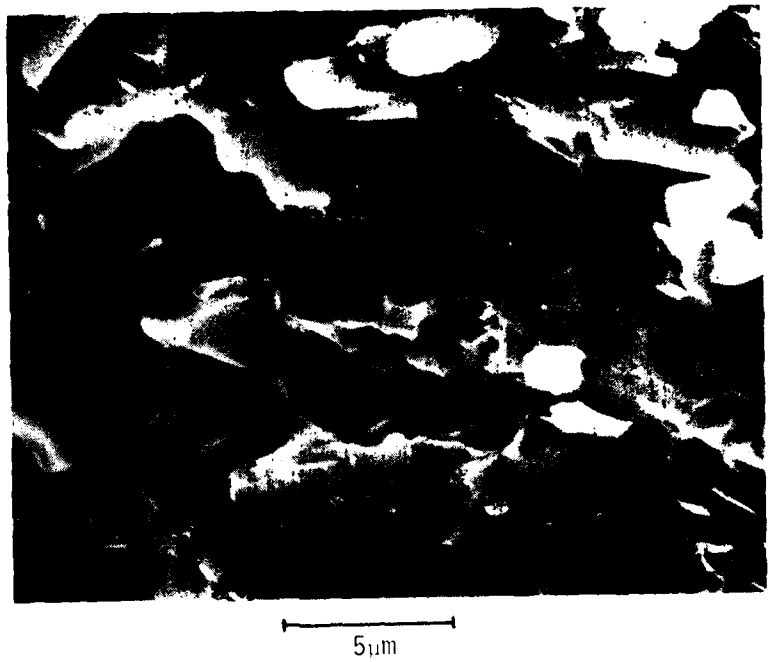

a

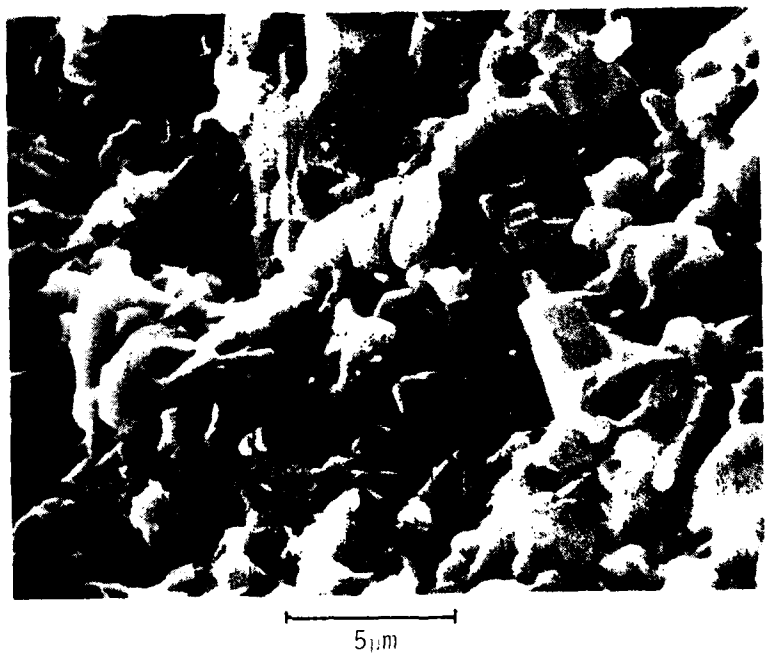

b

Fig. 1. Scanning electron fractographs of BeO-SiC composites showing the triple points and micro-cracks initiating from triple point. Composition: (a) 30% SiC and (b) 50% SiC by weight.

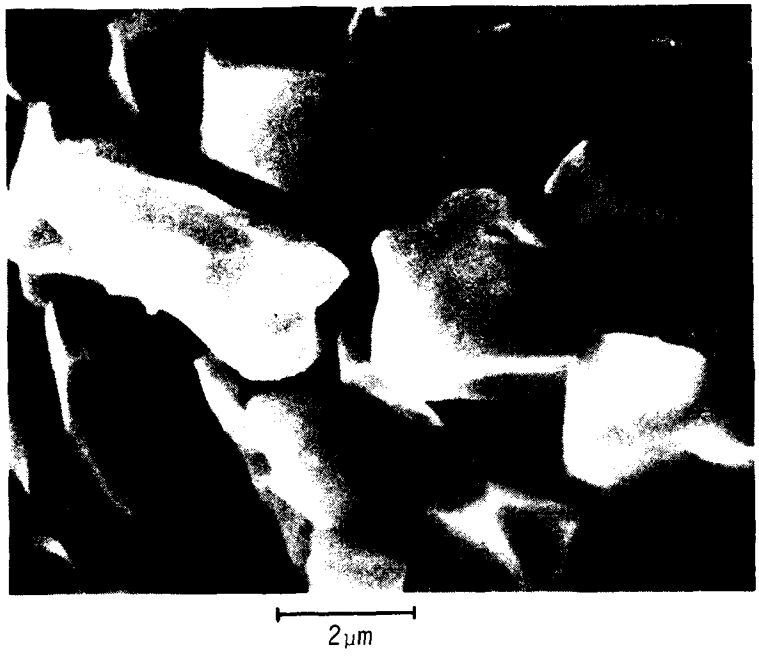

C

Fig. 1c. Scanning electron fractograph of BeO-SiC composite (containing 80% SiC by weight) showing the triple points and micro-cracks initiating from triple point.

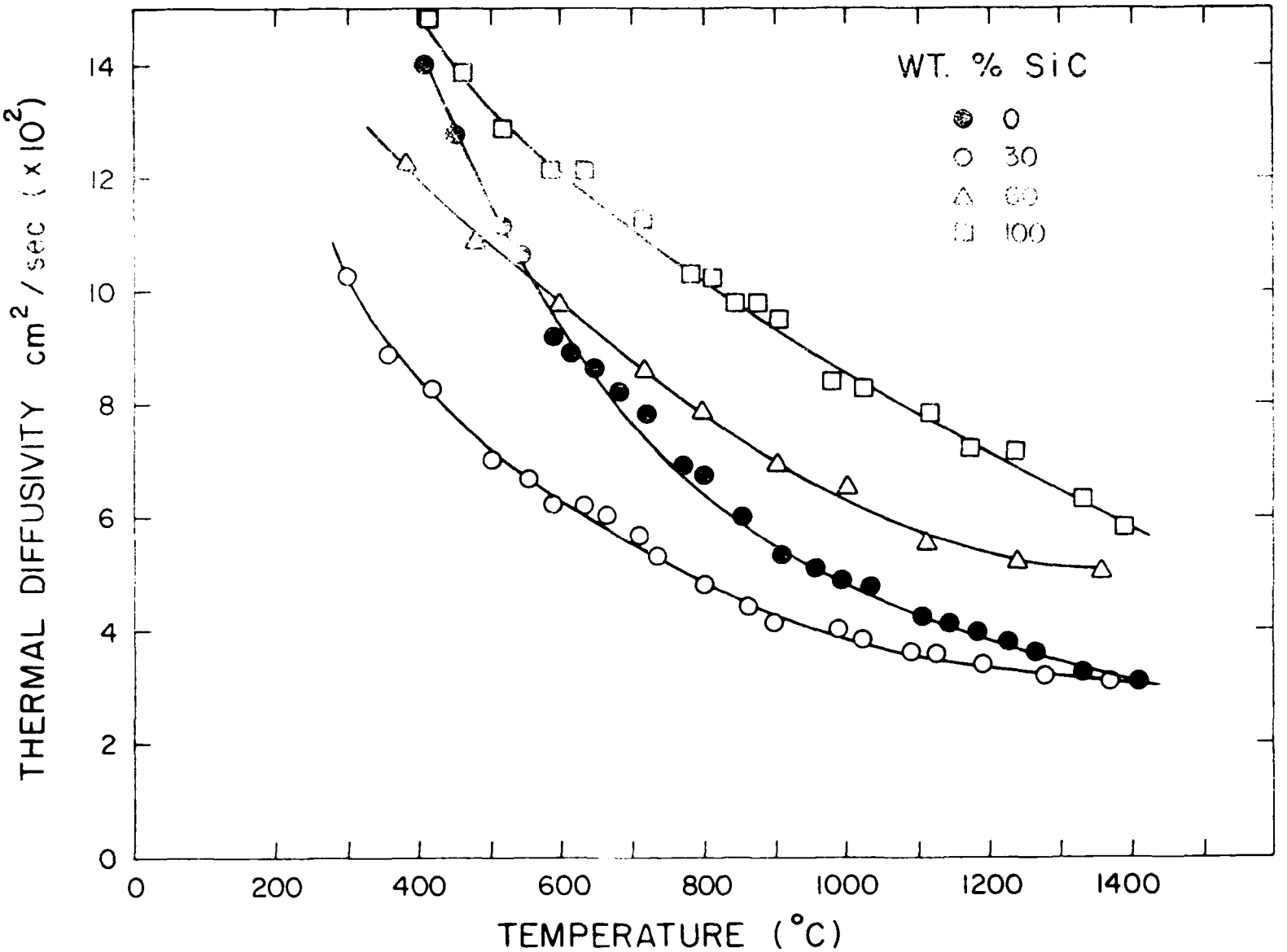

Fig. 2. Thermal diffusivity of BeO-SiC composites as a function of temperature.

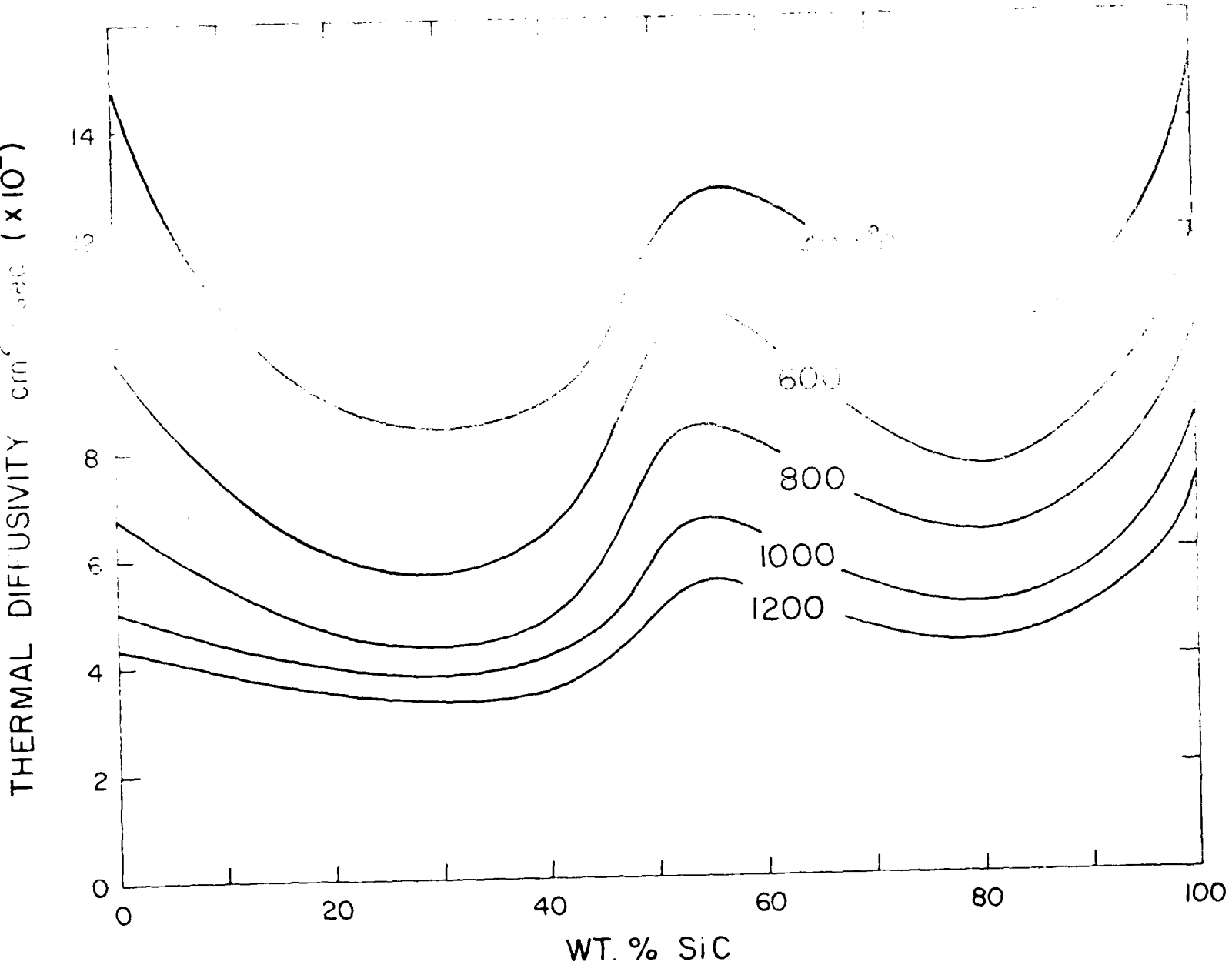

Fig. 3. Effect of SiC content on thermal diffusivity of BeO-SiC composites.

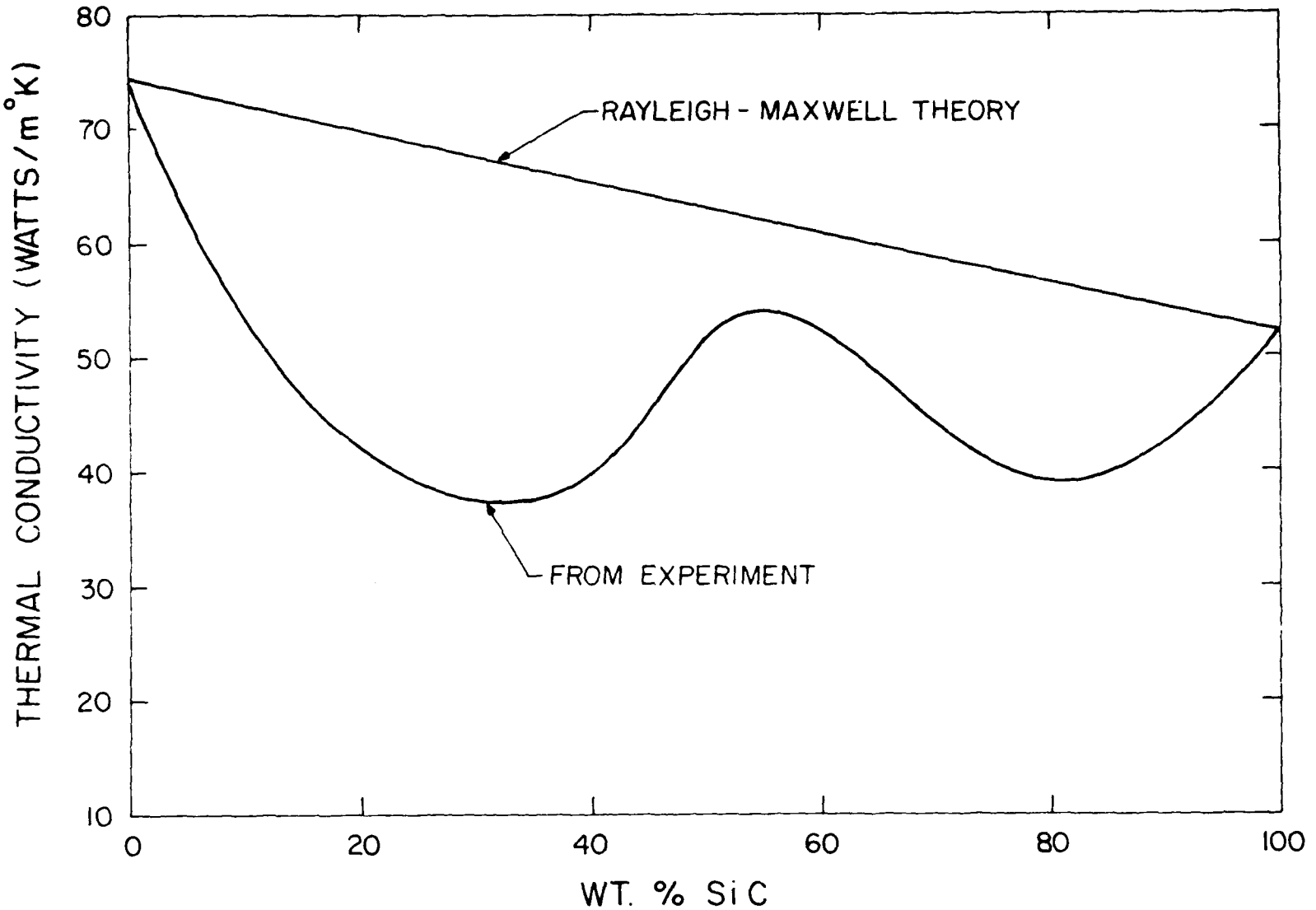

Fig. 4. The values of thermal conductivity of BeO-SiC composites as a function of SiC content calculated from the diffusivity values in Figure 3 at 400°C. Included in the figure is also the calculated values for thermal conductivity based on Rayleigh Maxwell theory.

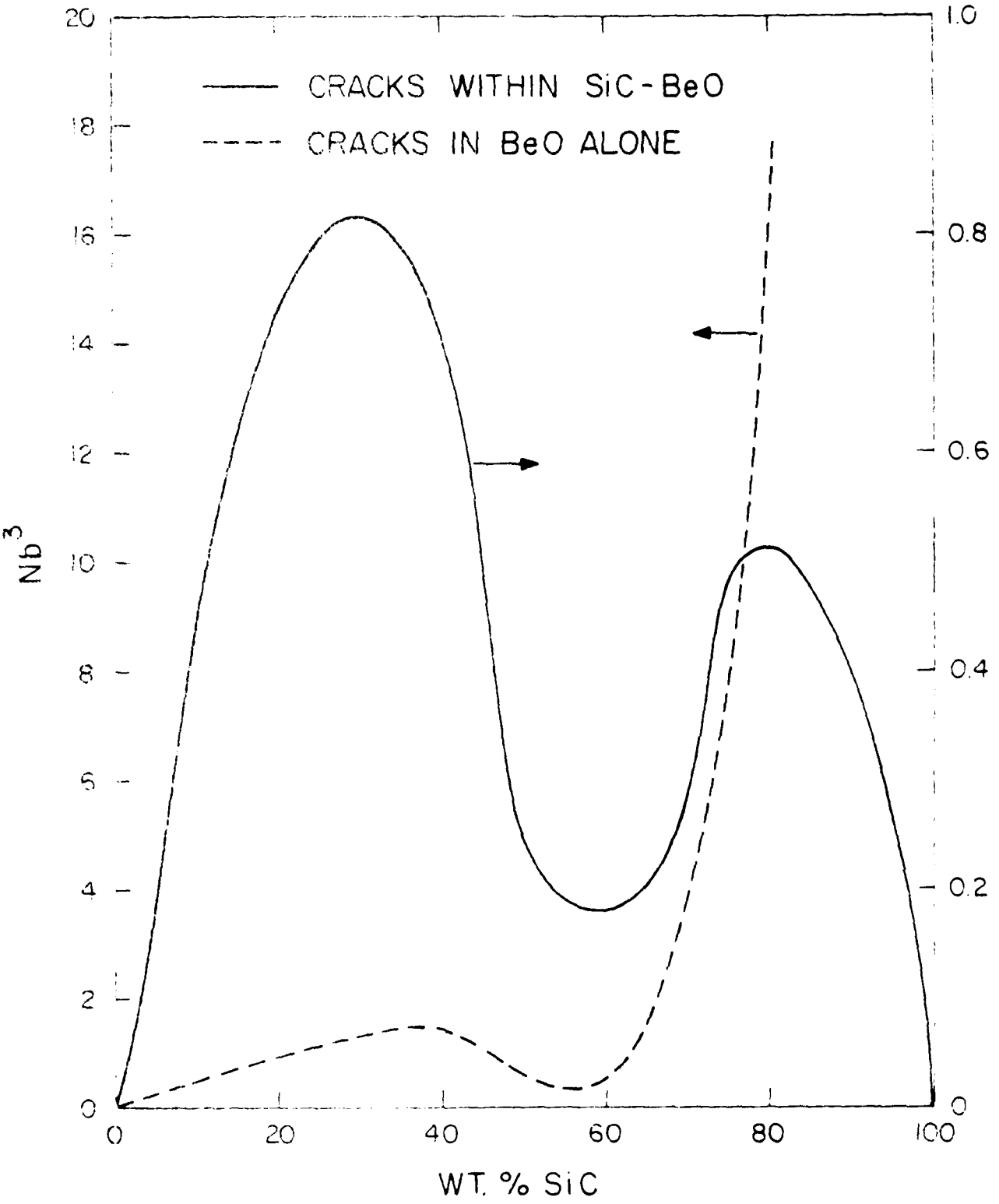

Fig. 5. The effect of SiC content on the values of Nb^3 as calculated from equations 2 and 3.

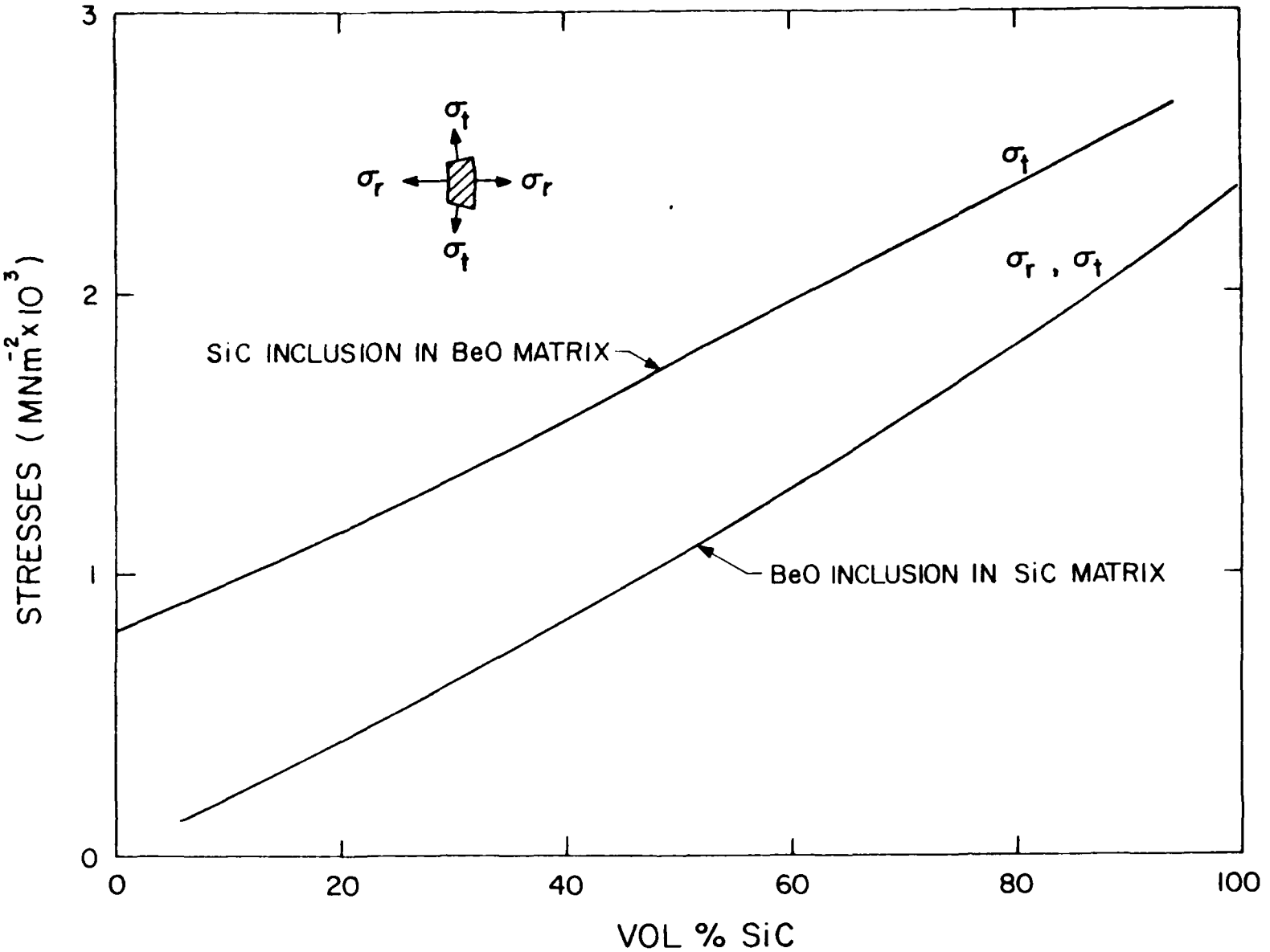

Fig. 6. Calculated values of tensile stresses in BeO phase at BeO-SiC interface based on composite sphere model. σ_r and σ_t represent radial and tangential stresses respectively.

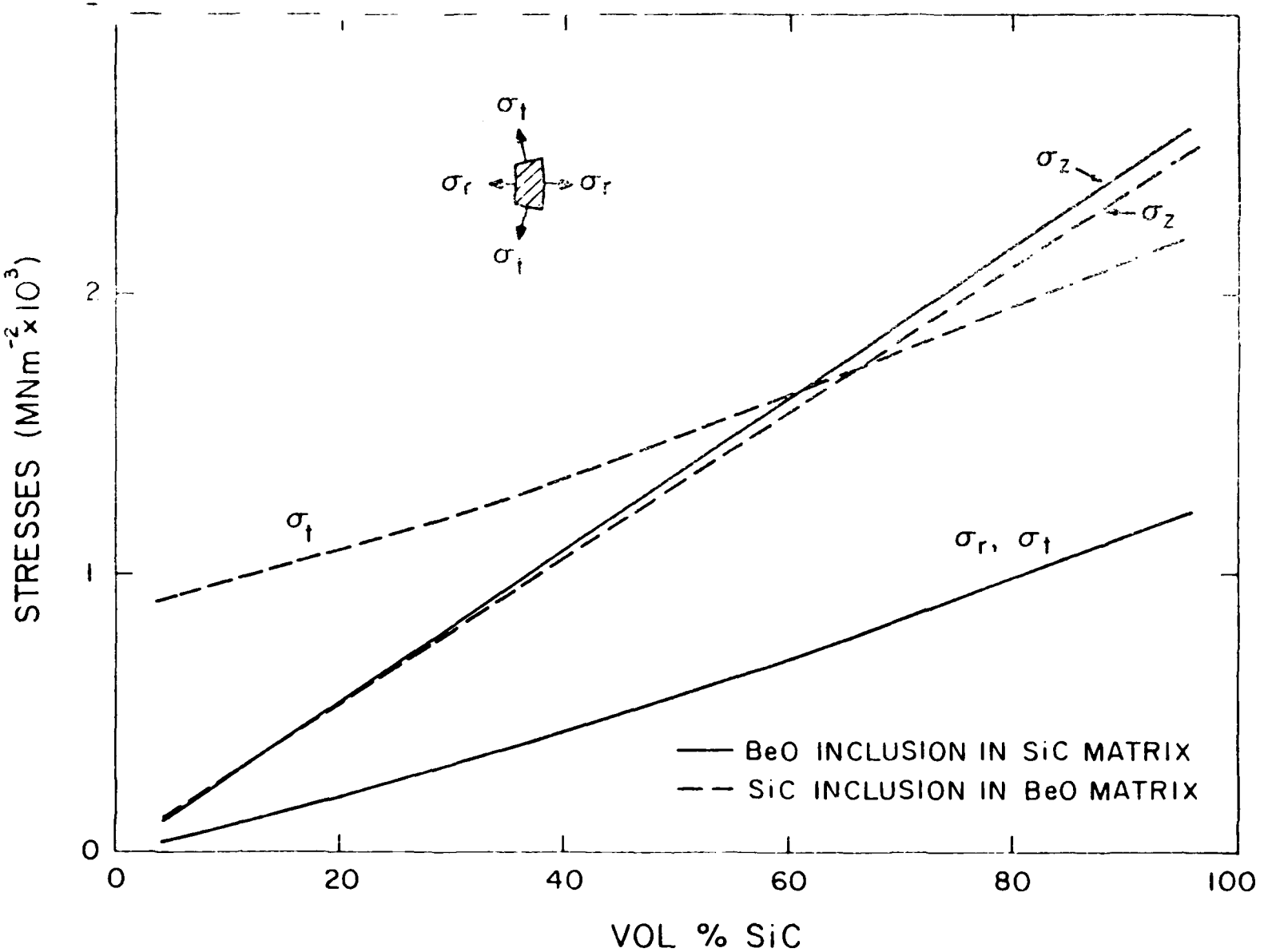

Fig. 7. Calculated values of tensile stresses in BeO phase at BeO-SiC interface based on composite cylinder model. σ_r, σ_t and σ_z represent radial, tangential and axial stresses respectively.

CHAPTER X

TRANSIENT THERMAL STRESSES IN CYLINDERS WITH SQUARE CROSS-SECTION UNDER CONDITIONS OF CONVECTIVE HEAT TRANSFER

by

K. Satyamurthy[§], J. P. Singh[*], D. P. H. Hasselman[*] and M. P. Kamat[§]

[*]Department of Materials Engineering

and

[§]Department of Engineering Science and Mechanics
Virginia Polytechnic Institute
Blacksburg, Virginia 24061

ABSTRACT

The transient thermal stresses in a long cylinder with square cross-section resulting from convective heating or cooling by a sudden change in ambient temperature were calculated by the finite element method. On heating, the maximum tensile stresses occur in the center of the rod, whereas the maximum principle stresses occur along the diagonal of the cross-section. On cooling, the maximum tensile stresses occur at the center of the faces. The results obtained are discussed in terms of experimental measurement of the thermal stress resistance of brittle ceramics. Possible failure modes during heating and cooling are discussed. Comparison with literature data shows that for a given value of the Biot number the magnitude of the maximum tensile stresses on cooling, in a rod with square cross-section exceeds those in a rod with circular cross-section.

I. INTRODUCTION

Brittle ceramic materials are highly susceptible to catastrophic failure under non-isothermal conditions involving high levels of thermal stress.[1] For purposes of reliable engineering design, characterization of the thermal stress resistance of ceramics for high-temperature structural application is essential.

A favorite method for measuring the thermal stress resistance of ceramics consists of quenching appropriate specimens into a quenching medium which is at a temperature different from the initial temperature of the specimens. Such quenching media may consist of water,[2,3] liquid metals,[4] oils,[5] fluidized beds[6] or eutectic mixtures of salts.[7] The initial temperature of the specimens may be above or below the temperature of the quenching medium. The specimen geometry can consist of spheres,[4,7] solid cylinders with circular[2] or square cross-section.[3]

For interpretation of the results for the spherical specimen[8] or the solid circular cylinders,[9] analytical solutions for the transient temperatures and thermal stresses are available in the literature. Unfortunately for cylindrical specimens with square cross-section no such solutions are available. For this reason, experimental quenching data for such specimen can be used to establish the relative thermal stress resistance of different materials. But a quantitative estimate of the magnitude of thermal stress at which a square specimen fail cannot be made. A brief analytical study carried by one of the present authors some years ago revealed that the lack of availability of analytical solutions for the thermal stresses in square cylinders, under convective heat transfer, appears to be attributable to the lack of rapid convergence of the product of two infinite series involved in the general solu-

tion. It may be noted that under conditions of a constant heat flux, no such problems are encountered.[10]

An alternative approach to evaluation of thermal stresses in square cylinders is to solve them by numerical methods, such as the finite element method, which formed the basis of the present study.

II. PROCEDURE

The cylinder with square cross-section located at $-a < x < a$ and $-a < y < a$ was assumed to be infinite in extent in the Z-direction in order to avoid end-effects. The cylinder initially at thermal equilibrium is subjected to thermal stresses by heating or cooling by an instantaneous change in ambient temperature. Heat transfer was assumed to occur by Newtonian convection, i.e., a rate of heat transfer proportional to the instantaneous temperature difference between the surface and the ambient environment. Heat transfer was assumed to be uniform along the length in order to avoid an axial component of the heat flow. The severity of the heat flux was expressed in terms of the non-dimensional Biot number, $\beta = ah/k$ where a is the half-thickness of the cylinder, h is the heat transfer coefficient and k is the thermal conductivity of the specimen.

The transient temperatures and thermal stresses were evaluated with the finite element computer program developed for a number of previous studies. The reliability of this program was checked out by verifying analytical results reported in the literature for the thermal stresses in a solid circular cylinder[9] subjected to convective heat transfer and for the thermal stresses in a hollow cylinder with spatially varying thermal conductivity under conditions of steady-state heat transfer.[15] Excellent agreement between the analytical and numerical results was obtained.

In view of the symmetry of the temperature and thermal stress distribution around the x- and y- axes of the square cross-section of the cylinder, the finite element computations were simplified by considering only one of the four quadrants of the cross-section located at $0 < x < a$ and $0 < y < a$. This quadrant was subdivided into 64 elements of equal size with the element at the corner (a,a) further subdivided into 4x4 equal size element. For values of the Biot number as high as 20, this finite element mesh gave identical results with a mesh for which the corner element was divided into 6x6 sub-elements. The calculations were not extended to values of the Biot number $\beta > 20$, as the high temperature gradients for these high values of β, required an even finer mesh size, requiring excessive computer time. All pertinent material properties were assumed to be independent of temperature.

For convenience all the results for the transient temperature, T are reported in terms of the non-dimensional temperature, T^* defined by $T^* = (T_i - T)/T_i - T_f)$ for convective cooling and $T^* = (T - T_i)/(T_f - T_i)$ for convective heating, where T_i is the initial temperature of the rod, and T_f is the temperature of the ambient to which the rod is subjected.

The transient thermal stresses, σ are reported in terms of the non-dimensional stress, $\sigma^* = \sigma(1-\nu)/\alpha E\Delta T$, where ν is Poisson's ratio, α is the coefficient of thermal expansion, E is Young's modulus of elasticity and $\Delta T = |T_i - T_f|$. The time dependence of the temperatures and stresses is expressed in terms of the non-dimensional time $t^* = \alpha t/a^2$ where α is the thermal diffusivity and t is the time. For simplicity the term "non-dimensional" will be deleted from the further discussion.

III. RESULTS AND DISCUSSION

Typical temperature and stress distributions will be examined first.

Because of the symmetry of the square cross-section about both the x- and y- axis as well as the diagonal, it is sufficient to present the temperature and stresses within an octant only.

Figure 1a shows the distribution of the temperature and the transverse stress, σ_y at the time it reaches its maximum value for convective heating with $\beta = 5$. The transverse stress σ_y at (o, o) reaches its maximum value at the same instant as the axial stress, σ_z (o, o). The maximum value of the compressive transverse stress (σ_y) is obtained at the center of the face (a, o). As expected, the edge of the rod has attained the highest value of temperature at the time of maximum transverse stress.

Figure 1b shows the axial and principal stresses at the time of their respective maximum values on heating for Biot number, $\beta = 5$. The maximum value of the axial tensile stress occurs at the center of the rod. Apart from a slight stress gradient near the edge, the axial stresses are fairly uniform along the faces of the rod. The maximum values of the principal stress occur along the diagnoal of the cross-section, in general agreement with the results of Cheung et. al.[10] for heating of a rectangular prism by a constant heat flux.

Figure 1c shows the temperatures and axial stresses at the instant of maximum axial stress, σ_z (a, a) for convective cooling with $\beta = 5$. The maximum value of tensile axial stress occurs at the edge of the rod. The maximum compressive stress occurs at the center of the rod. Again, with the exception of the immediate edge region, the axial stresses are nearly uniform along the rod face.

Figures 2a-d give the time dependence of the transverse σ_y (a, o), the axial stresses σ_z (o, o), σ_z (a, a) and the principal stress for a range of

values of Biot number, β. Comparison of these stress values show that on cooling, the transverse stress σ_y (a, o) reaches the highest value. It should also be noted, however, that the value of the axial stress, σ_z (a, a) exceeds the value of transverse stress σ_y (a, o) at short times.

Figure 3a gives the values of the maximum tensile axial (σ_z), transverse (σ_y), and principal stress (σ_p) for convective heating and cooling as a function of the Biot number, β. In general, these results indicate that the tensile stresses developed during cooling exceed the corresponding values obtained during heating.

In Fig. 3b, the curves marked (C) indicate the temperatures at various positions in the rod at the time of maximum tensile axial σ_y(a, o) obtained during convective cooling as a function of Biot number. Similarly, the curves marked (H) indicate the temperature at various positions at the time of maximum axial stress, σ_z (o, o) at the center of the rod. These results indicate, as expceted that the temperature differences within the rod at the time of maximum stress increase with increasing Biot number.

For purposes of comparing the results of various thermal shock tests, it is of interest to compare the present results for the magnitude of the maximum tensile stresses developed during cooling in a cylinder with a square cross-section with those in a cylinder with circular cross-section. These results are shown in Fig. 4. For the limiting cases of β = o, ∞ these stresses should be identical. At intermediate values the magnitude of the thermal stresses in the square rod exceeds the values of stress in the circular rod. Particularly for values of β frequently encountered in laboratory thermal shock test, ($0.5 < \beta$ 5.0), the relative difference in stress can amount to as much as 50 percent.

From the point of the interpretation of thermal shock tests, it is of interest to speculate on the mode of failure of the rods with square cross-section. Thermal shock by cooling, as found in a quench test, will be considered first. If it is assumed that failure occurs at a predetermined value of tensile stress, failure would be expected to occur at the center of the face under the influence of the transverse stress. Because of the axial stress, the stress state at the center of the face is nearly uniform biaxial. This makes the center of the face an even more likely site of failure because the biaxial state of stress increases the probability of failure for those brittle materials for which fracture is controlled by statistical considerations.

In assessing the site of failure, however, it should be recognized that during the initial stages of the thermal shock (i.e. at times less than the time of maximum stress), the axial stress at the specimen edge exceeds the transverse stress at the face center, as pointed out earlier. For this reason, in case of a thermal shock overload in which the maximum stresses exceed the fracture stress significantly, failure more likely will be initiated at the specimen edge than at the face center.

During preparation of thermal shock specimens with square cross-section, such defects as nicks, scratches and other flaws more likely are introduced in the specimen edges than in the specimen face. This provides a further reason, why thermal stress failure in square rods will be initiated at the specimen edges rather than at the center of the faces. This effect will be enhanced further in stress-corrosive environments which will promote more sub-critical crack growth in flaws at the edges because of the more rapid rise in the magnitude of thermal stress than in the case of the face centers.

For these combined reasons, it is speculated here that for most brittle engineering materials tested in practice, the specimen edge may well be the preferred site of failure.

On heating, failure could occur under the influence of the tensile stress in the specimen center. Alternatively, failure can be initiated by the principal stresses along the diagonals of the cross-section. The observations of Chueng et. al.[10] suggest that the latter may be the preferred mode of failure for brittle materials.

A final comment should be made about the finding that for a given value of the Biot number, on cooling the maximum value of tensile stress in the square rod exceeds that for a circular rod. This implies that for a given quenching medium, square rods will require a lower critical temperature difference (ΔT_c) for the initiation of thermal stress failure. Firstly, this suggests that for a given quenching environment, the use of square rod specimens will permit comparative testing of a wider range of materials. Secondly, the use of square rod specimens with their lower values of ΔT_c will suppress changes in the heat transfer coefficient due to nucleate boiling or vapor formation in quenching media with high vapor pressures. This will facilitate the interpretation of data for the comparative thermal shock resistance of materials with large differences in ΔT_c.

ACKNOWLEDGMENTS

The present study was conducted as part of a larger program on the thermal-mechanical and thermal properties of engineering ceramics supported by the Office of Naval Research under contract No. N00014-78-C-0431.

REFERENCES

1. W. D. Kingery, "Factors Affecting Thermal Stress Resistance of Ceramic Materials," J. Am. Ceram. Soc., 38 [1] 3-15 (1955).

2. D. P. H. Hasselman, "Strength Behavior of Polycrystalline Alumina Subjected to Thermal Shock," J. Am. Ceram. Soc., 53 (9) 490-95 (1970).

3. T. K. Gupta, "Critical Grain Size for Non-Catastrophic Failure in Al_2O_3 Subjected to Thermal Shock," J. Am. Ceram. Soc., 56, (7) 396 (1973).

4. C. -Y. King and W. W. Webb, "Internal Fracture of Glass under Triaxial Tension Induced by Thermal Shock," J. Appl. Phys., 42, (6) 2386-95 (1971).

5. J. Gebauer, D. A. Krohn and D. P. H. Hasselman, "Thermal-Stress Fracture of a Thermomechanically Strengthened Alumina Silicate Ceramic," J. Amer. Ceram. Soc., 55 (4) 198-201 (1972).

6. D. P. H. Hasselman, E. P. Chen, C. L. Ammann, J. E. Doherty and C. C. Nessler, "Failure Prediction of the Thermal Fatigue of Silicon Nitride," J. Am. Ceram. Soc. 58, 513 (1975).

7. W. B. Crandall and J. Ging, "Thermal Shock Analysis of Spherical Shapes," J. Am. Ceram. Soc., 38 (1) 44-54 (1955).

8. G. Gruenberg, "State of Stress in an Isotropic Sphere with Non-Uniform Heating," Z. der Physik, 35, 548-55 (1925).

9. J. C. Jaeger, "On Thermal Stresses in Circular Cylinder," Phil. Mag., 36, 418-28 (1945).

10. J. B. Cheung, Kuppusamy Thirumalai and Ta-Shen Chen, "Transient Thermal Stress in Rectangular Prism," Proc. Am. Soc. Civil Eng., J. Eng. Mech. Div., 100, 463-67 (1974).

11. K. Satyamurthy, M. P. Kamat and D. P. H. Hasselman, "Effect of Spatially Varying Thermal Conductivity on Magnitude of Thermal Stress in Convective Heating," J. Am. Ceram. Soc., (in review)

REFERENCES (CONT'D)

12. K. Satyamurthy, J. P. Singh, M. P. Kamat and D. P. H. Hasselman, "Effect of Spatially Varying Porosity on Magnitude of Thermal Stress During Steady State Heat Flow," J. Am. Ceram. Soc., (in review).

13. K. Satyamurthy, J. P. Singh, M. P. Kamat and D. P. H. Hasselman, "Thermal Stress Analysis of Brittle Ceramics with Density Gradients Under Conditions of Transient Convective Heat Transfer," Proc. Brit. Ceram. Soc., (in press).

14. D. P. H. Hasselman and G. E. Youngblood, "Enhanced Thermal Stress Resistance of Structural Ceramics with Thermal Conductivity Gradient," J. Am. Ceram. Soc., 61, (1) 49-52 (1978).

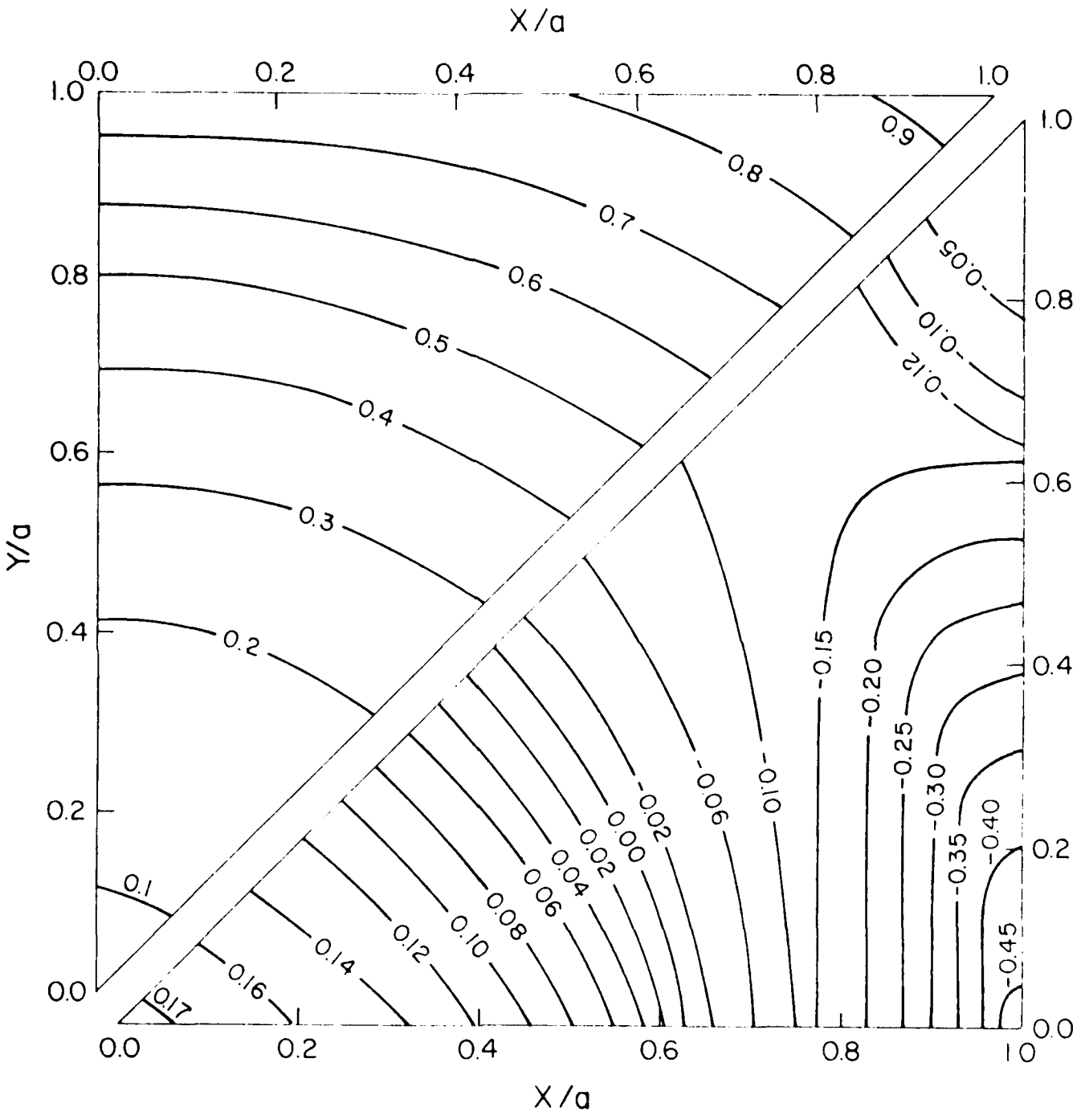

Figure 1a. Distribution of, a: temperature and b: transverse stress, σ_y at the time of maximum transverse σ_y (0,0) and axial stress, σ_z (0,0) in a long cylinder with square cross-section subjected to sudden convective heating for a Biot number, β=5.

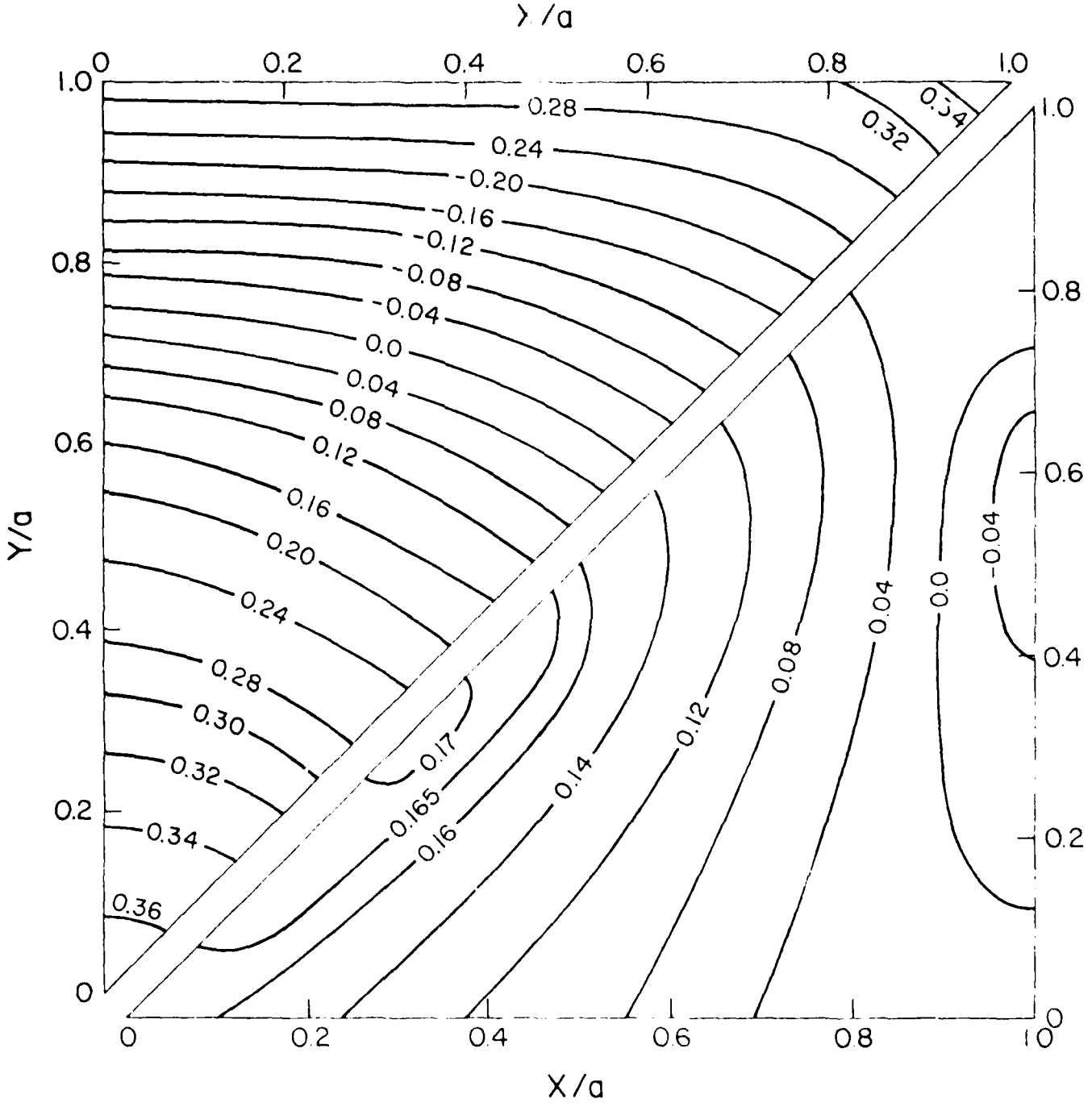

Figure 1b. Distribution of, a: axial stress, σ_z and, b: principal stress, σ_p at the time of their maximum value in a long cylinder with square cross-section subjected to sudden convective heating for a Biot number, β=5.

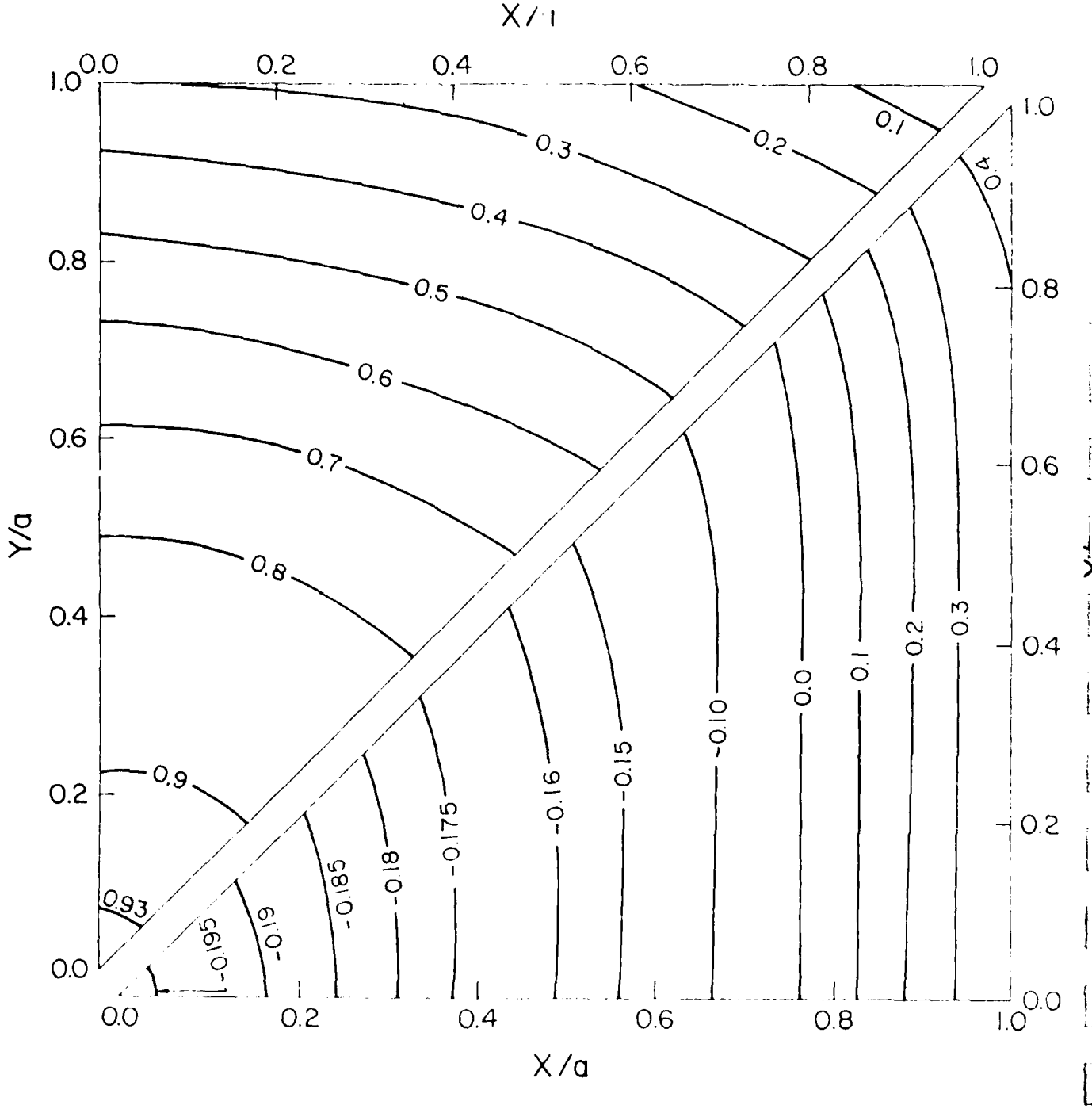

Figure 1c. Distribution of, a: temperature and, b: axial stress, σ_z at the time of maximum axial stress, σ_z (a,a) in a long cylinder with square cross-section subjected to sudden convective cooling, for a Biot number, B=5.

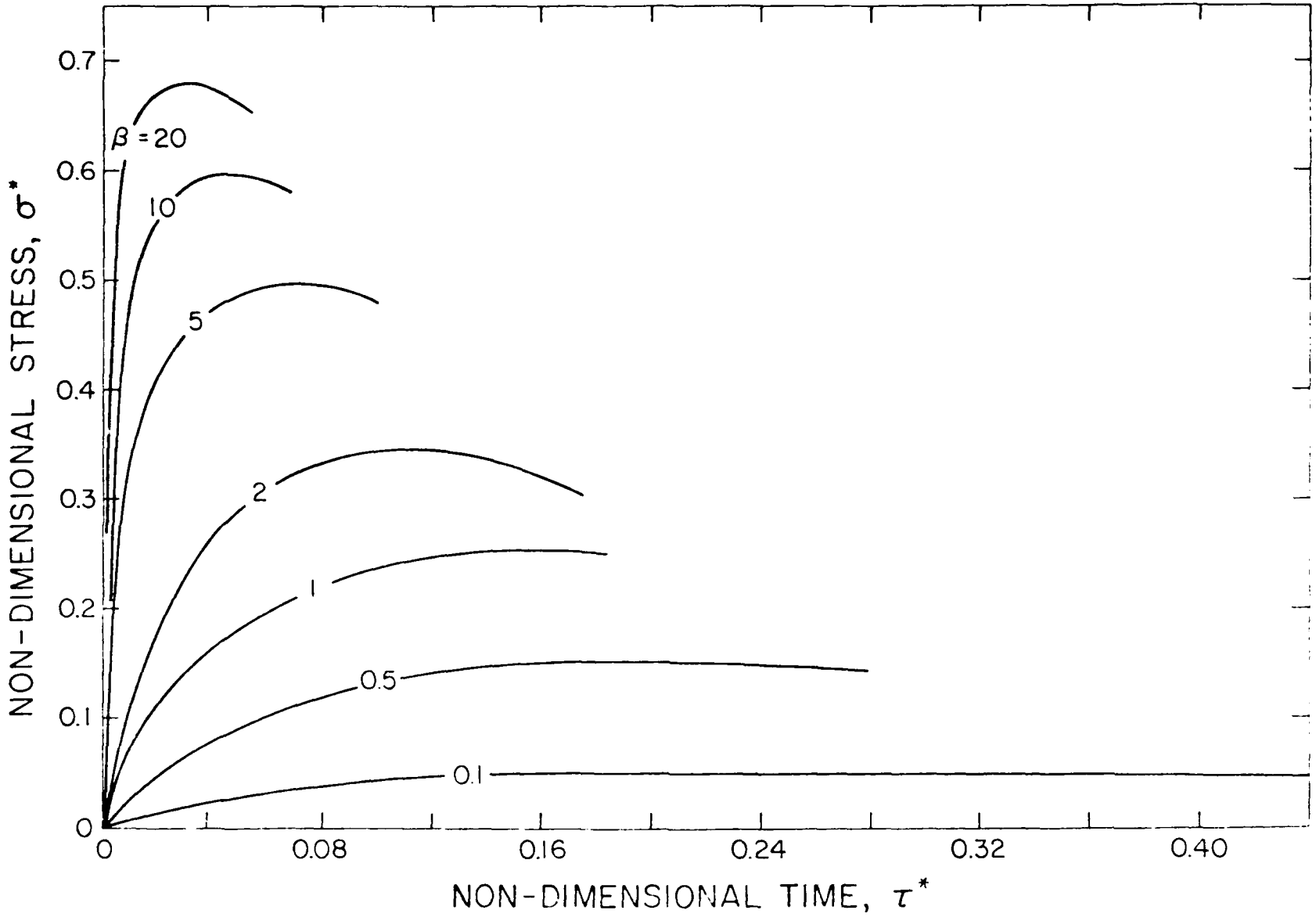

Figure 2a. Time dependence of the transverse stress, σ_y (a,o) at the center of the faces of a long cylinder with square cross-section subjected to sudden convective heat transfer for a range of values of Biot number. (Cooling: stress is tensile; Heating: stress is compressive).

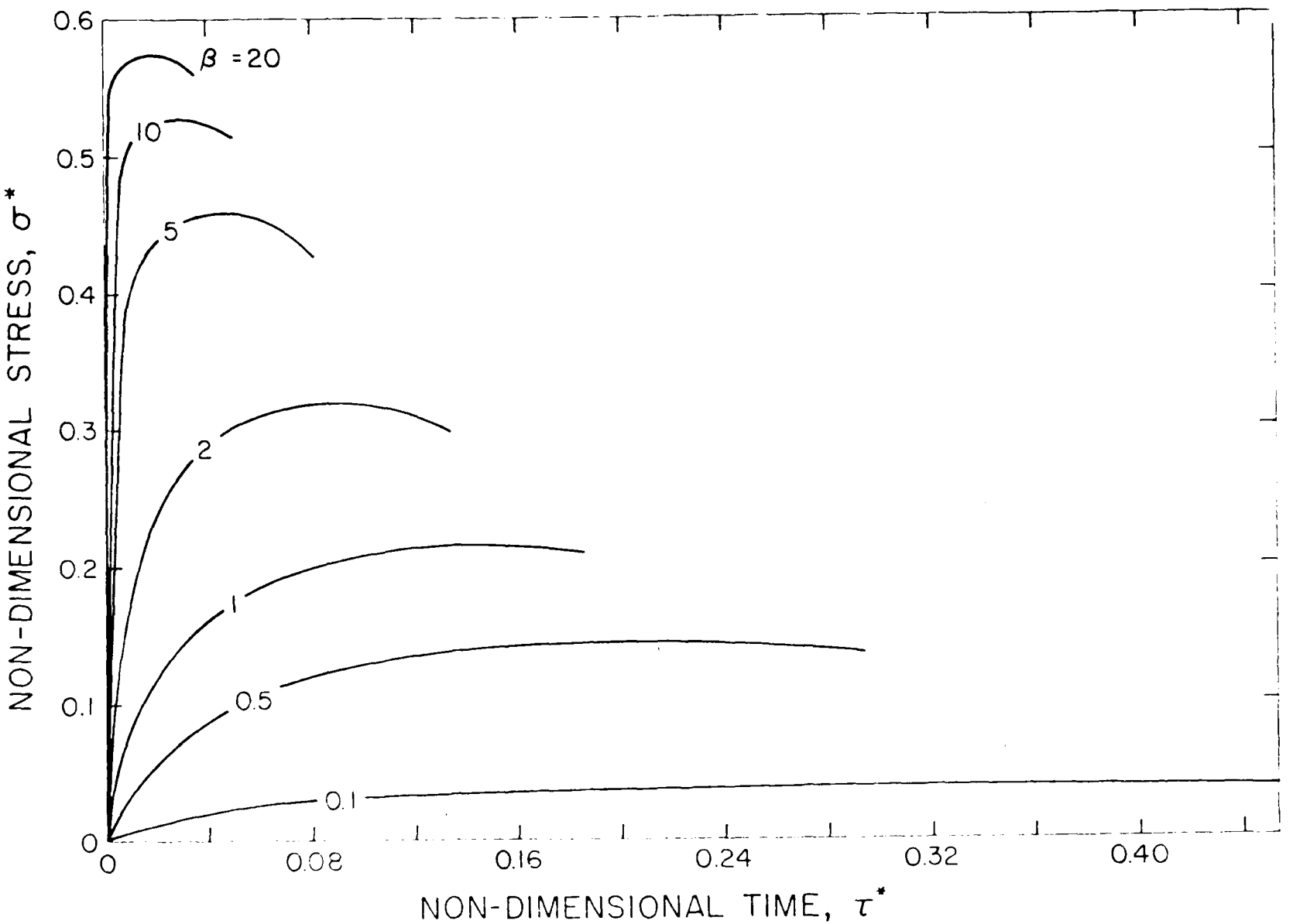

Figure 2b. Time dependence of the axial stress, σ_z (o,o) at the center of a long cylinder with square cross-section subjected to sudden convective heat transfer for a range of values of Biot number. (Cooling: stress is compressive; Heating: stress is tensile.)

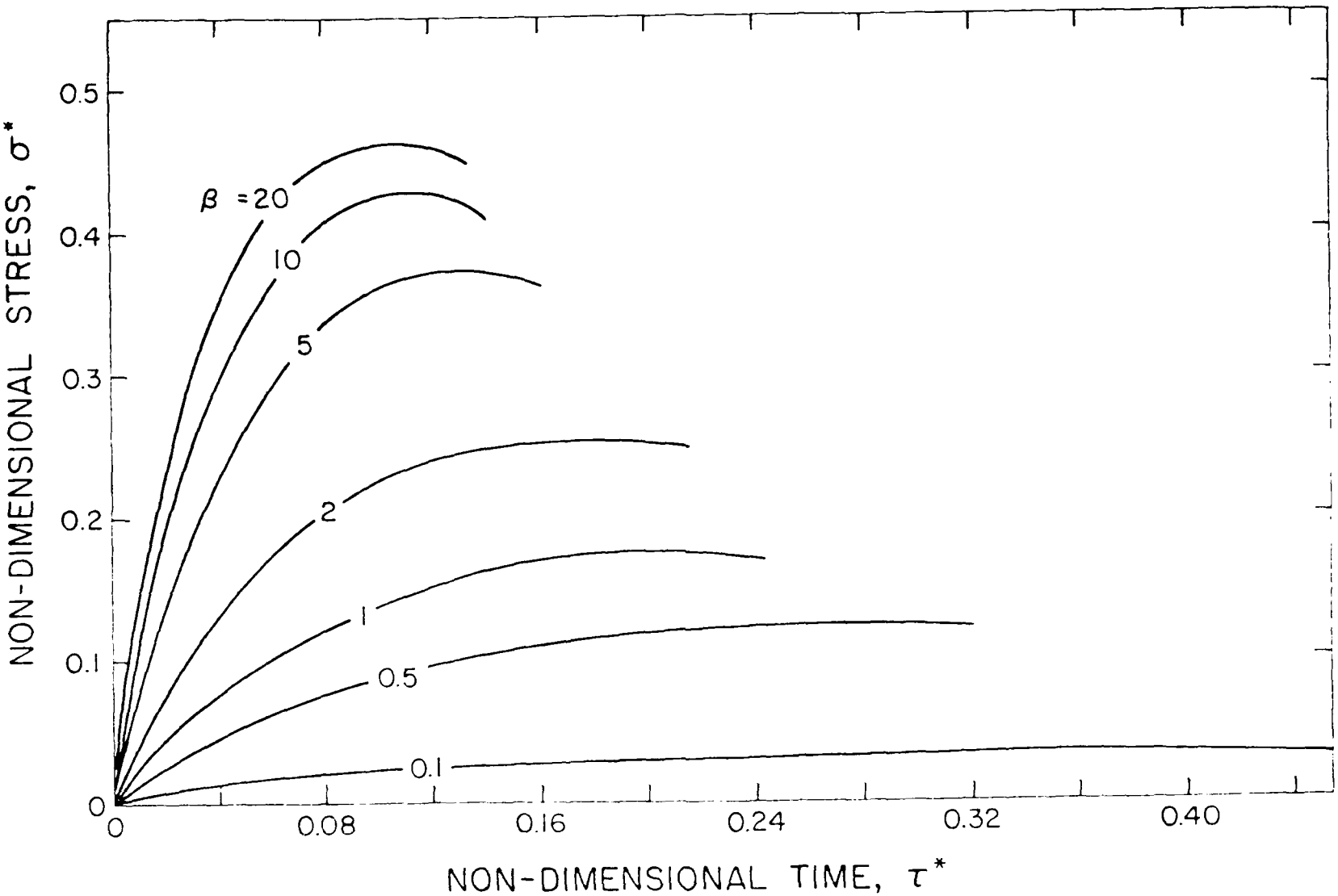

Figure 2c. Time dependence of the axial stress σ_z (a,a) at the corner of a long cylinder with square cross-section subjected to sudden convective heat transfer for a range of values of Biot number. (Cooling: stress is tensile; Heating: stress is compressive).

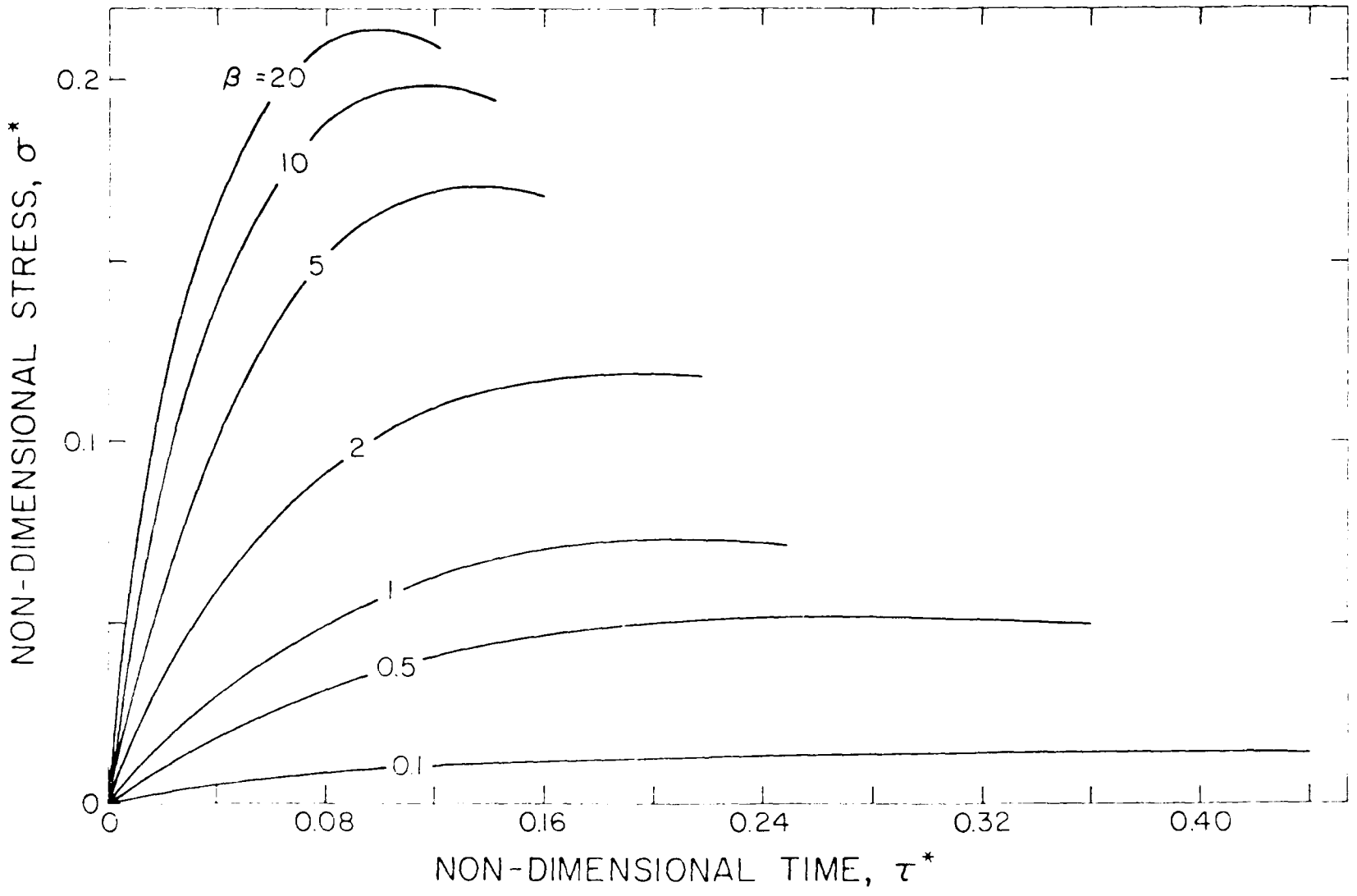

Figure 2d. Time dependence of the maximum tensile principal stresses in a square rod subjected to sudden convective heat transfer.

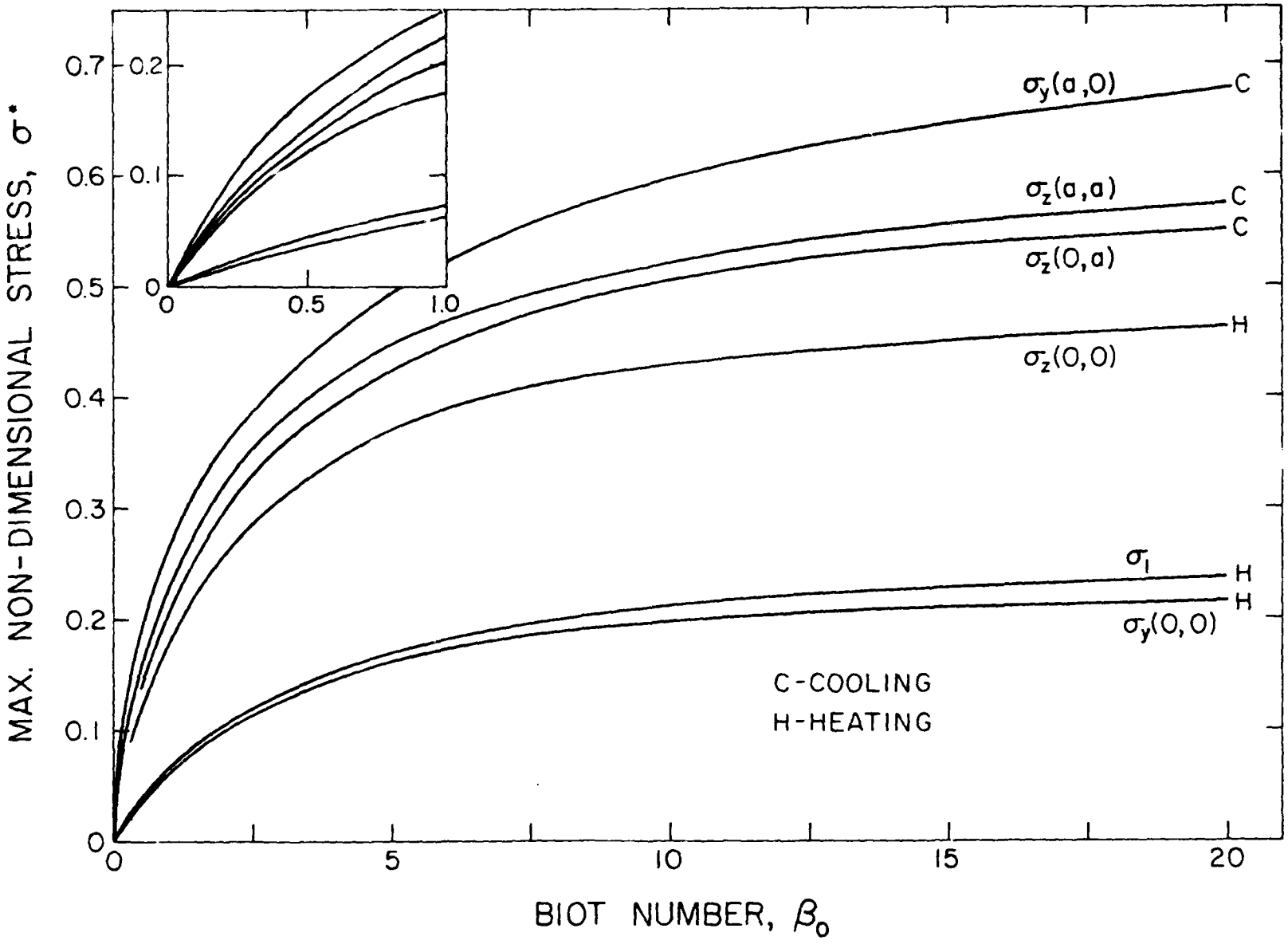

Figure 3a. Maximum tensile axial (σ_z), transverse (σ_y) and principal stress (σ_p), as a function of the Biot number in a long cylinder with square cross-section subjected to sudden convective heating (H) or cooling (C).

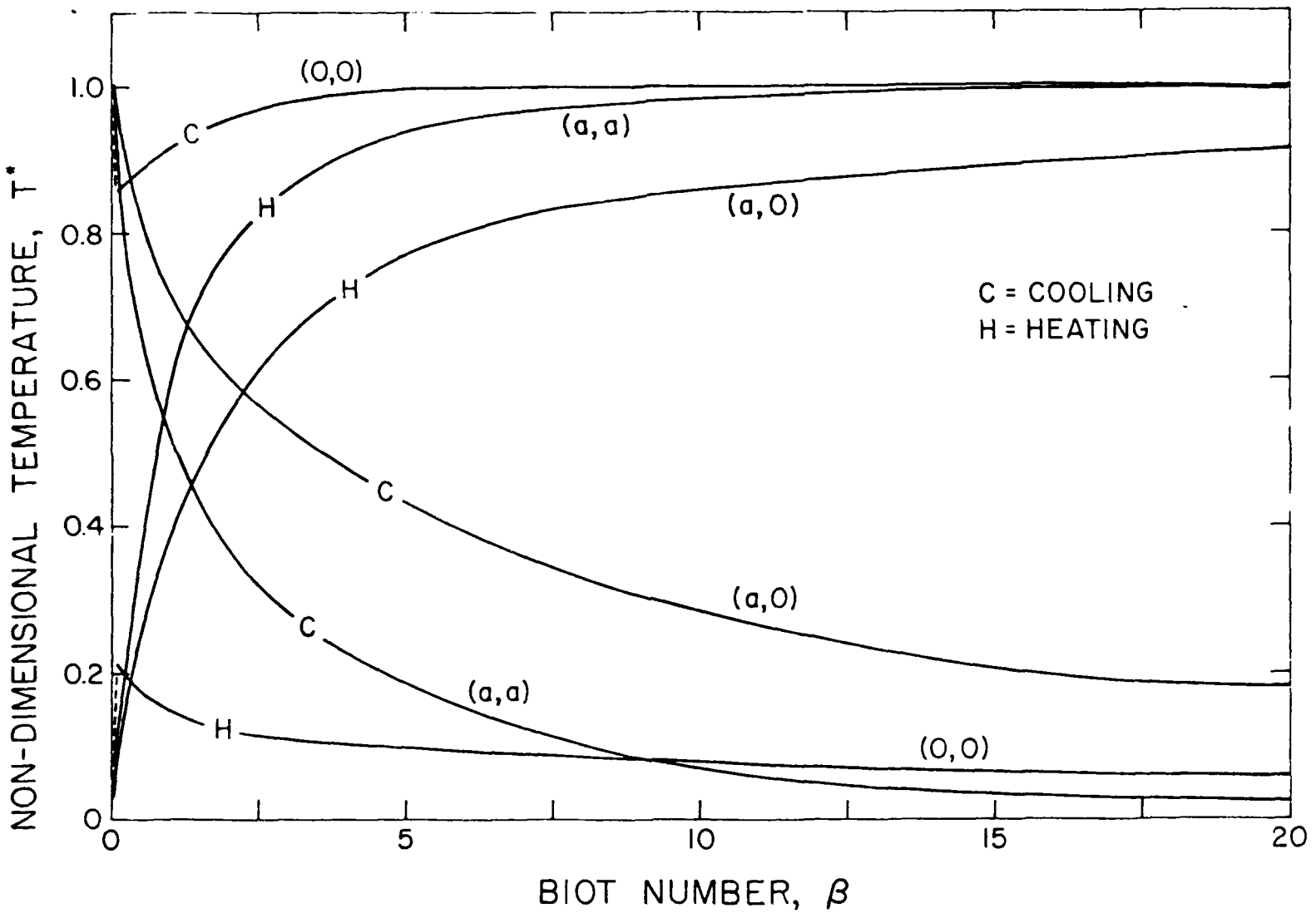

Figure 3b. Temperatures at various positions in a long cylinder with square cross-section at the time of maximum tensile axial, σ_z (o,o) and transverse σ_y (o,o) stresses for heating (H), and at the time of maximum axial tensile stress σ_y (a,o) for cooling (C) as a function of Biot number, β.

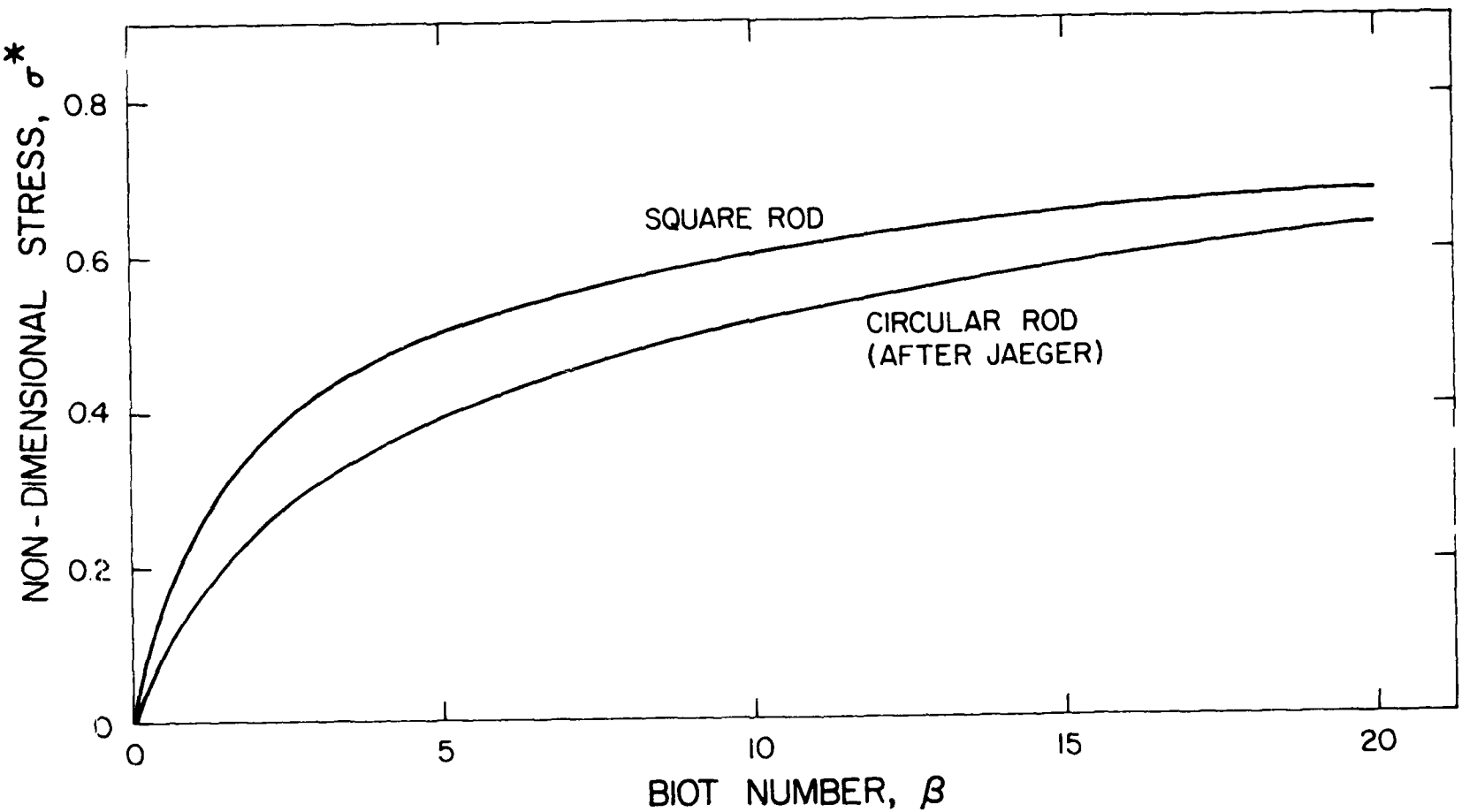

Figure 4. Comparison of the magnitude of the maximum tensile stress in cylinders with circular and square cross-section subjected to convective cooling as a function of Biot number, β.

CHAPTER XI

EFFECT OF MICRO-CRACKING ON THERMAL CONDUCTIVITY: ANALYSIS AND EXPERIMENT

D. P. H. Hasselman
Department of Materials Engineering
Virginia Polytechnic Institute and State University
Blacksburg, Virginia 24061

ABSTRACT

High densities of micro-cracks can have a profound effect on the conduction of heat through materials. An analysis of this effect on thermal conductivity is presented. The variables which affect the formation of micro-cracks in brittle materials due to thermal expansion mismatches are discussed. It is shown that micro-cracking results in a "thermo-mechanically" coupled thermal conductivity which is a function of elastic properties, the coefficient of thermal expansion, fracture toughness, microstructural variables such as grain size, as well as the closure and healing of cracks at higher temperatures.

These effects are demonstrated by experimental data for the temperature dependence of the thermal diffusivity of polycrystalline iron titanate, magnesium dititanate, composites of alumina with silicon carbide, and a glass containing a dispersed phase of nickel.

INTRODUCTION

Materials with high densities of micro-cracks are of current or potential interest for engineering applications involving high temperature. Such cracks can arise from creep-deformation, fatigue or mechanical failure due to thermal shock. High densities of micro-cracks can result from the thermal expansion anisotropy of the individual grains of polycrystalline aggregates. Mismatches in the coefficient of thermal expansion of the component materials in a composite also represents an important source of micro-crack formation.

High densities of cracks are expected to have a large effect on material properties. A quantitative understanding of such effects is essential for purposes of material selection, prediction of performance and failure analysis. Previous experimental and analytical studies have shown that extensive micro-cracking can promote significant increases in thermal shock resistance[1,2] with corresponding large decreases in the moduli of elasticity and Poisson's ratio[3,4] and large increases in fracture toughness[5]. Of significance also is that micro-cracking in brittle materials changes the usual highly catastrophic (unstable) failure mode to a stable, far more controllable, mode of failure[2]. This latter effect is very important for materials of construction of many high-temperature structures or components, which frequently are expected to provide satisfactory performance even while in a fractured condition. For these various reasons, micro-cracking constitutes a very effective mechanism for obtaining significant improvements in the engineering properties of brittle materials.

The thermal conductivity of materials also is expected to be affected strongly by the presence of micro-cracks especially at relatively low temperatures at which heat transfer by radiation across the cracks is minimal.

The purpose of this paper is to review previous analytical results for the effect of micro-cracking on thermal conductivity. The thermo-mechanical properties which affect micro-cracking to result in a "thermo-mechanically" coupled thermal conductivity will be discussed. Experimental data which illustrate this effect will be presented.

ANALYSIS

A. Effect of Cracks on Thermal Conductivity

Solutions for the effect of cracks on thermal conductivity were presented by Willis[6] for crack oriented perpendicularly to the direction of heat flow. The present writer[7] analyzed the effect on thermal conductivity of cracks oriented randomly, perpendicularly and parallel to the direction of heat flow. These latter analyses were based on the theoretical work of Fricke[8] and Powers [9] on the thermal conductivity of composites consisting of a continuous matrix with dilute dispersions in the shape of oblate ellipsoids of revolution with major axis b and minor axis a. By setting the thermal conductivity and minor axis equal to zero, solutions are obtained for the effect of infinitely thin pores in the form of circular (penny-shaped) cracks on thermal conductivity, as follows:

a. Randomly oriented cracks

For the solution of Fricke[8] and Powers[9] the thermal conductivity (k) of a matrix with randomly oriented circular cracks of zero thickness and zero thermal conductivity can be written:

$$K = K_o(1+2bV/3\pi a)^{-1} \tag{1}$$

where K_o is the thermal conductivity of the matrix without cracks and V is the volume fraction occupied by the cracks. However, for infinitely thin cracks, a = 0 and V = 0, which on substitution, renders eq. 1 indeterminate. Fortunately, this indeterminacy can be removed by noting that for an oblate ellipsoid the volume equals $4\pi ab^3/3$. For N cracks per unit volume, the total volume V occupied by the cracks equals:

$$V = 4\pi Nab^2/3 \tag{2}$$

which upon substitution into eq. 1 yields:

$$K = K_o(1+8Nb^3/9)^{-1}$$

b. Cracks oriented perpendicular to the direction of heat flow.

Following the same approach as for randomly oriented cracks, the solutions of Fricke and Powers with the aid of eq. 2 for the effect of cracks oriented perpendicular to the heat flow on thermal conductivity, becomes:

$$K_{\perp} = K_o(1+8Nb^3/3) \tag{4}$$

c. Cracks parallel to heat flow.

For this case the solutions of Fricke and Powers indicate that the cracks do not inhibit heat flow such that

$$K_{\parallel} = K_o \tag{5}$$

Comparison of eqs. 3, 4 and 5 indicates that cracks oriented perpendicularly to the direction of heat flow are most effective in reducing the thermal conductivity, followed by randomly oriented cracks in turn followed by cracks parallel to the heat flow, which have no effect at all. It is also of interest to note that the dependence of cracks on thermal conductivity expressed by the quantity Nb^3 was also found for the effect of cracks on elastic behavior. Furthermore, for a given value of Nb^3, the relative effect of cracks on elastic moduli is about twice the relative effect on thermal conductivity.

Figure 1 shows the relative thermal conductivity of a matrix with cracks of various orientations as a function of Nb^3.

B. Material Variables Which Control Micro-Crack Formation

To provide additional background for the experimental data to be presented, the material properties and other variables which control the formation and nature of micro-cracks should be examined. The formation of micro-cracks in brittle materials is due primarily to mismatches in the coefficients of thermal expansion. For single-phase polycrystalline materials such a mismatch can arise from the thermal expansion anisotropy of the individual grains. For composites, differences in the coefficients of thermal expansion of the components give rise to a thermal expansion mismatch.

Such thermal expansion mismatches result in the generation of "internal" stresses, whenever the temperature is changed from the value at which the differences in thermal strains are zero. This latter temperature usually corresponds to the temperature at which the polycrystalline material or composite was manufactured.

The material properties which affect the magnitude of the "internal stress" can be determined from the solution of the radial stress component (σ_r) at the interface between a single spherical isotropic inclusion contained within an infinite matrix, derived by Selsing[10]:

$$\sigma_r = \frac{\Delta\alpha\Delta T E_d}{(1+\nu_m)(E_d/2E_m)+(1-2\nu_d)} \tag{6}$$

where $\Delta\alpha$ is the difference in the coefficients of thermal expansion, E is Young's modulus, ν is Poisson's ratio and the subscripts d and m refer to the inclusion and matrix, resp.

Eq. 6 indicates that in addition to the thermal expansion mismatch, the magnitude of internal stress is a function of the elastic properties as well. More complex solutions for the internal stresses in composite circular cylinders[11] and composite spheres[12] show that the magnitude of the internal stresses is a function of the volume fractions of each component as well. Very important to note is that all literature solutions indicate that the magnitude of internal stress is independent of the dimensions of the grains in polycrystalline materials or inclusions in composites.

If brittle materials failed at some pre-determined stress level, micro-cracks could form whenever the magnitude of internal stress exceeds the value of strength. The latter value usually corresponds to the tensile strength, since brittle materials are most prone to failure in tension. Generally, however, fracture in brittle materials does not occur at a predetermined stress level, but depends on the size and geometry of defects or flaws at which failure is initiated. The same should hold for failure resulting in micro-cracks.

The variables and their relationships which control micro-crack formation should be examined. An isotropic inclusion will be considered, which is placed in a state of uniform triaxial tension due to a mismatch in thermal expansion with a surrounding rigid matrix. The inclusion contains a precursor flaw in the form of a small circular (penny-shaped) crack. By a slight modification of the analytical theory for crack stability under conditions of thermal stress[2] the critical temperature difference (ΔT_c) required for instability of the precursor flaw can be shown to be:

$$\Delta T_c = \{\pi G(1-\nu_m)^2/2E_d(\Delta\alpha)^2(1-\nu_m)\ell\}^{1/2} \qquad (7)$$

where G is the surface fracture energy required to create unit area of new crack surface and ℓ is the radius of the precursor flaw.

Eq. 7 indicates that if for a precursor flaw of given size ΔT does not exceed ΔT_c, micro-cracks will not form. Conversely, for a given value of ΔT, the size of the precursor flaw must exceed some minimum size before micro-cracking will occur.

The defects thought to be primarily responsible for micro-crack formation in brittle materials are residual pores located at grain boundaries or at triple-points[13]. Such pores generally have a flat shape and can act as effective cracks. The size of such pores generally is proportional to the grain size. For this reason it is expected that, although the magnitude of internal stress is independent of grain size, micro-crack formation is expected to be related to the grain size in view of the inverse square root dependence of ΔT_c on precursor crack size. For this reason, the effect of micro-cracking on thermal conductivity is expected to be grain-size dependent.

Once the condition for micro-crack formation as expressed by eq. 7 is satisfied, strain-relief and eventual crack arrest will follow. On reheating the material (i.e., reducing ΔT) two effects will occur. First, depending on

crack geometry crack closure can take place. Such closure will provide direct contact across the crack surfaces, which should result in a positive dependence of thermal conductivity on temperature. Secondly, at sufficiently high temperatures, "crack-healing" can occur by diffusional or other transport processes. This latter effect will reduce the crack size and lead to the partial or complete recovery of the thermal conductivity to its original value before micro-crack formation. For this reason, the thermal conductivity of micro-cracked materials is expected to be a function of thermal history.

A number of the above effects are demonstrated by experimental data described below.

EXPERIMENTAL

A. Materials

Experimental results for the effect of micro-cracking on thermal transport behavior are reported for four different materials, namely polycrystalline iron titanate[14], polycrystalline magnesium dititanate[15], composites of beryllium oxide and silicon carbide[12] and a glass containing a dispersed phase of spherical nickel inclusions[16]. In the iron titanate and magnesium titanate micro-cracking results from the thermal expansion anisotropy of the individual grains. In the BeO-SiC composites, micro-cracking is due to the mismatch between the coefficients of thermal expansion of the BeO and SiC, with crack formation occurring in the component with the higher coefficient of thermal expansion, i.e. the BeO. In the glass-nickel composites micro-cracking takes the form of de-cohesion at the glass-Ni interface, due to poor mechanical bonding. All materials, which were nearly fully dense, were made by hot-pressing. For the details of their synthesis and micro-structures, the reader is referred to the original papers (12,14,15,16).

B. Experimental Method.

The effect of micro-cracks on thermal transport was determined experimentally by measurement of the thermal diffusivity by the laser-flash technique [17]. Details of the equipment are described in the original studies [12,14,15, 16]. The specimen temperature was monitored by either an IR-detector or by a thermocouple.

Micro-cracking has little or no effect on density. Furthermore the specific heat is uneffected by the presence of micro-cracks. For this reason, the relative effect of micro-cracking on thermal diffusivity at a given temperature is expected to be nearly identical to the relative effect of micro-cracking on thermal conductivity.

C. Experimental Results and Discussion

1. Iron titanate

Figure 2 shows the thermal diffusivity of iron titanate as a function of temperature for a complete heating and cooling cycle for three thermal anneals.

These annealing treatments promoted grain growth to result in a bi-modal grain size distribution, the fraction of large grains increasing with increasing time of anneal.

The experimental data for the thermal diffusivity indicate a number of effects. Firstly, the values of the thermal diffusivity at a given temperature decrease with increasing time of anneal, i.e., increasing fraction of large grains. Secondly, the negative temperature dependence of the thermal diffusivity on the heating part of the cycle decreases with increasing fraction of large grains. Thirdly, the two materials subjected to grain-growth show a pronounced hysteresis on heating and cooling.

These observations are in accordance with the expected effect of the microstructural variables on micro-cracking and thermal transport behavior, discussed earlier. The fine-grained (non-annealed) material shows the typical temperature dependence for a dielectric material in which heat conduction occurs primarily by phonon conduction. The reproducibility of the experimental data on heating and cooling also is typical for dielectric materials which do not undergo a microstructural change on thermal cycling. In contrast, the thermal diffusivity of the sample which underwent grain-growth is less than the value for the fine-grained material by as much as a factor of three. This effect can be attributed to the micro-cracking which occurred as the result of the grain-growth. Clearly, in the fine-grained material the size of the precursor flaws was too small for micro-cracks to form. In the coarse-grained materials the number and size of the micro-cracks was difficult to ascertain quantitatively. However, if it is assumed that the micro-cracks were of uniform size and randomly oriented, the quantity of Nb^3 in eq. 3 for the coarse-grained material is of the order of about two.

The more positive temperature dependence of the coarse-grained material, compared to the fine-grained material, is the direct result of crack closure with increasing temperature. Possibly the effect may also be attributed in part to an increased contribution of radiation across the crack to the heat conduction.

Of particular interest is the counter-clockwise hysteresis observed on cooling after initial heating. This behavior is indicative of permanent crack closure due to recombination of atomic bonds across the crack surface or due to diffusional processes. After such crack healing, the material must be cooled over some range of temperature before the micro-crack can form again, automatically leading to a hysteresis effect. At least qualitatively, all the above phenomena can be explained in terms of the variables which control micro-cracking and in terms of the effect of temperature on the size of the micro-cracks and thermal diffusivity.

2. Magnesium dititanate

The data for the temperature dependence of the thermal diffusivity for magnesium dititanate with two different grain sizes are shown in Fig. 3. For the finer-grained material, the hysteresis on heating and cooling is clock-wise in contrast to the counter-clockwise behavior observed for the iron-titanate. The coarse-grained magnesium dititanate exhibits a combination of clockwise as well as counter-clockwise behavior. Comparing these results with those in Fig. 2, it can be concluded that the mechanism of micro-crack formation in magnesium dititanate differs considerably from that in iron titanate.

It is suggested here that micro-crack formation in the magnesium dititanate involves substantial subcritical crack growth in contrast to iron titanate which involves catastrophic crack propagation. Crack extension by sub-critical crack-growth requires time. For this reason, it is conceivable that during the time period of cooling the specimen from the hot-pressing temperature the total extent of crack growth was relatively significant. For this reason, on reheating the thermal diffusivity will exhibit the typical temperature dependence of a dielectric material. On reaching sufficiently high temperatures, however, additional crack growth can occur leading to a decrease in the thermal diffusivity and a clock-wise hysteresis. On the other hand, substantial micro-crack formation by catastrophic crack propagation must have occurred during the initial cooling from the hot-pressing temperature, as indicated by the lower value for the thermal diffusivity at the beginning of the thermal cycle in comparison to the fine-grained material. Such cracks are expected to close or heal, leading to the counter-clockwise hysteresis, at least at the higher temperature range of the thermal cycle. The decrease in thermal diffusivity to a value less than the original value observed during heating can be attributed to additional micro-crack formation to yield a crack density in excess of the original value. For this reason, the clockwise and counter-clockwise hysteresis appears to be the result of the competitive effects between crack closure and healing and additional crack formation. This explanation, if correct, suggests that in assessing the effect of micro-cracks on thermal conductivity information on the kinetics of subcritical crack growth may be required as well.

3. Beryllium oxide-silicon carbide

The thermal diffusivity of these composites with a range of values for the volume fraction silicon carbide was measured over the temperature range from approximately 300°C to 1400°C, as shown in Fig. 4. Figure 5 shows the calculated thermal conductivity at 400°C as a function of silicon carbide content. Included in the figure is the thermal conductivity predicted by the Rayleigh-Maxwell theory for the crack-free composites. The experimental data show a large decrease near 20 and 80 percent silicon carbide, whereas near 40% SiC, the value of the thermal diffusivity is near the crack-free material. For an interpretation of these results it should be noted that detailed calculations have shown that the magnitude of the internal stress in the BeO phase increases linearly with increasing volume fraction SiC.[12] For this reason, the dependence of the thermal diffusivity on SiC content cannot be explained by corresponding variations in the magnitude of the internal stress. A more likely explanation is based on the changes in stress distribution with increasing silicon carbide content. At the low and high concentraitons of SiC, beryllium oxide is the continuous and dispersed phase respectively. However, near 50% SiC both phases are expected to be continuous. For one of the phases to be continuous the internal stress distribution will approximate that in a composite sphere, with a multi-axial stress state. For both phases to be continuous near 50% SiC, the stresses are more closely described by a composite cylinder. For such a model the stresses in the BeO are uniaxial. For a precursor flaw of given size, micro-crack formation is more likely to occur under a multi-axial stress state for which the orientation of the flaw is less important, than for a uniaxial stress state under which failure will occur only for a flaw oriented perpendicular (or nearly so) to the stress. If this explanation for the data in

Fig. 4 is indeed proven to be correct, it indicates that estimates of micro-crack formation and its effect on heat transport behavior, in addition to the variables discussed above, should take the statistical nature of brittle fracture into account as well. Also, this explanation illustrates that the existence of an internal stress of given magnitude is a necessary but not sufficient condition of micro-crack formation.

4. Glass-Ni Composites

These composites were made by vacuum hot-pressing at 700°C glass powders and Ni spheres with a diameter of approximately 50 μm. The coefficient of thermal expansion of the Ni ($\alpha \simeq 13.4 \times 10^{-6}K^{-1}$) exceeded the value of the glass ($\sim 7 \times 10^{-6}K^{-1}$) by nearly a factor of two. As a result, on cooling these composites the relative shrinkage of the Ni is larger than for the glass. Nickel and glass generally show very poor mutual adhesion. As a result, on cooling a gap will form at the interface between the glass and Ni. In effect, at the lower temperatures, the nickel will occupy a cavity in the glass larger than the size of the nickel particles. In analogy to the effect of cracks on thermal conductivity, such gaps should have an effect on the transport of heat through the composite.

Figure 6 shows the data for the thermal diffusivity as a function of temperature for the glass with 0, 15, 30 and 45 vol.% Ni. Included in the figure is the thermal diffusivity calculated by means of the Bruggeman variable dispersion relation, which assumes no resistance to heat flow at the interface[18]. The large negative deviation of the experimental data from the calculated is indicative of the effect of the resistance of the interfacial barrier to heat flow. The positive temperature dependence of the thermal diffusivity is expected from the closure of the gap with increasing temperature.

In spite of the existence of the interfacial gap, the data indicate that the Ni still contributes to the conduction of heat as indicated by the presence of the Curie point and also by the fact that the thermal diffusivity increases with increasing Ni content. This latter observation would not be expected if the Ni did not aid conduct heat. Heat conduction through the nickel presumably occurs as the result of multiple contact between the Ni particles and the wall of the cavity. As a final observation it should be noted that for the glass with 45% Ni, at the highest temperature, the measured value for the thermal diffusivity exceeds the calculated value. This effect is thought to be the result of Ni particle-to-particle contact, not accounted for in the Bruggeman theory.

DISCUSSION

The experimental data presented above qualitatively illustrate many of the expected effects of microcracking on thermal diffusivity. Because of the quantitative uncertainties in calculations of microcrack formation, it appears unlikely that quantitatively reliable estimates of thermal diffusivity of micro-cracked materials can be made at this time. From a practical point of view, however, the present observations suggest that micro-cracking represents an effective mechanism by which the thermal diffusivity of solid materials can be tailored to specific values.

The present data also indicate that although the basic understanding of heat transport phenomena appears to be well developed, many uncertainties still exist at the microstructural level which offer excellent opportunities for further theoretical analysis.

Acknowledgments

The present review was prepared as part of a research program on the thermo-mechanical and thermal properties of structural materials for high-temperature applications funded by the Office of Naval Research under contract: N00014-78-C-0431.

References

1. R. C. Rossi, Bull. Amer. Ceram. Soc., 48 (1969) 736.
2. D. P. H. Hasselman, J. Amer. Ceram. Soc., 52 (1969) 600.
3. R. L. Salganik, Izv. An. SSSR, Mekhanika Tverdogo Tela, 8 (1973) 149.
4. B. Budiansky and R. J. O'Connell, Int. J. Solid Structures, 12 (1976) 81.
5. J. A. Kuszyk and R. C. Bradt, J. Amer. Ceram. Soc., 56 (1973) 420.
6. J. R. Willis, J. Mech. Phys. Solids, 25 (1977) 185.
7. D. P. H. Hasselman, J. Comp. Mat., 12 (1978) 403.
8. H. Fricke, Phys. Rev., 24 (1924) 575.
9. A. E. Powers, KAPL-2145, March 1961.
10. J. Selsing, J. Amer. Ceram. Soc., 44 (1961) 419.
11. B. E. Gatewood, Thermal Stresses, McGraw Hill (1957).
12. J. P. Singh, D. P. H. Hasselman, W. M. Su, J. A. Rubin and R. Palicka, J. Mat. Sc. (in press).
13. A. G. Evans, Acta Met. 26 (1978) 1845.
14. H. J. Siebeneck, D. P. H. Hasselman, J. J. Cleveland and R. C. Bradt, J. Amer. Ceram. Soc., 59 (1976) 241.
15. H. J. Siebeneck, D. P. H. Hasselman, J. J. Cleveland and R. C. Bradt, J. Amer. Ceram. Soc., 60 (1977) 336.
16. Bob R. Powell, Jr., G. E. Youngblood, D. P. H. Hasselman and Larry D. Bentsen, J. Am. Ceram. Soc., (in press).
17. W. J. Parker, R. J. Jenkins, C. P. Butler and G. L. Abbott, J. Appl. Phys., 32 (1961) 1679.
18. D. A. G. Bruggeman, Ann. Physik, 24 (1935) 636.

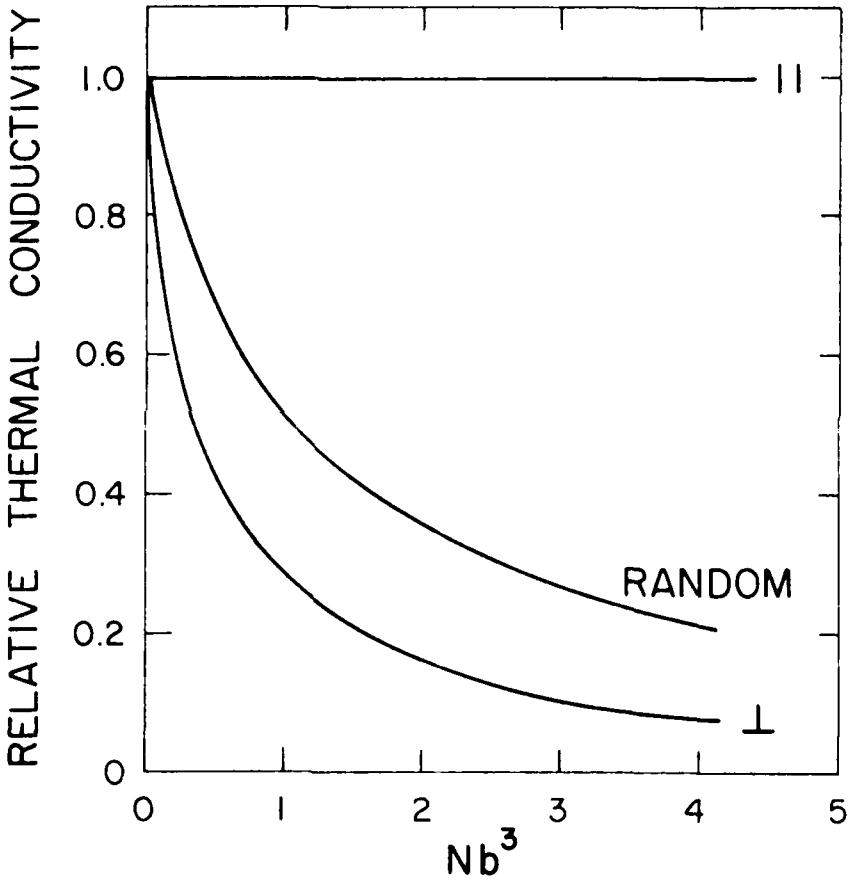

Figure 1. Effect of micro-cracking on thermal conductivity for various crack orientations.

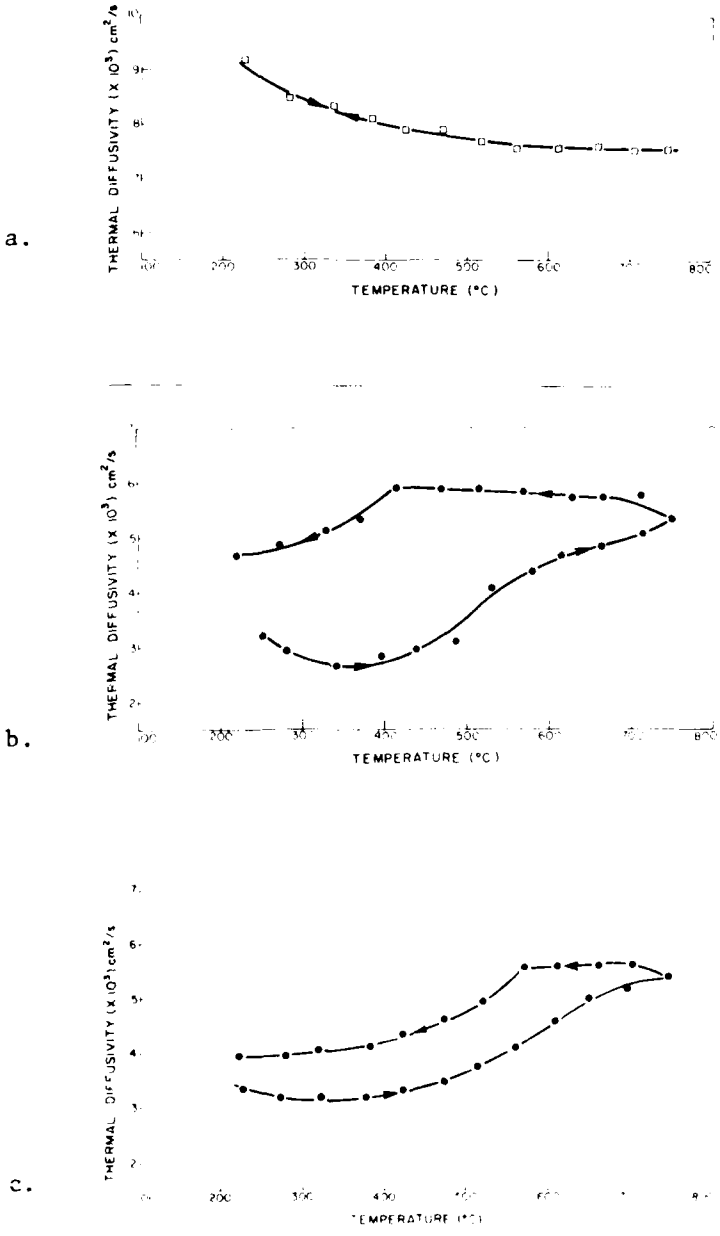

Fig. 2. Temperature dependence of the thermal diffusivity of iron titanate for three thermal anneals to promote grain-growth. a: As-prepared; b: Annealed 16 hrs; c: Annealed 32 hrs. (After Siebeneck, et al [14]).

AD-A081 915 VIRGINIA POLYTECHNIC INST AND STATE UNIV BLACKSBURG --ETC F/G 11/4
THERMAL-MECHANICAL AND THERMAL BEHAVIOR OF HIGH-TEMPERATURE STR--ETC(U)
DEC 79 D P HASSELMAN, P F BECHER, L D BENTSEN N00014-78-C-0431

UNCLASSIFIED

NL

3 OF 3

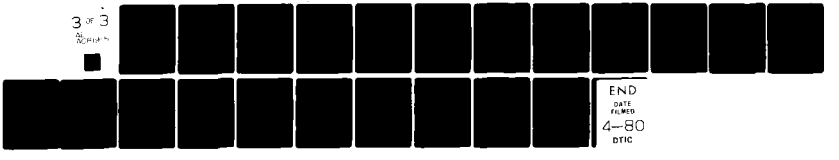

END
DATE FILMED
4-80
DTIC

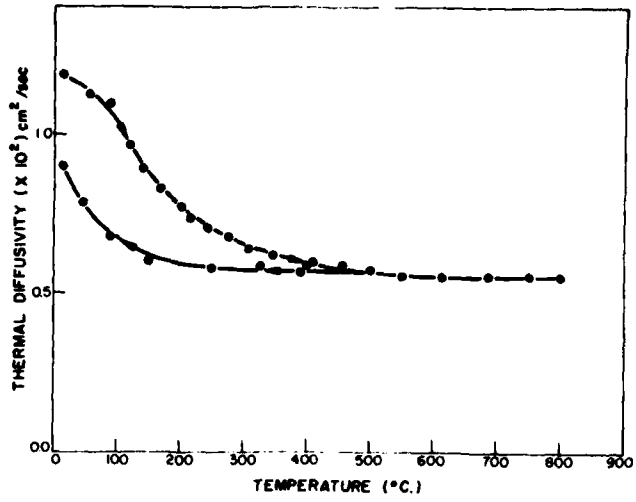

a.

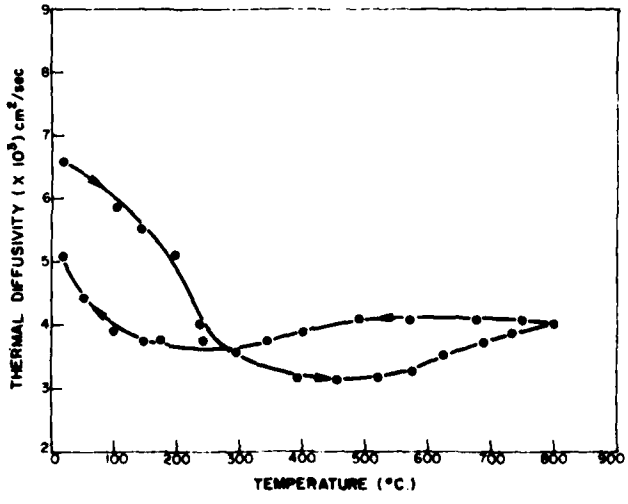

b.

Fig. 3. Temperature dependence of thermal diffusivity of magnesium dititanate for two different mean grain sizes, a: 1.0 μm and b: 70 μm (After Siebeneck et al [15].

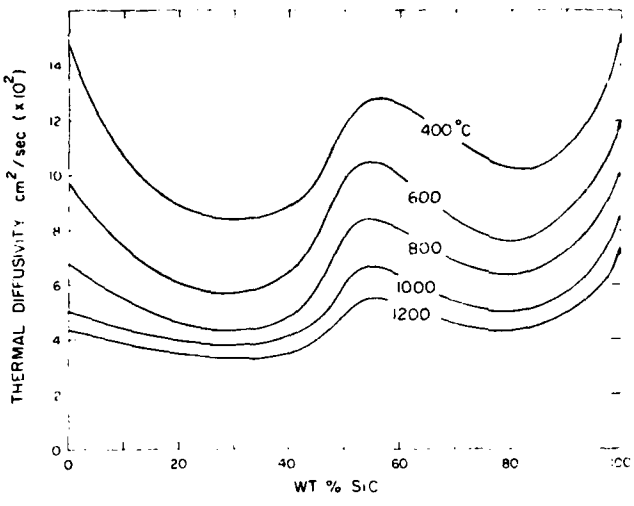

Fig. 4. Thermal diffusivity of SiC-BeO composites as a function of SiC content for a range of temperatures (After Singh, et al [12].

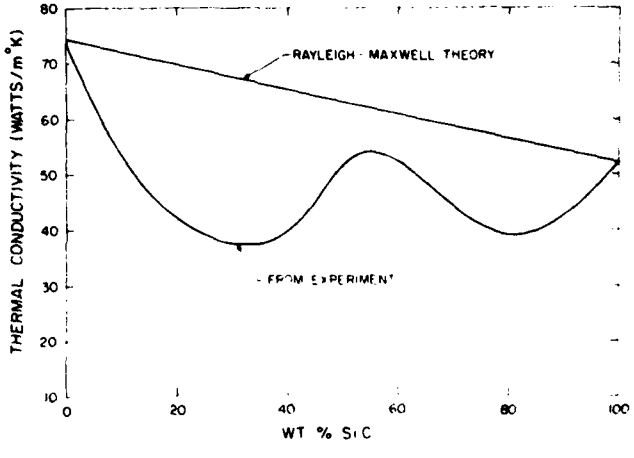

Fig. 5. Thermal conductivity of SiC-BeO composites as a function of SiC content at 400°C (After Singh, et al [12].

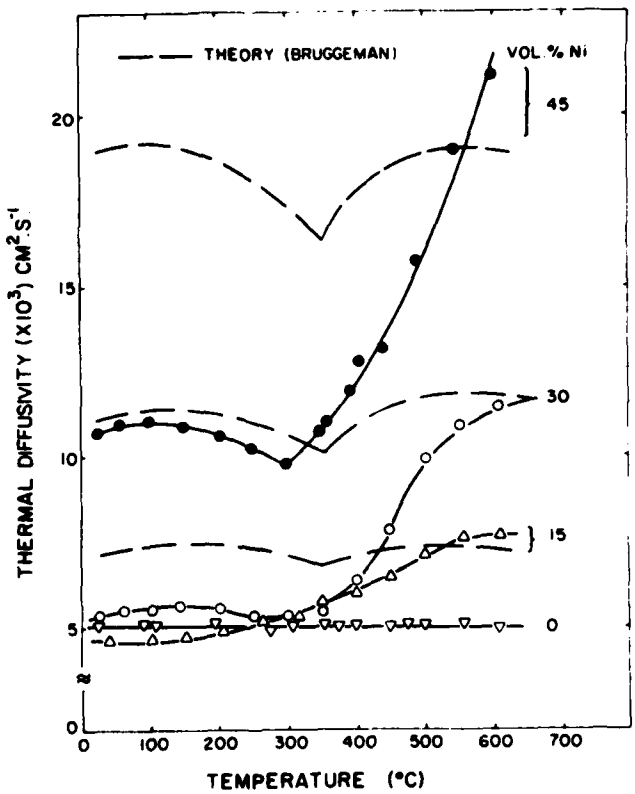

Fig. 6. Comparison between theory and experimental data for the thermal diffusivity of composites of a glass with various volume fractions of Ni spherical inclusions. (After Powell, et al., [16].

CHAPTER XII

ROLE OF THERMAL EXPANSION IN THERMAL STRESS RESISTANCE OF SEMI-ABSORBING BRITTLE MATERIALS SUBJECTED TO SEVERE THERMAL RADIATION

J. R. Thomas, Jr., J. P. Singh and D. P. H. Hasselman

Departments of Mechanical and Materials Engineering

Virginia Polytechnic Institute and State University
Blacksburg, Virginia 24061

ABSTRACT

An analysis is presented of the thermal stresses resulting from "thermal trapping" in semi-absorbing brittle ceramic materials in the form of a thin flat plate subjected to intense thermal radiation. Solutions for the thermal stresses are presented for symmetric and assymmetric radiation heating and convective cooling with limiting values of the heat transfer coefficient, $h = 0$ and ∞. For $h = \infty$, the stresses are identically equal to zero for values of the optical thickness μa of 0 and ∞, and reach their maximum value at $\mu a \simeq 1.3$ and 2.0 for symmetric and assymmetric heating respectively. For $h = 0$, the magnitude of thermal stress increases with increasing optical thickness.

Expressions are derived for the maximum radiation heat flux to which the plate can be subjected without failure, in terms of the pertinent material properties. These properties are combined in "figures-of-merit" for the selection of material with the optimum thermal stress resistance, appropriate for given heating and cooling conditions. These figures-of-merit, which may contain as many as seven material properties, indicate that high thermal stress resistance requires low values of the coefficient of thermal expansion, Young's modulus, Poisson's ratio, emissivity, and the absorption coefficient in combination with high values of tensile strength and thermal conductivity.

I. INTRODUCTION

Non-uniform thermal expansions in materials or structures subjected to non-linear temperature distributions result in thermal stresses. The magnitude of these thermal stresses can be sufficiently high to result in catastrophic failure. This problem is particularly severe for brittle materials which do not permit thermal stress relief by plastic flow. Thermal stress analysis is (or should be) an essential element in the design of engineering structures or components operating under non-uniform temperature conditions.

In practice, the problem of thermal stress failure can be solved by a structural re-design. An alternative solution is to select a material with the optimum combination of properties which keep the magnitude of the thermal stresses well below the failure stress. The magnitude of thermal stress is not only a function of the coefficient of thermal expansion, but also depends on the elastic properties, the thermal conductivity and diffusivity and many other properties depending on the nature of heat transfer, performance criteria and mechanisms of failure [1]. The choice of the optimum material to avoid thermal stress failure for a given thermal environment can be based on "thermal stress resistance parameters" or "figures-of-merit." The two best known thermal stress resistance parameters are [1,2]:

$$R = S_t(1 - \nu)/\alpha E$$

and

$$R' = S_t(1 - \nu)k/\alpha E,$$

in which S_t is the tensile strength, ν is Poisson's ratio, k is the thermal conductivity, α is the coefficient of thermal expansion and E is Young's modulus. Materials with higher values of the parameters R and R' will have higher thermal stress resistance than those with lower values of these parameters. A review of some thirty other thermal stress resistance parameters was presented some time ago. The tensile strength, S_t, is present in R and R' because of the high ratio of compressive to tensile strength of brittle materials, which makes them most susceptible to failure in tension.

Radiation represents an important mechanism of heat transfer, especially at high temperatures. The incidence of thermal stress failure under conditions of radiative heat transfer is receiving increased attention lately as the direct result of the importance of solar radiation as an energy source. An analysis of the thermal stress failure of brittle materials opaque to incident black-

body radiation was presented some time ago [3]. This analysis was extended to include materials opaque above a given wavelength of incident black-body radiation and completely transparent below this wavelength [4].

The absorption properties of many materials are such that incident radiation transmitted through the surface is absorbed throughout the thickness. This results in the so-called "thermal trapping" effect, in which the temperature in the interior of a material can greatly exceed the temperature of the ambient environment. An analysis of the thermal stresses which result from this type of heat transfer was performed recently [5] for a flat plate symmetrically heated by normally incident radiation and cooled by convection with heat transfer coefficients $h = 0$ and ∞.

The purpose of this paper is to report these latter results, together with results for the thermal stresses in a plate assymmetrically heated by radiation and cooled by convection again for h values of 0 and ∞. In this paper, special attention is paid to the interaction between the coefficient of thermal expansion and the other material properties which control the magnitude of thermal stress. Only the principal analytical results will be highlighted. For the mathematical details the reader is referred to the original report [5,6].

II. ANALYSIS

The analysis of thermal stresses first requires obtaining the solutions for the temperature distributions. From these, expressions are derived for the thermal stresses. By equating the maximum tensile thermal stress to the tensile strength, an expression can be obtained for the maximum incident radiation heat flux to which the material can be subjected without causing failure.

For the analysis, the following simplifying assumptions were made. First, reflectivity of the material of the plate is sufficiently low that the effect of multiple internal reflections can be neglected. Secondly, the plate will be assumed to be at low enough temperature that the maximum value of thermal stress is reached before the plate becomes sufficiently hot that re-emission of the absorbed radiation must be taken into account. Indeed, the validity of this latter assumption is easily demonstrated with numerical examples [5]. Finally, it was also assumed that the emissivity and absorptivity of the plate are independent of wavelength. If required, the spectral dependence of these properties can easily be taken into account in the analysis.

For the various types of radiative heating and convective cooling conditions and the rates of internal heat generation, the general approach used for the solutions and the expressions for the maximum value of tensile thermal stresses are as follows.

A. Symmetric radiative heating and convective cooling

For normally incident symmetric thermal radiation, the rate of internal heat generation (g''') within the plate can be derived to be:

$$g''' = 2\mu\varepsilon q_o e^{-\mu a} \cosh(\mu x) \tag{1}$$

where μ is the absorption coefficient, ε is the emissivity ($\varepsilon = 1 - r$, where r is the reflectivity), q_o is the intensity of the incident heat flux at each side of the plate, a is the half-thickness of the plate and x is the through-the-thickness coordinate with $x = 0$ at the center of the plate.

Derivation of the transient temperature (T) requires solution of the differential equation [7]

$$\partial^2 T/\partial x^2 + g'''(x)/k = (1/\beta)\partial T/\partial t \tag{2}$$

where k is the thermal conductivity, t is the time, and β is the thermal diffusivity.

The thermal stresses in the plane of the plate are obtained by substitution of the solution for the temperature in [8]:

$$\sigma_{y,z} = \frac{\alpha E}{1 - \nu}\left[-T + \frac{1}{2a}\int_{-a}^{a} T\,dx + \frac{3x}{2a^3}\int_{-a}^{a} Tx\,dx\right] \tag{3}$$

For the two cooling conditions, the initial and boundary conditions used for the solution of Eq. (2) and the maximum tensile stresses and maximum permissible heat flux are as follows:

1. Heat transfer coefficient $h = 0$.

Initial and boundary conditions:

$$T(x,0) = T_o;\ \partial T/\partial x(0,t) = \partial T/\partial x(a,t) = 0 \tag{4}$$

For these conditions the maximum tensile thermal stresses which occur at $x = 0$ and $t = \infty$ can be derived to be:

$$\sigma_{y,z} = \frac{\alpha E \varepsilon q_o e^{-\mu a}}{(1-\nu)k} \{\frac{2}{\mu} + (\frac{a}{3} - \frac{2}{a\mu^2})\sinh(\mu a)\} \qquad (5)$$

In general, by equating the maximum tensile thermal stress to the tensile strength, Eq. (5) can be rearranged into an expression for the maximum permissible heat flux, q_{max}, such that thermal stress failure is avoided. For the limiting cases of an optically thick ($\mu a \to \infty$) and optically thin ($\mu a << 1$) plate, simple analytical expressions for q_{max} can be obtained:

$$q_{max} = 6S_t(1-\nu)k/\alpha E\varepsilon a \qquad (\mu a \to \infty) \qquad (6a)$$

$$q_{max} = 180S_t(1-\nu)k/7\alpha E\varepsilon\mu^3 a^4 \qquad (\mu a << 1) \qquad (6b)$$

2. Heat transfer coefficient h = ∞.

For this case the initial and boundary conditions are:

$$T(x,0) = T_o;\ \partial T/\partial x\ (0,t) = 0 \qquad (7a)$$

$$T(a,t) = T(-a,t) = T_o \qquad (7b)$$

The tensile thermal stresses are a maximum at t = ∞ and x = -a,a and can be derived to be:

$$\sigma_{y,z}(a,\infty) = \frac{4\alpha E(\mu a)\varepsilon q_o e^{-\mu a}}{(1-\nu)ka^2} \cosh(\mu a) \sum_{n=0}^{\infty} \{(\mu^2 + \lambda_n^2)(a\lambda_n^2)\}^{-1} \qquad (8)$$

where $\lambda_n = (n + 1/2)\pi/a$

In analogy to Eq. (6), the maximum permissible radiation heat flux q_{max} for the optically thick and optically thin plate can be derived to be:

$$q_{max} = \infty \qquad (\mu a \to \infty) \qquad (9a)$$

$$q_{max} = \frac{S_t(1-\nu)k\pi^4}{64\alpha E\mu\varepsilon a^2} \qquad (\mu a << 1) \qquad (9b)$$

B. Assymmetric radiation heating and convective cooling

The thermal stresses will be given specifically for a plate subjected to incident radiation on one face (x = -a) and convective cooling on the opposite face (x = a).

For this case the rate of internal heat generation is:

$$g''' = q_o \varepsilon \mu e^{-\mu(x + a)} \tag{10}$$

1. Heat transfer coefficient h = 0.

The initial and boundary conditions are

$$T(x,0) = T_o;\ \partial T/\partial x(-a,t) = \partial T/\partial x(a,t) = 0 \tag{11}$$

The solutions for the stresses indicate that the tensile thermal stresses reach their maximum value at t = ∞, but that the position of the maximum tensile stress can occur anywhere within the plate, depending on the value of optical thickness. The complete solution for the thermal stresses at t = ∞ as a function of the coordinate x is:

$$\begin{aligned}\sigma_{y,z} = {} & \frac{\alpha E q_o \varepsilon}{(1 - \nu)k}\left[\frac{e^{-\mu(x + a)}}{\mu} - \frac{(x + a)^2}{4a}(1 - e^{-2\mu a}) + (x + a)\right] \\ & + \frac{\alpha E q_o \varepsilon}{(1 - \nu)k}\left[\frac{e^{-2\mu a} - 1}{2\mu^2 a} + \frac{a}{3}(1 - e^{-2\mu a}) - a\right] \\ & + \frac{3\alpha E q_o \varepsilon x}{2(1 - \nu)a^3 k}\left\{\frac{1}{\mu^3}[e^{-2\mu a}(\mu a + 1) + (\mu a - 1)]\right. \\ & \left. + \frac{a^3}{3}(1 - e^{-2\mu a}) - \frac{2a^3}{3}\right\}\end{aligned} \tag{12}$$

For the optically very thick plate the maximum tensile stresses occur at x = 0 and can be written:

$$\sigma_{y,z}(0,\infty) = \frac{\alpha E q_o \varepsilon a}{12(1 - \nu)k} \qquad (\mu a \to \infty) \tag{13a}$$

For the optically very thin plate the maximum tensile thermal stress occurs at x = -a, and is given by:

$$\sigma_{y,z}(-a,\infty) = \frac{\alpha E q_o \varepsilon \mu a^2}{(1- \nu)k} \qquad (\mu a << 1) \tag{13b}$$

The expressions for the maximum permissible heat flux become

$$q_{max} = 12 S_t (1 - \nu)k/\alpha E \varepsilon a \qquad (\mu a \to \infty) \tag{14a}$$

$$q_{max} = S_t (1 - \nu)k/\alpha E \varepsilon \mu a^2 \qquad (\mu a << 1) \tag{14b}$$

2. Heat transfer coefficient $h = \infty$.

The initial and boundary conditions are:

$$T(x,0) = T(a,t) = T_o;\ \partial T/\partial x(-a,t) = 0$$

The tensile thermal stresses have their maximum value at $x = -a$ and $t = \infty$, and are given by

$$\sigma_{y,z} = -\frac{\alpha E}{1-\nu} \sum_{n=\text{ odd}}^{\infty} \frac{16q_o\varepsilon\mu a}{n^2\pi^2 k} \frac{\mu + (n\pi/4a)e^{-2\mu a}}{\mu^2 + (n\pi/4a)^2}$$

$$+\frac{\alpha E}{1-\nu} \sum_{n=\text{odd}}^{\infty} \frac{8q_o\varepsilon\mu}{n^2\pi^2 k} \frac{\mu + (n\pi/4a)e^{-2\mu a}}{\mu^2 + (n\pi/4a)^2} \frac{1}{\lambda_n}(-1)^{\frac{n-1}{2}}$$

$$-\frac{3\alpha E}{a(1-\nu)} \sum_{n=\text{odd}}^{\infty} \frac{8q_o\varepsilon\mu}{n^2\pi^2 k} \frac{\mu + (n\pi/4a)e^{-2\mu a}}{\mu^2 + (n\pi/4a)^2} \left[\frac{a}{\lambda_n}(-1)^{\frac{n-1}{2}} - \frac{1}{\lambda_n^2}\right] \qquad (15)$$

where $\lambda_n = n\pi/4a$ with $n = 1, 3, 5, 7 \ldots$

For the optically thick and optically thin plates Eq. (15) can be simplified to:

$$\sigma_{y,z}(-a,\infty) = 0 \qquad (\mu a \to \infty) \qquad (16a)$$

$$\sigma_{y,z}(-a,\infty) = \frac{0.2719\alpha E q_o \varepsilon \mu a^2}{(1-\nu)k} \qquad (\mu a << 1) \qquad (16b)$$

which yield for the maximum incident heat flux:

$$q_{max} \to \infty \qquad (\mu a \to \infty) \qquad (17a)$$

$$q_{max} = \frac{3.677 S_t (1-\nu)k}{\alpha E \varepsilon \mu a^2} \qquad (\mu a << 1) \qquad (17b)$$

III. NUMERICAL RESULTS AND DISCUSSION

For the symmetrically heated plate, Fig. 1 shows the maximum tensile thermal stress as a function of the optical thickness, μa. For $h = \infty$, the stresses are identically equal to zero for $\mu a = 0$ and ∞, with a maximum at $\mu a = 1.34$. For $\mu a = 0$, no thermal stress will arise, because no heat is absorbed. For $\mu a = \infty$, the radiation is absorbed in the immediate surface and removed by

the convective medium. Again, no heating of the plate occurs. At $\mu a = 1.34$, the thermal trapping effect is a maximum with the corresponding highest values of temperature increase and thermal stresses within the plate. These results suggest that in general for a highly efficient solar collector ($\mu a \to \infty$), the heat should be removed from the plate at the same side as the incident radiation. For $h = 0$, the stresses are zero for $\mu a = 0$ and increase monotonically with increasing value of μa.

Figure 2 shows the maximum values of tensile stress as a function of the optical thickness of the plate heated on one side by the incident radiation and cooled on the other side by convection. Qualitatively, Fig. 2 looks similar to Fig. 1. The magnitude of the stresses for the assymmetrically heated plate, however, is much less than that for the symmetrically heated plate. The principal reason for this is that in the assymmetrically heated flat plate, the non-uniform thermal expansions in part can be accommodated by bending.

For $h = \infty$ and $\mu a = 0$, no stresses occur because no heat is absorbed. For $\mu a = \infty$ and $h = \infty$, however, although the heat is transmitted through the plate, no stresses occur because at $t = \infty$ the temperature distribution is linear, which results in zero thermal stress. For $h = 0$, the stress is zero for $\mu a = 0$ and increases monotonically with increasing μa. Included in Fig. 2 are the values of the maximum transient stresses for $h = \infty$. For these, the reader is referred to the original study [6] for further details.

Attention can now be focused on the role of the coefficient of thermal expansion and its interaction with the other material properties establishing the magnitude of the thermal stress resistance of semi-absorbing ceramics. It may be noted that the various expressions for q_{max} are a function of a numerical constant, the thickness of the plate, and a number of material properties. For a given heating and cooling condition and plate thickness, thermal stress resistance is governed only by the material properties. For the purpose of selection of the material with optimum thermal stress resistance, so-called "thermal-stress-resistance" parameters or figures-of-merit can be separated from the expressions for q_{max} as follows:

$$\frac{S_t(1-\nu)k}{\alpha E \varepsilon \mu}; \quad \frac{S_t(1-\nu)k}{\alpha E \varepsilon \mu^3}; \quad \frac{S_t(1-\nu)k}{\alpha E \varepsilon} \tag{18}$$

Materials with higher values of these figures-of-merit have better thermal stress resistance than materials with lower values. For this reason, high thermal stress resistance is associated with high values of tensile strength and thermal conductivity, coupled

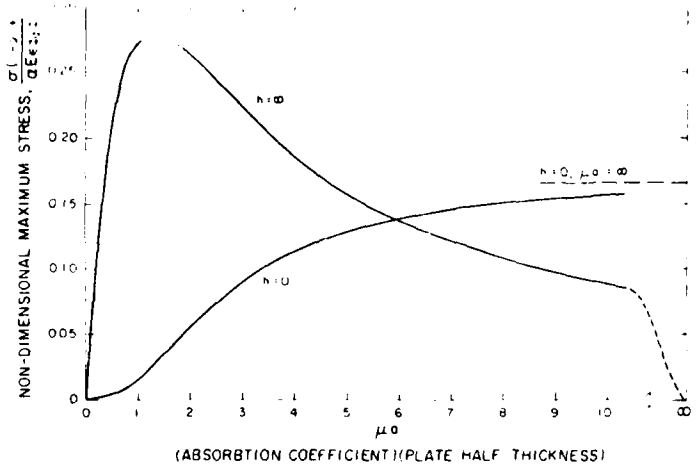

Fig. 1 Magnitude of maximum tensile thermal stresses as a function of optical thickness in flat plate symmetrically heated by thermal radiation and cooled by convection.

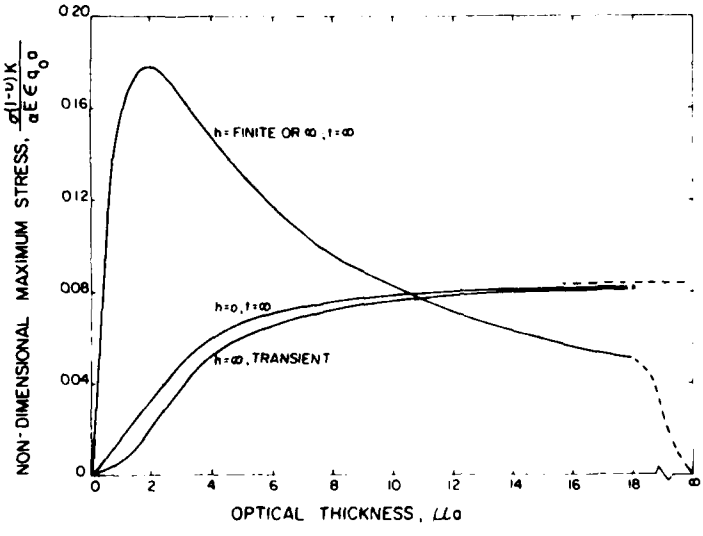

Fig. 2 Magnitude of maximum tensile thermal stresses as a function of optical thickness in flat plate assymmetrically heated by thermal radiation on one side and cooled by convection on the opposite side.

with low values of the coefficient of thermal expansion, Young's modulus, emissivity and absorption coefficient. For optically thin materials ($\mu a << 1$), thermal stress resistance is inversely proportional to μ or μ^3 depending on the heating and cooling condition, but is independent of μ for optically thick materials and $h = 0$. Of course, since the objective of solar collectors is to absorb as much radiation as possible, the values of ε and μ should be non-zero. For this reason, trade-offs in design and material properties may be required.

In terms of the objective of the present conference, it is of interest to note that in establishing the values for the figures-of-merit in Eq. (18), the coefficient of thermal expansion interacts with as many as six other material properties, including optical, thermal as well as mechanical properties. As far as the present writers are aware, no figure-of-merit for materials in such engineering fields as aerospace, thermoelectricity, etc. contains as many dissimilar material properties such as those given by Eq. (18). Clearly, the coefficient of thermal expansion will play a significant role in determining the feasibility of high-intensity solar energy collectors.

ACKNOWLEDGEMENTS

This study was conducted as part of a research program on the thermal properties of engineering ceramics for structural applications supported by the Office of Naval Research under contract N00014-78-C-0413.

REFERENCES

1. W. D. Kingery, J. Amer. Ceram. Soc., 38(1955)3.

2. D. P. H. Hasselman, Ceramurgia, 4(1978)147.

3. D. P. H. Hasselman, J. Amer. Ceram. Soc., 46(1963)229.

4. D. P. H. Hasselman, J. Amer. Ceram. Soc., 49(1966)103.

5. D. P. H. Hasselman, J. R. Thomas, Jr., M. P. Kamat and K. Satyamurthy, J. Amer. Ceram. Soc. (in press).

6. J. R. Thomas, Jr., J. P. Singh and D. P. H. Hasselman, J. Amer. Ceram. Soc. (in press).

7. H. S. Carslaw and J. C. Jaeger, Conduction of Heat in Solids, Oxford at the Clarendon Press (1960).

8. B. Boley and J. Wiener, Theory of Thermal Stresses, John Wiley and Sons, New York (1960).

December 1979

BASIC DISTRIBUTION LIST

Technical and Summary Reports

Organization	No. of Copies
Defense Documentation Center Cameron Station Alexandria, Virginia 22314	(12)
Office of Naval Research Department of the Navy	
Attn: Code 471	(1)
Code 102	(1)
Code 470	(1)
Commanding Officer Office of Naval Research Branch Office 495 Summer Street Boston, Massachusetts 02210	(1)
Commanding Officer Office of Naval Research Branch Office 536 South Clark Street Chicago, Illinois 60605	(1)
Office of Naval Research San Francisco Area Office One Hallidie Plaza, Suite 601 San Francisco, California 94102	(1)
Naval Research Laboratory Washington, D.C. 20390	
Attn: Code 6000	(1)
Code 6100	(1)
Code 6300	(1)
Code 6400	(1)
Code 2627	(1)
Naval Air Development Center Code 302 Warminster, Pennsylvania 18974 Attn: Mr. F. S. Williams	(1)
Naval Air Propulsion Test Center Trenton, New Jersey 08628 Attn: Library	(1)
Naval Construction Batallion Civil Engineering Laboratory Port Hueneme, California 93043 Attn: Materials Division	(1)
Naval Electronics Laboratory Center San Diego, California 92152 Attn: Electron Materials Science Division	(1)
Naval Missile Center Materials Consultant Code 3312-1 Point Mugu, California 93041	(1)
Commanding Officer Naval Surface Weapons Center White Oak Laboratory Silver Spring, Maryland 20910 Attn: Library	(1)
David W. Taylor Naval Ship R&D Center Materials Department Annapolis, Maryland 21402	(1)
Naval Undersea Center San Diego, California 92132 Attn: Library	(1)
Naval Underwater System Center Newport, Rhode Island 02840 Attn: Library	(1)
Naval Weapons Center China Lake, California 93555 Attn: Library	(1)
Naval Postgraduate School Monterey, California 93940 Attn: Mechanical Engineering Dept.	(1)
Naval Air Systems Command Washington, D.C. 20360	
Attn: Code 52031	(1)
Code 52032	(1)

BASIC DISTRIBUTION LIST (Cont'd)

Organization	No. of Copies
Naval Sea System Command Washington, D. C. 20362 Attn: Code 035	(1)
Naval Facilities Engineering Command Alexandria, Virginia 22331	(1)
Scientific Advisor Commandant of the Marine Corps Washington, D.C. 20380 Attn: Code AX	(1)
Naval Ship Engineering Center Department of the Navy Washington, D.C. 20360 Attn: Code 6101	(1)
Army Research Office P.O. Box 12211 Triangle Park, N.C. 27709 Attn: Metallurgy & Ceramics Program	(1)
Army Materials and Mechanics Research Center Watertown, Massachusetts 02172 Attn: Research Programs Office	(1)
Air Force Office of Scientific Research Bldg. 410 Bolling Air Force Base Washington, D.C. 20332 Attn: Chemical Science Directorate	(1)
Electronics and Solid State Science Directorate	(1)
Air Force Materials Lab (LA) Wright-Patterson AFB Dayton, Ohio 45433	(1)
Library, Bldg 50, Rm 134 Lawrence Radiation Laboratory Berkeley, CA 94720	(1)

Organization	No. of Copies
NASA Headquarters Washington, D. C. 20546 Attn: Code RRM	(1)
NASA Lewis Research Center 21000 Brookpark Road Cleveland, Ohio 44135 Attn: Library	(1)
National Bureau of Standards Washington, D.C. 20234 Attn: Metallurgy Division	(1)
Inorganic Materials Division	(1)
Defense Metals and Ceramics Information Center Battelle Memorial Institute 505 King Avenue Columbus, Ohio 43201	(1)
Office of Naval Research, Branch Office 1030 East Green Street Pasadena, CA. 91106	(1)
Metals and Ceramics Division Oak Ridge National Laboratory P.O. Box X Oak Ridge, Tennessee 37380	(1)
Los Alamos Scientific Laboratory P.O. Box 1663 Los Alamos, New Mexico 87544 Attn. Report Librarian	(1)
Argonne National Laboratory Metallurgy Division P.O. Box 229 Lemont, Illinois 60439	(1)
Brookhaven National Laboratory Technical Information Division Upton, Long Island New York 11973 Attn: Research Library	(1)

BASIC DISTRIBUTION LIST (Cont'd)

Organization	No. of Copies	Organization	No. of Copies

Director Applied Physics Laboratory (1)
University of Washington
1013 Northeast Forthieth Street
Seattle, Washington 98105

SUPPLEMENTARY DISTRIBUTION LIST

Technical and Summary Reports

Advanced Research Project Agency
Materials Science Director
1400 Wilson Boulevard
Arlington, VA 22209

Mr. George Boyer
Sensor Systems Program
Office of Naval Research
Code 222
Arlington, VA 22217

Professor R. Bradt
Ceramics Section
Materials Sciences Department
The Pennsylvania State University
University Park, PA 16802

Professor L. E. Cross
The Pennsylvania State University
Materials Research Laboratory
University Park, PA 16802

Dr. A. G. Evans
Department Materials Science
and Engineering
Hearst Mining Building
University of California
Berkeley, CA 94720

Dr. Gene Haertling
Motorola Corporation
3434 Vassar, NE
Albuquerque, NM 87107

Dr. L. L. Hench
Department of Metallurgy
University of Florida
Gainesville, FL 32603

Dr. A. A. Heuer
Professor of Ceramics
Case Western Reserve University
University Circle
Cleveland, OH 44106

Dr. Paul Jorgensen
Stanford Research Institute
333 Ravenswood Avenue
Menlo Park, CA 94025

Dr. R. N. Katz
Army Materials and Mechanics
Research Center
Watertown, MA 02172

Dr. H. Kirchner
Ceramic Finishing Company
P.O. Box 498
State College, PA 16801

Dr. B. G. Koepke
Honeywell, Inc.
Corporate Research Center
10701 Lyndale Avenue South
Bloomington, MN 55420

Mr. Frank Koubek
Naval Surface Weapons Center
White Oak Laboratory
Silver Spring, MD 20910

Dr. J. Lankford
Southwest Research Institute
8500 Culebra Road
San Antonio, TX 78284

Professor P. B. Macedo
The Catholic University of America
Washington, DC 20017

Dr. N. Perrone
Code 474
Office of Naval Research
800 N. Quincy Street
Arlington, VA 22217

Dr. R. Rice
Naval Research Laboratory
Code 6360
Washington, DC 20375

SUPPLEMENTARY DISTRIBUTION LIST (Cont'd)

Dr. A. M. Alper
GTE Sylvania Inc.
Towanda, PA 18848

Dr. W. H. Rhodes
GTE Laboratories Inc.
40 Sylvan Rd.
Waltham, MA 02154

Dr. D. C. Larson
IIT Research Inst.
10 W. 35th Street
Chicago, IL 60616

Dr. B. Butler, Chief
Materials Branch
Solar Energy Research Institute
1536 Cole Blvd
Golden, CO 80401

Dr. M. Berg
AC Spark Plug Division
General Motors Corp.
1601 N. Averill Avenue
Flint, MI 48556

Dr. I. K. Naik
Airesearch Casting Corp.
Garrett Corp.
2525 W. 190th Street
Torrance, CA 90509

Dr. R. J. Bratton
R&D Center
Westinghouse Electric Corp.
Pittsburgh, PA 15235

Dr. W. Reilly, Director
PPG Industries
P.O. Box 31
Barberton, OH 44203

Dr. D. J. Godfrey
Admiralty Materials Laboratory
Ministry of Defense
(Procurement Executive)
Holton Heath
Poole, Dorset
BH16 6 JU
UNITED KINGDOM

Dr. Wm. Kessler
AFML
Wright-Patterson Air Force Base
OH 45433

Dr. S. F. Galasso
United Aircraft Research Laboratori
East Hartford, CN 06108

Dr. J. A. Coppola
The Carborundum Comp.
P.O. Box 1054
Niagara Falls, NY 14302

Dr. W. D. Tuohig
Bendix Research Laboratories
Southfield, MI 48076

Dr. Robert Ruh
AFML/LLM
Wright-Patterson AFB
OH 45433

Dr. R. A. Penty
Hague International
3 Adams Street
South Portland, Maine 04106

Dr. S. Musikant
General Electric Company
3198 Chestnut Street
Philadelphia, PA 19101

Dr. D. W. Richerson
Airesearch Man. Comp. Code 503-44
Garrett Corp.
111 S. 34th Str., Box 5217
Phoenix, AZ 85034

Dr. Frank Recny
General Electric Company
Court Street
Plant Building C
Box 1122
Syracuse, NY 13201

Globe-Union, Inc.
5757 North Green Bay Avenue
Milwaukee, WI 53201
Attn: G. Goodman

SUPPLEMENTARY DISTRIBUTION LIST (Cont'd)

Dr. J. H. Rosolowski
General Electric Company
Research and Development Center
P.O. Box 8
Schenectady, NY 02301

Dr. J. H. Simmons
Catholic University of America
Washington, DC 20064

Dr. P. L. Smith
Naval Research Laboratory
Code 6361
Washington, DC 20375

Dr. R. W. Timme
Naval Research Laboratory
Code 8275
Underwater Sound Reference Division
P.O. Box 8337
Orlando, FL 32806

Dr. Charles C. Walker
Naval Sea Systems Command
National Center #3
2531 Jefferson Davis Highway
Arlington, VA 20390

Dr. Paul D. Wilcox
Sandia Laboratories
Division 2521
Albuquerque, NM 87115

Dr. Murray Gillen
Australian Embassy
Washington, DC 33801

Dr. C. O. Hulse
United Aircraft Research Labs
United Aircraft Corporation
East Hartford, CT 06108

Dr. S. M. Wiederhorn
Physical Properties Section
Bldg. 223, Rm. A355
National Bureau of Standards
Washington, DC 20234

Dr. P. F. Becher
Code 6362
U.S. Naval Research Laboratory
Washington, D.C. 20375

Dr. R. Jaffee
Electric Power Research Institute
3412 Hillview Avenue
P.O. Box 10412
Palo Alto, CA 94303

Dr. B. A. Wilcox
Ceramics Programs, Room 336
Metallurgy and Materials Research
National Science Foundation
Washington, DC 20550

Dr. H. E. Bennett
Naval Surface Weapons Center
Research Department Code 601
China Lake, CA 93555

Dr. R. J. Charles
General Electric Company
Research and Development Center
Schenectady, NY 12301

Dr. A. R. C. Westwood
Martin-Marietta Laboratories
1450 South Rolling Road
Baltimore, MD 21227

Dr. N. S. Corney
Ministry of Defense
(Procurement Executive)
The Adelphi
John Adam Street
London WC2N 6BB
UNITED KINGDOM

Dr. D. E. Niesz
Battelle Memorial Institute
505 King Avenue
Columbus, OH 43201

Dr. R. E. Engdahl
Deposits and Composites, Inc.
318 Victory Dr.
Herndon, VA 22070

Professor W. D. Kingery
Ceramics Div. Rm. 13-4090
MIT
77 Mass. Avenue
Cambridge, MA 02139

SUPPLEMENTARY DISTRIBUTION LIST (Cont'd)

Mr. J. F. McDowell
Sullivan Park
Corning Glass Works
Corning, NY 14830

Dr. E. K. Beauchamp, Div. 5846
Sandia Laboratories
Albuquerque, NM 87185

Dr. J. A. Rubin
Kyocera International, Inc.
8611 Balboa Avenue
San Diego, CA 92123

Dr. W. V. Kotlensky
Materials Technology Department
TRW, Inc.
One Space Park
Redondo Beach, CA 90278

Dr. N. N. Ault
NORTON Comp.
One New Bond Street
Worcester, MA 01606

Dr. Hayne Palmour III
Engineering Research Division
N.C. State University
P.O. Box 5995
Raleigh, NC 27650

Dr. D. Ulrich
AFOSR, Code NC
Chemical Sciences Div.
1400 Wilson Blvd.
Arlington, VA 22209

Dr. V. J. Tennery
Oak Ridge Nat. Lab.
Oak Ridge, TN 38730

Dr. E. D. Lynch
Lynchburg Research Center
Babcock and Wilcox Co.
Box 1260
Lynchburg, VA 24505

Dr. S. C. Dixon
SDD-Thermal Structure Branch
Mail Stop 395
NASA Langley Research Center
Hampton, VA 23665

Dr. F. W. Clinard, Jr.
Los Alamos Scientific Lab.
MS 546
P.O. Box 1663
Los Alamos, NM 87544

Dr. D. DeCoursin
Fluidyne Eng.
5900 Olson Memorial Hwy.
Minneapolis, MN 55422

Dr. F. F. Lange
Rockwell International
P.O. Box 1085
1049 Camino Dos Rios
Thousand Oaks, CA 91360

Dr. T. Vasilos
AVCO Corporation
Research and Advanced Development
Division
201 Lowell Str.
Wilmington, MA 01887

Dr. W. R. Prindle
National Materials Adv. Brd.
2101 Const. Avenue
Washington, DC 20418

Dr. S. Dutta
NASA-Lewis Research Center
Mail Stop 49-3
21000 Brookpark Rd.
Cleveland, OH 44135

Mr. B. Probst
NASA-Lewis Research Center
21000 Brookpark Rd.
Cleveland, OH 44135

Dr. S. W. Freiman
Deformation and Fracture Group
Physical Properties Section, Bldg 22
National Bureau of Standards
Washington, DC 20234

Mr. W. Trombley
Garrett Corporation
1625 Eye Str. NY
Suite 515
Washington, DC 20006

SUPPLEMENTARY DISTRIBUTION LIST (Cont'd)

Mr. R. T. Swann
MD-Materials Research Branch
Mail Stop 396
NASA Langley Research Center
Hampton, VA 23665

Dr. K. H. Holko, Manager
Materials Applications
General Atomic Company
P.O. Box 81608
San Diego, CA 92138

Dr. W. Bakker
EPRI
3412 Hillview Avenue
P.O. Box 10412
Palo Alto, CA 94303

Dr. P. A. Miles, Research
Raytheon Company
28 Seyon Str.
Waltham, MA 02154

Dr. J. Ritter
University of Massachusetts
Dept. of Mech. Engr.
Amherst, MA 01002

Dr. M. E. Gulden
International Harvester Company
Solar Division
2200 Pacific Highway
San Diego, CA 92138

Dr. G. E. Youngblood
MERDI
Butte, MT 59701

Mr. C. E. Bersch
Code 52032
Naval Air Systems Command
Washington, DC 20361

Dr. M. A. Adams
Jet Propulsion Laboratory
California Institute of Technology
4800 Oak Grove Drive
Pasadena, CA 91103

Dr. Clifford Astill
Solid Mechanics Program
National Science Foundation
Washington, DC 20550

Dr. R. J. Gottschall
U.S. Dept. of Energy
Div. of Materials Science
Mail Stop J309
Washington, DC 20545

Prof. R. Roy
Pennsylvania State Univ.
Materials Research Lab.
University Park, PA 16802

Dr. R. Ruh
AFML - WPAFB
Dayton, OH 45433

Mr. J. Schuldies
Airesearch
Phoenix, AZ

Mr. J. D. Walton
Engineering Exp. Station
Georgia Inst. of Technology
Atlanta, GA 30332

Dr. W. F. Adler
Effects Technology, Inc.
5383 Hollister Avenue
P.O. Box 30400
Santa Barbara, CA 92105

Mr. D. Richarson
Airesearch Manufacturing Company
4023 36th Street
P.O. Box 5217
Phoenix, AZ 85010

Dr. N. MacMillan
Materials Research Laboratory
Pennsylvanis State University
College Park, PA 16802

Mr. W. B. Harrison
Honeywell Ceramics Center
1885 Douglas Drive
Golden Valley, MN 55422